CARBON MONOXIDE OXIDATION UNDER OXIDIZING AND REDUCING CONDITIONS WITH ALKALI-METAL AND PALLADIUM DOPED TIN DIOXIDE

A THESIS SUBMITTED TO
THE GRADUATE SCHOOL OF NATURAL AND APPLIED SCIENCES
OF
MIDDLE EAST TECHNICAL UNIVERSITY

BY

BURCU MİRKELAMOĞLU

IN PARTIAL FULFILLMENT OF THE REQUIREMENTS
FOR
THE DEGREE OF DOCTOR OF PHILOSOPHY
IN
CHEMICAL ENGINEERING

SEPTEMBER 2006

Approval of the Graduate School of Natural and Applied Sciences

Prof. Dr. Canan Özgen
Director

I certify that this thesis satisfies all the requirements as a thesis for the degree of Doctor of Philosophy.

Prof. Dr. Nurcan Baç
Head of Department

This is to certify that we have read this thesis and that in our opinion it is fully adequate, in scope and quality, as a thesis for the degree of Doctor of Philosophy.

Assoc. Prof. Dr. Gürkan Karakaş
Supervisor

Examining Committee Members

Prof. Dr. Timur Doğu (METU,CHE)

Assoc. Prof. Dr. Gürkan Karakaş (METU,CHE)

Prof. Dr. Suna Balcı (Gazi Ünv., CHE)

Prof. Dr. Hayrettin Yücel (METU,CHE)

Assist. Prof. Dr. Ayşen Yılmaz (METU, CHEM)

I hereby declare that all information in this document has been obtained and presented in accordance with academic rules and ethical conduct. I also declare that, as required by these rules and conduct, I have fully cited and referenced all material and results that are not original to this work.

Name, Last name : Burcu Mirkelamoğlu

Signature :

ABSTRACT

CARBON MONOXIDE OXIDATION UNDER OXIDIZING AND REDUCING CONDITIONS WITH ALKALI-METAL AND PALLADIUM DOPED TIN DIOXIDE

Mirkelamoğlu, Burcu
Ph.D., Department of Chemical Engineering
Supervisor: Assoc. Prof. Dr. Gürkan Karakaş

September 2006, 181 pages

The investigation of CO oxidation with supported noble metal catalysts to develop a fundamental understanding of the nature of the active sites, adsorbate-surface interactions, surface reaction pathways and the role of promoters is of prime importance for development of highly active and selective catalyst formulations for low temperature oxidation of carbon monoxide. Low temperature CO oxidation catalysts find applications in monitoring and elimination of CO in chemical process exhaust gases, in on-board control and diagnostics devices, automobile exhaust gas treatment systems for the development of zero-emission vehicles and, in closed-cycle CO_2 lasers for remote sensing. Moreover, the investigation of the interaction of CO with noble metals and noble metals catalyzed oxidation of CO have important outcomes for upstream fuel processing systems and for the development of more CO tolerant anode materials for H_2 fuel cell.

Palladized tin dioxide is a well-known and highly active catalyst for CO oxidation which possesses the potential to satisfy the need for CO oxidation catalysts in the abovementioned areas however, research on this material is concentrated mostly around empirical studies which focus solely on CO sensing applications. This current research is undertaken to investigate both the mechanism of CO oxidation with Pd/SnO_2 at the molecular scale and the possibility of promoting the CO activity of this catalyst by the application alkali-metal modifiers.

Alkali-metal modified PdO/SnO_2 catalysts were characterized by XPS, XRD and SEM and, tested with regard to their oxidation/reduction and CO oxidation behavior by *in-situ* dynamic methods such as, temperature-programmed reaction/reduction/desorption and impulse techniques. Modification of PdO/SnO_2 by alkali-metals, namely Li, Na and K, resulted in catalyst formulations with different surface characteristics and reduction/oxidation behaviors that lead to superior activity in low temperature CO oxidation and selectivity towards CO in the presence of H_2. Studies have shown that these catalysts are potential candidates for CO oxidation catalysts in a wide range of areas.

Keywords: CO oxidation, alkali-metal promotion, palladium, tin dioxide, characterization

ÖZ

ALKALİ METAL VE PALLADYUM KATKILI KALAY OKSİT İLE İNDİRGEN VE YÜKSELTGEN KOŞULLARDA KARBON MONOKSİT OKSİDASYONU

Mirkelamoğlu, Burcu
Doktora, Kimya Mühendisliği Bölümü
Tez Danışmanı: Doç. Dr. Gürkan Karakaş

Eylül 2006, 181 sayfa

Soy metal katkılı katalizörlerle CO oksitlenmesi üzerine yapılan çalışmanın hedefi, düşük sıcaklıklarda yüksek aktiviteye ve seçiciliğe sahip CO oksidasyon katalizörleri geliştirebilmek adına; aktif alanların doğası hakkında bir anlayış edinebilmek, adsorbat-yüzey etkileşimi, yüzey reaksiyon işleyişini ve katkıların katalizör üzerindeki rolünü anlayabilmektir. Düşük sıcaklıklarda aktivite gösteren CO oksitleme katalizörleri; kimyasal süreçlerin atık gazlarında karbon monoksit tespiti ve giderilmesi, motorlu taşıt dahili kontrol ve tanı cihazları, egzos gazı işleme sistemleri ve kapalı devre CO_2 lazerleri için kullanılabilmektedir. Bunun yanında, karbon monoksitin soy metallerle etkileşiminin ve karbon monoksit oksidasyonunda soy metallerin katalitik etkisinin araştırılması; H_2 yakıt pilleri için yakıt işleme sistemleri ve karbon monoksite daha toleranslı anot maddelerinin geliştirilmesi açısından da önem taşımaktadır.

Paladyum katkılı kalay oksit, CO oksidasyonunda yüksek aktiviteye sahip olduğu bilinen ve yukarıda sözü geçen alanlarda ihtiyacı karşılayacak potansiyele sahip bir katalizördür, ancak; bu madde üzerinde yapılan çalışmalar çoğunlukla ya ampirik düzeyde kalmış ya da yalnızca CO gazı algılama uygulamaları üzerine eğilmişlerdir. Bu çalışma hem Pd/SnO_2 katalizörünün CO oksidasyon mekanizmasını moleküler düzeyde çözümlemek hem de alkali metal katkıları uygulayarak bu katalizörün CO aktivitesini arttırmak üzere yürütülmüştür.

Alkali-metal katkılı PdO/SnO_2 katalizörlerin karakterizasyonu X-ışını fotoelektron spektroskopisi (XPS), X-ışını saçınımı (XRD) ve taramalı elektron mikroskopisi (SEM) teknikleri kullanılarak, yükseltgenme/ indirgenme davranışları üzerine olan testler ise, sıcaklığa bağlı oksidasyon tepkilerini gözlemlemek adına, TPD (Isıl Programlı Desorpsiyon), TPR (Isıl Programlı İndirgeme), TPRS (Isıl Programlı Reaksiyon) gibi "*anında*" gözlemlenen dinamik tekniklerle ve impulse tekniği ile yapılmıştır. Lityum, sodyum ve potasyum gibi alkali metal katkıları uygulanmış olan farklı formülasyonlara sahip PdO/SnO_2 katalizörler, hem yüzey karakterleri, hem de yükseltgenme/indirgenme davranışlarında, düşük sıcaklıkta yüksek CO oksidasyonuna ve H_2 varlığında yüksek CO seçiciliğine varan farklılıklar sergilemiştir. Sonuçlar göstermiştir ki; üretilen bu katalizörler geniş uygulama alanlarında yer bulacak CO oksidasyon katalizörleri arasında yer almaya adaydır.

Anahtar Kelimeler: CO oksitlenmesi, alkali-metal katkısı, paladyum, kalayoksit, karakterizasyon

To My Parents

ACKNOWLEDGMENTS

First and the most, I would like to take this opportunity to express my sincere gratitude to my supervisor, Assoc. Prof. Dr. Gürkan Karakaş for introducing me to this field of research, his invaluable scientific and academic guidance and, providing me with support and encouragement during the course of this research. I also wish to express my grateful thanks to Ph.D Examining Committee members, Prof. Dr. Timur Doğu and Prof. Dr. Suna Balcı, for their critical and constructive comments and insights on the progress of the work.

The help of all the technicians and machine shop workers of the Department of Chemical Engineering is gratefully acknowledged. I also would like to thank Belma Soydaş for the XRD analysis. The Central Laboratory and Department of Materials and Metallurgical Engineering of the Middle East Technical University are acknowledged for the XPS and SEM analysis. Thanks are due my friends; İrem Sert, Başak Kurbanoğlu and Ayşegül Ersayın Yaşınok, for their support and I also would like to acknowledge the former and present members of my research group.

Last but not the least; my cordial thanks are due my parents for their support and unshakeable faith in me.

TABLE OF CONTENTS

PLAGIARISM iii

ABSTRACT iv

ÖZ V

DEDICATION vii

ACKNOWLEDGEMENTS ix

TABLE OF CONTENTS x

LIST OF TABLES xiv

LIST OF FIGURES xv

LIST OF SYMBOLS AND ABBREVIATIONS xix

CHAPTER

1. INTRODUCTION 1

1.1 Closed-Cycle CO_2 Lasers 1

1.2 Automobile Exhaust Catalysis 2

1.3 Fuel Cell Applications 3

2. LITERATURE REVIEW 7

2.1 Carbon Monoxide Oxidation in CO-O_2 Mixtures 7

2.2 Selective Oxidation of Carbon Monoxide in CO-H_2-O_2 Mixtures 9

2.3 Tin Dioxide Based Catalysts 12

2.3.1 Tin Dioxide Based Gas Sensors and the Gas Sensing Mechanism 12

2.3.2 Tin Dioxide and Tin Dioxide Supported Platinum Group Catalysts 14

2.3.3 Interaction of SnO_2 Surfaces with Water Vapor and the Effect of Adsorbed Water and Hydroxy Species on the Activity of SnO_2-based Catalysts 17

2.4 Alkali-Metal Promoters of Red-Ox Reactions 19

3. EXPERIMENTAL 23

3.1 Catalyst Preparation 23

3.2 Experimental Set-up 25

3.3 Experimental Design and Parameters 28

3.4 Catalyst Characterization with Instrumental Analysis Techniques 31

3.5 Catalysts Characterization with In-situ Dynamic Techniques 32

3.5.1 Temperature Programmed Desorption (TPD) Studies 35

3.5.2 Temperature Programmed Reaction Spectroscopy (TPRS) Studies 36

3.5.3 Temperature Programmed Reduction (TPR) Studies 37

3.5.4 Steady-State CO Oxidation Activities of PdO/SnO_2-based Catalysts 38

4. RESULTS AND DISCUSSION 40

4.1 Characterization of PdO/SnO_2 and Na-PdO/SnO_2 40

4.1.1 XPS Analysis 40

4.1.1.1 XPS Analysis of Pd 3d Envelope of Oxidized and Reduced PdO/SnO_2 41

4.1.1.2 XPS Analysis of Pd 3d Envelope of Oxidized and Reduced Na-PdO/SnO_2 44

4.1.1.3 Quantitative Analysis of XPS Data 46

4.1.2 Scanning Electron Microscopy (SEM) and Energy Dispersive X-Ray Spectroscopy (EDX) 49

4.1.3 Temperature-Programmed Reaction Spectroscopy (TPRS) Studies 50

4.1.4 Steady-State CO Oxidation Activity 58

Temperature Programmed Desorption (TPD) Studies 60

4.1.5.1 CO Adsorption-O_2 TPD Studies 60

4.1.5.2 CO and O_2 Co-adsorption-O_2 TPD Studies 69

4.1.6 Surface Titration Experiments with Impulse Technique 75

4.2 Characterization of Li-PdO/SnO_2 and K-PdO/SnO_2 84

4.2.1 X-Ray Diffraction Analysis 85

4.2.1.1 X-Ray Diffraction Analysis of K-PO/SnO_2 85

4.2.1.2 X-Ray Diffraction Analysis of Li-PdO/SnO_2 86

4.2.2 XPS Analysis 89

4.2.2.1 XPS Analysis of Pd 3d Envelope of Oxidized and Pre-Reduced Li-PdO/SnO_2 90

4.2.2.2 XPS Analysis of Pd 3d Envelope of Oxidized and Pre-reduced K-PdO/SnO_2 90

4.2.3 Temperature-Programmed Reaction Spectroscopy (TPRS) Studies 94

4.2.4 Temperature Programmed Reduction (TPR) Studies with CO 97

4.3 Competitive Oxidation of CO and H_2 over Alkali-metal Modified PdO/SnO_2 105

4.3.1 Temperature Programmed Reduction with CO-H_2 Mixtures 105

4.3.2 Temperature-Programmed Reaction Spectroscopy (TPRS) Studies 111

4.3.3 Time-on-stream Activity – Under Fuel-Cell Conditions 122

4.4 Effect of Alkali-Metal Concentration on Properties of PdO/SnO_2-Based Catalysts 124

4.4.1 Effect of Modifier Concentration on the Crystal Structure 125

4.4.2 Effect of Modifier Concentration on the CO Oxidation Activity 127

4.4.3 Effect of Modifier Concentration on the Reduction Characteristics 131

5. CONCLUSIONS 138

REFERENCES 145

APPENDICES

A. MASS SPECTROMETRY 163

A.1 Basic Principles 163

A.2 Quantitative Analysis of Mass Spectra 163

B. FORTRAN 90 CODE FOR AREA UNDER THE CURVE CALCULATIONS FOR IMPULSE EXPERIMENTS 167

C. FORTRAN 90 CODE FOR AREA UNDER THE CURVE CALCULATIONS FOR O_2-TPD EXPERIMENTS 170

D. SAMPLE CALCULATIONS 173

D.1 Calculation of Crystallite Size 173

D.1 Calculation of Rates of CO Oxidation Reaction 173

D.2 Calculation of CO Selectivity in the Presence of H_2 175

E. N_2 ADSORPTION ISOTHERMS FOR BET AND PSD ANALYSIS 177

CURRICULUM VITAE 180

LIST OF TABLES

Table 3.1 Palladium and alkali-metal loading of the catalysts tested 25

Table 4.1 XPS analysis of Pd 3d envelope of Na-PdO/SnO_2 and PdO/SnO_2 47

Table 4.2 XPS analysis of Pd 3d envelope of Li-PdO/SnO_2 and K-PdO/SnO_2 93

Table 4.3 Rates of CO oxidation 95

Table 4.4 Rates of CO and H_2 oxidation and CO Selectivity at $X_{O_2} = 0.5$ ... 122

Table A.1. Cracking patterns of traced species 164

Table A.2 Traced ions and species contributing to traced ions 166

Table D.1 Rates of CO conversion (%) at 150°C under different reactor feed conditions 175

Table D.2 Rates of CO reaction (μmol/m^2.min) at 150°C under different reactor feed conditions 175

LIST OF FIGURES

Figure 3.1 Experimental set-up 26

Figure 4.1 Sn 3d XP spectra of (a) oxidized SnO_2, (b) oxidized PdO/SnO_2 and (c) oxidized Na-PdO/SnO_2 before (solid line) and after (dashed line) Ar-ion etching 42

Figure 4.2 Pd 3d XP spectra of (a) oxidized PdO/SnO_2 and (b) pre-reduced PdO/SnO_2 43

Figure 4.3 Pd 3d XP spectra of (a) oxidized Na-PdO/SnO_2 and (b) reduced Na-PdO/SnO_2 45

Figure 4.4 SEM images of (a) PdO/SnO_2 and (b) Na-PdO/SnO_2 49

Figure 4.5 CO conversion rates over oxidized PdO/SnO_2 (------), reduced PdO/SnO_2 (–··–··), oxidized Na-PdO/SnO_2 (———) and reduced Na-PdO/SnO_2 (.....) 51

Figure 4.6 CO conversion rates over oxidized PdO/SnO_2 (------), reduced PdO/SnO_2 (–··–··), oxidized Na-PdO/SnO_2 (———) and reduced Na-PdO/SnO_2 (.....) 52

Figure 4.7 CO conversion rates over oxidized PdO/SnO_2 (------), reduced PdO/SnO_2 (–··–··), oxidized Na-PdO/SnO_2 (———) and reduced Na-PdO/SnO_2 (.....) 53

Figure 4.8 Variation of rates of CO oxidation with TPRS feed composition 54

Figure 4.9 Water evolution profiles during TPRS, (a) reduced PdO/SnO_2, (b) oxidized PdO/SnO_2, (c) reduced Na-PdO/SnO_2 and (d) oxidized Na-PdO/SnO_2 57

Figure 4.10 Conversion rate of CO over SnO_2 (▼) PdO/SnO_2 (●) and Na-PdO/SnO_2 (○) under different [CO]/[O] ratios (a)S = 0.9 and (b)S = 1.1 59

Figure 4.11 CO_2 evolution profiles during post CO adsorption O_2 TPD (a) oxidized SnO_2, (b) reduced SnO_2, (c) oxidized PdO/SnO_2, (d) reduced PdO/SnO_2, (e) oxidized Na-PdO/SnO_2 and (f) reduced Na-PdO/SnO_2 61

Figure 4.12 H_2O evolution profiles during post CO adsorption O_2 TPD (a) oxidized SnO_2, (b) reduced SnO_2, (c) oxidized PdO/SnO_2, (d) reduced PdO/SnO_2, (e) oxidized Na-PdO/SnO_2 and (f) reduced Na-PdO/SnO_2 65

Figure 4.13 CO_2 profiles during CO adsorption (a) oxidized SnO_2, (b) reduced PdO/SnO_2 and (c) reduced Na-PdO/SnO_2 66

Figure 4.14 O_2 consumption/evolution profiles during post CO adsorption O_2 TPD (a) oxidized SnO_2, (b) reduced SnO_2, (c) oxidized PdO/SnO_2, (d) reduced PdO/SnO_2, (e) oxidized Na-PdO/SnO_2 and (f) reduced Na-PdO/SnO_2 68

Figure 4.15 CO_2 evolution profiles during post CO-O_2 co-adsorption O_2 TPD (a) oxidized SnO_2, (b) reduced SnO_2, (c) oxidized PdO/SnO_2, (d) reduced PdO/SnO_2, (e) oxidized Na-PdO/SnO_2 and (f) reduced Na-PdO/SnO_2 70

Figure 4.16 O_2 consumption/evolution profiles during post CO-O_2 co-adsorption O_2 TPD (a) oxidized SnO_2, (b) reduced SnO_2, (c) oxidized PdO/SnO_2, (d) reduced PdO/SnO_2, (e) oxidized Na-PdO/SnO_2 and (f) reduced Na-PdO/SnO_2 73

Figure 4.17 H_2O evolution profiles during post CO-O_2 co-adsorption O_2 TPD (a) oxidized SnO_2, (b) reduced SnO_2, (c) oxidized PdO/SnO_2, (d) reduced PdO/SnO_2, (e) oxidized Na-PdO/SnO_2 and (f) reduced Na-PdO/SnO_2 74

Figure 4.18 CO_2 evolution profiles during post CO-O_2 co-adsorption He TPD (a) oxidized SnO_2, (b) reduced SnO_2, (c) oxidized PdO/SnO_2, (d) reduced PdO/SnO_2, (e) oxidized Na-PdO/SnO_2 and (f) reduced Na-PdO/SnO_2 75

Figure 4.19 CO and CO_2 evolution from (a) oxidized SnO_2 (20ºC), (b) pre-reduced SnO_2 (20ºC), (c) oxidized SnO_2 (150ºC) and (d) pre-reduced SnO_2 (150ºC) 77

Figure 4.20 CO (○) and CO_2 (●) evolution from (a) oxidized PdO/SnO_2 (150ºC), (b) oxidized Na-PdO/SnO_2 (150ºC), (c) oxidized PdO/SnO_2 (20ºC) and (d) oxidized Na-PdO/SnO_2 (20ºC) 78

Figurez4.21 CO (○) and CO_2 (●) evolution from (a) pre-reduced PdO/SnO_2 (150ºC), (b) pre-reduced Na-PdO/SnO_2 (150ºC), (c) pre-reduced PdO/SnO_2 (20ºC) and (d) pre-reduced Na-PdO/SnO_2 (20ºC) 80

Figure 4.22 CO_2 evolution from (a) pre-reduced Na-PdO/SnO_2 and (b) oxidized Na-PdO/SnO_2 81

Figure 4.23 CO (○) and CO_2 (●) evolution from (a) oxidized PdO/SnO_2 (150ºC), (b) oxidized Na-PdO/SnO_2 (150ºC), (c) oxidized PdO/SnO_2 (20ºC) and (d) oxidized Na-PdO/SnO_2 (20ºC) during intermittently delayed injections of CO 83

Figure 4.24 CO (○) and CO_2 (●) evolution from (a) pre-reduced PdO/SnO_2 (150 ºC), (b) pre-reduced Na-PdO/SnO_2 (150 ºC), (c) pre-reduced PdO/SnO_2 (20 ºC), (d) pre-reduced Na-PdO/SnO_2 (20 ºC) during delayed injections of CO 84

Figure 4.25 XRD pattern of oxidized 0.1 wt. % K- 1 wt. % PdO/SnO_2 86

Figure 4.26 XRD patterns of: (a) oxidized 0.03 wt. % Li-1. wt. % PdO/SnO_2 (Li/0.53), (b) reduced 0.03 wt. % Li-1. wt. % PdO/SnO_2 (Li/0.53), (c) oxidized 0.1 wt. % Li- 1 wt. % PdO/SnO_2 (Li/1.77) and (d) oxidized 0.1 wt. % Li/SnO_2 88

Figure 4.27 Sn 3d XP spectra of (a)oxidized K-PdO/SnO_2 and (b)oxidized Li-PdO/SnO_2 before (solid line) and after (dashed line) Ar-ion etching 89

Figure 4.28 Pd 3d XP spectra of: (a) oxidized Li-PdO/SnO_2 (Li/0.53) and (b) pre-reduced Li-PdO/SnO_2 (Li/0.53) 91

Figure 4.29 Pd 3d XP spectra of: (a)oxidized K-PdO/SnO_2 and (b)reduced K-PdO/SnO_2 92

Figure4.30 Rates of CO conversion over oxidized Li-PdO/SnO_2 (———), reduced Li-PdO/SnO_2 (.....), oxidized K-PdO/SnO_2 (- - - - -) and reduced K-PdO/SnO_2 (– · · – · ·) 97

Figure 4.31 Temperature-programmed reduction CO_2 traces of (a)reduced SnO_2, (b) oxidized SnO_2, (c) reduced PdO/SnO_2, (d) oxidized PdO/SnO_2, (e) reduced K-PdO/SnO_2, (f) oxidized K-PdO/SnO_2, (g) reduced Na-PdO/SnO_2, (h) oxidized Na-PdO/SnO_2 (i) reduced Li-PdO/SnO_2 and (j) oxidized Li-PdO/SnO_2 102

Figure 4.32 Temperature-programmed reduction H_2O traces of (a)reduced SnO_2, (b) oxidized SnO_2, (c) reduced PdO/SnO_2, (d) oxidized PdO/SnO_2, (e) reduced K-PdO/SnO_2, (f) oxidized K-PdO/SnO_2, (g) reduced Na-PdO/SnO_2, (h) oxidized Na-PdO/SnO_2 (i) reduced Li-PdO/SnO_2 and (j) oxidized Li-PdO/SnO_2 103

Figure 4.33 Temperature-programmed reduction CO_2 traces of (a) reduced K/SnO_2, (b) oxidized K/SnO_2, (c) reduced Na/SnO_2, (d) oxidized Na/SnO_2, (e) reduced Li/SnO_2 and (f) oxidized Li/SnO_2 104

Figure 4.34 CO_2 evolution profiles during CO/H_2-TPR (a) K-PdO/SnO_2, (b) Na-PdO/SnO_2, (c) Li-PdO/SnO_2 and (d) PdO/SnO_2 106

Figure 4.35 H_2O evolution profiles during CO/H_2-TPR (a) K-PdO/SnO_2, (b) Na-PdO/SnO_2, (c) Li-PdO/SnO_2 and (d) PdO/SnO_2 107

Figure 4.36 H_2O Evolution profiles during H_2-TPR (a) PdO/SnO_2, b) Li-PdO/SnO_2, (c) Na-PdO/SnO_2 and (d) K-PdO/SnO_2 110

Figure 4.37 CO (- - - - -), O_2 (———) and H_2 (.....) conversion over oxidized (a) PdO/SnO_2, (b) Li-PdO/SnO_2, (c) Na-PdO/SnO_2 and (d) K-PdO/SnO_2 112

Figure 4.38 Water evolution profiles of (a) PdO/SnO_2, (b) Li-PdO/SnO_2, (c) Na-PdO/SnO_2 and (d) K-PdO/SnO_2 113

Figure 4.39 CO (- - - - -), O_2 (———) and H_2 (.....) conversion over oxidized (a) PdO/SnO_2, (b) Li-PdO/SnO_2, (c) Na-PdO/SnO_2 and (d) K-PdO/SnO_2 114

Figure 4.40 CO (- - - - -), O_2 (———) and H_2 (.....) conversion over oxidized (a) PdO/SnO_2, (b) Li-PdO/SnO_2, (c) Na-PdO/SnO_2 and (d) K-PdO/SnO_2 117

Figure 4.41 CO (- - - - -), O_2 (———) and H_2 (.....) conversion over oxidized (a) oxidized PdO/SnO_2, (b) reduced PdO/SnO_2, (c) oxidized Li-PdO/SnO_2, (d) reduced Li-PdO/SnO_2, (e) oxidized Na-PdO/SnO_2 (f) reduced Na-PdO/SnO_2, (g) oxidized K-PdO/SnO_2 and (h) reduced K-PdO/SnO_2 121

Figure 4.42 Steady-state CO (●) and O_2 (○) conversions and CO selectivity (▼) (a) PdO/SnO_2, (b) Na-PdO/SnO_2 and (c) K-PdO/SnO_2 123

Figure 4.43 XRD patterns of (a) Na/0.32, (b) Na/1.50, (c) K/0.32 and (d) K/1.50 126

Figure 4.44 Broadening of (211) reflection from cassiterite with sodium (i) and potassium (ii) content: (a) A:Pd = /1.50, (b) A:Pd = 0.53 and (c) A:Pd = 0.32 127

Figure 4.45 CO conversion rates over oxidized Na-PdO/SnO_2 (Na/0.32) (———), reduced Na-PdO/SnO_2(Na/0.32) (·····), oxidized Na-PdO/SnO_2 (Na/1.50) (------), reduced Na-PdO/SnO_2(Na/1.50) (–··–) 128

Figure 4.46 CO conversion rates over oxidized K-PdO/SnO_2 (K/1.5) (-----), oxidized K-PdO/SnO_2(K/0.53) (———), oxidized K-PdO/SnO_2(K/0.32) (·····) 129

Figure 4.47 CO conversion rates over reduced K-PdO/SnO_2 (K/1.5) (-----), reduced K-PdO/SnO_2(K/0.53) (———), reduced K-PdO/SnO_2(K/0.32) (·····) 130

Figure 4.48 Variation of CO oxidation rate with alkali-metal content 131

Figure 4.49 CO_2 evolution profiles (a) reduced Na-PdO/SnO_2 (Na/0.32), (b) oxidized Na-PdO/SnO_2 (Na/0.32), (c) reduced Na-PdO/SnO_2 (Na/0.53), (d) oxidized Na-PdO/SnO_2 (Na/0.53), (e) reduced Na-PdO/SnO_2 (Na/1.50) and (f) oxidized Na-PdO/SnO_2 (Na/1.50) 134

Figure 4.50 H_2O evolution profiles (a) reduced Na-PdO/SnO_2 (Na/0.32), (b) oxidized Na-PdO/SnO_2 (Na/0.32), (c) reduced Na-PdO/SnO_2 (Na/0.53), (d) oxidized Na-PdO/SnO_2 (Na/0.53), (e) reduced Na-PdO/SnO_2 (Na/1.50) and (f) oxidized Na-PdO/SnO_2 (Na/1.50) 135

Figure 4.51 CO_2 evolution profiles (a) reduced K-PdO/SnO_2 (K/0.32), (b) oxidized K-PdO/SnO_2 (K/0.32), (c) reduced K-PdO/SnO_2 (K/0.53), (d) oxidized K-PdO/SnO_2 (K/0.53), (e) reduced K-PdO/SnO_2 (K/1.50) and (f) oxidized K/PdO/SnO_2 (K/1.50) 136

Figure 4.52 H_2O evolution profiles (a) reduced K-PdO/SnO_2 (K/0.32), (b) oxidized K-PdO/SnO_2 (K/0.32), (c) reduced K-PdO/SnO_2 (K/0.53), (d) oxidized K-PdO/SnO_2 (K/0.53), (e) reduced K-PdO/SnO_2 (K/1.50) and (f) oxidized K/PdO/SnO_2 (K/1.50) 137

Figure E.1 N_2 adsorption (●) and desorption (o) isotherm for SnO_2 177

Figure E.2 N_2 adsorption (●) and desorption (o) isotherm for PdO/SnO_2 178

Figure E.3 N_2 adsorption (●) and desorption (o) isotherm for Na-PdO/SnO_2 178

Figure E.4 N_2 adsorption (●) and desorption (o) isotherm for K-PdO/SnO_2 179

LIST OF SYMBOLS AND ABBREVIATIONS

Symbols

A	Alkali-metal
B	Integral breadth, rad
c_i	Concentration of species i
F_i	Molar flow rate of species i
I	Intensity
K	Scherrer's constant
m	Mass
M	Metal
N	Number of moles, mol
P_i	Partial pressure of species i
R	Alkyl group
$R_{i,s}$	Surface reaction rate with respect to species I, μmol/m^2.min
$\Re$	Universal gas constant
Sg	Specific surface area, m^2/g
S_i	Percent selectivity with respect to species I
t	Crystallite size, nm
T_{50}	Light-off temperature (°C)
X_i	Conversion of species i
z	ionic charge

Greek Letters

υ	Volumetric flow rate, ml/min
λ	Wavelength, nm

Subscripts

lat	lattice

Abbreviations

EDX	Energy dispersive X-ray

ESCA	Electron spectroscopy for chemical analysis
ICE	Internal combustion engine
PEMFC	Proton exchange membrane fuel cell
PGM	Platinum group metal
PROX	Preferential oxidation
PSD	Pore size distribution
RS	Relative ionization gauge sensitivity
SEM	Scanning electron microscopy
SMSI	Strong metal-support interaction
TGA/MS	Thermogravimetric analyzer/mass spectrometer
TPD	Temperature programmed desorption
TPR	Temperature programmed reduction
TPRS	Temperature programmed reaction spectroscopy
TWC	Three-way catalysis
WGS	Water-gas shift reaction
XPS	X-ray photoelectron spectroscopy
XRD	X-ray diffraction

CHAPTER 1

INTRODUCTION

Carbon monoxide oxidation reaction is an industrially important reaction and has been subject to extensive heterogeneous catalysis research. The development of low-temperature CO oxidation catalyst formulations, which can effectively oxidize carbon monoxide at low temperatures in the presence or absence of other gaseous components such as hydrogen, hydrocarbons and water vapor and, in a wide range of gas phase compositions from CO-rich to CO-lean is necessary for application in automobile exhaust gas sensing systems for on-board-control and on-board-diagnostics devices, automobile exhaust catalysis, closed cycle CO_2 lasers and fuel cells.

1.1 Closed-Cycle CO_2 Lasers

Closed-cycle CO_2 lasers are utilized for remote sensing in space applications where, energy and space limitations exist. In these lasers, the optical gain occurs through a uniform electric discharge in a CO_2, N_2 and He gas mixture which is maintained at atmospheric pressure. The maximum amount of pulses that can be obtained in a single fill of gas is limited to $2X10^3$ pulses because the electrical discharges used to excite the laser decompose CO_2 to CO and O_2 and, the presence of oxygen is the most important factor that limits the number of pulses achievable before the discharge degenerates into localized arcs [1]. In order to prolong the lifetime of laser achievable with a single fill, sealed CO_2 lasers incorporate a CO oxidation catalyst to recombine stoichiometric amounts of CO and O_2 formed in the lasing process [1-3]. Stark and Harris [2] demonstrated the applicability of a heated platinum wire in recombination of CO and O_2 in a mixture containing 32% CO_2, 20% N_2, 40% He, 6% CO and 2% O_2 to resemble the degraded, high-power UV-preionization $CO_{2\ TEA}$ lasers. However, the catalyst needed heating up to 1000°C. Significant improvements in the sealed life of the laser were reported with the application of unheated tin dioxide-precious metal catalysts [1,3,4]. Stark and Harris [1] investigated a number of supported noble metal catalysts, compared their activity with that of

hopcalite under the operating conditions of sealed lasers and reported that the most active catalyst was SnO_2-Pd, which was 70 times more active than hopcalite even after exposure to humid laboratory air. Later, they investigated the effect of placing SnO_2-Pd in the mainstream of the gas circulating inside the laser on the sealed life of the laser and reported that when an unheated SnO_2-Pd catalyst was present, the life of the laser was improved by three orders of magnitude through the recombination of the dissociation products, CO and O_2 [3]. Gardner et *al.* [5] screened a number of noble metal/reducible oxide materials for application in low-temperature CO oxidation in sealed CO_2 lasers and reported that Au/MnO_X performed better than tin dioxide based catalysts in terms of catalyst activity and decay. In a later report, Gardner et *al.* [6] showed that 10% Au/MnO_X catalyzed CO oxidation reaction without any decay in the activity at 50°C for over 10 hours whereas, significant deactivation of 19.5% Pt/SnO_2 and 2% Pt/SnO_2 catalysts was observed under same conditions.

1.2 Automobile Exhaust Catalysis

Noble metal catalyzed oxidation of carbon monoxide in exhaust gases is also very important from an environmental pollution abatement point of view. Carbon monoxide is one of the major polluting components of automobile exhaust gases and regulations, which set limits for the release of carbon monoxide as well as hydrocarbons and nitrogen oxides, are now being adopted and tightened all over the world. Carbon monoxide is a product of incomplete combustion that indicates insufficient oxygen supply to the engine. At normal operating conditions, typical exhaust gas contains 0.5 vol. % carbon monoxide, 350 vppm unburned hydrocarbons, 900 vppm nitrogen oxides, 0.17 vol. % hydrogen, 10 vol. % water, 10 vol. % carbon dioxide and 0.5 vol. % oxygen [7]. Although the three-way catalyst (TWC) performs efficiently under normal driving conditions to simultaneously oxidize carbon monoxide and hydrocarbons and meanwhile, reduce NO_X; great amounts of CO and HC's are emitted during the first 10 minutes of engine switch-on when the catalyst is cool [8]. As the catalyst is heated up oxidation of CO starts first, which is followed by HC's and NO_X [7]. Low temperature oxidation of carbon monoxide during the engine cold-start period is a critical issue for the performance of the catalytic converters because, carbon monoxide adsorption inhibits the adsorption of HC's and reduces the efficiency of the catalytic converter [9].

Reduction of the light-off temperature (T_{50}) of the TWC for CO oxidation for efficient operation of the catalytic converters during the cold-start period is a challenge for heterogeneous catalysis. The light-off temperature (T_{50}) is defined as the temperature at which 50% conversion of the reactants is achieved and the typical light-off temperature for the TWC lies in 470-570°C range [10]. The modern three-way catalysts consist of precious metals namely Pt, which is responsible for the oxidation of CO and HC, and Rh, which is responsible for NO_X reduction and; CeO_2 is used as oxygen storage agent. The precious metals and ceria are mixed with γ-Al_2O_3 wash coat which is stabilized with La_2O_3 or BaO against sintering at the very high operating temperatures [11]. Among the platinum group metals (PGM's) Pt, Pd and Rh are the most widely applied metals in automobile exhaust catalysis as, they exhibit sufficiently high activity at high space velocities and also, they possess acceptable tolerance against sulfur poisoning [9]. Although palladium is known to exhibit higher activity than Pt in the oxidation of carbon monoxide and unsaturated hydrocarbons [14,15], it is not applied as widely as platinum and rhodium as, it is more sensitive towards poisoning by Pb [12,13]. With the recent improvements in the fuel quality (i.e. reduction of Pb content of gasoline), palladium started to partially substitute Pt and Rh in TWC. Reduction in the light-off temperatures are achieved by the utilization palladium in the TWC and improved TWC catalyst formulations involving Pd are being developed for meeting the tighter future emission regulations [16].

1.3 Fuel Cell Applications

The concerns about environmental pollution and the limited availability of fossil fuels resulted in a motive to create cleaner and more fuel efficient energy technologies, which could serve as alternatives to fossil fuels and help eliminate the dependence of societies on these fuels. Fuel cells are lean and energy efficient alternatives to the conventional combustion systems used in stationary and mobile applications thus; much emphasis is given to the commercialization of fuel cells and their widespread application in mobile and stationary systems.

The internal combustion engine (ICE) releases approximately 12 kg of CO_2, which is a greenhouse gas; to the atmosphere for each gallon of gasoline used [17] whereas, the only by-product of the fuel cell operated with pure hydrogen is water vapor. Moreover, huge amounts of atmospheric pollutants are emitted to

the atmosphere from fossil fuelled plants whereas, only little amounts of CO and CO_2 are emitted from the fuel cell operated plants.

The conventional thermo-mechanical methods for converting chemical energy to electrical energy comprise inefficient intermediate steps which are restricted with the efficiency of the Carnot cycle. These include the combustion of fossil fuels to obtain heat energy which is, then, converted to mechanical energy in a piston or a turbine. The mechanical energy is converted to electrical energy in a generator. Fuel cells, on the other hand, convert chemical energy directly into electrical energy and thus; are twice as much efficient as the ICE extracting more amount of work than the ICE from the same amount of fuel [18].

The type of the electrolyte determines the temperature window of operation of the fuel cell which in turn, defines the catalysts to be used and the purity of the fuel to be fed to the fuel cell. Several types of fuel cells for different applications are currently under development [17,19,20]. Among these, Proton Exchange Membrane Fuel Cell (PEMFC) is the most widely used fuel cell in transport applications due to its low temperature of operation (~80°C) and high power density [20] and; more than 90% of all fuel cell powered vehicles on the road are equipped with a PEMFC [21]. The handicap of PEMFC is that it has a very low CO tolerance and the anode electrokinetics is greatly hindered by traces of CO present from hydrocarbon steam reforming and water-gas shift reaction processes. At the operating temperature of the PEMFC, only platinum based catalysts exhibit sufficient activity to be used as the electrode materials however, when hydrogen from reformed hydrocarbons is used as the feed stream these catalysts are severely poisoned by the CO contained in the H_2 stream as CO is preferentially adsorbed on the catalyst, blocking the active sites for H_2 dissociation/oxidation and reducing the performance of the fuel cell dramatically [22].

Hydrogen to be supplied to the fuel cell is produced by reforming the readily available conventional fuels, such as natural gas (NG), liquefied petroleum gas (LPG), gasoline or methanol, to produce fuel cell grade hydrogen. In the long term, hydrogen to be used in the fuel cell would be generated by the use of renewable energy sources such as wind energy and solar energy; a transitional approach is to use the existing infrastructure for supplying hydrogen and use the conventional fuels after reforming. Although the ultimate aim is the hydrogen fuelling of the fuel-cell powered vehicles, an on-board fuel cell processor employing conventional hydrogen production techniques from carbogenic fuels

presents the short-term solution to the current hydrogen supply problem arising from the lack of hydrogen infrastructure. The conventional processes for producing hydrogen from carbogenic fuels include steam reforming (SR), catalytic partial oxidation (CPO) and autothermal reforming. When compared to CPO, the SR produces higher amount of hydrogen per mole of fossil fuel consumed and has slightly higher efficiency [23]. In addition, SR is an endothermic process which allows recycling the heat generated in other parts of the system.

Typical composition of the effluent from the reformer is 8% CO, 10% CO_2, 43% H_2, 25% H_2O and balance N_2 [24]. In order to generate more H_2 and further decrease the CO level, the reformate is fed to high temperature (~350 – 400°C) and low temperature (~200°C) water-gas shift reactors. Due to the thermodynamic limitations, the CO concentration of H_2 feed stream may be decreased to 5000 ppm – 1% range by water-gas shift reaction (Reaction 1.1). However; further reduction is not possible as water-gas shift reaction is reversible. The typical composition of the effluent from the water-gas shift reactor is 40-75% H_2, 0.5-1% CO, 15-25% CO_2, 15-30% H_2O and 0-25% N_2.

$$CO + H_2O \rightleftharpoons H_2 + CO_2 \tag{1.1}$$

Unfortunately, these conventional hydrogen production technologies yield product streams containing CO_2 and H_2 and as well small amounts of CO, which causes loss in the efficiency of the fuel cell. The efficiency loss of the fuel cell arising from the CO poisoning of the anode electrocatalyst can be avoided either by the development of more CO tolerant anodes or by the reduction of the CO content of the H_2 feed stream. More CO tolerant state-of-art Pt anodes, such as PtMo or PtRh; that can operate up to 100 ppm CO have been proposed [25].

The reduction in the CO content of the H_2 stream can be achieved in several ways [18,26]; one alternative is the separation of hydrogen by diffusion through a Pd/Ag membrane [27] however, this method requires high pressure gradients and the flux is generally very low. Carbon monoxide content of the H_2 feed stream could also be eliminated by methanation [28]. Methanation (Reaction 1.2) is a very effective and commonly practiced method for the removal of traces of CO in ammonia plants however; this process consumes 3 molecules of hydrogen per molecule of CO and releases methane, which is a greenhouse gas.

$$CO + 3H_2 \rightarrow CH_4 + H_2O \tag{1.2}$$

Another, and yet the most studied; alternative is the preferential oxidation (PROX) of carbon monoxide with minimum loss of hydrogen [29]. Ideally, the catalyst to serve for this purpose must selectively oxidize 1% CO to <5 ppm without oxidizing any of the 40-70% H_2 present in the reformate [30]. Oxidation of H_2, thus the formation of water decreases the amount of H_2 to be fed to the fuel cell reducing the overall efficiency of the fuel cell. For this reason the amount of oxygen to be supplied to the PROX reactor should be kept at minimum, which requires a very high selectivity of the PROX catalysts towards CO.

The CO PROX catalyst to be utilized in the CO clean-up system in the H_2 fuel cell mush exhibit both high activity and high selectivity towards carbon monoxide and should be able to operate at temperatures in between the temperature of the upstream low-temperature WGS unit (250-300°C) and the downstream PEMFC (80-100°C). The development of such a catalyst with high CO oxidation rate and selectivity is still a challenge for heterogeneous catalysis. Current research is concentrated around oxide-supported gold; PGM and copper based catalysts with or without promoters and inputs from fundamental studies on the interaction of absorbed carbon monoxide and hydrogen and; the reaction pathways leading to the oxidation of these components are required for the development of active and selective catalyst formulations.

In the present work, PdO/SnO_2-based catalysts, which are known to be active in low-temperature CO oxidation, were characterized and investigated with regard to their activity in CO oxidation under oxidizing and reducing conditions. Alkali-metal (Li, Na and K) promotion was applied to investigate the possibility of further enhancing the CO oxidation activity of these catalysts and the effect of different alkali-metals on catalyst structure and morphology; reduction and CO oxidation behavior and; on the extent of incorporation of subsurface oxygen in CO oxidation was investigated with XRD, XPS, and SEM and; with temperature programmed techniques, surface titration experiments and steady-state activity measurements. The results of the experiments carried out under a number of oxidizing and reducing conditions have shown that alkali-metals can be used to alter the reduction behavior of PdO/SnO_2-based catalysts and promote the low-temperature CO oxidation activity. The study has shown that alkaline modified PdO/SnO_2 catalysts are effective low-temperature CO oxidation catalysts which possess the potential of application in CO_2 lasers, automobile exhaust catalysts and H_2 fuel-cell applications and; deserve further attention.

CHAPTER 2

LITERATURE REVIEW

2.1 Carbon Monoxide Oxidation in CO-O_2 Mixtures

Catalyst formulations involving a noble metal component dispersed over a reducible metal oxide, that can be supported on an inert oxide such as SiO_2 or Al_2O_3, are the most widely investigated formulations for low temperature CO oxidation [31-37]. In addition to these noble metal based catalysts; base metal oxides [38-40]; especially copper oxides and; perovskite type catalysts [41,42] have been reported to exhibit CO oxidation activity.

Noble metal catalysts are well recognized for their high activity in CO oxidation reaction and the oxidation of CO over a number of oxide-supported noble metal systems as well as single crystals, bulk films, wires and ribbons of Pt, Pd and Rh have been extensively studied [31-37,43-47]. It is well established that carbon monoxide oxidation over noble metal catalysts proceeds with Langmuir-Hinshelwood mechanism, where both of the reactants are chemisorbed over the surface [37,43,46-48]. Carbon monoxide irreversibly adsorbs on and strongly interacts with noble metal surfaces [49] such that, under oxidation conditions the surface is practically covered with adsorbed CO species and the reaction rate is controlled by the rate of CO desorption from the surface [50,51]. Fuchs et *al.* [45] have investigated the kinetics of CO oxidation over polycrystalline Pd, Pt and Rh foils, ribbons and wires in oxidizing and reducing gas mixtures and reported that in oxidizing gas mixtures, the rate was first order with respect to P_{CO} and independent of P_{O_2} whereas, in reducing gas mixtures, the reaction order was +1 with respect to P_{O_2}, while the rate was independent of P_{CO} at the high temperature range and was inhibited by CO at the low temperature range. Santra and Goodman [47] investigated CO oxidation over Pd, Ir and Rh and observed that at a O_2-to-CO ratio of 12:1 the reaction rate with respect to P_{O_2} started to decrease from positive first order down to negative order while, the reaction order with respect to P_{CO} changed from negative to positive. Engel and Ertl [43] observed that oxygen adsorption was completely inhibited over CO

precovered surface whereas, no inhibition of CO adsorption was present over oxygen precovered Pd(111) surface. Over Pd(110), Goschnick et *al.* [52] observed a drastic decrease in the sticking probability of CO when oxygen was present as an adsorbate and reported that each oxygen atom adsorbed on Pd(110) blocked ten sites for CO adsorption. Piccolo et *al.* [53] studied Pd clusters mainly exhibiting (111) and (100) facets and reported a similar observations for the inhibition of CO chemisorption over oxygen pre-saturated surface.

In line with single crystal studies, studies on polycrystalline palladium catalysts supported on a number of reducible metal oxides have shown that the reaction rate was controlled by the desorption of CO from the metallic particles to allow oxygen chemisorption [32,33,37]. Duprat et *al.* [32] studied the kinetics of CO oxidation over Pd supported on SiO_2 and Al_2O_3 under typical conditions of atmospheric pollution and reported negative reaction order with respect to P_{CO} and positive order with respect to P_{O_2}. Similarly, Kalinkin et *al.* [33] reported negative first order reaction with respect to P_{CO} and positive first order with respect to P_{O_2} over Pd/Fe_2O_3 under stoichiometric feed conditions, implying that the reaction was inhibited by strong adsorption of CO. An irreversible kinetic surface model for CO oxidation was developed by Ziff et *al.* [54] to model the kinetic phase transitions that correspond to the poisoning of surfaces with CO and O_2. The authors observed a region of steady-state reaction, where the mole fraction of CO (y_{CO}) was in the region 0.389-0.525. For gas phase CO fractions lower than 0.389, the system was poisoned by oxygen and alternatively, when the CO fraction was higher than 0.525, CO poisoning occurred.

As the reaction kinetics discussed above implies, both CO and O_2 compete for the same sites and tend to inhibit the CO oxidation reaction by hindering the adsorption of the other. Therefore, the catalyst that could efficiently oxidize CO at low temperatures must be able to simultaneously accommodate CO chemisorption and O_2 ionosorption. Another critical factor, which is in close relation with the chemisorption of CO and O_2, is the tendency of the catalyst to donate its oxygen and this determines the activity of a catalyst. If the oxide is easily reducible then the oxygen would easily be donated and the catalyst could be expected to be active but not selective. Alternatively, when the oxygen-metal bond is strong then the oxygen would not be donated so easily and the catalyst would be expected to exhibit low activity. Therefore, a correlation between the

activity of the catalyst in oxidation reactions and the bonding strength of the oxygen bond exists and; catalytically most active oxides are characterized by low energy of the surface oxygen [55]. The kinetics of oxidation reactions over palladium oxide based surfaces is known to follow a Mars-van-Krevelen mechanism, which involves the donation of oxygen species by oxide during the oxidation of chemisorbed species and the re-oxidation of the oxide by gaseous oxygen to regenerate active oxygen species [46,56-59]. On the other hand, the CO oxidation reaction kinetics over metallic Pd reflects a Langmuir-Hinshelwood mechanism, where the reaction takes place between adsorbed CO molecules and O atoms adsorbed on neighboring sites [37,43,46-48].

The high activity of palladium-based catalysts in oxidation reactions have been attributed to a dual mechanism where both PdO and Pd are active in catalyzing the reaction [55,59,60]. Belousov et *al.* [55] studied the low temperature reduction of supported palladium catalysts and concluded that the catalytically active form of the catalyst was an oxide cluster incorporating partially reduced Pd chemically bound to the oxide. Similarly, Burch and Urbano [60] stated that approximately four monolayers of oxygen was necessary for palladium clusters to exhibit good catalytic activity and Muller et *al.* [59] proposed a mechanism involving the reduction/oxidation of the surface and a few submonolayers.

2.2 Selective Oxidation of Carbon Monoxide in CO-H_2-O_2 Mixtures

The investigation of the CO oxidation activity of noble metal catalysts in the presence of other reducing agents such as hydrogen or hydrocarbons is of particular importance for application in automotive exhaust catalysis, where the effluent gas contains unburned hydrocarbons and hydrogen as well as, steam, carbon dioxide and NO_X. Furthermore, the effect of the presence of hydrogen on CO interaction with noble metals is also important for fuel cell applications, both for the CO clean-up system, where a noble metal based catalyst is employed for the elimination of the CO content of the H_2-feed and, for the development of more CO tolerant anode materials, which are poisoned by the presence of traces of CO present in H_2.

Although the behavior of noble metal systems towards CO adsorption/oxidation is well established, the simultaneous adsorption of CO and H_2 and, their simultaneous oxidation in CO-H_2-O_2 gas mixtures is not fully understood. As the chemisorption of CO on noble metal surfaces is much stronger when compared

to the chemisorption of O_2 and H_2 species [50, 61], CO induces a blanketing effect, interfering with the adsorption/oxidation of other compounds [27,49,62-64]. Czerwinski et *al.* [63] have studied the effect of carbon monoxide on hydrogen adsorption on thin films of palladium and reported that H_2 oxidation was hindered by adsorbed CO which saturates the surface and leaves out only a limited number of free adsorption centers for H_2. Similarly, Yepez and Scharifker [49] studied the oxidation of CO on hydrogen loaded palladium and observed that carbon monoxide interfered with the oxidation of organic compounds. Lischka et *al.* [64] performed density functional theory calculations to show that H_2 adsorption is completely eliminated on a CO precovered Pd(210) surface.

A general work on the selective oxidation of CO in the presence of hydrogen was reported by Oh and Sinkevitch [65], where the authors investigated a number of noble metal (Ni, Pt, Pd, Rh, Ru, Ag) catalysts supported on alumina and base metals (Co/Cu, Ni/Co/Fe, Ag, Cr, Fe, Mn) under very dilute conditions, i.e. 8500 ppm H_2, 900 ppm CO, 800 ppm O_2 and balance N_2, and compared the performance of alumina with other possible base metal oxides. Among the base metal catalysts, the highest activity was reported for the Co-containing catalysts and the CO oxidation activity of the supported noble metal catalysts decreased in the order Ru/Al_2O_3 > Rh/Al_2O_3 > Pt/Al_2O_3 > Pd/Al_2O_3.

While CO has an inhibiting effect on H_2 oxidation over noble metal catalysts, several authors have reported the promotion of CO oxidation in the presence of H_2 [62, 66-69]. Both Langmuir-Hinshelwood and Eley-Rideal mechanisms require desorption of sufficient amount of CO from the surface to allow the dissociative adsorption of oxygen and the exposure of the catalytically active sites so that, the catalytic reaction would commence. The promoting effect of the presence hydrogen on CO oxidation has been attributed to the elimination of the inhibiting effect. Muraki et *al.* [69] have reported that CO oxidation activity of alumina supported Pt, Pd and Rh catalysts was promoted by the presence of steam and H_2 in the feed gas. The degree of the promotion effect decreased in the order of Pt>Pd>Rh and the authors have attributed the effect to the decrease in the CO-inhibition effect. Stetter and Blurton [67] have observed a similar promotion effect of H_2 on the CO oxidation rate on asbestos supported Pt and silica gel supported Pd and reported a 50 K decrease in the onset temperature for CO oxidation when H_2 was added to the reaction mixture. According to these authors, the decrease in the CO inhibition effect is associated with the formation of a complex such as H-CO on the catalyst surface that can be desorbed at much

lower temperatures than CO and, the CO oxidation reaction takes place at lower temperatures. Over Pt wires, Dabill et *al.* [68] reported a 34°C decrease in the onset temperature of CO oxidation reaction and a 100°C increase in the onset temperature of H_2 oxidation reaction when the two agents are coexisted in the reaction mixture. These authors suggested that gas-phase CO would react with oxygen ad-species at room temperature to yield gas-phase CO_2 and vacant surface sites. The resulting surface sites would be filled with CO which would block the surface until the temperature is high enough to initiate desorption of CO to vacate these sites for dissociative adsorption of O_2. Surface species such as -CHOH have been postulated to form and desorb from the surface at lower temperatures than CO. Goldsmith et *al.* [66] have also observed the promoting effect of the presence of hydrogen in CO feed over Pd/SiO_2 and attributed the effect to the alloying of Pd in the presence of hydrogen which would promote the oxygen adsorption.

Many of the PROX catalyst formulations developed for application in H_2 fuel cells involve a noble metal component, which is generally Pt [70-73] or gold [74-76]. Early patents involving Pt based catalysts for CO oxidation in H_2 streams for fuel cell applications belong to Engelhard [77]. The Selectoxo™ catalyst and process developed and commercialized by Engelhard for H_2 plants for the removal of CO to provide feed stream to ammonia plants, is based on 0.3-0.5% Pt catalyst supported on γ-alumina 1/8" (3 mm) tablets promoted with a base metal oxide. This catalyst exhibits high selectivity towards CO, reducing up to 10 000 ppm CO to less than 5 ppm without significantly oxidizing 70% H_2 in the reformate. However, the Selectoxo™ process cannot be implemented to the fuel cell as the CO removal unit for fuel cell applications need to operate under transient conditions at very high space velocities and in the presence of large amounts of CO_2 and H_2O. Recently, a modification of the Selectoxo™ catalyst where a cordierite monolith was wash-coated by an aqueous slurry of 5% Pt promoted by a base metal oxide impregnated onto γ-alumina has been reported to exhibit good activity and selectivity towards CO under fuel cell conditions [72].

Kahlich et *al.* [70] have investigated the kinetics of CO oxidation with Pt/Al_2O_3 with simulated reformer gas and have reported a two-fold increase in the rate of CO oxidation in the presence of H_2. The authors proposed a mechanism where, adsorbed CO blocked adsorption/dissociation of O_2 and resulted in the observed high selectivity. At temperatures higher than 250°C a loss in CO selectivity was

observed and has been attributed to the onset of CO desorption and increase in the H_2 oxidation rate.

Although palladium is known as an active CO oxidation catalyst, which can catalyze the reaction between CO and O_2 at temperatures as low as -27°C [1], supported palladium catalysts have been observed to have inferior activity relative to Pt based catalysts in selectively oxidizing CO in the presence of H_2 [65, 78-80]. In a study where they reported Ru/Al_2O_3 and Rh/Al_2O_3 to be active CO-PROX catalysts, Oh and Sinkevitch [65] identified Pd/Al_2O_3 as the least active catalyst. They have observed a similar behavior of all of these catalysts towards carbon monoxide oxidation till 60°C and above that temperature CO conversion over Pd/Al_2O_3 showed a weaker dependence of temperature and diverged from the conversion profiles of the two other catalysts. The authors have attributed the unusual temperature dependence of CO conversion over Pd/Al_2O_3 to the onset of the oxidation of catalytically highly active Pd to PdO, which is catalytically less active. Similarly, Pozdnyakova et *al.* [80] have investigated the PROX activity of ceria supported Pt and Pd and reported that, Pd exhibited inferior catalytic activity relative to Pt, although it is known as an active CO oxidation catalyst in the absence of H_2. In efforts to provide a mechanistic explanation to the poor activity of Pd/CeO_2, the authors identified the formation of Pd β-hydride phase in the presence of hydrogen. They have suggested that this phase greatly suppressed the CO oxidation as oxygen from both gas-phase and the surface would rapidly react with H to form water and CO was retained on the surface as formyl (-CHO) species rater than being oxidized to CO_2.

2.3 Tin Dioxide Based Catalysts

Tin dioxide is an industrially important semiconducting metal oxide which has found applications in gas sensing with solid state gas sensor devices, photocatalytic degradation of microorganisms, development of self cleaning surfaces and in heterogeneous catalysis as a red-ox catalyst for carbon monoxide, methane and NO_X [81].

2.3.1 Tin Dioxide Based Gas Sensors and the Gas Sensing Mechanism

Tin dioxide is a well-recognized and widely investigated semiconducting metal oxide. It is the most widely applied metal-oxide-semiconductor (MOS) in solid state gas sensor devices for the detection of flammable and toxic gases under

ambient conditions [82,83]. Much research has been devoted to the elucidation of the gas sensing mechanism with SnO_2-based sensors and improvement of the response and recovery times and, the specificity of these sensors for the detection of different gases [84-101].

The basic operating principle of solid-state gas sensor devices is the monitoring of the changes in the electrical resistance behavior of the sensing element, which has a high surface-to-bulk ratio and secured on a heated substrate with attached metallic electrodes. Adsorption of oxygen on tin dioxide surface leads to the formation of O_2^- and O^- species which would result in the build-up of negative charge at the surface and increase the resistance of the sensing material [84, 85]. During the exposure of this ionosorbed oxygen covered tin dioxide surface to a reducing gas, such as CO, reaction of the reducing gas with the previously adsorbed oxide species would take place and this would result in the ejection of electrons to the conduction band, which would, again, alter the resistance of the sensing material. Therefore, any change in the ambient concentration of a trace gas would result in a change in the availability/mobility of the free charge carriers through; adsorption, surface reaction and desorption of the gas phase molecules. The change in the availability and/or mobility of the charge carriers available at the surface would be manifested as a change in the resistance behavior of the material and; the response would be proportional to the concentration of the trace gas in the ambient atmosphere. As the foregoing discussion implies, gas sensing with solid-state gas sensor devices arises from catalytic reactions taking place at the surface of the sensing material for which the electrical consequences are manifested all through the volume of the material and, in fact, heterogeneous catalysis phenomena namely adsorption, surface migration, activation, surface reaction, desorption; prevail in the gas detection mechanism. Therefore, inputs from research focusing on the fundamentals of the sensing mechanism are needed for further development of the technology [84,86].

In line with the principles of heterogeneous catalysis, secondary or even ternary, metallic compounds that are more active than tin dioxide in adsorbing and oxidizing the reducing agents, were introduced to tin dioxide layers, in efforts to increase the sensitivity and selectivity of tin dioxide based gas sensors towards different flammable and toxic gases [87-96]. The effect of the addition of a number of transition metals such as; nickel [87], platinum [87-90], palladium [87-96] and gold [90] on the selectivity and sensitivity of SnO_2-based sensors

for CO detection have been investigated and it has been shown that the introduction of these metals to tin dioxide structure promoted the CO sensitivity and selectivity of these sensors. Among the transition metals introduced into the tin dioxide matrix, palladium has been observed to result in the most pronounced effect in terms of increasing selectivity and sensitivity, decreasing the optimum operating temperature and reducing the response and recovery times of the sensor [87,90]. Although the promoting effect of addition of palladium to tin dioxide has been documented by various studies in the literature [87-96], there is still debate on the role of palladium in the sensing mechanism. It has been proposed that the observed enhancement in the sensor response functions resulted from either a chemical [89, 94] or an electronic [86] interaction. The chemical mechanism, which is also named as the spill-over process, comprises the movement of adsorbed molecules, which do not interact with the oxide in the absence of palladium, from the metallic cluster to the oxide surface. Alternatively, in the electronic mechanism, the reaction with the gas molecules takes place on the introduced metal clusters, not on the metallic oxide. The state of these clusters change which leads to a change in the electrical resistivity behavior of the supporting oxide. Moreover, Kappler et *al.* [96] have proposed that palladium addition changed the density of the reaction sites. Also, introduction new states to the band structure of the material and changes in the surface morphology of doped surfaces are frequently discussed in attempts to explain the role of transition metal additives in the gas sensing mechanism [87].

2.3.2 Tin Dioxide and Tin Dioxide Supported Platinum Group Catalysts

Although recent research on tin dioxide is mainly concentrated on the gas sensing applications of the material, tin dioxide is also a well known CO oxidation catalyst which oxidizes chemisorbed CO through a mechanism of lattice oxygen abstraction with the participation of oxygen in the surface layers at temperatures above 300°C [83,102,103].

In early 90's, tin dioxide has also attracted particular attention as the support material for platinum and palladium catalysts for application as low-temperature CO oxidation catalysts in space applications [1,3,4,103-107]. Low-temperature CO oxidation catalysts are needed in CO_2 lasers, as the electrical discharges used to excite the lasers decompose some CO_2 to CO and O_2 reducing the lifetime of the CO_2 laser. The application area of these lasers, such as remote sensing from

space vehicles, does not allow the addition of make-up gas or the removal of the decomposition products because of volume and weight constraints of space applications. Moreover, as energy supply is limited in such applications, the catalyst to be utilized in closed-cycle CO_2 lasers should be able to reoxidize CO and O_2, which are present in stoichiometric amounts, without the need for heating to minimize power consumption. During the search for a low-temperature CO oxidation catalyst for extending the lifetime of CO_2 lasers, Stark and Harris [1] have shown that platinized and palladized tin dioxide systems were more active than the noble metals and tin dioxide in isolation are and that, these systems actively catalyzed the CO oxidation reaction at temperatures as low as -27°C. Till the end of 1990's, much research was done to elucidate the mechanisms leading to this synergy between tin dioxide and palladium (platinum) [103,104-113]. Although no consensus is present on the exact cause of this synergistic effect, a number of factors are frequently discussed to explain the metal-support interactions in tin dioxide supported platinum group catalysts:

(i) *Spillover of activated species from the transition metal to the oxide:* Although CO readily adsorbs over transition metal surfaces [103], negligible amount of CO and O_2 are adsorbed over tin dioxide surface at temperatures below 400°C [105] and thus, at temperatures below 400°C, the rate limiting step for CO oxidation over bare tin dioxide would be the adsorption of the reactant species. Sheintuch et *al.* [106] have proposed that CO monoxide migrated to SnO_2 surface after it has been adsorbed on Pd centers and then, it is oxidized by the incorporation of either gas phase oxygen or oxygen chemisorbed from the gas phase. Thus, the role of the support was explained as accelerating the rate by increasing the active surface area and reducing the effect of CO inhibition on the noble metal. Similarly, Kulshreshtha and Sasikala [107] reported that H_2 and CO treatment of Pt/SnO_2 and Pd/SnO_2 led to the formation of more Sn^{2+} relative to reduction pretreatment of bare SnO_2 and explained the effect by spillover of activated CO and H_2 from metal sites to oxide support however the authors did not completely exclude the possibility of localized increase in the temperature of the metal centers leading to enhanced rates. In a more recent work, Amalric-Popescu and Bozon-Verduraz [108] investigated SnO_2 supported Pd catalysts by surface spectroscopic techniques and, postulated that the role of palladium was to adsorb

CO which then spills over SnO_2 where it reacts with oxygen anions, generating oxygen vacancies.

(ii) *Reverse spillover of oxygen from tin dioxide to the metal:* Although the noble metal reacts strongly with CO and increases its surface coverage, CO generally acts as a catalyst poison and tends to inhibit the adsorption of oxygen over the noble metal surface. Therefore, the rate limiting step for CO oxidation over palladium catalysts might also be the adsorption oxygen to participate in oxidation reaction. Boulahouache et *al.* [109] have observed the presence of an induction period in the reaction of preadsorbed CO with oxygen whereas, preadsorbed oxygen directly reacted with CO and attributed the effect to the attacking of the adsorbed CO layer by oxygen spilling over from the support before oxygen from the gas phase could chemisorb and react on the surface. Similar observations were also presented in a report by Grass and Lintz [110] where they attributed the synergism between platinum and tin dioxide to the adsorption of oxygen mainly on the oxide surface and to the migration of these oxygen species to the reaction sites situated at the border between noble metal and the oxide.

(iii) *Formation of Pt(Pd)/Sn alloy:* The strong metal-support interaction (SMSI) between Pd and Sn that is caused by treatment of the catalyst samples in reducing atmospheres at temperatures above 200°C has been observed to lead to the formation of Pd_ySn_x alloys through the hybridization Pd 3d and Sn s states and; the formation of these alloys have been reported to alter chemisorption properties and influence the catalytic behavior of the Pd-SnO_x [103,104,114] and Pt-SnO_x [115] systems and bimetallic Pd-Sn catalysts supported on different oxides [116-118]. Schryer et *al.* [111] have observed enhanced CO oxidation rate over samples that have been subjected to reduction pretreatment relative to the ones subjected to oxidizing pretreatment and postulated that, the presence of a PtSn alloy which has formed during reduction pretreatment of the catalyst, led to increased oxygen chemisorption rates as the rate determining step for CO oxidation over Pt/SnO_2 was oxygen chemisorption because of the low sticking coefficient of oxygen [112]. Similarly, Takeguchi et *al.* [113] have studied CO adsorption over Pd/SnO_2

catalysts and have observed that the catalysts adsorbed little amount of CO when they are subjected to reduction pretreatment. The authors have interpreted the phenomena as the formation Pd-Sn alloy which hardly adsorbs CO due to the strong interaction between Pd and SnO_2.

(iv) *Localized temperature increase in the vicinity of metal centers:* Through Mössbauer investigations on Pd/SnO_2, Gadgil et *al.* [103] have observed increased amount of Sn^{2+} upon exposure to CO indicating that reduction of Sn^{4+} was facilitated in the presence of the noble metal. The authors have associated the effect with the energy release during the chemisorption of CO or O_2 which was postulated to lead to localized temperature increase in the vicinity of the metal centers resulting in enhanced oxygen abstraction from the solid matrix.

2.3.3 Interaction of SnO_2 Surfaces with Water Vapor and the Effect of Adsorbed Water and Hydroxy Species on the Activity of SnO_2-based Catalysts

Adsorption of water on tin dioxide surfaces results in the formation of physisorbed water molecules and hydroxy groups, which strongly interact with the surface. Two different types of hydroxy species have been reported [85]:

(i) Isolated hydroxy species, which are hydroxy groups bound to tin atoms. These species can be formed by the reaction of adsorbed water with preadsorbed O^- species [119] trough Reaction 2.1.

$$H_2O + O^- + 2Sn_{lat} \rightarrow 2(Sn-OH) + e^- \qquad (2.1)$$

(ii) Rooted hydroxy species, which are formed by protons attached to lattice oxygen species. These species can be formed by the interaction of adsorbed water molecules with lattice tin and oxygen species through Reaction 2.2 [100].

$$H_2O + Sn_{lat} + O_{lat} \rightleftharpoons (OH-Sn_{lat}) + (O_{lat}H)^+ + e^- \qquad (2.2)$$

These ad-species are strongly bound to the tin dioxide surface and pretreatment of catalysts at temperatures in the order of 100°C eliminates molecularly adsorbed water and reduces the concentration of hydroxy groups

[99, 104, 120] however, effective dehydroxylation of the surface requires annealing under HV at 600°C [98, 104, 120].

Although a number of reports on the inhibition of hydrocarbon combustion reactions by water ad-species on palladium catalysts exist [121-124], the presence of these surface hydroxyl groups and adsorbed water molecules have been observed to promote carbon monoxide oxidation over Pd/SnO_2 and Pt/SnO_2 catalysts [125,126] moreover, the presence of these ad-species have been observed to be necessary for stable and reproducible sensoric interactions as they mediate the sensing activity [98]. Regarding the role of water ad-species in carbon monoxide oxidation over pure SnO_2, Thornton and Harrison [127] proposed a mechanism where, CO molecules initially become associated with surface hydroxyl groups and react with adjacent surface oxide species forming CO_2 molecule adsorbed onto a lower-valent tin specie rather than interacting with coordinatively unsaturated tin atoms. For Pd/SnO_2 system, Croft and Fuller [125] have postulated that the hydroxylated sites formed through the adsorption of water molecules acted as chemical bridges to mediate the spillover of Pd-activated CO species.

Alternative reaction pathways involving the incorporation hydroxy species in CO oxidation have also been proposed in attempts to elucidate the role of adsorbed water species in promoting CO oxidation on SnO_2-based catalysts [85, 97, 100, 112, 126] and it has been postulated that the reaction pathway leading to the reaction with OH groups was favored at low temperatures [85].

On SnO_2-based surfaces chemisorbed CO can oxidize to CO_2 through either one of the following pathways:

i. Reaction with surface water to formic acid (HCOOH) through Reaction 2.3. Formic acid can dissociate to proton (H^+) and formate ($HCOO^-$).

$$H_2O + CO \rightleftharpoons HCOOH \rightleftharpoons H^+ + HCOO^- \qquad (2.3)$$

ii. Reaction with preadsorbed oxygen species to yield surface carboxylate species (Reaction 2.4),

$$CO + O^- \rightarrow CO_2^- \qquad (2.4)$$

iii. Reaction with hydroxyl species to yield formate through Reaction 2.5 [97, 100, 112]. Upon heating, formate can decompose to carbon dioxide and proton and, the decomposition of formate through Reaction 2.6 has been shown to influence the CO/CO_2 ratio [128]. Alternatively, formate can react with adsorbed oxygen through Reaction 2.7 to yield carbonate species [97, 112] which immediately decomposes to yield CO_2.

Chemisorbed carbon monoxide can also react with two adjacent hydroxyl groups to yield bicarbonate (Reaction 2.8). Unlike carbonate, the decomposition of bicarbonate proceeds at lower rates and thus, formation of bicarbonate slows down the CO oxidation reaction [112].

$$CO + M-OH \rightleftharpoons M-COOH \tag{2.5}$$

$$M-COOH \rightleftharpoons CO_2 + M-H \tag{2.6}$$

$$M-COOH + M-O \rightleftharpoons M-CO_3 + M-H \tag{2.7}$$

$$CO + 2(OH-M) \rightleftharpoons M-COOOH + M-H \tag{2.8}$$

2.4 Alkali-Metal Promoters of Red-Ox Reactions

Promotion is the action of one or more substances, that are introduced in trace quantities to a catalyst, to improve the activity, selectivity or useful lifetime of the catalyst by either augmenting a desired reaction or suppressing an undesired one [129]. Alkali metals are well known electropositive promoters of red-ox reactions which have found applications as promoting agents in a number of industrially important reactions such as, CO hydrogenation to yield methanol and C_{2+} alcohols [130-133], C_2 oxygenation to yield acetic acid and acetaldehyde [134], oxidative coupling of methane [135], NO reduction by methane [136], propene [137,138] and propane [138] and; oxidation of hydrocarbons [139, 140]. The lithium-enhanced interaction of CO with Pd/SiO_2 and Pd/CeO_2 surfaces have been reported to facilitate CO dissociation and insertion reactions to lead to high activity for methanol synthesis from synthesis gas [130,132]. Sodium has been reported to significantly enhance the performance of $Pd/\gamma\text{-}Al_2O_3$ and Pt/Al_2O_3 catalysts in NO reduction with C_3H_6 and C_3H_8 under simulated three-way catalysis conditions [137,138]. Similarly, potassium has been observed to promote selectivity of Rh-based catalysts in Fischer-Tropsch synthesis by suppressing alkane and promoting alkene and primary alcohol formation [141].

Alkali metals are Group 1A elements of the periodic table, which have the lowest ionization potentials among the members of their respective periods because of the loosely bound –s electron in their outermost shell and, upon the removal of this electron they assume stable noble gas electron configuration. Hence, alkali metals are highly reactive and react readily with water and halogens. When alkali metals are present at the surface of noble metal based catalysts, they act as electronic modifiers, which donate electrons and increase the basic strength of the surface by increasing the electron density on the transition metal [139]. In the XPS spectra, the increased electron density on the transition metal in the presence alkali has been observed as downward shift in the binding energies of Pd 3d electrons [142, 143]. In general, alkali-metal adsorption on transition metal surfaces cause a decrease in the work function of the metal and a decrease in the surface work function would result in a decrease in the heat of adsorption of electropositive (electron-donor) adsorbates coupled with an increase in the heat of adsorption of electronegative (electron-acceptor) adsorbates [129]. The presence of the alkali metal has been observed to lead to enhanced chemisorption of CO, NO and O_2, which are electron acceptor adsorbates, at the expense of the chemisorption of hydrocarbons and hydrogen, which are electron donor adsorbates [137,144-150]. Therefore, alkali modified adsorption of diatomic molecules over transition metal surfaces result in an alteration of the relative surface coverages, dissociation and sticking probabilities of these molecules [144,152].

According to the Blyholder model for CO adsorption on transition metal surfaces, the carbonyl-surface interaction takes place through backdonation of electrons from Pd-3d orbitals to the antibonding π-molecular orbitals of the carbonyl and alkali-metals act to promote the carbonyl-surface interaction by enhanced backdonation of electrons from the metal [152]. For CO adsorption over sodium modified noble metal surfaces, this alkali mediated electron enrichment of the metal phase has been postulated to promote the interaction of CO with the surface and lead to the weakening of C-O bond [153-155], which has been observed as a downward shift of C-O bond stretching frequency in the IR spectra of CO chemisorbed on Na modified Pd [155,156]. Simultaneously, the alkali ion may interact with the oxygen of the carbonyl ligand forming a Pd-CO-Na^+ bridge to decrease the C-O bond order [155,156] which could result in the cleavage of the C-O bond even on metals which normally chemisorb CO molecularly [129]. Similar observations have been reported for alkali-modified N-O bond weakening and decomposition on Pd-based catalysts [137].

The effect of alkali-metal modification on oxygen adsorption involves the stabilization of oxygen, possibly through interaction with alkali modified sites and, the promotion of the maximum surface coverage of oxygen. Oxygen adsorbs dissociatively on transition metal surfaces and similar to CO, the adsorption of oxygen is also accompanied by charge transfer from the metal surface thus, oxygen behaves as a strong electron acceptor [129]. Alkali modification of oxygen adsorption on transition metal surfaces have been reported to enhance the interaction of oxygen with the surface by an increase in the sticking coefficient of oxygen [149-151], which is manifested as a shift in O_2 desorption to higher temperatures and for which, the effect become stronger from Na to Cs [149]. Furthermore, Kiskinova et *al.* [150] have reported an increase in the maximum surface coverage of oxygen in the presence of Cs and postulated a mechanism where the oxygen atoms initially adsorbed on Cs and spilt-over to the transition metal. Similarly, Seiki et *al.* [140] reported an increase in the oxygen storage capacity of Co-NaY catalysts by alkali modification via an increase in the oxygen affinity of cobalt species and facilitating the formation of cobalt oxide.

Alkali-metal modification of hydrogen adsorption of on transition metals have been reported to decrease the sticking coefficient of hydrogen as well as the saturation coverage and, to increase the activation energy for desorption of hydrogen from the alkali-modified surface. Lanzillotto et *al.* [157] reported a reduction in the saturation coverage of hydrogen in the presence of potassium. Resch et *al.* [146] also observed a decrease in the hydrogen coverage on potassium modified nickel surfaces and postulated an increased activation barrier for hydrogen adsorption in the vicinity of potassium atoms. Solymosi and Kovács [147] studied the adsorption of hydrogen on potassium promoted Pd(100) surface and, reported a decrease in both the sticking coefficient and uptake of hydrogen coupled with a simultaneous shift in the hydrogen desorption to higher temperatures. The authors attributed the effects to inhibition of hydrogen adsorption by potassium through a site blocking effect where, potassium blocked 4-5 adsorption sites for hydrogen and also to, the stabilization of hydrogen by potassium trough the formation of alkali metal hydride-like surface complexes. The formation of alkali metal hydride-like surface complexes has also been postulated by several other authors in attempts to explain the stabilization of hydrogen in the presence of alkali metals [146,148,158].

The introduction of alkali metals to noble metal-based catalysts is also subject to the formation of ternary oxides of palladium and the alkali metal [159-162], which can alter the catalytic properties of the noble metal systems. The formation of such ternary oxides of noble metals and alkali-metals readily takes place even at 400°C under oxygen atmosphere [159]. Similarly, Mitra et *al.* [162] have reported the formation of a ternary oxide of sodium and rhenium ($NaReO_4$) in Re_2O_4/TiO_2 and Re_2O_4/Al_2O_3 catalysts calcined at 450°C and the $NaReO_4$ phase was observed to alter the reduction behavior of the catalysts, which was well correlated with the amount of alkali metal added till Na/Re ratio was increased to 1, where sufficient sodium was present in the structure to stabilize all rhenium in $NaReO_4$ form.

Studies on the effect of alkali-metal promotion on selective CO oxidation in H_2-rich streams are rather rare. Tanaka et *al.* [163] have applied potassium promotion to Rh/SiO_2 and Rh/USY catalysts by the addition of K_2CO_3 and; reported dramatic increases in the CO oxidation selectivity, where >99% removal of CO was achieved with 50% selectivity. Pedrero et *al.* [164] applied Na, Rb and Cs promotion to Pt/SiO_2 system and reported selectivity in the order of 90% at H_2/CO ratios of ~100. The authors attributed the increase in the turnover rates and selectivity over the alkali modified surfaces to the titration of hydroxyl groups to inhibit spillover-mediated H_2 oxidation pathways, which lead to selectivity losses. Similarly, Kwak et *al.* [165] have reported that sodium promotion enhanced the catalytic performance of $PtCo/Al_2O_3$ catalysts for preferential oxidation of carbon monoxide. The authors attributed the fact to the joint effect of the promotion of oxygen adsorption and retardation of CO desorption to vacate sites for hydrogen adsorption, in the presence of sodium.

CHAPTER 3

EXPERIMENTAL

Unmodified and alkali-metal (Li, Na or K) modified PdO/SnO_2 catalysts were synthesized by sol-gel methods. These catalysts were characterized by XRD and XPS and; the CO oxidation activity of these catalysts were investigated by dynamic methods. In addition to the CO oxidation activity, the interactions between the support and the promoters and, the mechanistic aspects of CO oxidation with SnO_2-based catalysts were examined to determine the effect of different alkali modifiers on the catalysts morphology and the relative merits of these alkali-metal modifiers in promoting the low-temperature CO oxidation activity of PdO/SnO_2-based catalysts.

3.1 Catalyst Preparation

PdO/SnO_2, Li-PdO/SnO_2, Na-PdO/SnO_2 and K-PdO/SnO_2 catalysts were synthesized by a sol-gel route described in detail earlier [166]. $SnCl_4.5H_2O$ (Acros Organics, 98+%), $Pd(CH_3CO)_2$ (Aldrich, 98%) and, in the case of alkali metal modified samples, the chloride salts of the respective alkali metals; LiCl (Merck, 99.95%), NaCl (Merck, 99.99%) and KCl (Merck, >99.0%) were used as the precursors of Sn, Pd and alkali metals, respectively. Moreover, unpromoted and alkaline promoted SnO_2 samples were synthesized for the investigation of the contribution of the support in the observed activities and also, for examining the effects that the alkaline promoters might have on the support rather than Pd phase through control experiments.

The first step in the sol-gel synthesis of SnO_2 is the preparation of a tin alkoxide solution. As $SnCl_4.5H_2O$ rather than commercial tin alkoxide solutions was used as the tin precursor, the catalyst synthesis was initiated by the *in-situ* preparation of the tin alkoxide solution, which was accomplished by dissolving $SnCl_4.5H_2O$ in isopropyl alcohol (Riedel-de Haën, extra pure). For this purpose, 12.37 grams of the tin precursor was dissolved in 15 grams of isopropyl alcohol, for the synthesis of each batch of catalyst sample. After the solid was completely dissolved in the alcohol, a mixture of 3.42 grams of water and 10 grams of

isopropanol was added to this solution to initiate hydrolysis reactions to replace the alkoxy groups of the metalorganic molecule with hydroxyl groups (Reaction 3.1).

$$M-O-R + H_2O \rightarrow M-OH + R-OH \tag{3.1}$$

At this stage of synthesis, the solution is named as the *sol*. Whenever appropriate, the palladium and/or alkali metal precursors are introduced to the sol at this stage to ensure uniform distribution of the catalyst and the promoter in the resulting powder.

Following the addition of the catalyst and the promoter, the sol was continuously stirred at 300 rpm and aged overnight at room temperature. While the sol is being aged water and alcohol condensation reactions (Reactions 3.2 and 3.3)take place to link the partially hydrolyzed molecules. Finally, polymerization reactions lead to the formation of Sn containing polymers, which reach to macroscopic dimensions and extend throughout the solution. From this stage on the solution is named as the *gel*. The gel was dried in a water bath at 100°C for 6 hours to remove volatile organics and water located within the 3D network of the polymers and results in the shrinkage of the network. The catalyst preparation procedure was completed by the calcination of the gel in a home-made calcination oven where, the temperature of the dried gel was increased to 600°C (5°C/min) and kept at 600°C in dry air (600 ml/min) for 6 hours. Calcination removes residual organics and leads to the formation of the desired crystal structure. After the calcination step, the resulting material was grinded to a fine powder in an agate mortar and stored in desiccator before use.

$$M-OH + HO-M \underset{\text{hydrolysis}}{\overset{\text{water condensation}}{\rightleftharpoons}} M-O-M + H_2O \tag{3.2}$$

$$M-O-R + HO-M \underset{\text{alcoholysis}}{\overset{\text{alcohol condensation}}{\rightleftharpoons}} M-O-M + R-OH \tag{3.3}$$

The composition of the catalysts tested within the framework of this study is presented in Table 3.1. The amounts of noble metal and alkali metal loadings and the Pd-to-alkali metal atomic ratio represent the values calculated from the amounts of precursors of the respective constituent introduced to the *sol*. The catalysts with different alkali metal promoter contents will be referred to with their respective alkali metal (A)-to-palladium ratios in the remainder of the text and unless otherwise stated, catalysts with A-to-Pd ratio of 0.53 (i.e. Li/0.53, Na/0.53 and K/0.53) are subject to dynamic characterization experiments.

Table 3.1 Palladium and alkali-metal loading of the catalysts tested

Catalyst	Pd Loading (wt. %)	Alkali-Metal (A) Loading (wt. %)	A:Pd Atomic Ratio
PdO/SnO_2	1	-	-
Li-PdO/SnO_2 (Li/0.53)	1	0.03	0.53
Li-PdO/SnO_2 (Li/1.77)	1	0.10	1.77
Na-PdO/SnO_2 (Na/0.32)	1	0.06	0.32
Na-PdO/SnO_2 (Na/0.53)	1	0.10	0.53
Na-PdO/SnO_2 (Na/1.50)	1	0.28	1.50
K-PdO/SnO_2 (K/0.32)	1	0.10	0.32
K-PdO/SnO_2 (K/0.53)	1	0.17	0.53
K-PdO/SnO_2 (K/1.50)	1	0.48	1.50
Li/SnO_2	-	0.10	-
Na/SnO_2	-	0.10	-
K/SnO_2	-	0.10	-
SnO_2	-	-	-

3.2 Experimental Set-up

The experimental set-up utilized for the dynamic studies consists of the following three units (Figure 3.1):

- *Gas feed unit:* The gas feed system is a home-made assembly which is used to prepare synthetic gas mixtures with the desired reactant concentrations. Three six port valves, which were designed to provide the micro-reactor with impulse or step inputs of the desired reactant(s) during the catalyst pretreatment and dynamic testing stages and four gas mass flow controllers, calibrated for the specific test gases are installed within the gas feed unit. In addition to providing step and impulse inputs to the reactor, the gas feed unit was designed to enable by-pass/isolation of the reactor unit, as well as vacuum connection to the unit.

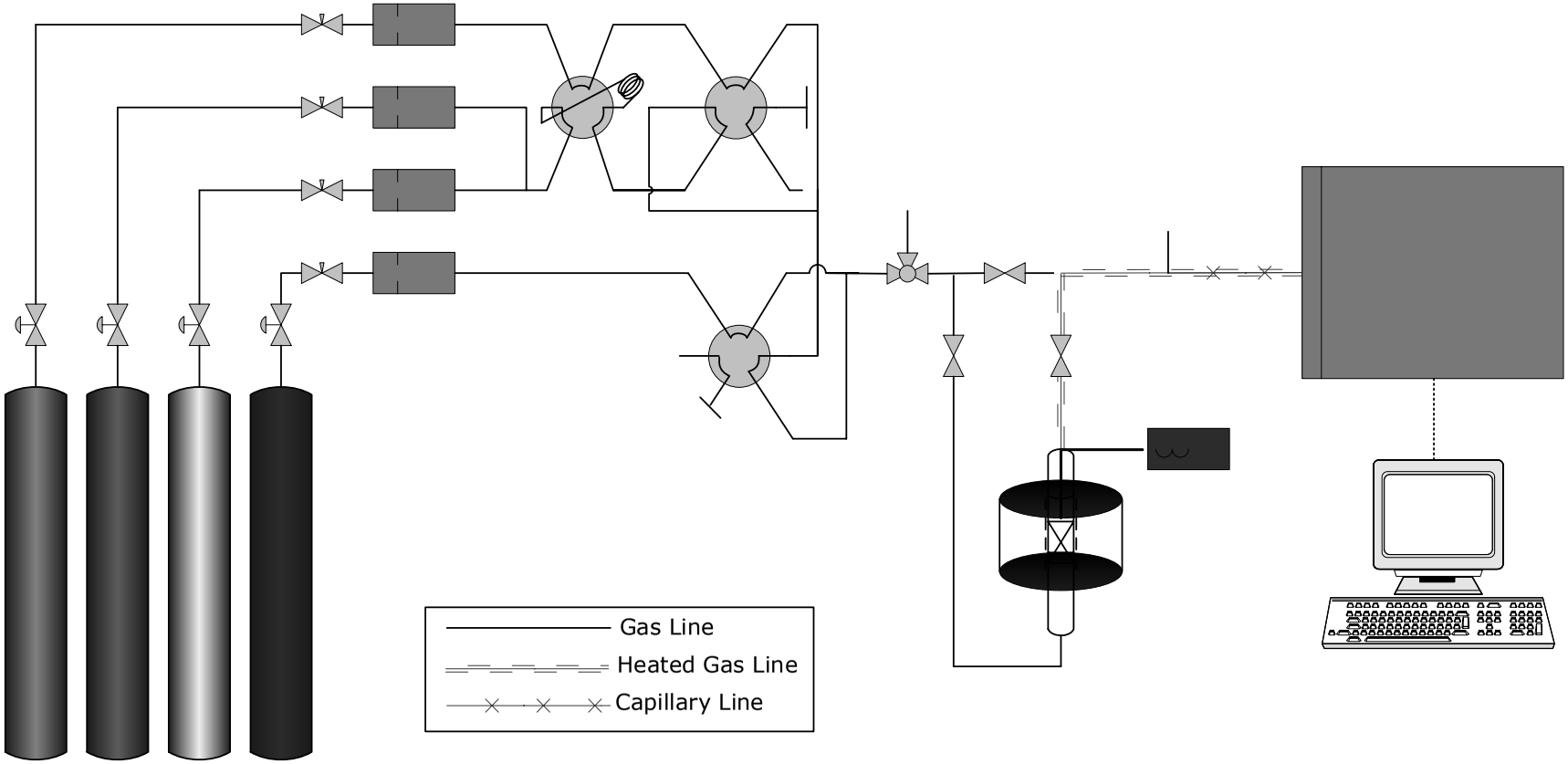

Figure 3.1 Experimental set-up

- *Reactor Unit:* The reactor unit comprises a micro-reactor and a fast-response furnace. The micro-reactor is made from quartz tubing with inner diameter (ID) of 4 mm. For each run, a pre-weighed amount of catalyst was packed inside the micro-reactor and secured in place with the aid of quartz wool plugs and; the reactor was connected to the gas line with Cajon® (Swagelok Company, USA) glass-to-steel fittings. The fast-response furnace (W.C. Heraeus Hanau, Mikro 1, 3/65) has the dimensions of ID 1.7 cm, OD 8.8 cm and height 6 cm and a power rating of 350 W. The temperature control of the reactor was accomplished by an auto-tune PID temperature controller with programmable ramp and soak feature (Love Controls, USA) and the reactor temperature readings were taken with the aid of a K-type sheathed thermocouple. The thermocouple was embedded inside the quartz wool plug securing the catalyst sample in position in the micro-reactor at the gas exit side. 1/8" 316 SS seamless tubing and fittings (Hoke Inc., USA) were used in the construction of all the gas lines and connections within the gas feed and reactor units and; reactor downstream to the gas analysis/data acquisition unit. The line from the exit of the micro-reactor to the gas analysis/data acquisition unit was equipped with a thermostated heating tape for preventing the contaminating species that might be present in the gas line during analysis from interfering with the collected mass spectra. The temperature of this gas line was controlled with another auto-tune PID temperature controller (Omron Corp., USA) and the temperature readings from the line were taken by the use of a K-type sheathed thermocouple embedded inside the heating tape. The temperature of the heated gas line was set to 110°C one hour ahead of the experiments and meanwhile, this gas line was purged with helium. The line was then thermostated at the same temperature during dynamic characterization tests for the collection of reproducible water vapor evolution profiles by hindering the condensation of water vapor before the reactor effluent was analyzed. The heated gas line had particular importance during analyzes where considerable amount of water vapor was present in the reactor effluent.

- *Gas Analysis/Data Acquisition Unit:* The gas analysis/data acquisition unit comprises an on-line quadruple mass spectrometer (HPR 20, Hiden Analytical Inc., UK) which is capable of scanning 2-200 amu range and is used to collect time-resolved concentration traces of the detected ions in the test gases or in the reactor effluents. The mass spectra were collected

during catalyst pretreatment and dynamic testing stages. For the dynamic tests involving a single reducing agent, i.e. carbon monoxide, the concentrations carbon monoxide, carbon dioxide, oxygen and water vapor were the traced components. For the tests where hydrogen was the reducing agent methane, methanol and formic acid species were also added to the traced components.

The evolution profiles of the traced species were corrected to account for the relative ionization gauge sensitivity factors and possible overlaps arising from the cracking of the traced ions, which would result in attenuated signals. The ions traced during the experiments together with sample calculations for correction of species concentrations due to the overlaps in mass signals arising from the cracking of the molecules are presented in Appendix A. Data acquisition was carried out with a desktop PC connected to the mass spectrometer.

3.3 Experimental Design and Parameters

There exist a number of studies in the literature on the red-ox behavior of tin dioxide-noble metal catalyst systems as the system exhibits strong metal support interaction (SMSI) and is an example of synergistic interaction between noble metal and semiconducting metal oxide leading to enhanced catalytic activity. Although these catalysts have been identified to exhibit high activity for low-temperature CO oxidation, alkali-metal promotion has not been applied to PdO/SnO_2 system previously. The motivation of the current study is to apply alkali metal promotion to PdO/SnO_2 system and develop a fundamental understanding of CO interaction with PdO/SnO_2 surface in the absence and presence of oxidizing/reducing species and of the effect and role of alkali metal promotion in this interaction. The work done within the framework of this study for the spectroscopic and dynamic characterization of unmodified and alkali-metal modified PdO/SnO_2 catalysts can be grouped under four phases, which are:

- *Application of alkali-metal promotion to PdO/SnO_2 and investigation of the effect of the addition of the alkali metal modifier on the CO activity of PdO/SnO_2:* The mechanism of CO oxidation over PdO/SnO_2 was investigated and alkali metal promotion was applied to PdO/SnO_2 system by using sodium as the representative alkali metal. The effect of sodium addition on the CO oxidation activity of PdO/SnO_2 was investigated under

transient conditions via temperature programmed reaction spectroscopy and in the long-run with steady-state reaction experiments. Instrumental analysis techniques namely, SEM and XPS and surface spectroscopic techniques namely, transient impulse technique and temperature programmed desorption were combined with previous characterization data [166] which comprises XRD and FTIR spectra to develop an understanding of sodium induced modifications in the catalyst structure and morphology leading to enhanced CO oxidation activity of sodium modified PdO/SnO_2.

- *Extension of alkali metal promotion of PdO/SnO_2 to cover lithium and potassium in addition to sodium:* As sodium modification of PdO/SnO_2 was observed to result in the promotion of the red-ox behavior and CO oxidation activity of PdO/SnO_2, the work on the alkali metal modification of PdO/SnO_2 catalysts was extended to cover two other alkali metals, namely lithium and potassium to observe the relative merits of different alkali metals in modifying the catalytic activity of PdO/SnO_2 and providing a broader view on the alkali metal promotion of PdO/SnO_2 catalysts. Lithium and potassium modified PdO/SnO_2 catalysts were synthesized by the same sol-gel route followed in the preparation of PdO/SnO_2 and Na-PdO/SnO_2 and, these catalysts were investigated with XRD and XPS in order to determine the alkali induced changes in the catalyst chemical structure and morphology. The effect of lithium and potassium on the CO oxidation activity of PdO/SnO_2 was investigated under transient conditions by temperature programmed reaction spectroscopy and the results were compared with the data on the CO activity of PdO/SnO_2 and Na-PdO/SnO_2. The influence of different alkali modifiers (Li, Na and K) on the reduction characteristics of PdO/SnO_2 and on the interaction of oxygen and carbon monoxide with the catalyst surface were investigated by temperature programmed reduction technique.

- *Investigation of the CO oxidation activity of the catalysts in the presence of another reducing agent, namely hydrogen:* In addition to the activity of the catalysts for CO oxidation reaction, their selectivity is another key issue for CO oxidation catalysis as CO co-exists with other reducing agents for most of the practical applications such as, hydrogen purification for the fuel cell and automobile exhaust catalysis. For this reason, the effect of the presence of another reducing agent, namely

hydrogen, on the CO oxidation activity of alkali-metal modified PdO/SnO_2 catalysts was investigated under transient and steady-state conditions. The interaction of surface oxygen with hydrogen and carbon monoxide when these two agents coexist in the reactor feedstream was investigated by TPR. Moreover, TPRS technique was utilized to investigate the selectivity of chemisorbed oxygen species between H_2 and CO oxidation reactions and the dependence of CO selectivity of surface oxygen on the surface coverage of these molecules.

- *Investigation of the effect of alkali metal modifier concentration on the reduction behavior and CO activity of the catalysts:* All the three of the alkaline modifiers introduced to PdO/SnO_2 catalysts have been observed to influence the morphology and catalytic behavior of the catalysts differently and, the catalysts modified by these alkali metals have been observed to present promising outcomes for different applications. The optimization of the catalytic activities of the alkali metal promoted catalysts is possible by alteration of the alkali content of the catalysts, such that at one concentration the alkali may behave as a catalyst poison while at another concentration it can behave as a promoter. Therefore, the alkali modifier concentration of the catalysts was considered as another parameter and its effect on the CO oxidation activity of the catalysts was investigated. PdO/SnO_2 catalysts modified with different amounts of sodium and potassium were investigated with TPR and TPRS techniques to observe the dependence of the reduction behavior of the catalysts on the amount of alkali metal introduced in the structure and to optimize the alkali metal concentration for CO oxidation with PdO/SnO_2 catalysts.

In addition to the abovementioned parameters, the effect of catalyst pretreatment on the CO activity and red-ox behavior of unmodified and alkali metal modified PdO/SnO_2 was investigated by subjecting the catalysts to *in-situ* pretreatment procedures prior to the dynamic characterization tests. Two types of pretreatment procedures; one of which was oxidizing and the other reducing in nature were adopted. The oxidation pretreatment procedure was adopted to saturate the catalyst surfaces with adsorbed oxygen species and comprises the following stages: a ten-minute helium flush (50 ml/min) at room temperature for the removal of air confined within the reactor, followed by heating to 150°C (50°C/min) under 1.3% O_2/He flow (50 ml/min). The samples were kept at

150°C under 1.3% O_2/He atmosphere for 30 minutes for the removal of ad-species, which might have formed by exposure to ambient air and, to provide saturation of the catalyst surface with oxygen species. The catalysts were then cooled to room temperature under the same atmosphere and kept at room temperature for another 30 minutes. At the end of this period, the temperature of the reactor was set according to the experiment to follow the pretreatment. Samples subjected to this type of pretreatment procedure are referred to as oxidized samples in the remainder of the text.

The reduction pretreatment procedure was adopted to partially eliminate surface oxygen species and it comprises a ten-minute helium flush (50 ml/min) at room temperature followed by heating to 150°C under the same atmosphere. After the reactor temperature has reached to 150°C hydrogen, which amounts 5% of the total flow was added to the reactor feed (helium) and the samples were kept at these conditions for 30 minutes. At the end of 30 minutes, hydrogen flow was switched off and the catalyst was kept at 150°C under helium atmosphere for another 30 minutes for the removal of physisorbed species. The reduction pretreatment was completed by adjusting the reactor temperature to the temperature set point of the following experiment. Catalysts subjected to abovementioned reduction pretreatment procedure are referred to as reduced samples in the remaining sections of the text. It is important to note that, at the adopted conditions reduction pretreatment cannot be expected to lead to complete reduction of all reducible species but rather, a partial reduction of the surface oxygen species should be considered.

The reagents used in catalyst pretreatment and dynamic testing were O_2 (5% in He, Airproducts), CO (1% in He, Airproducts), and H_2 (99.999% purity, Airproducts). These gases were either diluted with He (99.9999% purity, Airproducts) to specified concentration or used directly.

3.4 Catalyst Characterization with Instrumental Analysis Techniques

Lithium, sodium or potassium modified PdO/SnO_2 catalysts, as well as unmodified PdO/SnO_2 and bare SnO_2 were subject to characterization using BET, PDS and XRD analyzes and, XPS for the assessment of the effect of these alkali metal modifiers on the surface morphology, crystal and chemical structure of the catalysts.

The X-ray diffraction patterns of the catalysts between 20° – 80° Bragg angle values were collected in Philips, PW 1840 model powder diffractometer equipped with Cu target and Ni filter ($\lambda_{CuK\alpha}$=0.154 nm). The BET surface areas and the pore size distributions (PSD) of the catalysts were measured in IGA-003 model TGA/MS system (Hiden Isochema Ltd., UK) using N_2 sorption technique. The SEM images were collected in JSM-6400 model scanning electron microscope (Jeol Ltd., Japan) equipped with X-ray micro analyzer system (Noran Series II). Prior to the collection of the SEM images the samples were loosely cast into pellets. Tin dioxide-based catalysts synthesized by the sol-gel method presented above are conductive materials used in gas sensor devices and attempts to utilize *in-situ* DRIFTS techniques to identify surface species especially above ambient temperatures did not yield any IR spectrum because of the high opacity of the samples in the IR range.

The valence states of tin and palladium; and the alkali metals were investigated in UNI-SPECS ESCA system (Specs GMBH., Germany) with monochromator, using Mg K_α (λ =1253.6 eV) radiation as the X-ray source. In the case of the alkali metal promoted samples, the resolution of the bands related to the binding states of electrons of the alkali metal has been a formidable task due to the presence of the alkali metals in trace amounts in the structure however, XPS data regarding the binding states of the alkali metals have also been obtained when possible. In addition to the oxidized samples, some reduced samples were investigated with XPS to determine the effect of the different types of catalyst pretreatment procedures on the valence states of the support and the noble metal. In order to provide information on the variation of the concentration of palladium atoms with information depth of the XPS analysis, all of the samples were analyzed before and after sputter etching the catalysts with 5 kV Ar-ion beam for 5 minutes to increase the information depth. The XPS spectra were referenced to the binding energy of Au $4f_{7/2}$ which is located at 84.0 eV. A computer package program (XPSPeak4.1) was utilized to analyze the XPS data by background subtraction (Shirley method) and curve fitting for the studied envelopes.

3.5 Catalysts Characterization with *In-situ* Dynamic Techniques

Dynamic techniques namely; transient impulse technique, where a fixed amount of an inert or reactive tracer is injected to the carrier gas and the evolution of this tracer from the reactor is monitored; temperature programmed techniques

where, the adsorption/reaction/desorption of probe molecule(s) is monitored while the temperature of the catalyst is increased linearly and step response technique where, the activation/deactivation of the catalyst surfaces with time-on-stream at a specific temperature is monitored were utilized for the *in-situ* dynamic characterization of the PdO/SnO_2-based catalysts. These techniques are discussed in detail below.

Transient Impulse Technique: The transient pulse technique comprises the injection of a predetermined amount of tracer to the carrier gas at specified time intervals. The tracer can be inert or reactive. The change in the concentration of the tracer in the reactor effluent with time, allows the deduction of data related to the catalyst dispersion; reaction, adsorption and desorption kinetics of the tracer; the oxygen content of the surface, the accessibility of the reactive sites by the reactant and also, the rate of oxygen diffusion from subsurface layers.

Within the course of the impulse experiments a reactive tracer, i.e. carbon monoxide, was utilized and 1ml doses of 1% CO/He mixture (0.42 μmol of CO per injection) was injected consecutively to the reactor feed stream (He: 37 ml/min) through a 1ml gas sampling loop attached to a six-port impulse valve (Figure 3.1), until a steady response of the catalysts towards the recurring injections was observed. Duration between each successive injection was adjusted as two minutes. However, intermittently delayed doses of CO were also provided to the system to observe the mobility of oxygen species from the bulk to the catalyst surface. For this purpose, intermittently delayed doses of CO were injected to the system at 4th, 10th and 25th minutes following the last periodic dose of each run. The impulse experiments were carried out at 20°C and 150°C with both oxidized and reduced samples of unpromoted and sodium promoted PdO/SnO_2 and, control experiments were also performed over the bare support for being able to determine the extent of support contribution. It is most important to note that no oxygen was supplied to the reactor along with the reducing agent during the CO impulses which implies that, CO oxidation proceeded solely by the consumption of the available oxygen species over the catalyst surfaces and in the bulk of the catalysts thus, these experiments provide an indication of the availability/reactivity of oxygen ad-species over the catalysts as well as, the mobility of oxygen species in the bulk.

For the quantitative analysis of the data, the areas lying under CO and CO_2 peaks were calculated with the use of relative ionization gauge sensitivity factors which are given in Appendix A and, with the use of a Fortran 90 program which

computes areas under mass signal traces by 2nd order Lagrange polynomial on non-uniform grid for numerical integration (see Appendix B for the Fortran 90 code). The calculated areas were normalized with respect to the peak areas of reference CO injections which were, recorded while by-passing the reactor.

Temperature Programmed Techniques: Temperature programmed techniques are widely used surface science techniques that utilize temperature programming to study surface processes, i.e. adsorption/desorption and surface reaction, with different activation parameters. The basic experiment for temperature programmed characterization of the catalysts involve the introduction of probe molecule(s) to the reactor, usually at low temperatures that can go down to sub-ambient temperatures and, controlled heating of the reactor at a constant rate whilst analyzing the residual gas for the evolution of the probe molecule or reaction products. Several variations to this technique exist:

1. Temperature programmed desorption (TPD): When the adsorption/ desorption of a probe molecule, which reversibly adsorbs on the surface is studied with temperature programming, then the technique is called TPD. TPD can provide information on the different modes (or sites) of adsorption of a probe molecule together with the adsorption strength of each of these modes.

2. Temperature programmed reaction (TPRS): TPRS is a modification of TPD where, the adsorption of the probe molecule is irreversible and results in surface reactions upon temperature programming. TPRS experiment can provide information on the reactivity of the active sites of the catalyst.

3. Temperature programmed reduction (TPR): While oxidizing or reducing agents can be used as the probe molecule during TPD and TPRS, TPR is another modification of temperature programmed techniques which utilizes a reducing agent, usually H_2, as the probe molecule. TPR is used to study the abundance and reactivity of the reducible species over the catalyst surfaces. The probe molecule for TPR studies is generally hydrogen however, CO may also be used as the probe molecule especially if the activity of catalysts with regard to CO oxidation is under consideration.

The abovementioned temperature programmed techniques were utilized to study the interaction of CO, H_2 and; mixtures of CO-O_2, CO-H_2 and CO-O_2-H_2 with PdO/SnO_2 based surfaces, which lead to adsorption, reaction and desorption of the probe molecules and provide information on the number of the types and nature of the active sites together with the temperature dependence of the activity of these sites. The experimental details and procedures adopted during the temperature programmed experiments are presented below.

3.5.1 Temperature Programmed Desorption (TPD) Studies

TPD technique was utilized to investigate the types of active sites for CO adsorption and oxidation; and the surface reaction pathways leading to the CO oxidation activity of sodium promoted and unpromoted PdO/SnO_2. As CO and O_2 are known to adsorb competitively over noble metal based surfaces, the effect of the competition between CO and O_2 on the CO oxidation behavior of the catalysts was also investigated along with CO adsorption and oxidation at the catalyst surfaces.

TPD experiments comprised room temperature adsorption of CO, where the reactor feed contained 160 ppm CO in helium (40 ml/min). This isothermal CO adsorption stage lasted for 20 minutes and was followed by a temperature programmed stage with an ultimate set point of 530°C, which was reached at a ramp rate of 12°C/min and during which the reactor feed constituted 200 ppm O_2 in helium (40 ml/min). Post CO adsorption He TPD studies in the same temperature region have been carried out previously [166] however, these studies did not yield any desorption profiles of either CO or CO_2 and it has been concluded from these experiments that CO irreversibly bonded to the surface. As a result, an atmosphere which is slightly oxidizing in nature was utilized during the temperature programmed desorption stage.

For the investigation of the competition between CO and O_2, the experimental procedure for the TPD experiments was altered to co-adsorb CO and O_2 during the isothermal stage preceding the temperature programmed stage and another set of TPD experiments were conducted by the addition of 160 ppm O_2 to the reactor feed, which contained only 160 ppm CO in helium. For the comparability of the results with the CO adsorption-O_2 TPD the O_2-TPD stage was left unaltered and carried out with a gas phase oxygen concentration of 200 ppm O_2 in helium.

The amount of CO_2 evolution from the catalysts surfaces during the O_2-TPD experiments were calculated through the numerical integration of the areas lying under the CO_2 mass signal traces with the aid of a Fortran 90 program, which utilizes 2nd order Lagrange polynomial on non-uniform grid for numerical integration (see Appendix C for the Fortran 90 code).

With the motive of observing the CO oxidation activities of the catalysts at sub-ambient temperatures similar TPD experiments were carried out after shifting the CO and O_2 co-adsorption temperature to -68°C. The co-adsorption temperature of -68°C corresponds to 4°C higher than the dew point of CO_2 under atmospheric pressure. The experimental procedure for the sub-ambient CO and O_2 co-adsorption studies constituted an isothermal CO and O_2 co-adsorption stage during which the reactor feed was 160 ppm CO and 160 ppm O_2 in helium (40 ml/min) and, a succeeding temperature programmed stage to reach 550°C at a rate of 12°C/min, during which 200 ppm O_2 in helium was fed to the reactor.

3.5.2 Temperature Programmed Reaction Spectroscopy(TPRS) Studies

CO-O_2 TPRS: The activity of the catalysts with regard to CO oxidation was studied with temperature-programmed reaction spectroscopy (TPRS). The total feed flow rate was 40 ml/min and the oxygen concentration at the feed was varied to meet three different feed compositions. In one set of experiments the feed constituted 2400 ppm CO and 2400 ppm O_2 in helium which corresponded to a stoichiometric ratio {S = [CO]/[O]} of 0.5 and in the other set of experiments oxygen-lean feed {S = [CO]/[O]=0.91} and {S = [CO]/[O]=1.25} was supplied to the reactor in order to observe the effect of gas phase oxygen concentration on the catalyst activity. The amount of catalyst used for each run was 100 mg and the temperature of the reactor was raised from 20ºC to 250ºC at a ramp rate of 2ºC/min. The rates CO oxidation reaction and conversion were determined at 150ºC and reported after normalizing with respect to the active surface area of the catalysts (See Appendix D for sample calculations on rates of CO oxidation reaction). The light-off temperatures were obtained where 50% conversion of CO was achieved.

CO-H_2-O_2 TPRS: The CO oxidation activity and selectivity of unpromoted and alkali-metal promoted catalysts in the presence of H_2 were also tested with temperature-programmed reaction spectroscopy. The reaction mixture for the TPRS experiments contained 9000 ppm H_2, 2000 ppm CO and varying oxygen

concentrations. The oxygen concentration was adjusted to yield [CO]/[O] ratios of 1, 0.5, 0.25 and 0.17. The total flow rate was 45 ml/min over 100 mg of sample. The procedure for the TPRS experiments consisted of a 15-minute isothermal adsorption stage, which is carried out at room temperature, followed by a temperature programmed stage, where the temperature of the catalyst was raised at a ramp rate of 2°C/min to an ultimate set point of 500°C, where catalysts were then kept another 15 minutes.

3.5.3 Temperature Programmed Reduction (TPR) Studies

CO-TPR: The effect of palladium and alkali metals on the interaction of oxygen and hydroxy species with the catalyst surfaces leading to different activities of the catalysts towards CO oxidation reaction was investigated by utilizing temperature programmed reduction (TPR) technique. The reducing agent was 2000 ppm CO in helium (40 ml/min). The TPR experiment comprised an isothermal reduction stage which lasted for 10 minutes and which was followed by a temperature programmed stage. After the catalyst was subjected to either one of the abovementioned pretreatment procedures, the reducing agent was admitted to the reactor at 20°C for the onset of the isothermal reduction stage and succeeding the isothermal stage, the temperature of the reactor was increased at rate of 2°C/min to an ultimate set point of 530°C.

Oxidized and reduced samples of Li-PdO/SnO_2, Na-PdO/SnO_2 and K-PdO/SnO_2 were the catalysts tested within the framework of the TPR experiments, but in addition to those, control experiments were carried out with oxidized and reduced samples of the bare support and PdO/SnO_2, in order to observe both the effect of palladium addition on the reduction behavior of SnO_2 and the effect of alkali metal addition on the reduction behavior of PdO/SnO_2. Moreover, for being able to isolate the variations on the reduction behaviors of the alkali metal promoted catalysts that may arise from the ternary interaction between tin-palladium and the alkali metals from the binary interactions of these metals, control TPR experiments were also carried out with oxidized and reduced samples of palladium free Li/SnO_2, Na/SnO_2 and K/SnO_2. The mass signals of the traced species were corrected with the use of relative ionization gauge sensitivity factors and possible contributions to the traced mass signals from the fragments of the cracked parent species (see Appendix A).

H_2-TPR: The interaction of H_2 with the catalysts and reduction behavior of the catalysts were investigated by temperature programmed reduction spectroscopy

by utilizing H_2 as the sole reducing agent. The total flow rate was 45 ml/min and 100 mg of catalyst sample was packed between quartz wool plugs for each run. The temperature programmed reduction experiments spanned 20°C – 500°C region and the temperature of the sample was raised at 2°C/min. The reducing agent (9000 ppm H_2 in He) was admitted to the reactor at room temperature after the catalyst sample was subjected to *in-situ* oxidation pretreatment. After the admittance of H_2/He mixture to the micro-reactor at room temperature, the reactor was kept at room temperature for 15 minutes before the onset of the temperature program and similarly, another isothermal stage was present at the end of the temperature programmed stage, where the reactor temperature was held constant at 500°C for 15 minutes.

H_2-CO TPR: CO is known to have an adverse effect on the catalytic oxidation of H_2 with noble metal catalysts as, CO strongly interacts with the noble metals and produces a blanketing effect for H_2 adsorption. For the investigation of this effect temperature programmed reduction (TPR) experiments were conducted by the addition of 2000 ppm CO to the reaction mixture, which constituted 9000 ppm H_2 in helium. The total flow rate, the amount of catalyst and the temperature program was left unchanged for the comparability of the collected mass spectra.

3.5.4 Steady-State CO Oxidation Activities of PdO/SnO_2-based Catalysts

Time-on-stream CO oxidation activity of PdO/SnO_2-based catalysts in CO-O_2 mixtures: In addition to the transient conditions of the TPRS experiments, the CO oxidation activities of the catalysts at steady-state conditions were investigated. Oxidized samples of PdO/SnO_2 and Na-PdO/SnO_2 were tested with regard to their CO oxidation activities at 30°C, 50°C, 100°C, 150°C, 200°C and 250°C under two [CO]/[O] feed ratios (*S*) of 0.9 and 1.1 to represent oxygen lean and oxygen rich reaction conditions. Control experiments to determine the activity of the bare support under the same reaction conditions were conducted with oxidized SnO_2 samples.

For each run, 150 mg of catalyst sample was packed inside the reactor and the overall flow rate was adjusted to 50 ml/min, which resulted in a space velocity of 10,780 hr^{-1}. The CO conversion and reaction rates were calculated after correcting the data with the respective relative ionization gauge sensitivity factors of each of the traced species and these kinetic data represent the activity of the catalysts after 45 minutes-on-stream. Following the acquisition of the data to represent the activity after 45 minutes-on-stream at one of the temperature

set points, the reactor temperature was raised to match the temperature set point at the next data point and meanwhile, the reactor was purged with helium (40 ml/min). After the temperature set point was reached helium was replaced with the test gas.

Time-on-stream CO oxidation activity of PdO/SnO_2-based catalysts in CO-H_2-O_2 mixtures: Time-on-stream activity tests were carried out for the investigation of the applicability of PdO/SnO_2 based catalysts for the elimination of the CO content of the reformer gas for fuel cell applications the CO oxidation activity and selectivity of the catalysts were also investigated under hydrogen rich reactor feed conditions that resemble the fuel cell applications. For each run 100 mg of catalyst was packed inside the reactor between quartz wool plugs and the total flow rate was adjusted as 45ml/min. The reactor feed constituted 70% H_2, 2000 ppm CO, 2000 ppm O_2 and balance He. The steady-state CO oxidation activities of the catalysts were determined after 20 minutes on stream at 50°C, 80°C, 110°C and 140°C. After the collection of the necessary data for assessing the activity of the catalysts at one temperature point, the reactor was purged with helium (40 ml/min) while the temperature of the reactor was raised to match the temperature set point at the next data point.

CHAPTER 4

RESULTS AND DISCUSSION

4.1 Characterization of PdO/SnO_2 and Na-PdO/SnO_2

SnO_2, 1 wt. % PdO/SnO_2 and 0.1 wt. % Na–1 wt. % PdO/SnO_2 (Na/0.53) catalysts were prepared by the sol-gel route described in Section 3.1 and, characterized with XPS, SEM and dynamic techniques involving temperature programmed characterization. The surface areas of SnO_2, PdO/SnO_2 and Na-PdO/SnO_2 catalysts have previously been determined as 32, 52 and 54 m^2/g, respectively and the major crystal phase of the catalyst powders have been reported as mineral tin dioxide (cassiterite) [166].

Scherrer's method was utilized to determine the crystallite size using the previous XRD data. The crystallite size for bare SnO_2, PdO/SnO_2 and Na-PdO/SnO_2 was calculated as 15nm, 14.6 nm and 11.2 nm, respectively (see Appendix D for sample calculations on crystallite size). The pore size and the pore structure of these catalysts were investigated with gas sorption technique and the catalysts were observed to be made up of nonporous particles (see Appendix E for N_2 adsorption/desorption isotherms).

4.1.1 XPS Analysis

The chemical structure of PdO/SnO_2 and Na-PdO/SnO_2 surfaces was investigated by XPS to determine the effect of alkali-metal promotion and the *in-situ* pretreatment procedures on the chemical state of Pd. The Sn 3d doublet is observed as symmetric peaks with a full-width-at-half-maximum (FWHM) of 1.8 eV, $3d_{5/2}$ – $3d_{3/2}$ doublet splitting of 8.4 eV, $3d_{5/2}$ located at 487.4 eV and 487.8 eV in oxidized PdO/SnO_2 and Na-PdO/SnO_2, respectively (Figure 4.1b and 4.1c). To determine the effect of palladium on the binding state of tin, the spectra of bare support was also collected and the Sn $3d_{5/2}$ band was observed at 487.1 eV (Figure 4.1a). The shift of the Sn $3d_{5/2}$ band to higher binding energy levels in the presence of the noble metal and the alkali-metal promoter could be explained by the presence of more ionosorbed oxygen species on tin oxide

surface that are likely to be formed through the spillover of oxygen ad-species from the noble metal centers to the oxide support surface, creating an oxygen rich surface layer on Na-PdO/SnO_2 and PdO/SnO_2 samples. The analysis of Sn $3d_{5/2}$ band suggested that the band was made up of a single component that could be assigned to stoichiometric SnO_2 [114, 167] and no other peaks evidencing the presence of oxygen deficient states was observed.

4.1.1.1 XPS Analysis of Pd 3d Envelope of Oxidized and Reduced PdO/SnO_2

The analysis of the Pd 3d doublet in oxidized PdO/SnO_2 sample suggested the presence of three different states of Pd, with Pd $3d_{5/2}$ bands located at 336.6 eV, 337.7 eV and 339.1 eV (Figure 4.2a). Through a comparison of the binding energy values with the available literature, the first state was assigned to Pd^{2+} (PdO) [168-170] and the second state was assigned to Pd^{4+} (PdO_2) [168, 171]. PdO_2 is an unstable oxide of Pd which is known to exist in hydrous form [172] and decomposes to PdO above 200ºC [169, 171]. This tetravalent oxide has previously been observed in supported palladium catalysts [90,169]. It has been suggested that the lifetime of the PdO_2 species strongly depended on the environment of Pd^{4+} and that PdO_2 should be stabilized through the interaction with the supporting material even in the high vacuum environment of ESCA equipment [169]. For PdO/SnO_2 system the stabilization of PdO_2 species has been suggested to occur with exposure to ambient air though interaction of H_2O [170] and Pd^{4+}/Pd^{2+} ratio was observed to reach a maximum value upon thermal treatment at 600ºC [90,167], which is the calcination temperature of the catalysts tested in this study. The third state has been assigned to a higher surface oxide. The presence of a similar higher oxide has previously been reported on electrochemically prepared PdO films and this state has been assigned to PdO_3 [173,174]. The Pd 3d band of oxidized PdO/SnO_2 sample was also investigated after Ar-ion etching which decreased the Pd^{4+}/Pd^{2+} ratio and simultaneously resulted in the disappearance of the third oxide. Although Ar-ion etching process provides information about the subsurface layers, it might also lead to the reduction of the Pd species over the surface and this interference was cleared out with further analysis of the samples by subjecting the catalysts to reduction pretreatment prior to the analysis.

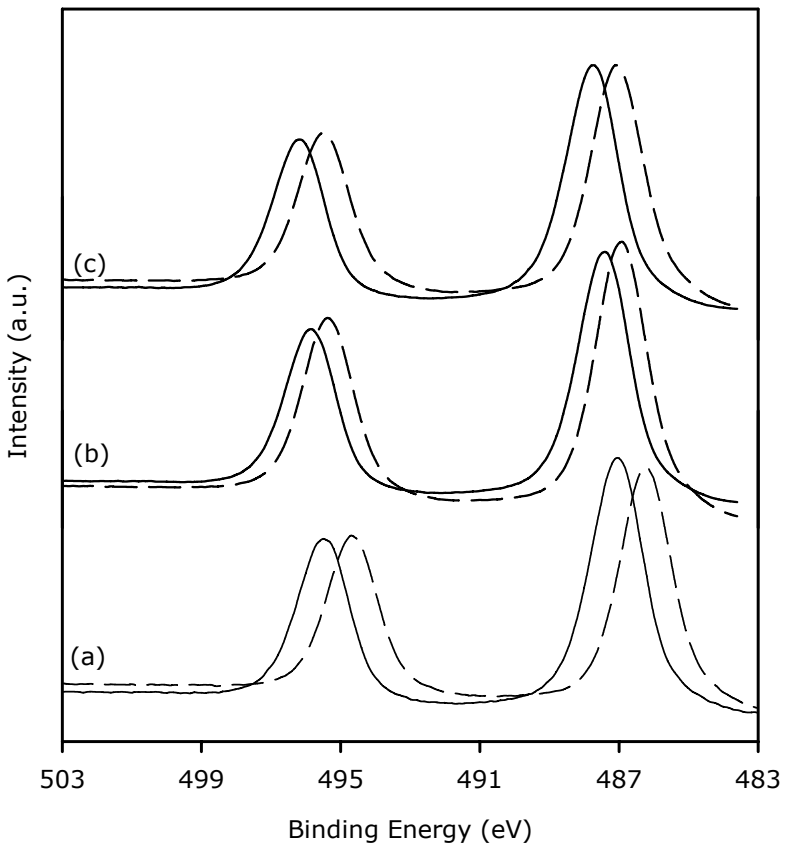

Figure 4.1 Sn 3d XP spectra of (a) oxidized SnO_2, (b) oxidized PdO/SnO_2 and (c) oxidized Na-PdO/SnO_2 before (solid line) and after (dashed line) Ar-ion etching

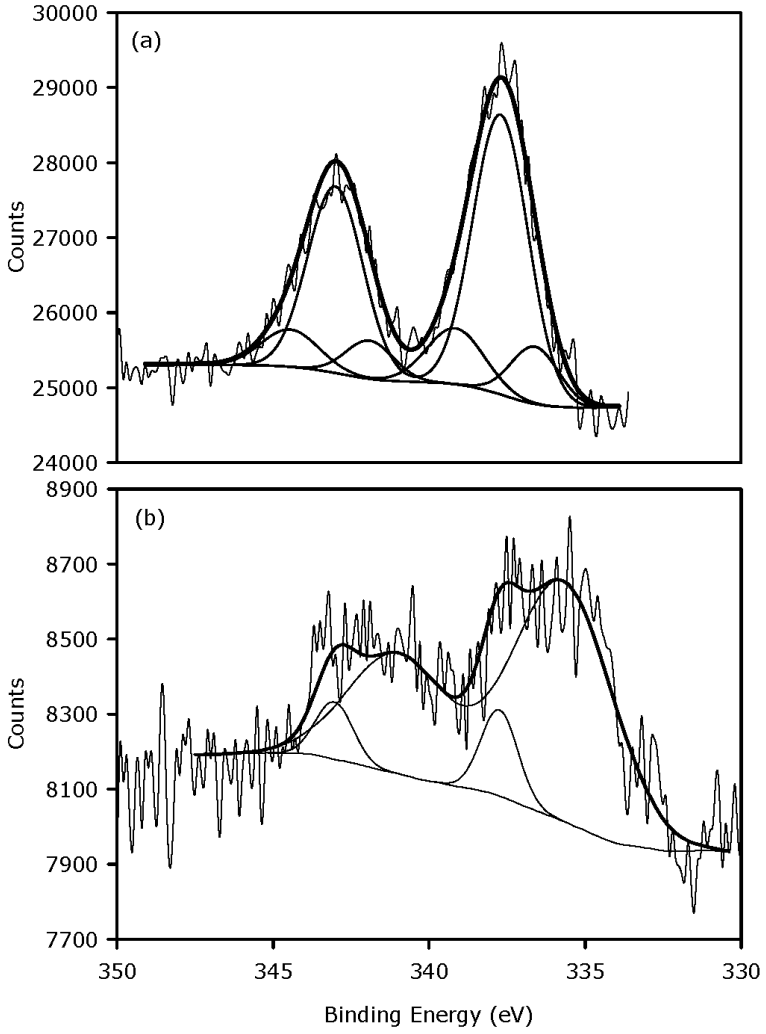

Figure 4.2 Pd 3d XP spectra of (a) oxidized PdO/SnO_2 and (b) reduced PdO/SnO_2

For observing the effect of reduction pretreatment on the chemical state of palladium, catalyst sample that has been subjected to the same reduction pretreatment procedure as the samples in activity tests was investigated by XPS. The analysis of the reduced catalyst confirmed that the reduction pretreatment reduced the palladium oxide rich systems to metallic palladium rich systems. The Pd 3d doublet in reduced PdO/SnO_2 sample was composed of three components located at 335.7 eV, 336.6 eV and 337.7 eV which have been assigned to Pd^0, Pd^{2+} and Pd^{4+} species (Figure 4.2b).

4.1.1.2 XPS Analysis of Pd 3d Envelope of Oxidized and Reduced Na-PdO/SnO_2

The X-ray photoelectron spectra of Pd 3d doublet in Na-PdO/SnO_2 sample was composed of broader peaks showing a tail at the high binding energy side and the envelope has shifted to higher binding energies relative to the Pd 3d envelope of PdO/SnO_2, indicating the presence of higher oxide rich surface layers (Figure 4.3a). The computer peak-fitting of the envelope suggested the presence of three states of palladium. The first two of these states, which are located at 337.7 eV and 339.1 eV, have been assigned to PdO_2 and PdO_3 through the analysis of Pd 3d doublet of PdO/SnO_2. The third state is unique to the sodium-promoted PdO/SnO_2 sample and located at 340.6 eV. It is most meaningful to associate this band located at 340.6 eV with super-oxide species formed in the presence of alkali-metal-promotion. Alkali-metals have previously been reported to facilitate the formation of higher oxides in some metal oxide systems and meanwhile, promote oxygen storage capacity these systems by increasing the electron density thus the oxygen affinity of the metal [140]. Therefore, the XPS results provide further support for the promotion of the interaction of oxygen with the catalyst surface by the presence of the alkali metal and the super-oxide specie that has been observed in the XPS spectra of the sodium modified sample may be postulated to result from such an interaction.

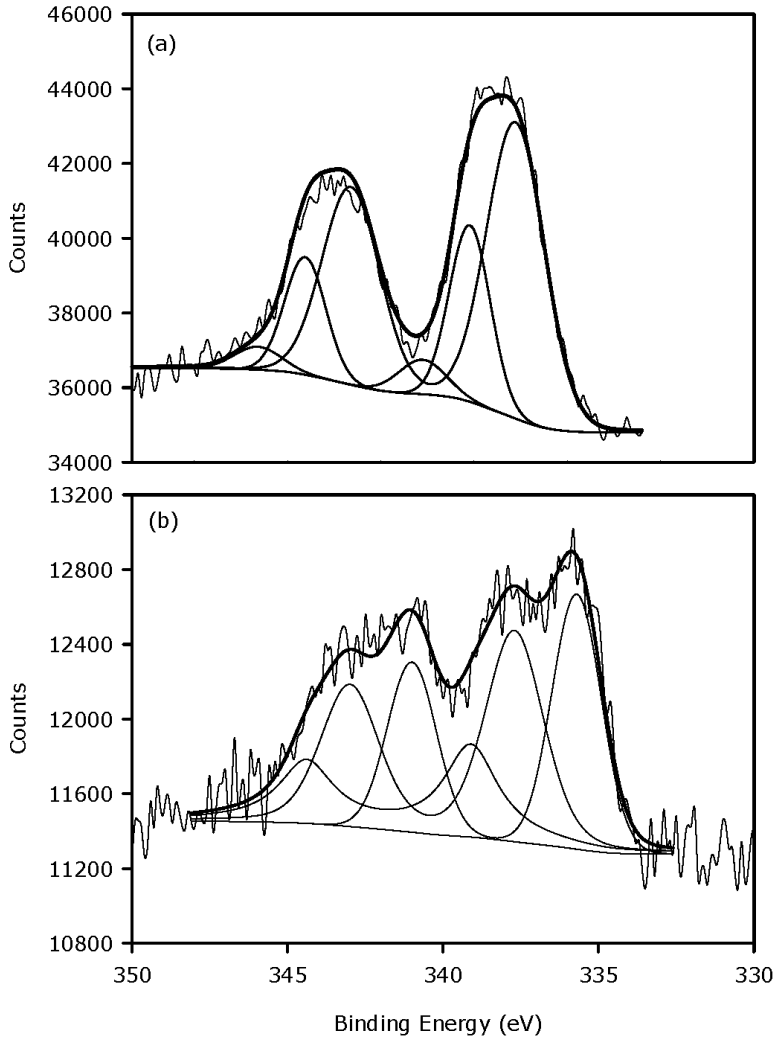

Figure 4.3 Pd 3d XP spectra of (a) oxidized Na-PdO/SnO_2 and (b) reduced Na-PdO/SnO_2

As it was the case in PdO/SnO_2, Ar-ion etching of the samples resulted in the disappearance of the two higher oxides located at 339.1 eV and 340.6 eV. Peak-fitting of the Pd 3d envelope after etching suggested the presence of PdO (336.6 eV) and PdO_2 (337.7 eV). The Pd^{2+}/Pd^{4+} ratio was calculated from the areas of the fitted Gaussian components and turned out to be 1.8 for Na-PdO/SnO_2 as opposed to 2.8 of PdO/SnO_2, after the same rate of ion bombardment procedure. The Pd^{2+}/Pd^{4+} ratios suggest that Pd^{4+} (PdO_2) species were stabilized in the presence of the alkali-metal in the structure.

The computer peak fitting of Pd 3d envelope of reduced Na-PdO/SnO_2 suggested the presence of three binding states of palladium, located at 335.7 eV, 337.7 eV, and 339.1 eV which could be assigned to Pd^0, Pd^{4+} and Pd^{6+}, respectively (Figure 4.3b). These findings are in agreement with XPS measurements after Ar-etching treatment.

The investigation of the chemical states of Pd and Sn in reduced catalysts is also subject to the formation of Pd-Sn alloys which alter the chemisorption properties, influence the catalytic behavior of Pd-SnO_x system [114], and bimetallic Pd-Sn catalysts supported on different oxides [116-118]. Although any binding states that could be assigned to a Pd-Sn alloy was not observed in the XPS spectra, the formation of a Pd-Sn alloy upon the reduction pretreatment, effecting the subsequent catalytic properties of the reduced samples should not be excluded.

4.1.1.3 Quantitative Analysis of XPS Data

The relative amounts of palladium oxide species were calculated from the areas of the fitted Gaussian components making up the Pd 3d envelope in oxidized and reduced PdO/SnO_2 and Na-PdO/SnO_2 (Table 4.1). The greater oxygen content of Na-PdO/SnO_2 in the surface layers was observed as the presence of greater amount of higher oxides in the in the alkali-metal promoted samples relative to the alkali-free catalyst. Pd^{4+}/Pd^{2+} ratio was larger in oxidized Na-PdO/SnO_2 than ratio in oxidized PdO/SnO_2. The data also showed that, even after reduction pretreatment a considerable amount of palladium in alkali-metal promoted PdO/SnO_2 existed in higher valance states while; most palladium in PdO/SnO_2 was reduced to metallic Pd upon reduction of PdO/SnO_2. A possible explanation for the oxygen enrichment of the palladium phase in alkali-metal promoted PdO/SnO_2 relative to the unpromoted PdO/SnO_2 is the alkali facilitated oxygen diffusion from the supporting oxide to the noble metal. The diffusion of oxygen

from subsurface layers to the surface of the catalysts has been tested by the application of impulse technique utilizing intermittently delayed injections. The results of these experiments will be discussed in Section 4.1.6. The stabilization of Pd^{4+} species in the presence of the alkali-metal could also account for the increase in Pd^{4+}/Pd^{2+} upon alkali-metal promotion of PdO/SnO_2.

Table 4.1 XPS analysis of Pd 3d envelope of Na-PdO/SnO_2 and PdO/SnO_2

	Binding Energy (eV)	PdO/SnO_2 (Oxidized)	PdO/SnO_2 (Reduced)	Na-PdO/SnO_2 (Oxidized)	Na-PdO/SnO_2 (Reduced)
Pd^0	335.7	-	85.3	-	37.1
PdO	336.6	18.2	2.1	-	-
PdO_2	337.7	60.2	12.5	67.4	40.9
PdO_3	339.1	21.6	-	26.4	22.0
Higher oxide	340.6	-	-	6.2	-

The Pd:Sn atomic ratios were calculated from the areas lying under the Pd 3d envelope and the Sn 3d envelope for PdO/SnO_2 and Na-PdO/SnO_2 catalysts in both oxidized and reduced state. In both of the cases, a two-fold increase in the Sn-to-Pd ratio was observed in sodium promoted sample relative to the unpromoted sample. Similarly, the quantification of XPS data showed that the amount of Pd present in the surface layers probed by XPS was doubled upon alkali-metal promotion of PdO/SnO_2. These observations suggest that sodium promotion resulted in the surface segregation of Pd atoms increasing the concentration of Pd in the surface layers.

A mechanism that could lead to the surface segregation of palladium atoms in the presence of the alkali is their interaction to form ternary oxide species. Alkali-metals and palladium are known to form ternary oxides [159-161]. In the present study, Na doping was achieved with the addition of 0.1 wt% of sodium to the catalysts which yields 0.53 Na:Pd atomic ratio. Thus, the amount of sodium introduced to the catalyst is sufficient to form $Na_xPd_3O_4$ phase. Furthermore, the formation of such ternary oxides of platinum group metals with alkali-metals was observed at 400ºC under oxygen atmosphere, which quite resembles the calcination procedure adopted in this study [159]. Similarly, Mitra et *al.* [162] have observed that a ternary oxide of sodium and rhenium ($NaReO_4$)

was formed on Re_2O_4/TiO_2 and Re_2O_4/Al_2O_3 catalysts and that the catalytic properties were altered in the presence of the ternary oxide. Although the diffusivity of these ternary palladate compounds in tin dioxide is yet unknown, the formation of these ternary oxide species may be postulated to lead to surface segregation of Pd possibly by stabilizing Pd species on the surface and suppressing the diffusion of these species through tin dioxide matrix.

Although tetravalent Pd species were observed to exist in both of the catalysts and spectroscopic differentiation of Pd^{4+} in $Na_xPd_3O_4$ and PdO_2 matrices has not been possible. This is not at odds with the postulation of the formation of $Na_xPd_3O_4$ species because, the difference between the Pd 3d binding energies of a Pd atom in PdO_2 environment and a Pd atom in a $Na_xPd_3O_4$ environment may not be large enough for spectroscopic differentiation of Pd atoms in either one of these environments. Nevertheless, the increased Pd^{4+}/Pd^{2+} ratio in Na-PdO/SnO_2 relative to the alkali-free catalyst may provide evidence for the stabilization of Pd atoms in tetravalent state in $Na_xPd_3O_4$ structures.

Quantification of the XPS data further showed that subjecting the catalysts to reduction pretreatment prior to the collection of X-ray photoelectron spectra resulted in an increase in the surface Pd:Sn atomic ratio of both PdO/SnO_2 and Na-PdO/SnO_2. This change in the Pd:Sn atomic ratio with reduction pretreatment at 150 °C might be attributed to the joint effect of palladium diffusion in and out of the tin dioxide matrix and the variation of palladium cluster size with pretreatment. As a result of the decrease in the atomic radius of Pd^0 with positive atomic charge, the diffusion of Pd^{2+} ions in tin dioxide network are favored over the diffusion of Pd^0 atoms [175] and several studies in the literature reported a decrease in the Pd^+/Sn ratio suggesting an inward diffusion of palladium ions with heat treatment [89,170]. Jimenez et *al.* [176] have reported an increase in the intensity of Pd 3d band after hydrogen treatment of Pd/SnO_2 at elevated temperatures and suggested that the diffusion of palladium ions penetrated in to the tin dioxide network to the surface of the catalyst took place during reduction. Under the reduction conditions adopted, another effect that accompanies the diffusion of palladium atoms in tin dioxide matrix to alter the Pd:Sn ratio is the wetting of tin dioxide surface by palladium. In this case, palladium atoms partially decorate tin clusters resulting in decreased concentration of tin atoms exposed and increased Pd:Sn ratios in catalysts subjected to reduction pretreatment. However, when the catalyst surfaces were etched with Ar-ion beam, the Pd:Sn ratio was either increased or remained

constant rather than decreasing suggesting that the contribution of the decorating effect of palladium was negligible when compared to the diffusional effects. Thus, it is probable that palladium ions were diffused from the tin dioxide bulk towards the surface of the catalysts where, these ions were reduced to metallic palladium or to lower oxides and because of the increase in their ionic radii, these species would remain within the surface layers.

4.1.2 Scanning Electron Microscopy (SEM) and Energy Dispersive X-Ray Spectroscopy(EDX)

The investigation of the catalysts powders with Scanning Electron Microscope revealed that the catalysts powders were made up of nano-scaled particles in the order of 80 nm (Figures 4.4a and 4.4b). The samples were also investigated by Energy Dispersive X-ray Spectroscopy (EDX) to observe the dispersion of palladium particles over the SnO_2 surface and the EDX data revealed that palladium particles were uniformly dispersed over the support material. Sodium promotion was observable neither through SEM images (Figure 4.4b) and nor through EDX analysis, and as inferred from these analyses, the particle morphology was not altered by the addition of sodium.

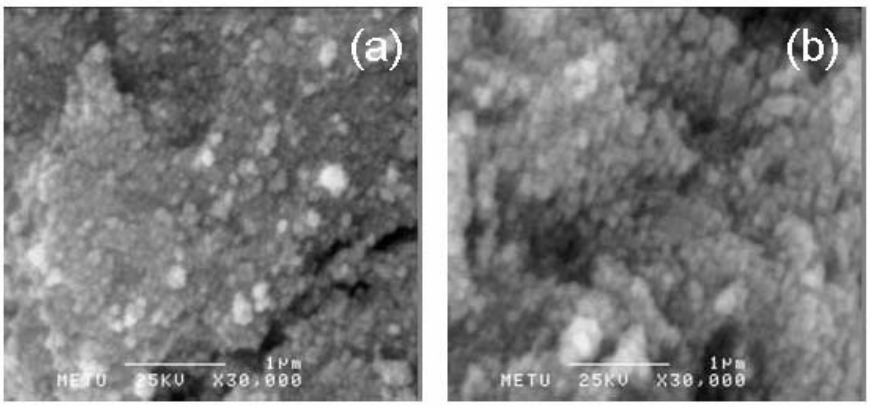

Figure 4.4 SEM images of (a) PdO/SnO_2 and (b) $Na\text{-}PdO/SnO_2$

4.1.3 Temperature-Programmed Reaction Spectroscopy (TPRS) Studies

For examining the effect of alkali metal promotion on the CO oxidation activity the CO oxidation activities of oxidized and reduced PdO/SnO_2 and Na-PdO/SnO_2 catalysts were tested via TPRS. Besides the initial oxygen coverage at the catalyst surfaces, another parameter determining the activity of the catalysts is the oxygen concentration at the gas phase thus, the CO activity of the catalysts were investigated under oxygen-lean (S = 1.25) and oxygen-rich (S = 0.91 and S = 0.5) reactor feed conditions in order to observe this effect.

The high CO oxidation activity of the PdO/SnO_2-based catalysts and the enhancement in the CO oxidation activity by sodium modification of the system is evidenced by TPRS experiments. Complete conversion of the CO in the reactor feed was achieved at temperatures in the order of 160°C (Figures 4.5 and 4.6). The investigation of the CO oxidation activities of the catalysts revealed that sodium modified catalysts subjected to oxidizing pretreatment were slightly less active than their unmodified counterparts under oxygen rich conditions (Figures 4.5 and 4.6). When the stoichiometric ratio (S) is 0.91, i.e. slightly oxygen rich reactor feed condition, the light-off temperatures for oxidized PdO/SnO_2 and Na-PdO/SnO_2 were recorded as 170°C and 174°C, respectively. Decreasing the stoichiometric ratio to 0.5 by increasing the oxygen concentration at the feed decreased the light off temperatures of oxidized PdO/SnO_2 and Na-PdO/SnO_2 to 169°C and 173°C, respectively. Reduction pre-treatment was observed to increase the activity of both of the catalysts (Figures 4.5 and 4.6) and, the effect of reduction pretreatment on the CO oxidation activity was more pronounced over Na-PdO/SnO_2 such that, a 17°C decrease to 152°C in the light-off temperature of PdO/SnO_2 was recorded as opposed to 30°C decrease recorded in the light-off temperature of Na-PdO/SnO_2 when the stoichiometric ratio is equal to 0.91. Similarly, when the stoichiometric ratio is 0.5, the light-off temperature of PdO/SnO_2 decreased by 21°C to 148°C by reduction pretreatment whereas, the light-off temperature of Na-PdO/SnO_2 decreased by 35°C to 138°C.

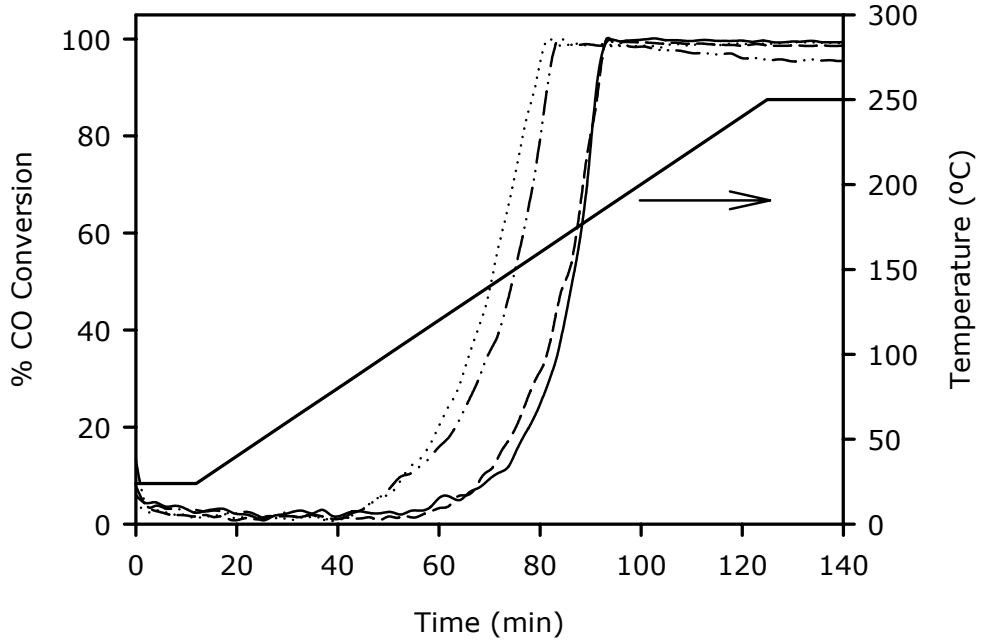

Figure 4.5 CO conversion rates over oxidized PdO/SnO_2 (------), reduced PdO/SnO_2 (–··–··), oxidized Na-PdO/SnO_2 (———) and reduced Na-PdO/SnO_2 (·····)

(*Reaction Conditions:* P = 1 atm; [CO]/[O] = 0.5; GHSV = 12 800 hr^{-1}; [CO] = 2400 ppm; catalyst weight = 100 mg; heating rate = 2°C/min)

Control experiments, under slightly oxygen rich condition, i.e. at a stoichiometric ratio of 0.91, were conducted on oxidized and reduced SnO_2 samples to observe the extent of the contribution of the support on the reported activity of palladium and sodium promoted catalysts. The reaction was observed to proceed at an insignificant rate till 250ºC and a CO conversion of 13% was observed at 250ºC over both oxidized and reduced samples of bare SnO_2 confirming that the reported catalytic activity was a consequence of palladium and sodium addition.

The effect of oxygen content of the feed on the performance of the catalysts in CO oxidation was further tested by decreasing the oxygen concentration while keeping CO concentration constant for the comparability of the results. The oxygen concentration was adjusted to yield CO-rich reactor feed, i.e. [CO]/[O] = 1.25. The effect of decreasing the oxygen concentration in the gas phase was observed as a shift in the CO conversion versus temperature curves of all of the catalysts to higher temperatures (Figure 4.7). At this feed condition, the light-off temperatures were recorded as 190°C and 168°C over oxidized and reduced PdO/SnO_2 and, 178°C and 143°C over oxidized and reduced Na-PdO/SnO_2. As it is clearly demonstrated by the light-off temperatures, the decrease in the

activity of Na-PdO/SnO_2 with decreasing oxygen concentration was less pronounced than its unmodified counterpart.

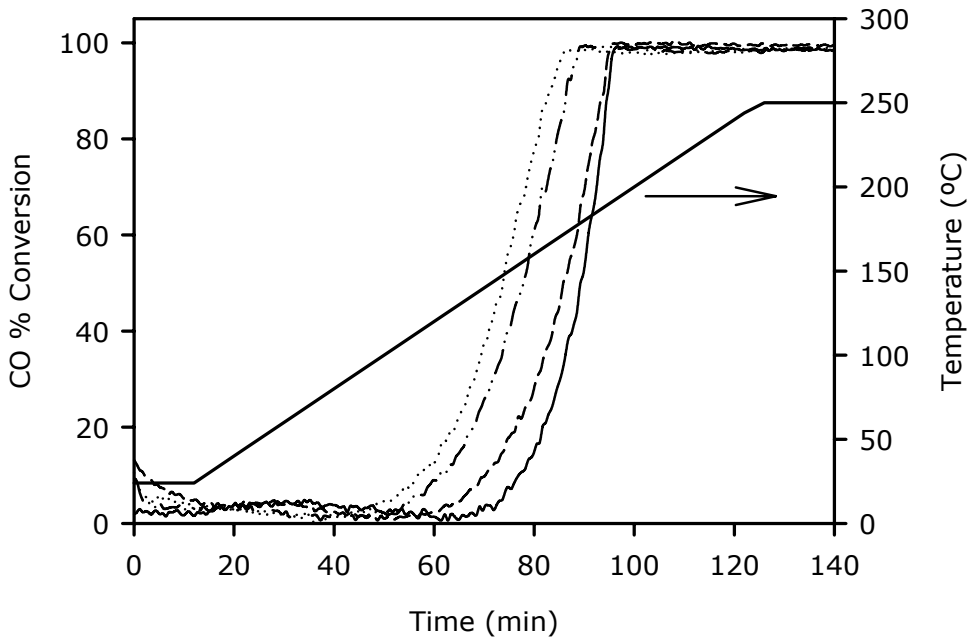

Figure 4.6 CO conversion rates over oxidized PdO/SnO_2 (------), reduced PdO/SnO_2 (–··–··), oxidized Na-PdO/SnO_2 (———) and reduced Na-PdO/SnO_2 (·····)

(*Reaction Conditions:* P = 1 atm; [CO]/[O] = 0.91; GHSV = 12 800 hr^{-1}; [CO] = 2400 ppm; catalyst weight = 100 mg; heating rate = 2°C/min)

The rates of CO oxidation reaction were calculated at 150°C to provide a basis for comparison of the activities of the catalysts tested and these values are presented in Figure 4.8 (see Appendix D for the calculation of reaction rates). Figure 4.8 shows that samples subjected to reduction pretreatment exhibited superior activity relative to samples subjected to oxidation pretreatment and among the catalysts tested, reduced Na-PdO/SnO_2 was observed to be the most active catalyst for CO oxidation under all three of the feed conditions. Furthermore, the activity of oxidized and reduced Na-PdO/SnO_2 was only slightly affected by decrease in the oxygen concentration of the reactor feed while, reduction in the oxygen concentration lead to significant reduction in the rate of CO oxidation over oxidized and reduced PdO/SnO_2. The effect is more readily observed in the case of oxidized samples: while oxidized Na-PdO/SnO_2 exhibited inferior activity relative to its unmodified counterpart under oxygen rich conditions, it is observed to possess superior activity under oxygen lean conditions.

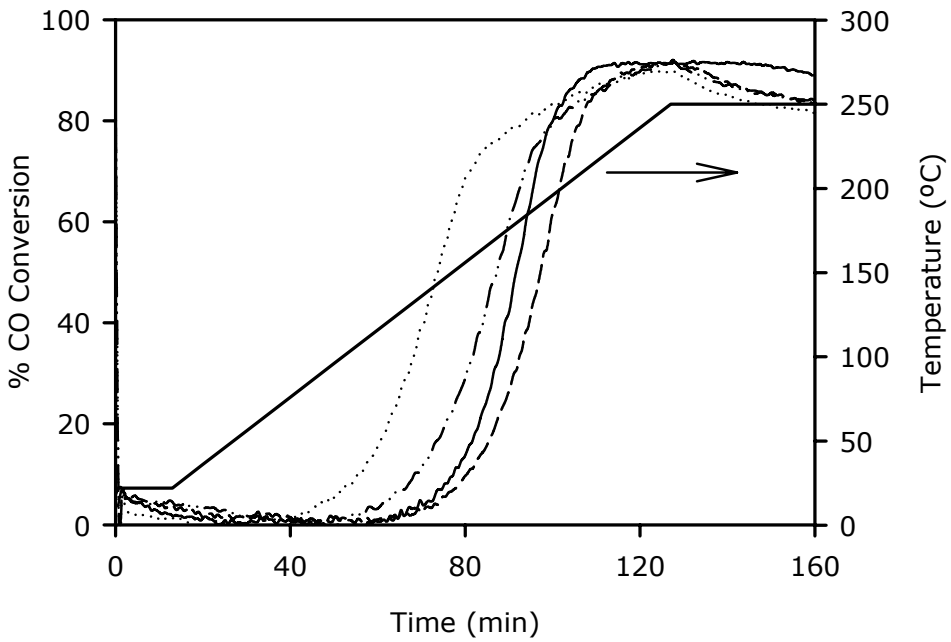

Figure 4.7 CO conversion rates over oxidized PdO/SnO_2 (------), reduced PdO/SnO_2 (–··–··), oxidized Na-PdO/SnO_2 (———), reduced Na-PdO/SnO_2 (·····)

(*Reaction Conditions:* P = 1 atm; [CO]/[O] = 1.25; GHSV = 12 800 hr^{-1}; [CO] = 2400 ppm; catalyst weight = 100 mg; heating rate = 2°C/min)

The enhanced rates CO oxidation over samples subjected to reduction pretreatment are in agreement with previous reports in the literature [6,104,111,112]. Although it is well established that oxygen adsorption on tin dioxide results in the formation of ionosorbed oxygen species and the reaction of chemisorbed CO with these ionosorbed species constitutes reaction pathway for CO oxidation [85], carbon monoxide and oxygen are known to competitively adsorb on noble metal surfaces [43,52,53] and the increase in the rates of CO conversion with reduction pretreatment of the catalysts may be associated with the inability of CO to adsorb over oxygen precovered surface. The oxidized catalyst surfaces are expected to be saturated with ionosorbed oxygen species as a result of the preceding oxygen treatment and these species would hinder the chemisorption of CO and the oxidation reaction would proceed with an insignificant rate until a certain temperature is reached, where desorption of molecular oxygen becomes significant that, vacant sites available for CO adsorption are created. On reduced catalysts, the catalyst surface effectively oxidized with oxygen from the gas phase and reduced during CO oxidation, in a cyclic manner and carbon monoxide is able to compete for active sites.

Therefore, the reaction proceeds at a higher rate over the catalysts activated in reducing atmospheres.

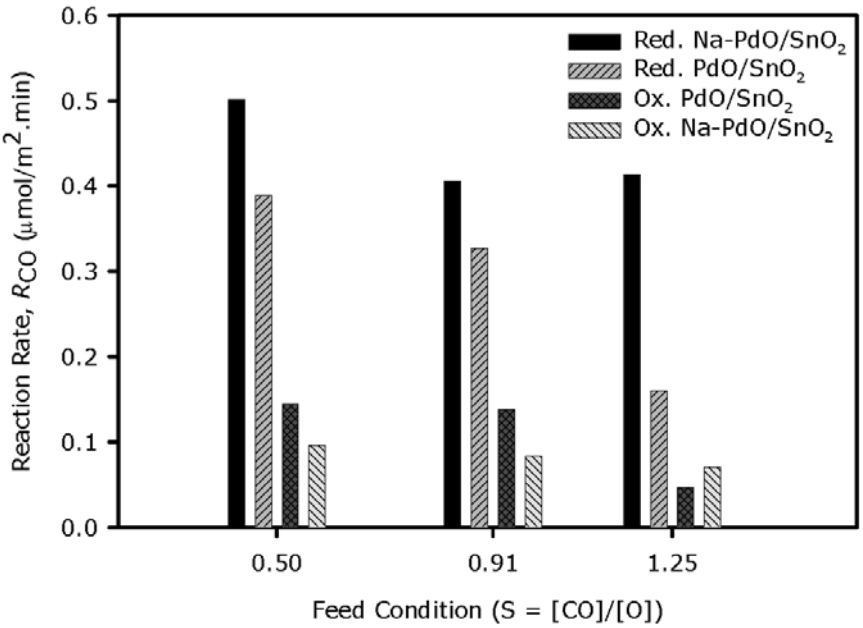

Figure 4.8 Variation of rates of CO oxidation with TPRS feed composition (*Reaction Conditions:* P = 1 atm; GHSV = 12 800 hr^{-1}; [CO] = 2400 ppm; catalyst weight = 100 mg; heating rate = 2°C/min)

The characterization of the catalysts with XPS have shown that sodium promotion resulted in an increase in the oxygen storage capacity of the catalysts by facilitating the formation of super-oxide species and as well, led to surface segregation of palladium atoms, which increases the number of available reaction sites. In line with the foregoing discussion, the increased oxygen storage capacity of Na-PdO/SnO_2 and the alkali-enhanced interaction of oxygen with the surface may be postulated to result in the inferior activity of oxidized Na-PdO/SnO_2 under oxygen rich reactor feed conditions. But, the same effect would counteract under oxygen lean conditions because of the greater amount of oxygen for oxidizing chemisorbed CO is present over oxidizing Na-PdO/SnO_2. Therefore, the effect of alkali-metal modifier in CO oxidation over PdO/SnO_2 depends on the gas phase concentrations which may affect the relative surface coverages of the reactants. Similarly, Yakovkin et *al.* [177] reported poisoning of Li modified Pt surface by oxygen under CO lean conditions and the effect was reversed under CO rich conditions. The effect has been attributed to amphoteric

nature of CO adsorption that involves donation and backdonation of electrons and results in electron donor-like behavior of CO in the presence of a coadsorbed electron acceptor, i.e. O [129]. Therefore, under CO-lean conditions modifier is expected to poison CO oxidation whereas, it would act to promote CO oxidation under CO-rich conditions.

Besides the alkali-induced changes in the relative surface coverages of CO and O_2, the enhanced reaction and CO conversion rates observed in the case of reduced Na-PdO/SnO_2 sample may be associated with the surface segregation of palladium atoms, which have been identified through XPS measurements. The increase in the surface concentration of palladium atoms have been concluded to originate from alkali-metal introduction to the structure and the increase in palladium surface concentration would increase the active sites for CO oxidation. Therefore, the increased initial oxygen content of the catalyst coupled with the increased number of reaction sites, which is a consequence of increased Pd concentration on the surface would lead to the superior performance of oxidized Na-PdO/SnO_2, under oxygen lean conditions.

Another important point that needs to be emphasized about the TPRS experiments carried out under oxygen-lean conditions is that a transient overshoot was observed in the experimental CO conversion rates, before they converge to the maximum theoretically attainable conversion value (80%) with time-on-stream at 250°C (Figure 4.7). CO consumption beyond the theoretically possible conversion rate may be explained by the presence of another mechanism which is coupled with the oxidation of chemisorbed CO with chemisorbed oxide species for CO oxidation over PdO/SnO_2-based catalysts. The presence of another mechanism for CO oxidation is also evidenced by the changes in the slopes of CO conversion curves of reduced Na-PdO/SnO_2 and reduced PdO/SnO_2, observed at 160°C for Na-PdO/SnO_2 and at 190°C for PdO/SnO_2 that may suggest the transition between two types of mechanisms; one of which definitely involves the oxidation of CO by oxygen species formed through chemisorption of oxygen from the gas phase. Such a transition in the reaction regime may involve the transition from surface reaction rate controlled region to bulk diffusion controlled regime, which implies the reduction of subsurface layers of the catalyst. These oxygen species would not be replenished during the course of the reaction as the chemisorbed oxygen species would be consumed to convert CO to CO_2 through reaction (4.1) rather than re-oxidizing the surface, therefore, the activity arising from the consumption of oxygen

contained in the subsurface layers of the catalyst would level-off when temperature of the reactor was kept constant at 250°C.

$$M-CO + M-O \rightarrow CO_{2\,(gas)} + 2M \tag{4.1}$$

Another mechanism that could account for the overshoot in the CO conversion rate and the transition between the two regimes is the involvement of surface hydroxy groups in the oxidation of chemisorbed CO through Reaction 4.2, to yield carbon dioxide and proton which is converted to water vapor through Reaction 4.3. Through O_2-TPD studies, the hydroxy reaction mechanism has previously been suggested to play a key role in the CO oxidation activity of alkali-metal promoted PdO/SnO_2-based catalysts and has been postulated to dominate in the 170 – 300°C region, especially over reduced catalysts. Drawdy et *al.* [104] have observed an increase in the abundance $Pt(OH)_2$ species after reduction pretreatment of Pt/SnO_2 catalysts at 175°C which is coupled with an increase in the CO oxidation activity of the catalysts. Furthermore, these authors reported a decrease in the catalyst activity when Pt/SnO_2 was subjected to reduction pretreatment at higher temperatures to eliminate hydroxyl species and concluded that $Pt(OH)_2$ sites played an important role in CO oxidation.

$$M-CO + M-OH \rightarrow M + M-H + CO_2 \tag{4.2}$$

$$M-H + M-OH \rightarrow 2M + H_2O \tag{4.3}$$

For providing further insights to the role played by the hydroxy species in CO oxidation mechanism over Pd/SnO_2 catalysts, the evolution of water vapor (m/z=18) during TPRS was also monitored along with the evolution of other components from the reactor (Figure 4.9). Two broad bands of water evolution were resolved over oxidized samples (Figure 4.9b and 4.9d). One of these bands corresponds just to the onset of the temperature programmed stage. It is not meaningful to associate these bands with the presence of physisorbed water due to exposure to ambient air. Although hydroxy groups are strongly bound to tin dioxide [178] and these species tend to remain on the surface at temperatures as high as several hundred °C under vacuum [98,104], heat treatment of SnO_2 surfaces at 75°C has been observed to reduce the amount of water and hydroxyl ad-species. Moreover, adsorbed water was reported to be completely eliminated upon pretreatment above 100°C [104] thus, prior to the activity tests the catalysts were subjected to in-situ pretreatment procedures at 150°C to remove

physisorbed water. The low temperature water evolution band completely diminished upon reduction pretreatment of the catalysts (Figures 4.9a and 4.9c).

Water evolution from unpromoted and sodium promoted PdO/SnO_2 in the same temperature range was also observed trough O_2-TPD studies (See Section 4.1.5). The most plausible explanation for water evolution at this temperature range was to associate these bands with the condensation of adjacent hydroxy groups to form adsorbed water, which would tend to desorb just at the onset of the temperature program. In fact, the decrease in the intensity of water evolution bands following reduction pretreatment further supports the hydroxy condensation mechanism because a decrease in the extent of this reaction is expected as reduction pretreatment would lead to the dehydration of the surface. It is also possible that water evolution may be a consequence of CO oxidation through Reactions 4.2 and 4.3 however; no clear correlation between the amount of low temperature water evolution and the CO oxidation activity of the catalysts has been observed.

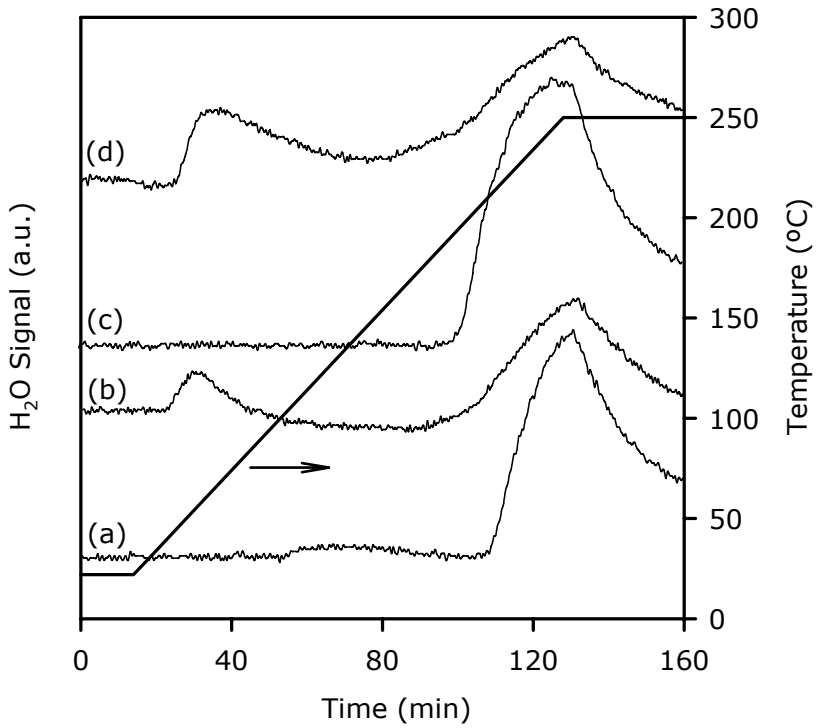

Figure 4.9 Water evolution profiles during TPRS, (a) reduced PdO/SnO_2, (b) oxidized PdO/SnO_2, (c) reduced Na-PdO/SnO_2 and (d) oxidized Na-PdO/SnO_2

(*Reaction Conditions:* P = 1 atm; [CO]/[O] = 1.25; GHSV = 12 800 hr^{-1}; [CO] = 2400 ppm; catalyst weight = 100 mg; heating rate = 2°C/min)

Over samples subjected to oxidation pretreatment onset of a second band was observed at 140°C whereas, reduction pretreatment led to the disappearance of the tail corresponding to 140°C-200°C region. In the same temperature range, the change in the slope of the CO conversion versus temperature curves of pre-reduced samples imply the suppression of the CO oxidation reaction possibly arising from the dehydroxylation of the surface during reduction pretreatment.

Palladized SnO_2 is already known as an effective low temperature CO oxidation catalyst [3] but, the reported reaction rate and light-off temperature data demonstrates that alkali-metal-promotion further enhanced the activity of palladized SnO_2 catalysts under different CO and O_2 concentrations. The enhanced activity of Na-PdO/SnO_2 relative to PdO/SnO_2 under oxygen-lean conditions need be associated with the availability/reactivity of the oxygen species over the catalysts in attempts to explain the concentration dependent role of the alkali-metal promoter.

4.1.4 Steady-State CO Oxidation Activity

As the TPRS data represent the CO oxidation activity of the catalysts under transient conditions, the TPRS data was coupled with steady-state CO activity tests for a more comprehensive representation of the CO oxidation characteristics of the SnO_2-based samples. As it was the case in the TPRS experiments, the effect of gas phase oxygen concentration on the catalyst activity was also studied and the CO oxidation activities of SnO_2, PdO/SnO_2 and Na-PdO/SnO_2 catalysts were tested under both oxygen rich (S = [CO]/[O] = 0.9) and oxygen lean (S = 1.1) reactor feed conditions.

During the steady-state activity tests of PdO/SnO_2 and Na-PdO/SnO_2 samples an initial CO oxidation activity was observed at 30°C under both of the feed conditions however, this activity appeared to be a transient one which leveled off with time-on-stream and, the CO oxidation reaction was observed to proceed at an insignificant rate below 150°C over all of the catalysts under both of the reactor feed conditions studied (Figures 4.10a and 4.10b). A rapid increase in the rates of CO oxidation and conversion were observed above 100°C and under the oxygen rich feed conditions, the rate of CO oxidation reaction was calculated as 0.531 μmol/min.m^2 cat. over PdO/SnO_2 at 150°C. The rate of reaction was 0.900 μmol/min.m^2 cat. over sodium modified sample which represents approximately two-fold increase in the rates of reaction and CO conversion

relative to PdO/SnO_2. At the same temperature, the rate of reaction thus, CO conversion was insignificant over SnO_2 relative to Na-PdO/SnO_2 and PdO/SnO_2 and, was calculated as 0.072 μmol/min.m^2 cat. Although the steady-state conversion of CO converges to the same value at 200°C and 250°C for both of sodium modified and alkali-free catalysts, the alkali-metal promoted catalyst was observed to perform significantly better than the alkali-free counterpart at temperatures below 200°C.

The alkali-metal promoted catalyst was observed to perform much better than the alkali-free catalyst in catalyzing the reaction between CO and O_2 under oxygen-lean reactor feed conditions (Figure 4.10b). Under this experimental condition, the rate of reaction at 150°C was calculated as 1.571 μmol/min.m^2 cat. over Na-PdO/SnO_2 and as 0.915 μmol/min.m^2 cat. over PdO/SnO_2. Unlike oxygen rich feed condition, where PdO/SnO_2 and Na-PdO/SnO_2 showed similar CO oxidation activity above 200°C, Na-PdO/SnO_2 was observed to exhibit superior catalytic activity when compared with the alkali-free counterpart at all temperatures under oxygen-lean reactor feed conditions.

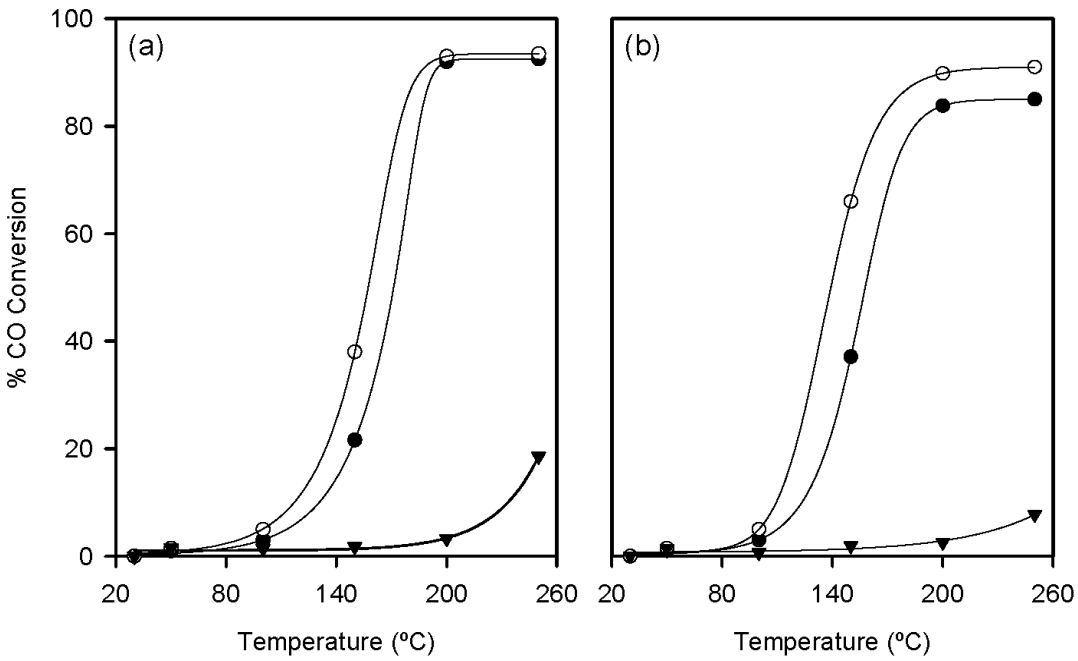

Figure 4.10 Conversion rate of CO over SnO_2 (▼) PdO/SnO_2 (●) and Na-PdO/SnO_2 (○): (a)[CO]/[O] = 0.9 and (b) [CO]/[O] = 1.1

(Reaction Conditions: P = 1 atm; [CO] = 2400 ppm, GHSV=10,780 hr^{-1}, catalyst weight = 150 mg)

Another observation which supports the superior CO oxidation activity of Na-PdO/SnO_2 is that; the rate of CO conversion over Na-PdO/SnO_2 reached 90% above 200°C, which is the maximum theoretically attainable CO conversion because of the feed stoichiometry however; the CO conversion was limited to 80% over PdO/SnO_2, which is below the theoretically attainable value. This indicates that the sodium promoted sample is effectively oxidized by chemisorbing oxygen from the gas phase and reduced through the consumption of these oxide species in CO oxidation while, replenishment of the oxide species of PdO/SnO_2 was not as effective as the sodium modified sample. The effect may be attributed the promotion of the interaction of oxygen with the sodium-modified surface. In fact, several studies in the literature reported the alkali-metal promotion of oxygen adsorption and a corresponding increase in the relative surface coverage of oxygen species [137,179] and the O_2-TPD studies discussed in section 4.1.5 also evidence the promotion of oxygen adsorption in the presence of sodium in the structure. Besides the oxygen chemisorption dynamics, the superior activity of the alkali-metal promoted catalyst may also be attributed to the alkali-induced Pd segregation at the surface. The XPD data have suggested increased palladium content of the surface of sodium modified sample which would lead to greater number of active sites for CO oxidation and increase the rates of CO oxidation and conversion.

4.1.5 Temperature Programmed Desorption (TPD) Studies

Previously, post CO adsorption He-TPD studies have been carried out on the catalysts [166] and no desorption bands of either CO or CO_2 has been observed from the mass signals traces collected during He-TPD studies. In the light of these He-TPD studies, it has previously been concluded that CO was irreversibly bonded to the surface and did not desorb even by heating to temperatures in the order of 500°C. For this reason, the TPD stage following the adsorption of CO or CO/O_2 mixture was carried our by the addition of oxygen to the carrier gas to facilitate the reaction of chemisorbed CO and the CO oxidation activity of SnO_2, PdO/SnO_2 and Na-PdO/SnO_2 were examined by O_2-TPD.

4.1.5.1 CO Adsorption-O_2 TPD Studies

Room temperature CO adsorption on oxidized PdO/SnO_2 resulted in two distinct CO_2 desorption peaks upon heating under oxygen atmosphere; the low temperature activity of the catalyst was observed just upon the onset of the

TPD, with the maxima appearing at 150ºC (Figure 4.11c). Upon subjecting PdO/SnO_2 to reduction pretreatment, the intensity of this low temperature peak significantly decreased, though not diminished completely (Figure 4.11d). The discrepancy in the activity caused by reduction pretreatment is readily observed in the amount of CO_2 evolution from the catalysts: 4.34 μmol of CO_2 was desorbed per unit surface area of the catalyst in the oxidized state as opposed to 0.45 $\mu mol/m^2$ cat. of CO_2 evolution from the reduced catalyst. Thus, this activity resulted most probably from the activity of Pd^{2+} (or PdO) sites which are abundant in oxidized catalysts and depleted to a great extent during reduction pretreatment. Same observation regarding the activity of Pd^{2+} phase has been reported previously, through room temperature IR studies over PdO/SnO_2 catalysts prepared by wet precipitation method [39].

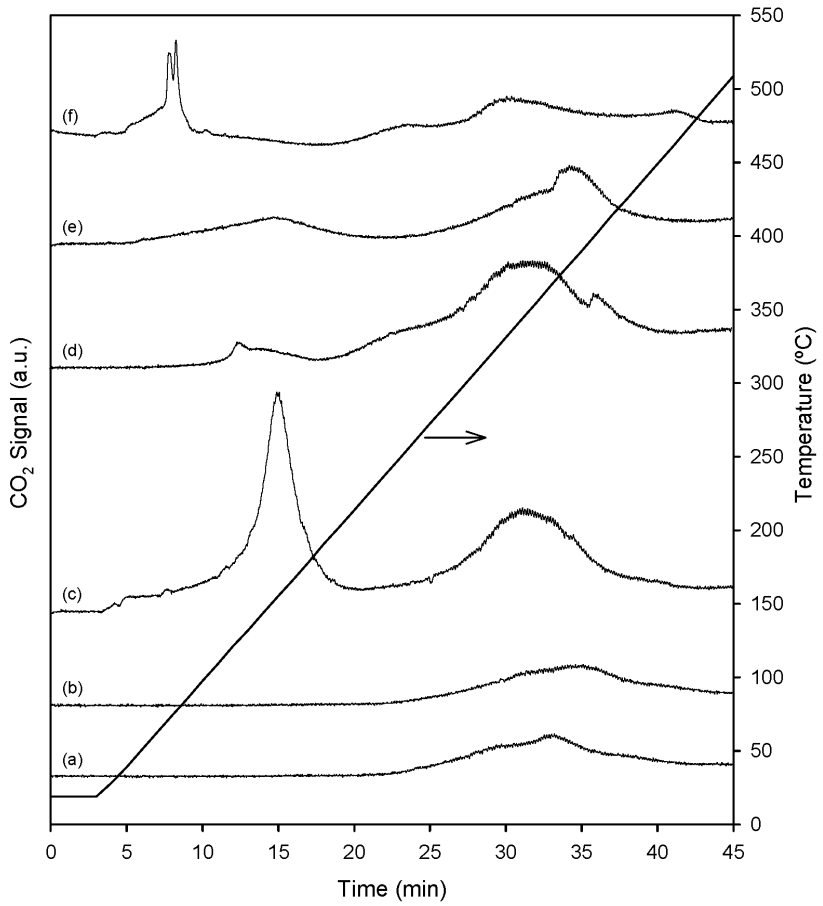

Figure 4.11 CO_2 evolution profiles during post CO adsorption O_2 TPD
(a) oxidized SnO_2, (b) reduced SnO_2, (c) oxidized PdO/SnO_2, (d) reduced PdO/SnO_2, (e) oxidized Na-PdO/SnO_2 and (f) reduced Na-PdO/SnO_2

(*Conditions:* P = 1 atm; [CO] = 160 ppm (adsorption); [O_2] = 200 ppm (TPD); GHSV = 12 800 hr^{-1}; catalyst weight = 100 mg; heating rate = 12°C/min)

The second CO_2 evolution corresponded to higher temperatures, specifically to the range 240-470ºC (maxima corresponded to, T_{max}= 345ºC), and the intensity of this band was quite unaffected by the nature of the pretreatment, i.e. whether it was reducing or oxidizing. Sodium promotion resulted in a broader and weaker CO_2 evolution peak in 40-230ºC (T_{max}= 155ºC) region but had no observable effect on the high temperature activity (Figure 4.11e). In the reduced state, sodium promotion resulted in a downward shift in the low temperature activity observed in PdO/SnO_2 via reducing the activation energy for CO to CO_2 conversion. A strong CO_2 desorption band was observed just at the onset of TPD till 100ºC (T_{max}= 70ºC) when Na-PdO/SnO_2 was subjected to reduction pretreatment (Figure 4.11f).

Similar to the unmodified catalyst, greater amount of CO_2 evolution was observed over oxidized Na-PdO/SnO_2 (1.08 μmol/m^2 cat.) than reduced Na-PdO/SnO_2 (0.38 μmol/m^2 cat.). In both oxidized and reduced Na-PdO/SnO_2 the high temperature activity was observed in 280-500ºC ($T_{max,\ reduced}$ = 340ºC, $T_{max,\ oxidized}$= 380ºC) region and the intensity was almost independent of pretreatment procedure. For determining the contribution of the support to the observed CO activity a similar control experiment was performed on tin dioxide. CO_2 evolution from tin dioxide was observed above 250ºC (T_{max}= 380ºC) and was unaffected by the pretreatment of the catalyst (Figures 4.11a and 4.11b). 3 μmol of CO_2 desorption was observed per m^2 of SnO_2 regardless of whether the catalyst was in reduced or oxidized state. Observation of CO_2 evolution indicates that at ambient temperatures SnO_2 surface is capable of adsorbing CO, though the extent is limited when compared to PdO/SnO_2 and Na-PdO/SnO_2, but incapable of oxidizing to and/or desorbing as CO_2 at low temperature range. The CO_2 evolution band over SnO_2 corresponded to the high temperature evolution peaks observed in both PdO/SnO_2 and Na-PdO/SnO_2. This indicated that the high temperature activity observed in 280-500ºC region was a consequence of the activity of the support. The presence of the noble metal and alkaline modifier had some influence on this activity of the support and on the average a 1.5-fold increase in the amount of CO_2 evolution per m^2 of catalyst was observed upon addition of these metals to tin dioxide. As evident from the foregoing discussion, tin dioxide is not just an inert support but rather itself is a CO oxidation catalyst capable of catalyzing CO/O_2 reaction at temperatures higher than 250ºC. The enhancement in the activity of SnO_2 in the presence of Pd or Na-Pd was a consequence of spillover of activated species from the metal to tin dioxide leading to increased coverage of tin dioxide surface, which does not have a

strong affinity towards reducing species and/or increased surface area of the catalyst in the presence of palladium.

Water profiles were also recorded during TPD experiments and these are presented in Figure 4.12. Two distinct water desorption bands were observed in all the catalysts, one of these corresponded to 50-190ºC and was observed to be more intense in the case of oxidized catalysts than their reduced counterparts (Figure 4.12). In this temperature range, evolution of 7.13 $\mu mol/m^2$ cat. of H_2O was observed from oxidized PdO/SnO_2 and this amount was decreased to 2.14 $\mu mol/m^2$ cat. over reduced PdO/SnO_2. As mentioned earlier, prior to the experiments the catalysts were subjected to *in-situ* pretreatment procedures at 150ºC, which is expected to remove physisorbed water species, thus, the water desorption peak below 100 ºC cannot be ascribed to physisorbed water formed due to exposure to ambient air. Moreover, a water desorption band, for which the maxima corresponded approximately to 100ºC, was observed, while the reactor temperature was raised to 150ºC during the pretreatment of the catalysts. Then water mass signal attained the background level observed in TPD stages before the end of pretreatment stage and this water evolution was a consequence of the presence of physisorbed water formed through the contact with ambient air. In addition, pretreatment of SnO_2 surfaces at 75ºC has been observed to reduce the amount of water and hydroxyl ad-species; adsorbed water was eliminated and hydroxyl groups are further depleted upon pretreatment above 100ºC [104]. This low temperature desorption band of water cannot be ascribed to the decomposition of palladium hydride species formed during the reduction pretreatment because this band was also observed over bare SnO_2. Two other effects may result in water desorption below 100ºC. The first of these effects is the reaction between two adjacent hydroxyl groups to yield water and surface oxygen species. It is well documented in the open literature that hydroxyl groups are strongly bound to tin dioxide [178] and have been observed to remain on the surface even under high vacuum conditions at temperatures as high as several hundred ºC [98,104]. Moreover, reduction pretreatment with H_2 had a negative effect on the intensity of this low temperature desorption peak. This provided further evidence to the hydroxyl reaction mechanism; as reduction pretreatment would lead to the dehydration of the surface, decreasing the abundance of surface hydroxyl species and thus, to lower amount of water production through the reaction between hydroxyl groups in the reduced state. During the reduction stage both rooted and isolated hydroxyl groups are supposed to be formed. Water, when formed through

reactions involving rooted hydroxyl groups, desorbs at around 130ºC. Whereas, condensation of isolated hydroxyl groups leads to water desorption above 400ºC [127]. Thus, the low temperature desorption peak may be attributed to the reaction of rooted hydroxyl groups.

The other possibility for the low temperature water desorption from catalysts, which have been subjected to pretreatment to remove physisorbed water, is the reaction between chemisorbed CO and surface hydroxyl groups yielding CO_2 and water for which the reaction sequence has been proposed above in Reactions 4.2 and 4.3. At 20ºC water formed through reaction (2), would remain over the surface and tend to desorb upon the onset of the TPD. A positive correlation between the amount of CO_2 production during the adsorption stage and the intensity of low temperature water desorption peak may be expected when Reactions 4.2 and 4.3 are considered as the prevailing reactions during adsorption stage. However, a comparison of CO_2 evolution profiles of reduced Na-PdO/SnO_2 and SnO_2 during adsorption stage reveals that, although comparable amounts of water desorption were present, CO_2 evolution from bare SnO_2 surface was lower than that of Na-PdO/SnO_2 (Figure 4.13a and 4.13c). Similarly, CO_2 evolution from reduced PdO/SnO_2 was much lower than that of oxidized SnO_2, though comparable amounts of water evolved from these catalysts (Figures 4.13a and 4.13b). As a result, there is no direct correlation between the low temperature water desorption peak and CO_2 evolution thus, the contribution of this pathway should rather be small at the temperature where adsorption was carried out. CO_2 evolution profiles presented in Figure 4.13 also depicts that the catalysts are active in CO oxidation reaction even at room temperature.

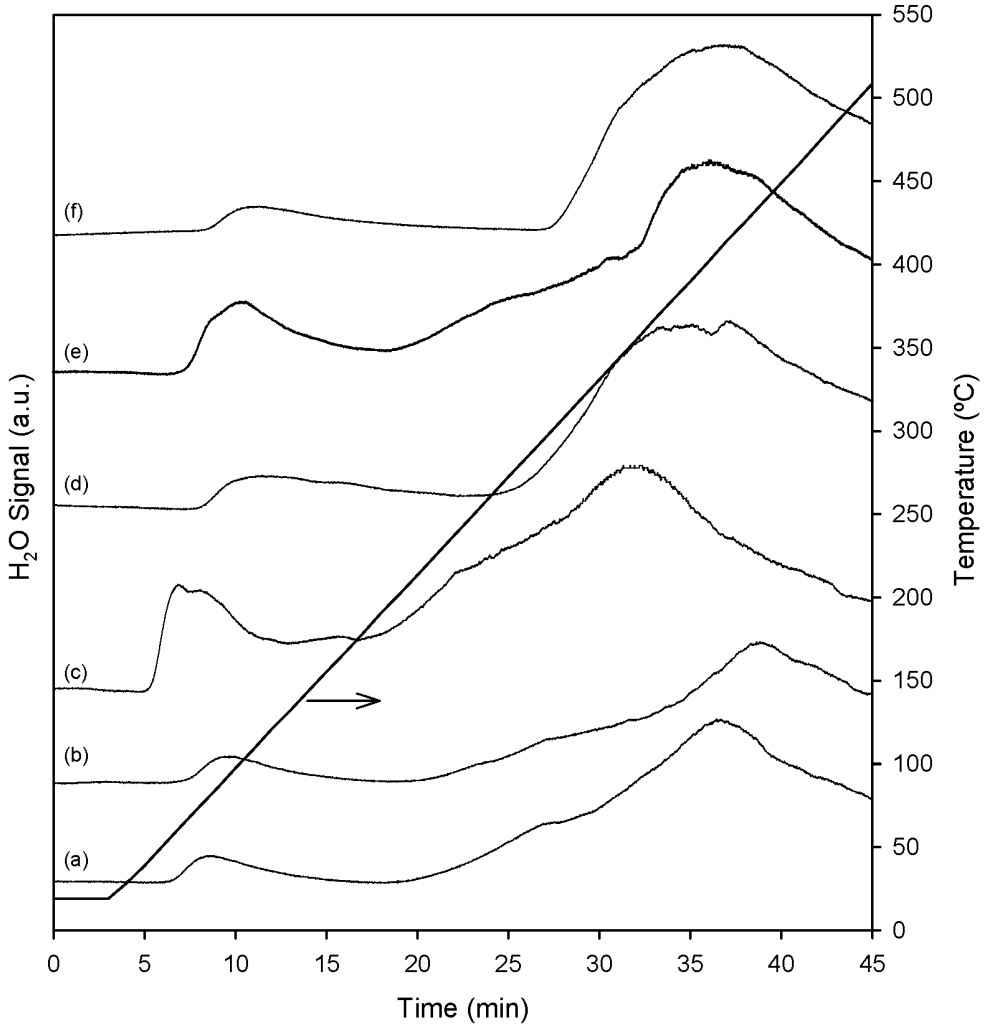

Figure 4.12 H_2O evolution profiles during post CO adsorption O_2 TPD (a) oxidized SnO_2, (b) reduced SnO_2, (c) oxidized PdO/SnO_2, (d) reduced PdO/SnO_2, (e) oxidized Na-PdO/SnO_2 and (f) reduced Na-PdO/SnO_2

(*Conditions:* P = 1 atm; [CO] = 160 ppm (adsorption); [O_2] = 200 ppm (TPD); GHSV = 12 800 hr^{-1}; catalyst weight = 100 mg; heating rate = 12°C/min)

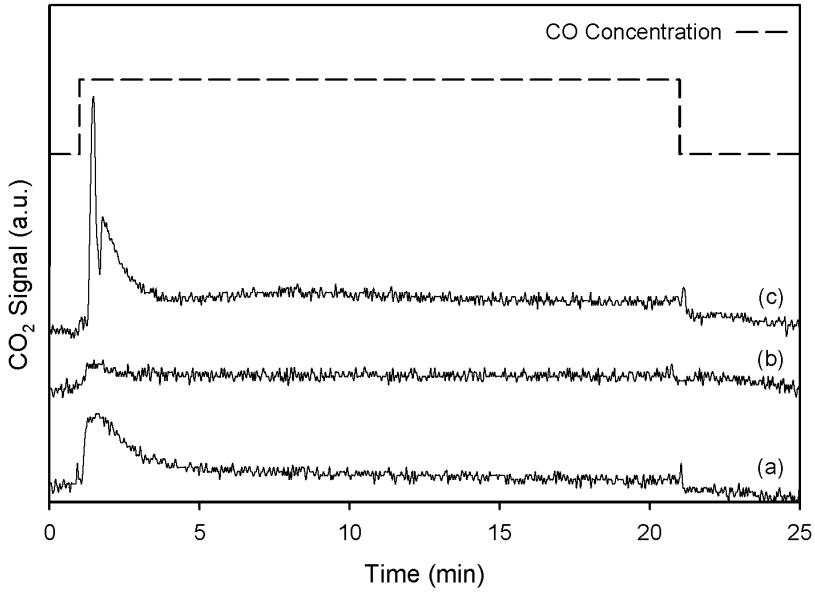

Figure 4.13 CO_2 profiles during CO adsorption (a) oxidized SnO_2, (b) reduced PdO/SnO_2 and (c) reduced Na-PdO/SnO_2

(*Conditions:* P = 1 atm; [CO] = 160 ppm; GHSV = 12 800 hr^{-1}; catalyst weight = 100 mg)

The surface dehydrating effect of reduction pretreatment was more readily observed in the low temperature shoulder of water desorption peak corresponding to 170-370ºC region. Disappearance of the shoulder corresponding to 170-300ºC over calcined samples was observed upon subjecting the catalysts to reduction pretreatment (Figures 4.12d and 4.12f). Meanwhile, a CO_2 evolution band was observed in the same temperature range over these catalysts (Figures 4.11d and 4.11f). Therefore, especially at high temperatures, the dominating reaction sequence should be Reactions 4.2 and 4.3 over reduced catalysts, where the surface abundance of hydroxyl groups was depleted during the reduction step by Reaction (4.4).

$$M-OH + H_2 \rightarrow M-H + H_2O \qquad (4.4)$$

Over oxidized catalysts, where greater amount of surface hydroxyls were present, the reaction sequence should comprise Reactions (4.1) and (4.5), below.

$$M-OH + M-OH \rightarrow H_2O + M-O + M \qquad (4.5)$$

This indicated that, in 200-300ºC region, reaction pathway leading to the formation of water through the reaction between hydroxyl groups was favored over oxidized catalysts, where surface hydroxyl groups are abundant. Over

reduced catalysts, the reaction pathway leading to the formation of CO_2 was favored as the surface has been dehydrated during the preceding reduction step.

The high temperature (200-500°C) water desorption band may result from the reaction between hydroxyl groups, but also, water production as a consequence of CO oxidation activity is another possibility. Chemisorbed carbon monoxide may react with certain hydroxyl groups to yield formate intermediate [82, 100] which decomposes above 230ºC [180] to yield CO_2 and adsorbed hydrogen atom, which may further react with a hydroxyl group to form water.

The oxygen consumption profiles of bare tin dioxide samples during temperature programmed desorption state exhibited explicit differences between the catalysts. Only a very weak oxygen uptake band was observed over both oxidized and reduced catalysts in 250-500ºC region, where a broad band of CO_2 desorption occurs from tin dioxide, indicating the incorporation of bulk oxygen in the oxidation reaction, creating an oxygen deficient tin dioxide matrix (Figures 4.14a and 4.14b). The absence of strong oxygen uptake bands in oxygen TPD evidenced that, either preceding reduction step carried out with hydrogen as the reducing agent was not sufficient to create an oxygen deficient structure at the temperature that reduction step was carried out or oxygen depleted in the reduction step could not be replenished by oxygen treatment of the support material in the temperature range studied. The fact that strong water evolution was observed in the same temperature region indicates that reaction between hydroxyl groups, leading to an oxidized surface is yet another possibility.

Low temperature CO_2 desorption from oxidized PdO/SnO_2 with the maxima at 150ºC was accompanied by O_2 uptake from the gas phase (Figure 4.14c). This indicated that surface oxygen species were immediately replenished by oxygen in the gas phase after being consumed in the reaction. This possibility has been considered as the reaction sequence of CO oxidation on PdO/SnO_2 in the presence of gas phase oxygen in the literature [51]. The oxygen uptake band observed above 250ºC was stronger in PdO/SnO_2 than in SnO_2, evidencing the influence of Pd on the activity of tin dioxide. Subjecting PdO/SnO_2 to reduction pretreatment resulted in a broad oxygen uptake band in the temperature range 150-450ºC, where surface oxygen species that have been depleted to a great extent in the preceding reduction treatment are rejuvenated (Figure 4.14d). Oxidized Na-PdO/SnO_2 gives rise to a weak oxygen uptake band in 150-180ºC region, and a high temperature oxygen uptake band which was stronger relative to the unpromoted counterpart (Figure 4.14e). Over reduced sample of Na-

PdO/SnO_2, a broad band of oxygen uptake was observed in 80-230ºC region, and this band corresponded to lower temperatures than the oxidation band of PdO/SnO_2 (Figure 4.14f). This indicated that, at temperatures below 200ºC, sodium promoted catalysts were more readily oxidized than unpromoted PdO/SnO_2.

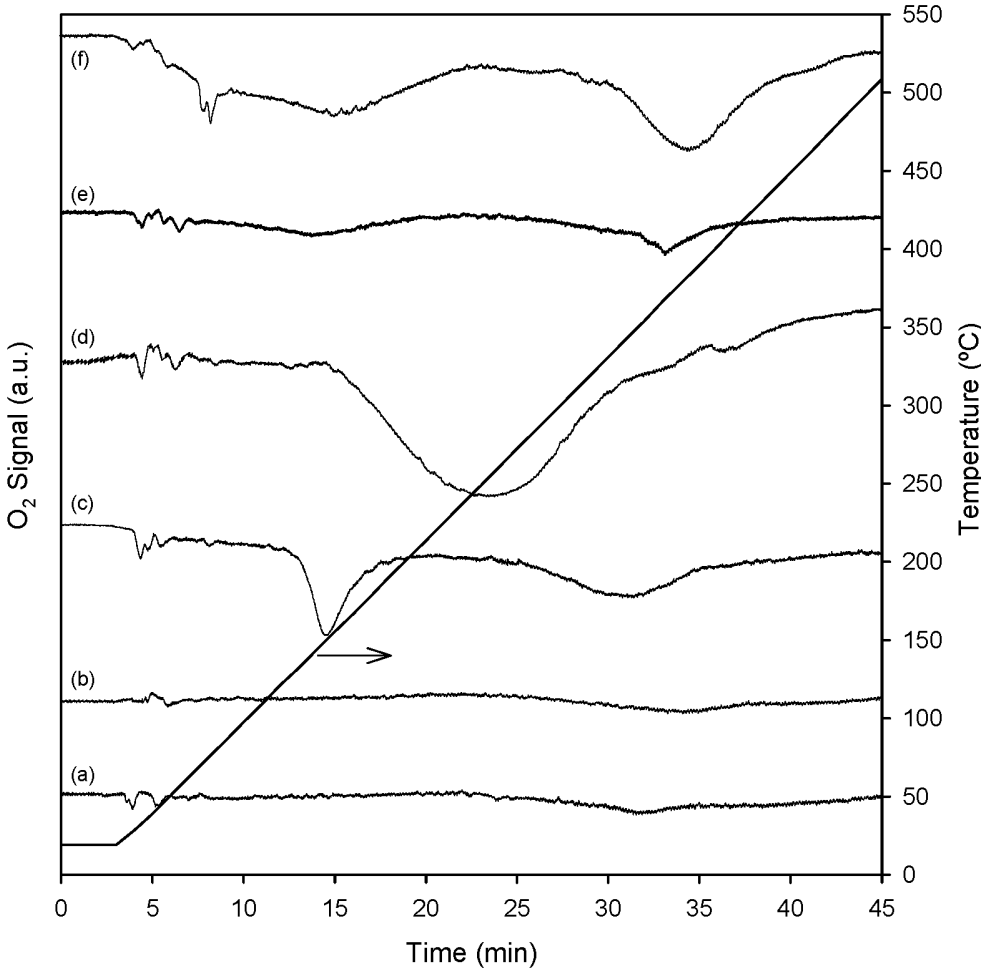

Figure 4.14 O_2 consumption/evolution profiles during post CO adsorption O_2 TPD (a) oxidized SnO_2, (b) reduced SnO_2, (c) oxidized PdO/SnO_2, (d) reduced PdO/SnO_2, (e) oxidized Na-PdO/SnO_2 and (f) reduced Na-PdO/SnO_2

(*Conditions:* P = 1 atm; [CO] = 160 ppm (adsorption); [O_2] = 200 ppm (TPD); GHSV = 12 800 hr^{-1}; catalyst weight = 100 mg; heating rate = 12°C/min)

Unlike SnO_2 and PdO/SnO_2, high temperature CO_2 evolution was accompanied by a strong oxygen uptake band for reduced sodium promoted catalyst. Similarly, no increase in CO_2 and water evolution was observed on sodium promoted catalyst relative to unpromoted PdO/SnO_2 and the bare support within the temperature range of 330-400°C, which could be coupled with the oxygen uptake band as it is seen from Figures 11f and 14f. It was concluded that this band resulted from the oxidation of the catalyst. Therefore, it is a strong possibility that, tin dioxide is also partially reduced during the pre-reduction step for sodium promoted catalysts as a result of surface oxygen bond weakening.

4.1.5.2 CO and O_2 Co-adsorption-O_2 TPD Studies

It is known that carbon monoxide and oxygen competitively adsorb on Pd surfaces [51-53] therefore, a study similar to the abovementioned CO adsorption/O_2 TPD studies was performed by co-adsorbing CO and O_2 on the catalysts, by keeping the oxygen during the TPD stage unchanged for the comparability of the results with CO adsorption/O_2 TPD experiments. The basic motive in supplying oxygen together with carbon monoxide was to validate that oxygen could not be adsorbed on carbon monoxide precovered transition metal surfaces as its adsorption was inhibited by the presence of CO [106, 109,110]. Therefore, changes in the species desorption profiles were expected as a natural consequence of co-adsorption of these molecules.

Post adsorption O_2 TPD studies performed with CO and O_2 co-adsorbed catalysts marked several important differences between catalysts, though the general appearance of the adsorption/desorption profiles of the species was not changed. The activity of the bare support was not affected by the addition of oxygen to the gas phase during adsorption stage (Figures 4.15a and 4.15b) and approximately the same amount of CO_2 evolution (3 $\mu mol/m^2$ cat.) as CO-only adsorbed catalyst was observed. Over oxidized and reduced PdO/SnO_2 co-adsorption resulted in a decrease in the intensity of both low and the high temperature CO_2 evolution bands (Figures 4.15c and 4.15d) with regard to the CO-only adsorption studies. Over oxidized PdO/SnO_2 1.44 $\mu mol/m^2$ cat. of CO_2 desorption was observed in the low temperature region and this corresponded to a three-fold decrease in the activity when compared to CO-only adsorbed catalyst. Similarly, in the high temperature range, 1.63 $\mu mol/m^2$ cat. of CO_2 evolution was present, which again corresponded to a three-fold decrease in the activity with respect to CO-only adsorbed catalyst. In the reduced state, 0.31

μmol/m^2 cat. of CO_2 evolution was observed from PdO/SnO_2 in the low temperature range, which was a quite insignificant decrease when compared to more than three-fold decrease in the activity in the high temperature range.

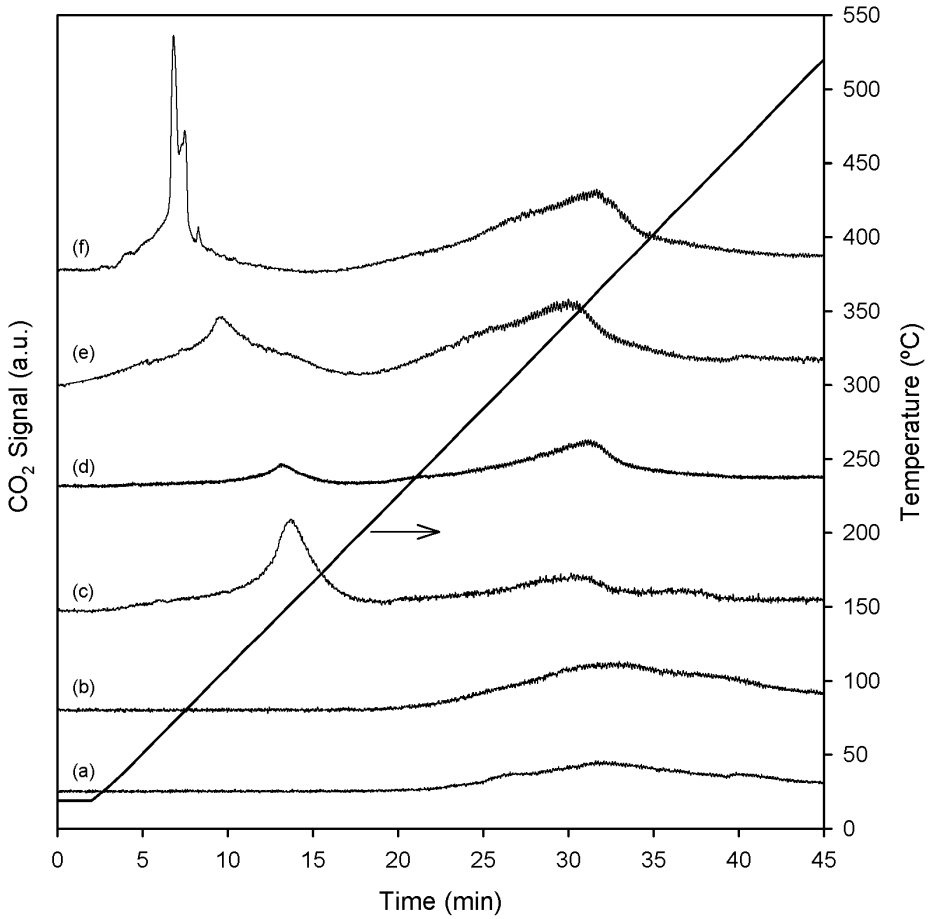

Figure 4.15 CO_2 evolution profiles during post CO-O_2 co-adsorption O_2 TPD (a) oxidized SnO_2, (b) reduced SnO_2, (c) oxidized PdO/SnO_2, (d) reduced PdO/SnO_2, (e) oxidized Na-PdO/SnO_2 and (f) reduced Na-PdO/SnO_2

(*Conditions:* P = 1 atm; [CO] = 160 ppm and [O_2] = 160 ppm(adsorption); [O_2] = 200 ppm (TPD); GHSV = 12 800 hr^{-1}; catalyst weight = 100 mg; heating rate = 12°C/min)

The oxygen uptake profile appeared to be parallel to the CO_2 profile. Over oxidized PdO/SnO_2, the intensity of oxygen uptake band was decreased, which is parallel to the decrease in the intensity of CO_2 evolution from this catalyst (Figure 4.16c) indicating both CO and O_2 are adsorbed over the surface and less CO is adsorbed when compared to CO adsorption. The intensity of the low temperature CO_2 evolution band was very sensitive to reduction pretreatment,

regardless of whether oxygen was supplied or not in the adsorption stage. The number of PdO sites decreases to a great extent in reduced catalysts as a consequence of contact with hydrogen, which is a strong reducing agent, and these sites could not be fully replenished by oxygen TPD of reduced catalysts below 150ºC, where the onset of a broad oxygen uptake band was observed, thus a decrease in the activity is observed when catalysts are subjected to reduction pretreatment. Baraton et *al.* [101] have also reported that the subsequent additions of oxygen did not totally restore the oxidation state of the catalyst but, instead, repetitive 'CO addition-evacuation-oxygen addition' sequences caused a steady overall reduction of tin dioxide powder at 150ºC. When oxygen was present in the gas phase the oxide catalyst is replenished by adsorbing oxygen from the gas phase. The oxygen uptake band observed over reduced PdO/SnO_2 was weaker over CO and O_2 co-adsorbed PdO/SnO_2 catalyst than over CO-only adsorption (Figure 4.16d). An increased number of sites would be occupied by ionosorbed oxygen during the adsorption and TPD stages and this would both hinder reduction of the surface by carbon monoxide because some sites for CO adsorption would be occupied by ionosorbed oxygen and decrease oxygen uptake of the surface during TPD.

Contrarily, on both oxidized and reduced Na-PdO/SnO_2, oxygen addition during CO adsorption had a positive effect on both low and high temperature activities and this is an indication that sodium promotion acted in a way to offset the inhibitory effect of both of the species on each other (Figures 4.15e and 4.15f). As opposed to a small increase in the amount of CO_2 desorption in both low and high temperature activity regions of oxidized Na-PdO/SnO_2 relative to CO-only adsorbed catalysts, 1.17 $\mu mol/m^2$ cat. of CO_2 evolution was observed over reduced Na-PdO/SnO_2 in the low temperature region. This corresponds to greater than three-fold increase in the activity. Similarly, in the high temperature range, amount of CO_2 evolution was increased from 1.09 $\mu mol/m^2$ cat. over CO-only adsorbed catalyst to 3.15 $\mu mol/m^2$ cat. over CO and O_2 co-adsorbed catalyst. Over oxidized Na-PdO/SnO_2, two weak oxygen uptake bands were observed and a broad band of oxygen uptake below 200ºC, which can be ascribed to the oxidation of the surface, accompanied these in the case of reduced Na-PdO/SnO_2 (Figures 4.16e and 4.16f). In control experiments performed with the oxidized and reduced support, it was observed that presence of gas phase oxygen had almost no effect on the activity of tin dioxide, thus, adsorption of CO, rather than oxygen adsorption, was the limiting factor for CO oxidation over tin dioxide surface (Figures 4.16a and 4.16b).

Together with the well documented role of weakening the C-O bond in CO chemisorbed on alkali metal promoted Pd surfaces, alkali metals tend to increase the adsorption strength of electronegative adsorbates, such as CO, NO and O_2, the effect being more pronounced in the case of oxidants [137]. The results in the present study also suggest that, addition of alkali metals also act to enhance oxygen adsorption, as sodium promoted catalysts subjected to reduction pretreatment are more readily oxidized than their unpromoted counterparts, Thus, especially in reduced state, Na promoted catalysts possess an increased oxygen affinity. As a result, oxygen coverage at the surface is increased while CO coverage decreases [181] when compared to PdO/SnO_2.

The effects observed during the O_2-TPD studies are understandable in terms of the alkali-mediated variation in the surface coverage of carbon monoxide and oxygen. In general, unpromoted PdO/SnO_2 catalysts perform well if oxygen competition for the active sites is not present during CO exposure while, sodium promoted PdO/SnO_2 exhibits a superior activity when oxygen is competitively adsorbed on the surface, especially when the catalyst is initially free from adsorbed oxygen species at the onset of adsorption. The promotion of oxygen interaction with PdO/SnO_2 surface by the presence of the alkali metal has been observed through XPS analysis and has been postulated to result in superior catalytic activity of Na-PdO/SnO_2 that has been observed through the activity tests under transient and steady state conditions. The increased oxygen chemisorption capacity of the sodium promoted surface is not readily observed in CO-only adsorption/O_2 TPD studies as sodium promotion also enhances CO adsorption. The increased CO chemisorption capability leads to hindrance of oxygen adsorption and hence, the activity of the surface is limited by oxygen depletion on the surface. Addition of oxygen during adsorption stage rules out this effect as oxygen would be capable of competing for the active sites. When oxygen is competitively adsorbed on PdO/SnO_2 surface, CO adsorption is hindered by the blockage of active sites by oxygen, and as oxygen adsorbs dissociatively it essentially blocks ten sites for CO adsorption [52]. Thus, during co-adsorption over PdO/SnO_2 though the surface becomes enriched in oxygen, the presence of oxygen on the surface tends to inhibit CO chemisorption and the activity of Pd clusters decreases due to CO depletion on the surface.

Figure 4.17 presents the water desorption profiles acquired during the experiments. The water desorption profiles were in agreement with those obtained during CO-only adsorption/O_2 TPD studies: two water desorption bands

were observed and the low temperature water desorption peak was larger in intensity for oxidized catalysts than in their reduced counterparts. Presence of gas phase oxygen during adsorption had a positive effect on the low temperature water desorption bands of sodium promoted catalysts (Figures 4.17e and 4.17f) while it had an adverse effect on PdO/SnO_2 (Figures 4.17c and 4.17d). Over oxidized PdO/SnO_2, in 50 – 190ºC range, evolution of 1.88 $\mu mol/m^2$ cat. of H_2O was observed and this presented approximately three-fold decrease relative to CO-only adsorbed catalyst. Contrarily, over oxidized Na-PdO/SnO_2 a two-fold increase to 9.41 $\mu mol/m^2$ cat. was observed upon CO and O_2 co-adsorption. The high temperature band was almost unaffected by the adsorption stage.

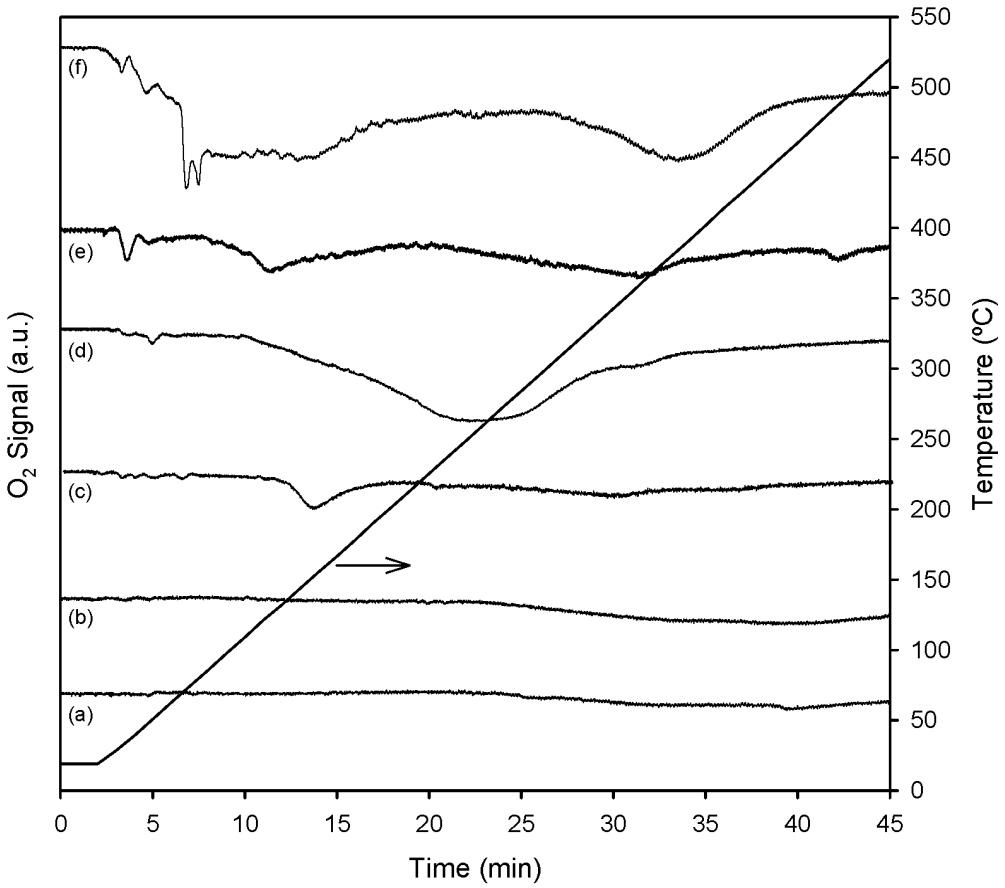

Figure 4.16 O_2 consumption/evolution profiles during post CO-O_2 co-adsorption O_2 TPD (a) oxidized SnO_2, (b) reduced SnO_2, (c) oxidized PdO/SnO_2, (d) reduced PdO/SnO_2, (e) oxidized Na-PdO/SnO_2 and (f) reduced Na-PdO/SnO_2

(*Conditions:* P = 1 atm; [CO] = 160 ppm and [O_2] = 160 ppm(adsorption); [O_2] = 200 ppm (TPD); GHSV = 12 800 hr^{-1}; catalyst weight = 100 mg; heating rate = 12°C/min)

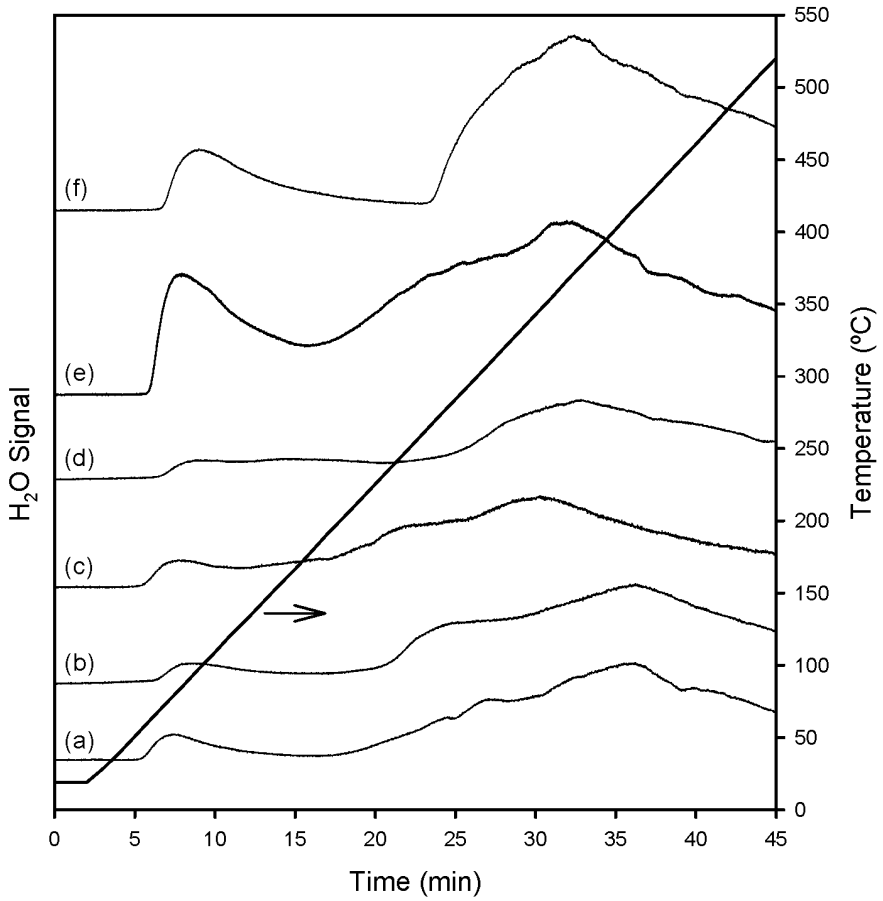

Figure 4.17 H_2O evolution profiles during post CO-O_2 co-adsorption O_2 TPD (a) oxidized SnO_2, (b) reduced SnO_2, (c) oxidized PdO/SnO_2, (d) reduced PdO/SnO_2, (e) oxidized Na-PdO/SnO_2 and (f) reduced Na-PdO/SnO_2

(*Conditions:* P = 1 atm; [CO] = 160 ppm and [O_2] = 160 ppm(adsorption); [O_2] = 200 ppm (TPD); GHSV = 12 800 hr^{-1}; catalyst weight = 100 mg; heating rate = 12°C/min)

As can be seen from Figure 4.13 the catalysts are active even at room temperature. With the motive of observing the activity of the catalysts at sub-ambient temperatures CO and O_2 were co-adsorbed on the catalyst surfaces at temperatures below room temperature. The co-adsorption temperature of -68ºC corresponds just above the freezing point of CO_2, which is -79ºC. Sub-ambient co-adsorption of CO and O_2 results in weaker desorption bands when compared to ambient co-adsorption (Figure 4.18). Besides an insignificant decrease in the intensity of the CO_2 desorption bands no change is observed in CO_2 evolution profiles of both calcined and reduced SnO_2 catalysts (Figures 4.18a and 4.18b). The high temperature CO_2 desorption band appears at 280-500ºC region (T_{max} = 400ºC) on SnO_2 catalysts. Meanwhile, the high temperature activity, which has

been attributed to SnO_2 previously, was observable again on PdO/SnO_2 and Na-PdO/SnO_2 catalysts with again an insignificant change in its intensity (Figures 4.18c to 4.18f). The changes in the intensity are more pronounced when the low temperature CO_2 evolution bands, with T_{max} around 150ºC, are compared. An additional strong CO_2 desorption band below -10ºC is observed on upon shifting the co-adsorption temperature to -68ºC and this constitutes the major difference between ambient and sub-ambient co-adsorption studies. This activity was observed to be highly sensitive to minor changes in the adsorption conditions on repeated experiments. However, the observed room temperature activity can be postulated to arise from the activity of these centers.

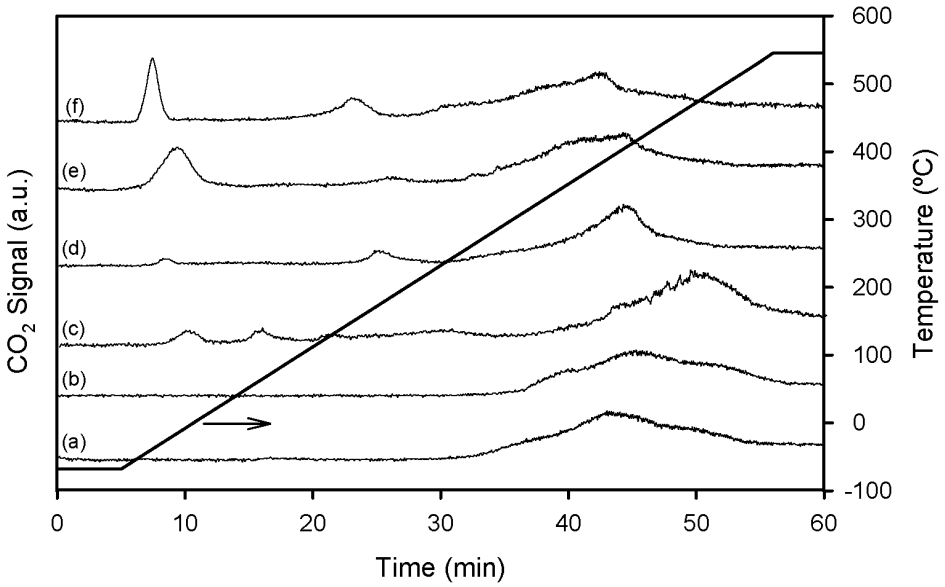

Figure 4.18 CO_2 evolution profiles during post CO-O_2 co-adsorption He TPD (a) oxidized SnO_2, (b) reduced SnO_2, (c) oxidized PdO/SnO_2, (d) reduced PdO/SnO_2, (e) oxidized Na-PdO/SnO_2 and (f) reduced Na-PdO/SnO_2

(*Conditions:* P = 1 atm; [CO] = 160 ppm and [O_2] = 160 ppm(adsorption); [O_2] = 200 ppm (TPD); GHSV = 12 800 hr^{-1}; catalyst weight = 100 mg; heating rate = 12°C/min)

4.1.6 Surface Titration Experiments with Impulse Technique

The transient pulse technique comprises the injection of a fixed amount of CO to the carrier gas at specified time intervals; the evolution of the reactive tracer from the reactor allows the deduction of data related to the catalyst dispersion, kinetics of the reaction, adsorption and desorption, the oxygen content of the surface, the accessibility of the reactive sites by the reactant and also, the rate

of oxygen diffusion from subsurface layers. 1 ml doses of 1 % CO/He (0.42 μmol CO/injection) were injected over oxidized and reduced samples of PdO/SnO_2 and Na-PdO/SnO_2 which were kept under inert He flow at 150ºC and 20ºC to observe the effect of both the initial state of the metal and temperature on the CO oxidation activity. Control experiments were also carried out over oxidized and reduced SnO_2 to observe the extent of SnO_2 contribution to the CO oxidation activity of the catalysts in absence of gas phase oxygen.

Over bare SnO_2, regardless of the pretreatment procedure, the evolution of an insignificant amount of CO_2 was observed at 20ºC (Figures 4.19a and 4.19b). Moreover, a comparison of the mass spectra collected at 20ºC with the one 150ºC showed that no pronounced effect of raising the reactor temperature from 20ºC to 150ºC was present on either oxidized or reduced SnO_2 (Figures 4.19c and 4.19d). When the amount of CO and CO_2 evolved from the reactor with each pulse was calculated by integrating the area under CO and CO_2 mass signal peaks, evolution of nearly the entire CO injected to the reactor (0.42 μmol) was observed, showing that the CO adsorption capacity of SnO_2 was poor as well, regardless of the preceding treatment procedure. Previously, SnO_2 was observed to be active in CO oxidation at temperatures above 200ºC, thus the presence of the negligible activity of the catalyst in transient pulse studies carried out below 200ºC is in line with the previous study. Moreover, any activity to be observed on PdO/SnO_2 and Na-PdO/SnO_2 can be isolated from the activity of the bare support and should be attributed to Na, Pd and as well to the interactions of Pd with Sn in these catalysts under the experimental conditions that were applied.

When successive doses of CO were injected over oxidized and reduced PdO/SnO_2 and Na-PdO/SnO_2 at 150ºC and 20ºC, oxidized catalysts were observed to exhibit a remarkable activity at 150ºC and a considerable loss of activity was observed upon decreasing the reactor temperature to 20ºC (Figure 4.20). This observation is clearly related to the decrease in the rates of reaction and to the mobility of ad-species with temperature.

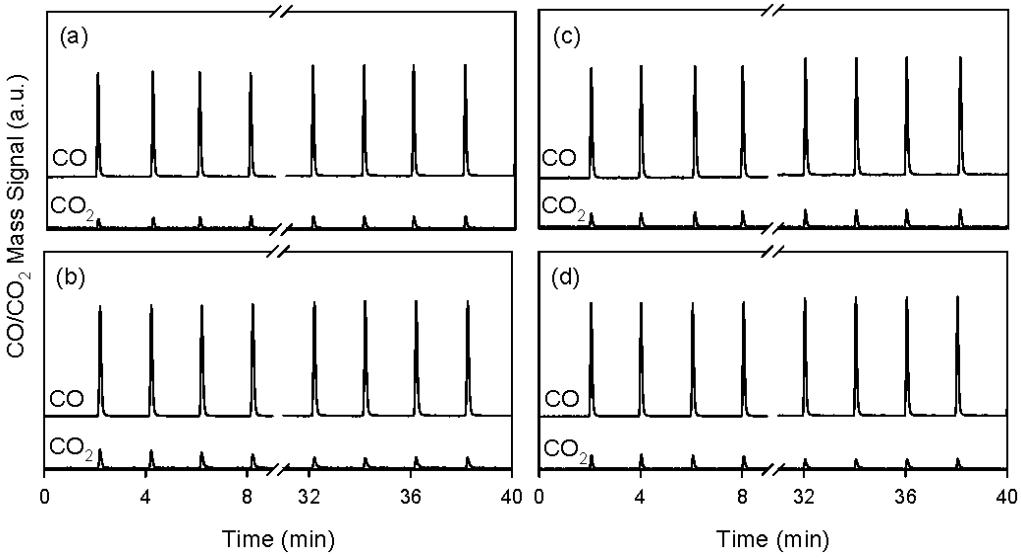

Figure 4.19 CO and CO_2 evolution from (a) oxidized SnO_2 (20ºC), (b) reduced SnO_2 (20ºC), (c) oxidized SnO_2 (150ºC) and (d) reduced SnO_2 (150ºC)

(*Conditions:* P = 1 atm; V_{inj} = 1 ml; n_{CO} = 0.42 μmol/injection; GHSV = 12 800 hr^{-1}; catalyst weight = 100 mg)

At 150ºC, PdO/SnO_2 yields better conversion of CO than Na-PdO/SnO_2 but, the amount of CO adsorbed on both of the surfaces was lower than the amount adsorbed at 20ºC (Figures 4.20c and 4.20d). This could be explained by assuming that, although the catalytically active phase for CO oxidation has been identified to be PdO, the existence of Pd^0 sites is necessary for CO adsorption. At 20ºC, the reduction of PdO to create vacancies for CO adsorption is not favored though CO adsorption is thermodynamically favored. The XPS data of Na-PdO/SnO_2 suggests that oxygen species were abundant in the surface layers of the catalyst and these species were stable even at the high vacuum environment of ESCA. Desorption of these oxygen species is not favored at 20ºC and they block CO adsorption sites thus only an insignificant amount of CO could be adsorbed on Na-PdO/SnO_2 surface. Similarly, amount of oxygen species is lower in PdO/SnO_2 and greater amount of CO could be adsorbed on the surface. In either case, regardless of the amount of CO adsorption, little amount of oxygen species would be reactive at 20ºC, therefore, only a small amount of CO would be oxidized and the remainder would hinder further adsorption of CO in subsequent doses. This is observed as the diminishing of the limited activity of PdO/SnO_2 catalyst after seven pulses.

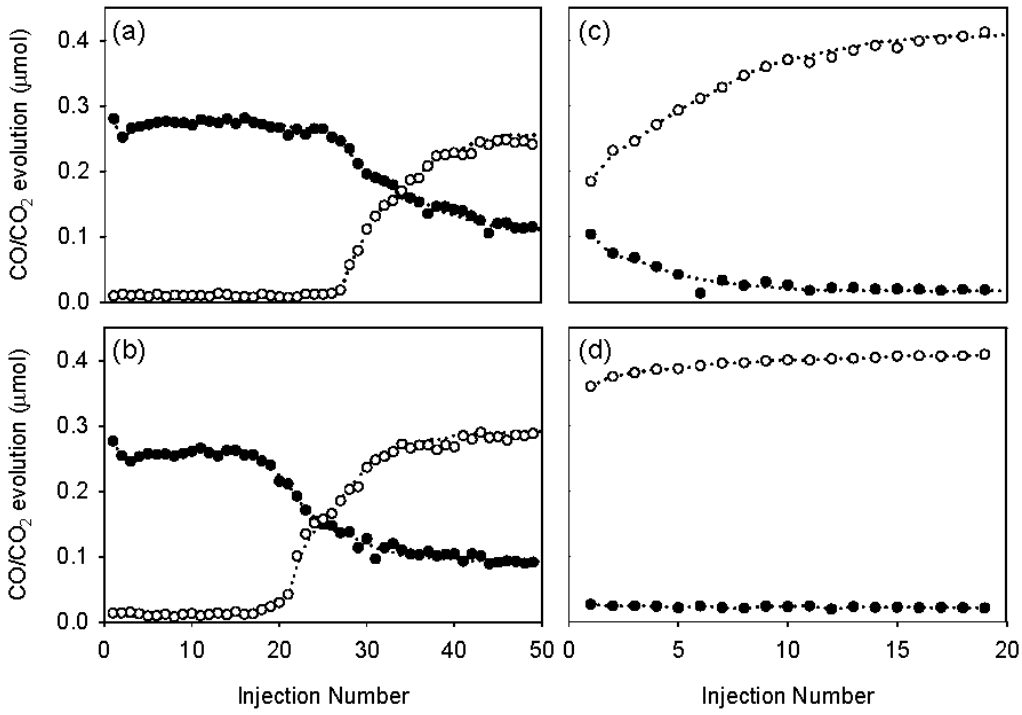

Figure 4.20 CO (○) and CO_2 (●) evolution from (a) oxidized PdO/SnO_2 (150ºC), (b) oxidized Na-PdO/SnO_2 (150ºC), (c) oxidized PdO/SnO_2 (20ºC) and (d) oxidized Na-PdO/SnO_2 (20ºC)

(*Conditions:* P = 1 atm; V_{inj} = 1 ml; n_{CO} = 0.42 μmol/injection; GHSV = 12 800 hr^{-1}; catalyst weight = 100 mg)

Over oxidized PdO/SnO_2, the first 27 doses of CO was converted to CO_2 at 150ºC and then the activity leveled off reaching a steady-state value (Figure 4.20a). The decrease in the activity in subsequent doses may be caused by two independent factors: the decrease in the amount of reactive oxygen species and the deposition and retaining the CO species over the surface. At this temperature, the most probable reaction pathway for the oxidation of CO to CO_2 is the reaction of chemisorbed CO with ionosorbed oxygen species, so that exactly the same amount of CO_2 as the amount of consumed CO would evolve from the surface. However, the evolution of smaller amount of CO_2 than the reaction stoichiometry was observed, and this suggests the accumulation of C-containing species over the surface. One probability is the CO_2 formation through Boudart's reaction (Reaction 4.6), which leads to the formation of adsorbed C-species. These carbon species would eventually be oxidized to CO_2 over the surface and desorb, but their retention over the surface would be longer and thus, these species would block the active sites. A mechanism for the oxidation of C-species involves the incorporation of bulk oxygen via diffusion of these

species to the surface layers (Reaction 4.7) and this mechanism will be discussed in detail together with the intermittently delayed injections.

$$M-CO + M-CO \longrightarrow M + M-C + CO_2 \quad (4.6)$$

$$M-C + M-O^{*}_{diffused} \rightarrow 2M + CO_2 \quad (4.7)$$

Yet, another surface blocking species is formate. Formate is an intermediate which forms during the course of the reaction of chemisorbed CO with hydroxy groups [100,182] and it is known to be stable on SnO_2 surface up to 230ºC [180], where it decomposes to CO_2 and hydrogen atom. At 150ºC, formation of formate, which is stable at that temperature, would decrease the activity as it would block sites for CO oxidation. Formation of formate rather than C-deposition could be more probable on oxidized catalysts since oxygen and hydroxy groups are abundant on the surface to oxidize CO through Reactions 4.1 and 4.2.

Over Na-PdO/SnO_2, a trend similar to PdO/SnO_2 was observed but the initial high activity transient lasted for the first 19 doses of CO only (Figure 4.20b). Considering the XPS data, this observation suggests that, though more surface oxygen was observed to exist on Na-PdO/SnO_2, these oxides are more stable than the surface oxides of PdO/SnO_2. Similar results were also reported for the alkali-metal promoted Re_2O_7/TiO_2 and Re_2O_7/Al_2O_3 systems where $NaReO_2$ ternary oxide increased the reduction temperature of the catalysts and the increase in temperature was well correlated with the amount of alkali added till Na/Re ratio increased to 1, where sufficient sodium was present in the structure to stabilize all rhenium in $NaReO_4$ form [162].

As a further investigation of the CO oxidation activity of the catalysts, samples were subjected to reduction pre-treatment by employing H_2 as the reducing agent. At 150ºC, the activity of PdO/SnO_2 observed in the oxidized sample was seen deteriorate upon reduction pretreatment and the first 5 doses of CO was chemisorbed in a decreasing extent over the surface (Figure 4.21a). The chemisorbed CO was not oxidized, most probably due to the lack of ionosorbed oxygen species. Unlike PdO/SnO_2, Na-PdO/SnO_2 was seen to preserve part of its activity after reduction pretreatment (Figure 4.21b). This activity was comparable to that of the oxidized sample however; it leveled off after the first five doses of CO. This indicates that some of the reactive oxygen species were more stable than the oxygen species of PdO/SnO_2 and thus, did not deteriorate

completely during reduction treatment which, may diffuse to the surface and promote the oxidation reaction at the surface.

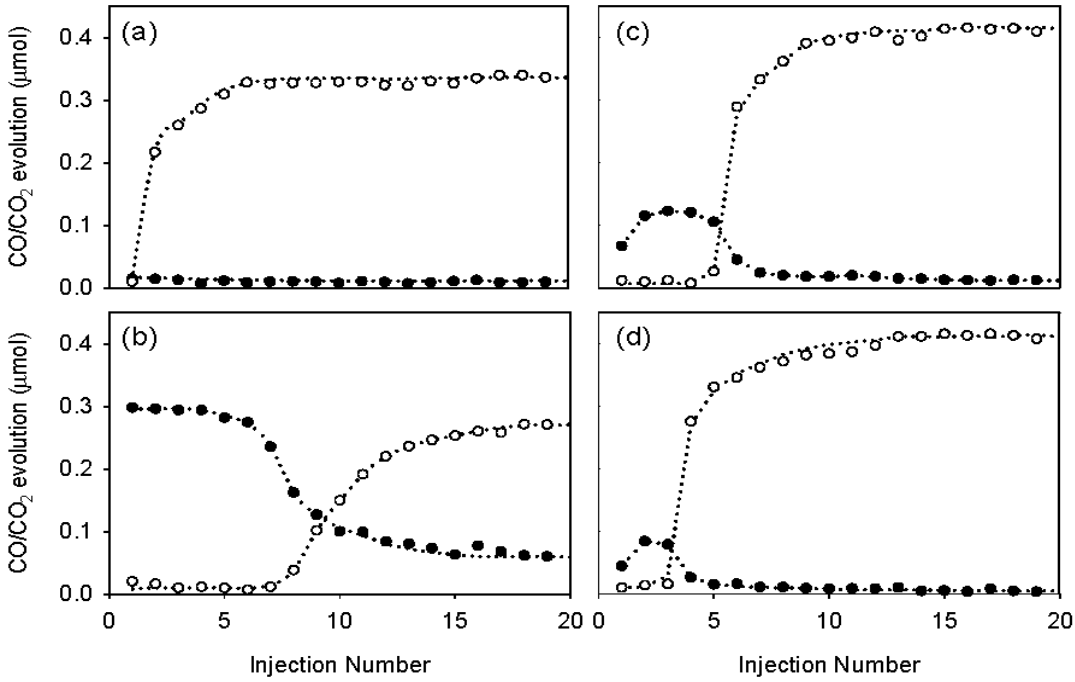

Figure 4.21 CO (○) and CO_2 (●) evolution from (a) reduced PdO/SnO_2 (150ºC), (b) reduced Na-PdO/SnO_2 (150ºC), (c) reduced PdO/SnO_2 (20ºC) and (d) reduced Na-PdO/SnO_2 (20ºC)

(*Conditions:* P = 1 atm; V_{inj} = 1 ml; n_{CO} = 0.42 µmol/injection; GHSV = 12 800 hr^{-1}; catalyst weight = 100 mg)

While the other evidences for oxygen diffusion from the bulk would be discussed later, the species mass signal peaks appeared to be much wider in the case of the reduced catalysts and as well, the longer time lag between the injection of the CO dose to the reactor and the observation of CO/CO_2 in the mass signal in reduced catalysts relative to oxidized ones also suggests that the process was limited with oxygen diffusion. Figure 4.22 presents the CO_2 mass signals collected after the 20th dose of CO injected over oxidized and reduced Na-PdO/SnO_2. As a consequence of the depletion of reactive oxygen species during reduction pretreatment, the rate of reaction appears to be much lower over reduced catalyst as opposed to the oxidized counterpart, and to provide a basis for better comparison, the CO_2 spectrum of the reduced catalyst was enlarged 5 times (Figure 4.22a). The FWHM of these peaks was measured as 10.7 and 25.3 seconds, for oxidized and reduced catalysts, respectively. The broadening of CO_2

evolution peak in reduced Na-PdO/SnO_2 suggested to be a consequence of the decreased rate of reaction, which is controlled by oxygen diffusion from the bulk of the catalyst.

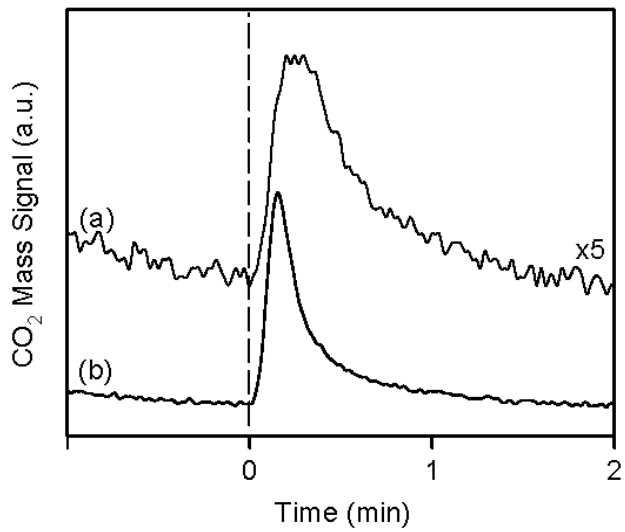

Figure 4.22 CO_2 evolution from (a) reduced Na-PdO/SnO_2 and (b) oxidized Na-PdO/SnO_2

(*Conditions:* P = 1 atm; V_{inj} = 1 ml; n_{CO} = 0.42 μmol/injection; GHSV = 12 800 hr^{-1}; catalyst weight = 100 mg)

Both of the catalysts were observed to behave similarly in reduced form at 20ºC (Figures 4.21c and 4.21d). An initial transient activity was observed in the first couple of CO doses and diminished upon successive injections. This observation supports the conclusion that the limiting step in CO oxidation over the oxidized catalysts was the occupation of the sites for CO adsorption by oxygen species, because when sites for CO adsorption were vacated through reduction pretreatment, CO was oxidized to CO_2 even by the reduced catalysts where reactive oxygen species were depleted by reduction pretreatment. This activity may result from the reaction of two chemisorbed CO molecules to yield CO_2 and adsorbed C. Yet, another alternative is the reaction of a chemisorbed CO with hydroxy species to yield formate species. During the experiments, formate species (m/z = 45 amu) was also monitored with MS however, the evolution of these species was not observed, most probably because these species were retained on the surface at the temperatures studied. Through TPD studies with these catalysts, water evolution coupled with CO_2 production was observed above 200ºC and a possible reaction pathway for water evolution has been

proposed as the decomposition of formate species to yield CO_2 and an adsorbed hydrogen atom where, this adsorbed atom further reacted with a hydroxy group to yield water. A transient pulse technique which has been applied in this study does not allow any further discussion about the hydroxy species because of the weak resolution of water (m/z=18) signal under the transient pulse conditions.

As well as the periodic doses, intermittently delayed doses of CO were injected to the reactor after the periodic doses to verify and strengthen the possibility of limitation of reaction by oxygen diffusion (Figures 4.23 and 4.24). Delayed doses were injected at 4th, 10th and 25th minute following the last dose of each run. Delayed injections did not cause changes in the amount of CO/CO_2 evolution in the case of bare SnO_2, which shows that neither CO adsorption nor CO_2 production was affected by delaying injections. Contrary to the bare support, increased pulse delays yields higher CO_2 evolution over PdO/SnO_2 and Na-PdO/SnO_2 catalysts. No change in the CO oxidation activity was observed over both of the oxidized catalysts at 20ºC, but a slight increase in the amount of CO chemisorbed was present (Figures 4.21c and 4.21d). In Figures 4.21 and 4.24 the amount of CO_2/CO evolved during the last dose of the periodic doses was included to demonstrate the trend observed upon delaying the pulses and this data constitutes the first data point in each set. Upon rising the temperature to 150ºC, CO_2 evolution increases on both of the catalysts, as a result of delayed injections (Figures 4.21a and 4.21b). The amount of CO_2 evolution was directly correlated with the amount delay between the intermittent injections. The effect of intermittent doses was more pronounced on Na-PdO/SnO_2. This suggests that at 150ºC a substantial extent of oxygen diffusion was present to promote the surfaces, but oxygen diffusion in Na-PdO/SnO_2 catalyst was more effective in promoting this catalyst, when compared to the alkali-free counterpart. Meanwhile, at 20ºC the effect of diffusion is not observed since the reaction is limited to CO adsorption rate rather than presence of oxygen species on the surface, over oxidized catalysts and the rate of oxygen diffusion in solid matrix is not favored at low temperatures.

Through the same type of experiments on reduced catalysts, it was observed that oxygen diffusion from the subsurface layers was not able to effectively promote PdO/SnO_2 surface at both of the temperatures studied, and delaying the pulses caused only a slight increase in the amount of CO_2 production relative to the last injection of the periodic doses upon delaying the injections (Figures 4.24a and 4.24c). However, an increasing amount of CO injected in each delayed

dose was adsorbed on the surface. This can be attributed to either the mobility of CO on the surface, that adsorbed species diffuse to other sites leaving vacant sites for adsorption but are not oxidized due to oxygen depletion or oxidation of CO through reaction with hydroxy groups, in the absence of oxygen species, that stable formate species are formed. In either case, evolution of CO_2 from the reactor would not be observed.

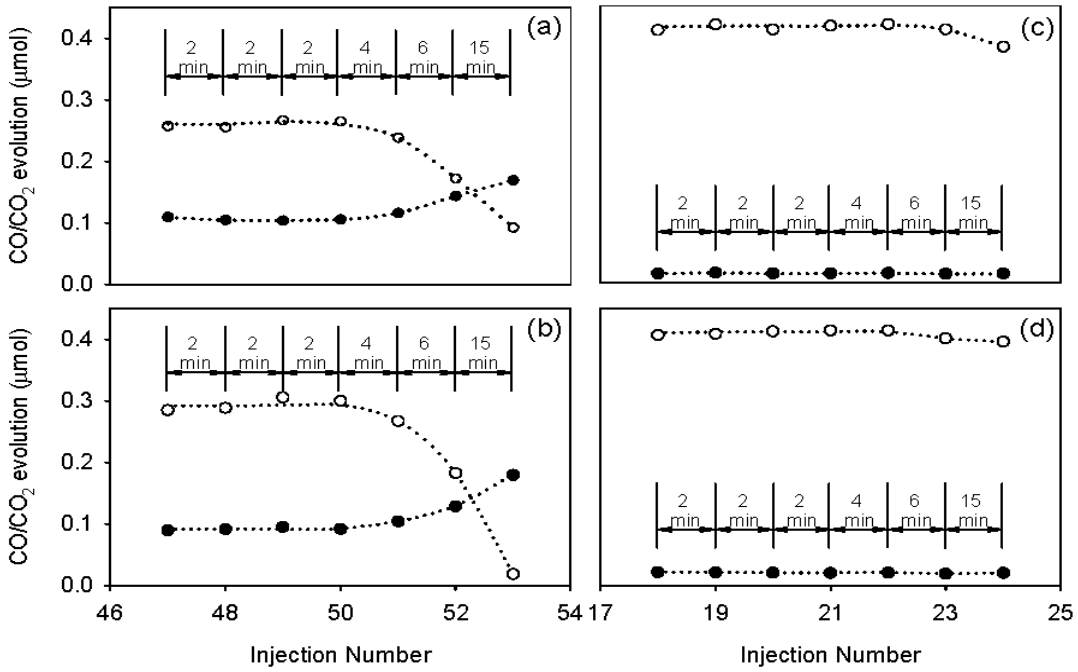

Figure 4.23 CO (○) and CO_2 (●) evolution from (a) oxidized PdO/SnO_2 (150ºC), (b) oxidized Na-PdO/SnO_2 (150ºC), (c) oxidized PdO/SnO_2 (20ºC) and (d) oxidized Na-PdO/SnO_2 (20ºC) during intermittently delayed injections of CO

(*Conditions:* P = 1 atm; V_{inj} = 1 ml; n_{CO} = 0.42 μmol/injection; GHSV = 12 800 hr^{-1}; catalyst weight = 100 mg)

Delayed injections resulted in an increase in the CO oxidation activity of alkali-metal promoted PdO/SnO_2 at 150ºC (Figure 4.24b) and caused no change at 20ºC (Figure 4.24d). At both of the temperatures the amount of CO evolving from the reactor was decreased but only at 150ºC adsorbed CO was oxidized to CO_2. These results show that, at 20ºC oxygen species are not mobile enough in either of the catalysts to replenish surface oxygen species and to increase the CO oxidation activity and at 150ºC oxygen species are more mobile in Na-PdO/SnO_2 and replenish the surface oxygen more effectively than PdO/SnO_2.

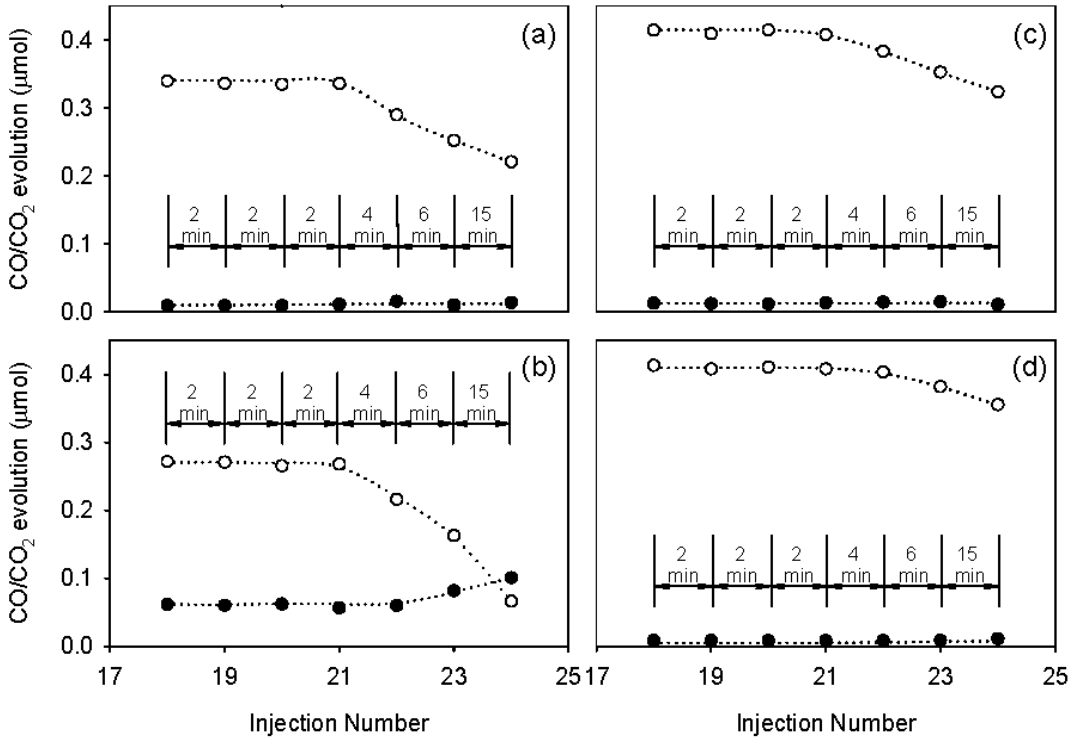

Figure 4.24 CO (○) and CO_2 (●) evolution from (a) reduced PdO/SnO_2 (150 ºC), (b) reduced Na-PdO/SnO_2 (150 ºC), (c) reduced PdO/SnO_2 (20 ºC), (d) reduced Na-PdO/SnO_2 (20 ºC) during delayed injections of CO

(*Conditions:* P = 1 atm; V_{inj} = 1 ml; n_{CO} = 0.42 μmol/injection; GHSV = 12 800 hr^{-1}; catalyst weight = 100 mg)

4.2 Characterization of Li-PdO/SnO_2 and K-PdO/SnO_2

After observing the sodium-induced enhancements in the interaction of PdO/SnO_2 surface with both CO and O_2 and the promotion of CO oxidation activity with sodium modification of the catalyst, lithium and potassium modified PdO/SnO_2 catalysts were prepared and tested with regard to their CO oxidation activity with the aim of comparing the effect of different alkali metals on the red-ox characteristics of PdO/SnO_2 and optimizing the type of the alkali modifier for enhancing the CO oxidation activity.

Lithium and potassium modified PdO/SnO_2 samples were characterized through XRD and XPS analyzes, to identify alkali-induced changes in the crystal structure and the binding states of palladium and tin. TPRS was utilized to investigate the CO oxidation characteristics of Li-PdO/SnO_2 and K-PdO/SnO_2 and to compare with the CO activity of Na-PdO/SnO_2 and PdO/SnO_2. Furthermore, CO-TPR was utilized to investigate the influence of different alkali metals on the reduction characteristics of SnO_2-based catalysts and to develop a comprehensive

understanding of the role of alkali-metal modification on CO oxidation with SnO_2-based catalysts.

The specific surface areas of Li-PdO/SnO_2 and K-PdO/SnO_2 samples were 55 m^2/g and 50 m^2/g, respectively. The analysis of the pore structure of these catalysts by N_2 sorption showed that the catalysts were made up of nonporous particles (see Appendix E).

4.2.1 X-Ray Diffraction Analysis

Li-PdO/SnO_2 and K-PdO/SnO_2 powders were investigated by X-ray diffraction to identify the crystal phases present in the catalysts and the alkali-induced changes in these crystalline phases.

4.2.1.1 X-Ray Diffraction Analysis of K-PdO/SnO_2

The X-ray diffraction pattern of potassium promoted sample possesses the reflections that are necessary to assign the major phase as cassiterite form of tin dioxide (Figure 4.25). No reflections that could be associated with metallic palladium were present in the diffraction patterns as great amount of palladium should be expected to exist as palladium oxide after calcination in air at 600°C for 6 hours during the last step in catalyst synthesis. Previously, palladium phase has been observed in cassiterite–palladium oxide systems with higher levels of loading [89] but, tin dioxide–palladium oxide containing systems present particular difficulty in identifying palladium phase with XRD, especially if the loading level is low (1 wt.% in the present study), due to the overlap of major reflections form palladium oxide, which appear at 33.8°, 54.7° and 71.2° and belong to (101), (112) and (202) planes respectively, with reflections from (101), (220) and (202) planes of tin dioxide. Through the XRD analysis of potassium modified 1wt.-percentage PdO/SnO_2, only weakly resolved reflections that could be associated with o palladium oxide were observed at 45.1° and 60.2°. These reflections correspond to minor reflections from (102) and (103) planes of PdO crystals.

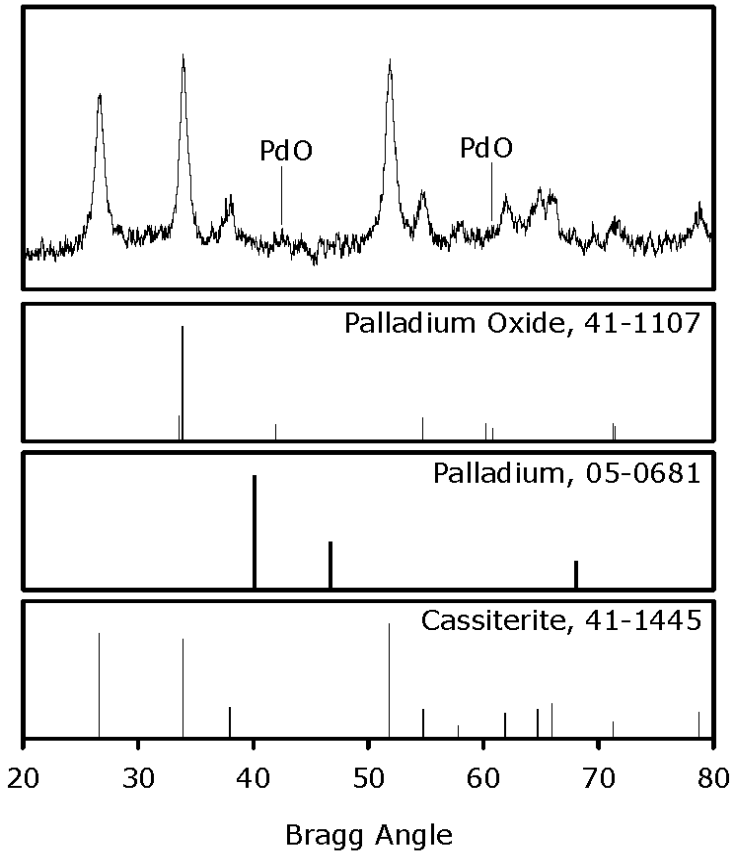

Figure 4.25 XRD pattern of oxidized 0.1 wt. % K- 1 wt. % PdO/SnO_2
(Reference XRD patterns of cassiterite, palladium oxide and palladium from the JCPDS database are provided for reference.)

4.2.1.2 X-Ray Diffraction Analysis of Li-PdO/SnO_2

In line with the XRD analysis of K-PdO/SnO_2, the major phase of Li-PdO/SnO_2 was also identified as tin dioxide in cassiterite form (Figure 4.26a). In addition to the reflections associated with cassiterite phase a unique peak was resolved at 44.7°. This unique reflection was accompanied wit changes in the XRD pattern at 38.4°, 65.0° and 78.4° where, peaks overlapping with those of cassiterite were observed. These reflections might be attributed to the interaction of lithium with cassiterite however, it has not been possible to associate the reflection resolved at 44.7° with any of the expected phases, i.e. cassiterite, palladium oxide and metallic palladium.

The development of crystal phases in tin dioxide by interaction with lithium is subject to various solid-state chemistry research for its potential to be used as the anode material in Li-ion batteries. Studies on lithium-intercalated tin oxide matrices have shown that lithium incorporation changed the chemical structure

of tin dioxide by reducing tin atoms through interaction with the oxygen bonded to these atoms to yield clusters of tin oxide or metallic tin and Li_2O [183,184]. The interaction of lithium with tin also gives rise to the formation of Li-Sn alloys with various stoichiometries [184,185]. Moreover, the ternary palladium-tin-lithium is subject to formation of lithium intercalated palladium stannide [186]. The relevance of crystallographic phases such as lithium-tin alloys, lithium intercalated tin dioxide, palladium stannide or bimetallic Li-Sn oxides have been investigated in attempts to identify the crystallographic phase formed by lithium addition in addition to cassiterite, palladium oxide or palladium metal and several other lithium modified catalysts were synthesized and analyzed by XRD to observe the dependence of this anomalous phase on the amount of lithium loading and pretreatment conditions.

The XRD analysis of another Li-PdO/SnO_2 sample with greater amount of lithium loading (Li:Pd = 1.70) also evidenced the presence of the anomalous crystal phase in addition to cassiterite(Figure 4.26c). Palladium-free Li/SnO_2 and reduced Li-PdO/SnO_2 samples were also investigated with XRD in order to assess the role of palladium/palladium oxide in the development of the lithium induced changes in the crystal structure of the catalysts samples (Figures 4.26b and 4.26d). In line with previous observations the major crystallographic phase in both of the samples was identified as cassiterite and no reflections that could be associated with LiSn and PdSn alloys was present implying that, reduction pretreatment had no effect on the crystal structure of SnO_2 that could be observed by XRD. The pattern of reduced Li-PdO/SnO_2 suggests the disappearance of the lithium-induced phase during reduction pretreatment (Figure 4.26b) whereas, the reflection resolved at 44.7° in the XRD pattern of oxidized Li-PdO/SnO_2 samples was also present in the diffractogram of Li/SnO_2, with a decrease in its intensity relative to Li-PdO/SnO_2.

In addition to LiSn alloys and oxygen deficient forms of tin dioxide, it is also possible that lithium incorporation to tin dioxide matrix result in the formation of $LiSnO_X$ type oxides. Lithium insertion to anatase TiO_2 as been observed to lead to the formation of lithium titanate ($Li_{0.5}TiO_2$) via anisotropic insertion of lithium ions along the *a* axes [187-189] and the formation of lithium stannate via insertion of lithium to tin dioxide which also has anatase structure might be considered. Similar reflections to the ones resolved in the XRD patterns of Li-PdO/SnO_2 samples were reported for $LiCoO_2$, which has a layered structure where Li^+ and Co^{3+} ions are ordered on alternate (111) planes of a rocksalt

structure [190]. Therefore, it is most meaningful to associate the third phase with lithium stannate that possibly formed through the intercalation of lithium in tin dioxide.

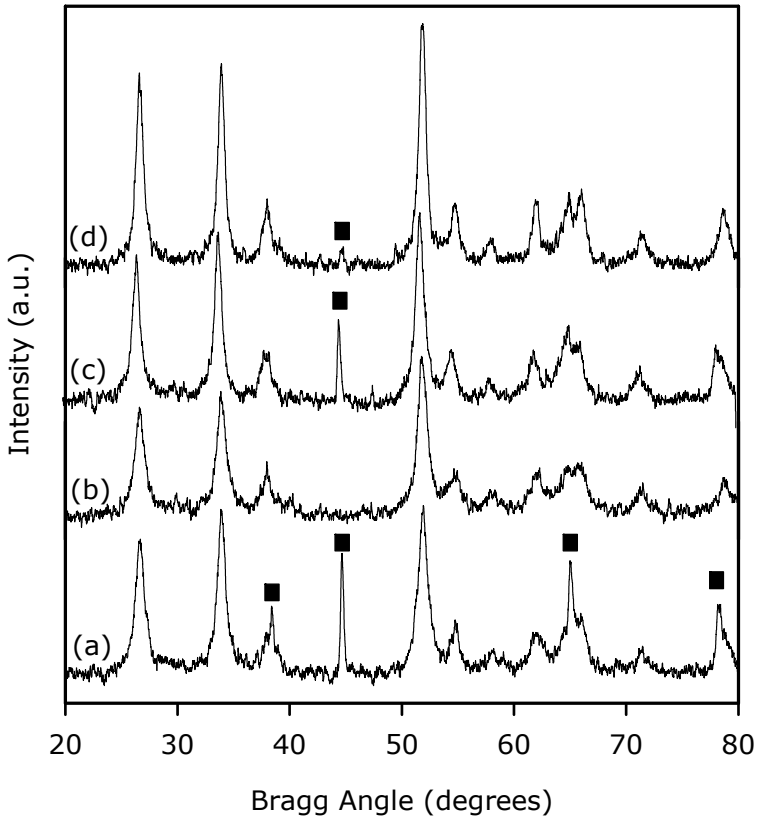

Figure 4.26 XRD patterns of: (a) oxidized 0.03 wt. % Li-1. wt. % PdO/SnO_2 (Li/0.53), (b) reduced 0.03 wt. % Li-1. wt. % PdO/SnO_2 (Li/0.53), (c) oxidized 0.1 wt. % Li- 1 wt. % PdO/SnO_2 (Li/1.77) and (d) oxidized 0.1 wt. % Li/SnO_2

Another important observation from the XRD pattern of the palladium-free Li/SnO_2 is the increase in the intensity and decrease in the peak broadenings of the reflections from cassiterite, which suggests either the formation of smaller crystallites and/or less ordered more defect structures in the palladium containing samples. The crystallite sizes were calculated by using Scherrer's method and turned out to be 14.9 nm for Li/SnO_2 whereas, values in the order of 14 nm were calculated for the Li-PdO/SnO_2 catalysts. These values suggest that the change in the crystallite size need be associated with palladium incorporation into the structure rather than the presence of lithium in the structure.

4.2.2 XPS Analysis

Sn 3d and Pd 3d envelopes of Li-PdO/SnO_2 and K-PdO/SnO_2; together with the relevant envelopes of the respective alkali-metals; were investigated with XPS in efforts to develop further insights to the alkali induced modifications in the chemical structure of alkali-metal promoted PdO/SnO_2 catalysts.

In both of the samples, the Sn 3d doublet was observed as symmetric peaks made up of a single component with $3d_{5/2}$-$3d_{3/2}$ doublet splitting of 8.4 eV and full-width-at-half-maximum (FWHM) of 1.8 eV. The Sn $3d_{5/2}$ was located at 487.2 eV and at 486.8 eV in Li-PdO/SnO_2 and K-PdO/SnO_2, respectively and sputter etching of the surfaces shifted the Sn $3d_{5/2}$ band to 486.3 eV in both of the catalysts (Figures 4.27a and 4.27b). These values are in well agreement with previously discussed results on Sn 3d doublets of bare SnO_2, PdO/SnO_2 and Na-PdO/SnO_2 samples. In the case of bare SnO_2, the Sn 3d band was resolved at 487.1 eV before etching of the surface and at 486.2 eV after the same rate of Ar-ion bombardment procedure (Figure 4.1).

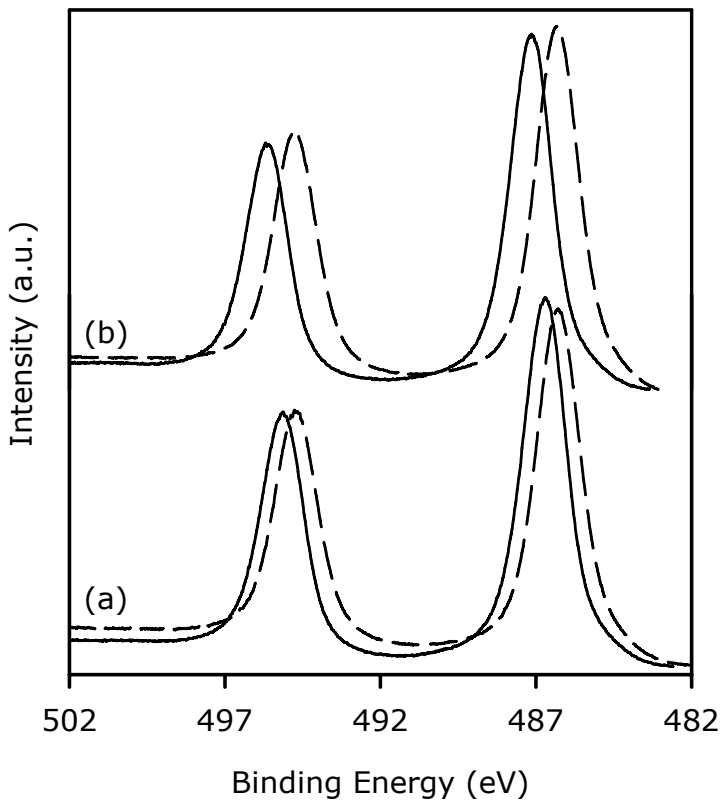

Figure 4.27 Sn 3d XP spectra of (a) oxidized K-PdO/SnO_2 and (b) oxidized Li-PdO/SnO_2 before (solid line) and after (dashed line) Ar-ion etching

The XPS data did not provide any evidence for the presence alkali-metal induced changes in the electronic structure of tin atoms and the binding states of Sn 3d electrons suggest that tin atoms existed in tetravalent coordination. Resolution of Li 1s and K 2p bands and the observation of the changes in the binding states of electrons of these atoms have not been possible since the alkali-metal loading was very low.

4.2.2.1 XPS Analysis of Pd 3d Envelope of Oxidized and Reduced Li-PdO/SnO_2

The analysis of Pd 3d envelope in oxidized Li-PdO/SnO_2 sample showed the presence of two different binding states of palladium with Pd $3d_{5/3}$ located at 337.7 eV and 339.1 eV (Figure 4.28a). In line with the investigation of PdO/SnO_2 and Na-PdO/SnO_2 catalysts with XPS, these states could be associated with Pd^{4+} (PdO_2) and Pd^{6+} (PdO_3) species. Following the reduction pretreatment of Li-PdO/SnO_2, Pd atoms existed as Pd^{2+} (336.6 eV), Pd^{4+} (337.7 eV) or Pd^{6+} (339.1 eV) and no bands that could be assigned to metallic palladium was present (Figure 4.28b). The relative amounts of different palladium species were calculated from the areas under the Gaussian components making up the Pd 3d envelope for both oxidized and reduced Li-PdO/SnO_2 samples (Table 4.2). The data shows that most of the palladium is present as higher oxides even after reduction pre-treatment.

4.2.2.2 XPS Analysis of Pd 3d Envelope of Oxidized and Reduced K-PdO/SnO_2

The computer peak fitting of the Pd 3d envelope of oxidized K-PdO/SnO_2 suggested that the envelope was composed of four components located at 335.7 eV, 336.6 eV and 337.7 eV and 339.1 eV (Figure 4.29a), which could be assigned to Pd^0, Pd^{2+} (PdO), Pd^{4+} (PdO_2) and Pd^{6+} (PdO_3) species through a comparison with previous XPS data on PdO/SnO_2 and Na-PdO/SnO_2 catalysts (Figure 4.29a).

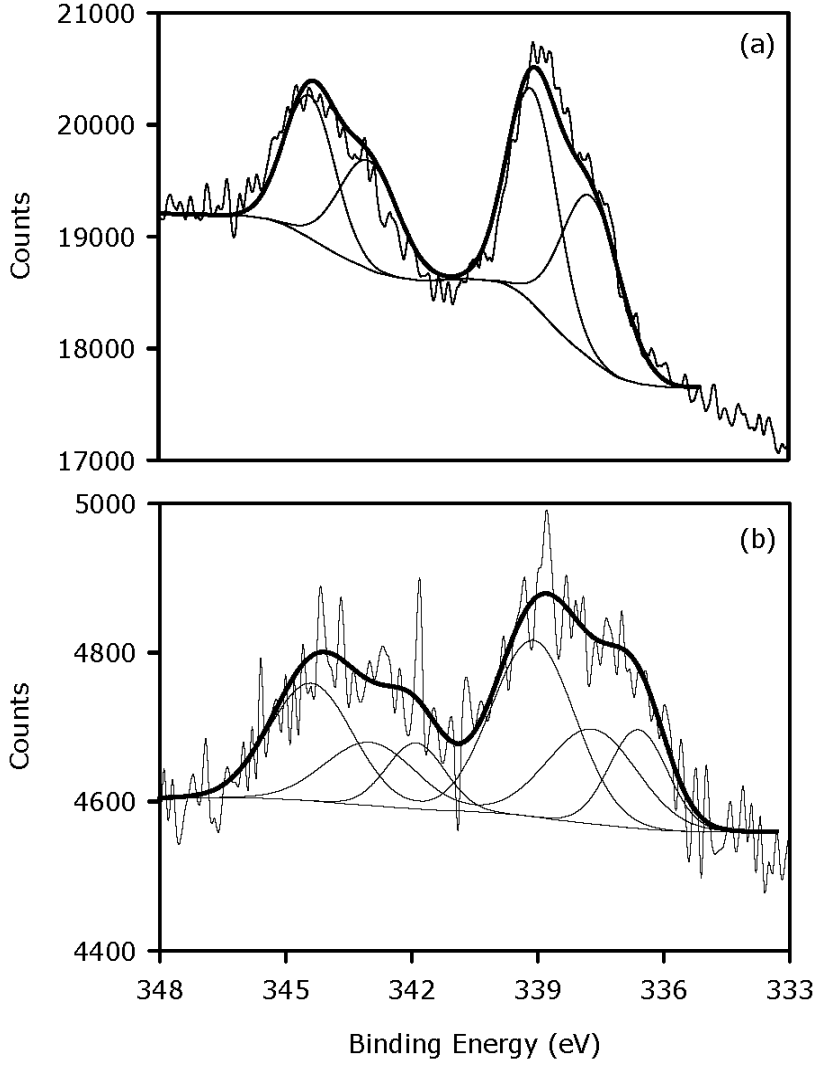

Figure 4.28 Pd 3d XP spectra of: (a) oxidized Li-PdO/SnO_2 (Li/0.53) and (b) reduced Li-PdO/SnO_2 (Li/0.53)

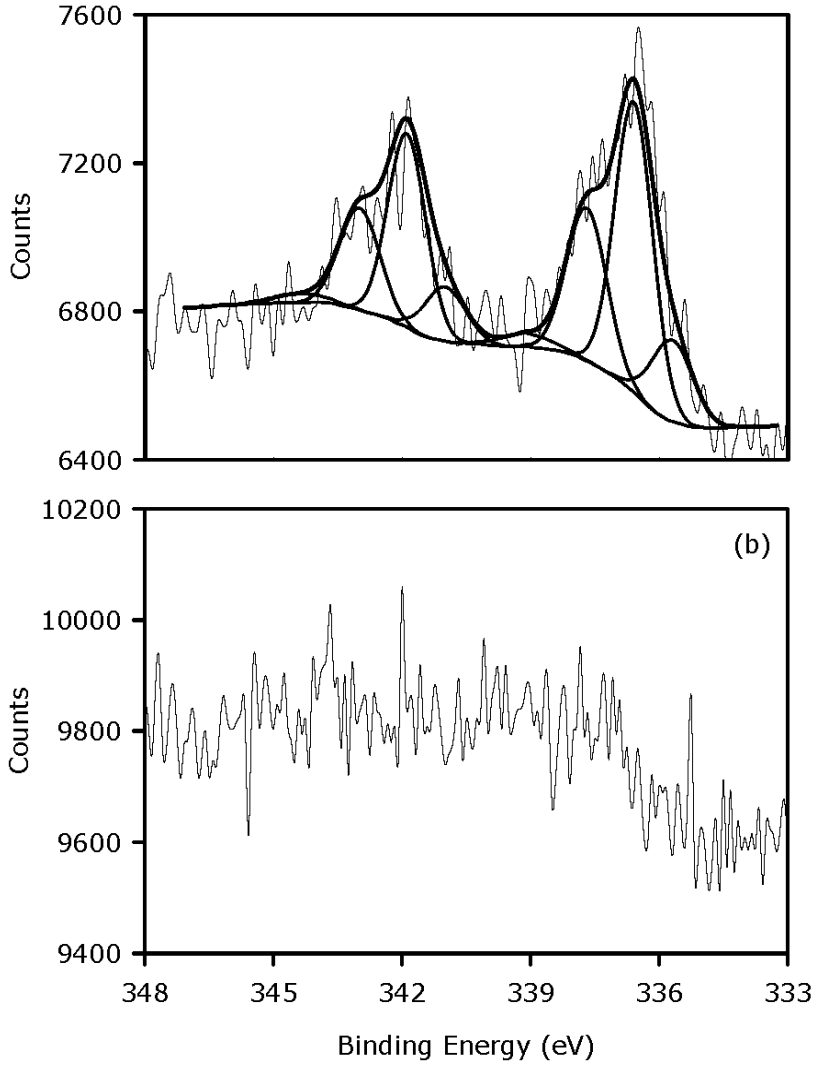

Figure 4.29 Pd 3d XP spectra of: (a) oxidized K-PdO/SnO_2 and (b) reduced K-PdO/SnO_2

The increase in the core-level binding energy of palladium metal (Pd^0) relative to clean metallic palladium films could be explained by the cluster size dependence of the core-level binding energies [191] however, the interaction between palladium clusters with the support should not be ruled out. The influence of the support on the oxidation state of palladium is well evident from the existence of a considerable portion of palladium in the form of higher oxides (Table 4.2), which are generally unstable and thus, were stabilized in PdO/SnO_2 catalysts through interaction with the support. Similar conclusions on the influence of the support on the oxidation state of palladium has been reported by Otto et *al.* [169] for $Pd/\gamma\text{-}Al_2O_3$ system. Table 4.2 shows that 15.7 % of palladium was present as metallic species in oxidized $K\text{-}PdO/SnO_2$, which indicates that the oxygen content of palladium phase of $K\text{-}PdO/SnO_2$ is much lower than the oxygen contents of unpromoted PdO/SnO_2 and $Na\text{-}PdO/SnO_2$, where the presence of Pd^0 was not observed in the oxidized samples. The deconvolution of Pd 3d envelope of reduced $K\text{-}PdO/SnO_2$ to its Gaussian components to represent various binding states of palladium has not been possible as the envelope was not resolved (Figure 4.29b), which probably arise from the diffusion of palladium atoms to SnO_2 bulk during pretreatment.

Table 4.2 XPS analysis of Pd 3d envelopes of alkali-metal modified PdO/SnO_2 samples*

	Pd^0	PdO	PdO_2	PdO_3	Higher oxide
Binding Energy (eV)	335.7	336.6	337.7	339.1	340.6
Oxidized PdO/SnO_2	-	18.2	60.2	21.6	-
Reduced PdO/SnO_2	85.3	2.1	12.5	-	-
Oxidized $Li\text{-}PdO/SnO_2$	-	-	47.0	53.0	-
Reduced $Li\text{-}PdO/SnO_2$	-	19.9	29.4	50.7	-
Oxidized $Na\text{-}PdO/SnO_2$	-	-	67.4	26.4	6.2
Reduced $Na\text{-}PdO/SnO_2$	37.1	-	40.9	22.0	-
Oxidized $K\text{-}PdO/SnO_2$	15.7	52.1	28.9	3.3	-
Reduced $K\text{-}PdO/SnO_2$	N/A	N/A	N/A	N/A	N/A

*Values for PdO/SnO_2 and $Na\text{-}PdO/SnO_2$ have been reproduced from Table 4.1

4.2.3 Temperature-Programmed Reaction Spectroscopy (TPRS) Studies

Temperature programmed reaction spectroscopy (TPRS) technique was utilized to complement previously discussed TPRS studies on PdO/SnO_2 and Na-PdO/SnO_2 and to compare the effect of different alkali-metal modifiers on the CO oxidation activity of PdO/SnO_2. The experiments were carried out under oxidizing conditions where, the reactor feed constituted 2400 ppm CO and the ratio of CO-to-O was 0.5. The initial oxygen coverage of the surfaces has been observed to have significant effect on the activity of the catalysts in CO oxidation thus, the effect of initial oxygen coverage of the surface on the CO activity was also investigated by subjecting the catalysts to *in-situ* oxidation and reduction pretreatment procedures prior to the activity tests.

A comparison of the CO conversion versus temperature curves of oxidized Li-PdO/SnO_2 and K-PdO/SnO_2 with that of oxidized PdO/SnO_2 under the same reactor feed conditions show a shift towards higher temperatures relative to unmodified PdO/SnO_2 (Figures 4.5 and 4.30). The light-off temperatures for oxidized Li-PdO/SnO_2 and K-PdO/SnO_2 are 220°C and 190°C, respectively. When compared to the light-off temperature of unmodified PdO/SnO_2, which is 169°C, these values also evidence the significant decrease in the CO activity of PdO/SnO_2. Reduction pretreatment increased the CO activities and for the catalysts subjected to reduction pretreatment, light-off temperatures were observed as 200°C for Li-PdO/SnO_2 and 160°C for K-PdO/SnO_2. As it can be seen in the light-off temperatures as well, reduction pretreatment was more effective in the case potassium modified sample than its lithium modified counterpart in shifting the CO oxidation activity to lower temperatures. These results are in agreement with previously discussed TPRS experiments on PdO/SnO_2 and Na-PdO/SnO_2 as, oxidized Na-PdO/SnO_2 was also observed to exhibit lower CO oxidation activity than oxidized PdO/SnO_2 and activation of these catalysts in reducing atmosphere also resulted in superior activity relative to their oxidized counterparts. In line with previous discussion on the effect of pretreatment procedures on catalyst activity, it is most meaningful to associate the increased activity of reduced catalysts with respect to their oxidized counterparts with oxygen saturation at the surface which would interfere with CO adsorption and result in the reduced activity of oxidized catalysts.

For providing another basis of comparison of the CO oxidation activities of the catalysts the rates of CO oxidation reaction over oxidized and reduced samples of Li-PdO/SnO_2 and K-PdO/SnO_2 were calculated at 150°C and these values are

presented in Table 4.3. Combining the TPRS and rate of reaction data presented in Section 4.1.3 with the ones presented in this section show that the CO oxidation activity of the oxidized catalysts decreased in the order PdO/SnO_2 > Na-PdO/SnO_2 > K-PdO/SnO_2 > Li/SnO_2. A comparison of these reaction rates with the rates observed over oxidized and reduced PdO/SnO_2 under the same conditions (Figure 4.8) also suggest that, regardless of the pretreatment procedure, lithium and potassium acted as catalysts poisons under these conditions and inhibited the CO oxidation activity rather than promoting it. Figure 4.8 also shows a similar poisoning effect over oxidized Na-PdO/SnO_2 under oxidizing feed conditions however, when the sample was pretreated under reducing conditions sodium modification was observed to promote the CO activity. Therefore, the CO oxidation activity of alkali-metal modified PdO/SnO_2 catalysts subjected to reduction pretreatment decrease in the order Na-PdO/SnO_2 > PdO/SnO_2 > K-PdO/SnO_2 > Li/SnO_2.

Table 4.3 Rates of CO oxidation over Li-PdO/SnO_2 and K-PdO/SnO_2

	Rate* $(\mu mol/m^2 \cdot min)$
Oxidized Li-PdO/SnO_2	0.011
Reduced Li-PdO/SnO_2	0.062
Oxidized K-PdO/SnO_2	0.060
Reduced K-PdO/SnO_2	0.249

**Reaction Conditions:* P = 1 atm; GHSV = 12 800 hr^{-1}; [CO] = 2400 ppm; [CO]/[O] = 0.5; catalyst weight = 100 mg

Alkali-metal modification presents a means of altering relative surface coverages of oxidizing and reducing components present in the gas phase and O_2 TPD data presented in Section 4.1.5 has shown that sodium modification promoted the interaction oxygen with the surface and as a result of this sodium modified catalysts were oxidized at lower temperatures than their unpromoted counterparts. Furthermore, the enhanced CO oxidation activity of sodium modified catalysts under both transient and steady-state conditions have been attributed to the promotion of the adsorption of electron acceptor species, especially oxidizing species, in the presence of sodium. Although the XPS data suggested that lithium exhibited a similar behavior in terms of promoting oxygen

adsorption and storage capacity of PdO/SnO_2, lithium modification also suppressed the CO oxidation activity. A plausible explanation for the suppression of CO activity by lithium would be a strong interaction between chemisorbed CO and lithium. As it has been discussed earlier, alkali metals lead to the electron enrichment of the metal phase which enhances the backdonation of electrons form the noble metal to antibonding molecular orbitals of CO [152-155]. This enhanced backdonation of electrons leads to the promotion of the interaction CO with the surface which could even result in dissociation of CO on surfaces which normally adsorb CO molecularly. Therefore, the aim in applying alkaline modification for promoting CO oxidation over noble metal-based catalysts should be promoting the interaction of CO without leading to the dissociation of the molecule. However, the interaction of CO with clean Li surface has been observed to be much stronger than Na and K surfaces and it resulted in the dissociation of CO even at 130K [192] and such a strong interaction between the modifier and chemisorbed CO that could even lead to cleavage of the C-O bond might hinder the oxidation of CO through the dissociation of the molecule. Even if the cleavage of the C-O bond does not take place, an interaction between CO and lithium may retain on the surface and may result in the suppression of CO activity. The poisoning effect of lithium may also be attributed to the formation of another crystal phase in the lithium modified samples and the lithium-induced poisoning of the catalytic activity of PdO/SnO_2-based catalysts may be correlated with these effects.

It should also be noted that, in addition to the type of the alkali-metal, the alkali-content of the catalysts need be optimized for developing catalyst formulations to exhibit superior catalytic activity under specific gas phase compositions of oxidizing and reducing components. Attempts have been made to provide further insights to the origins of the different CO activities of differently modified PdO/SnO_2 catalysts, which probably arise from the modification of the interaction of oxide/hydroxide species with surface and the influence of alkali-metal modifiers on the reduction behavior of this system has been investigated by CO-TPR.

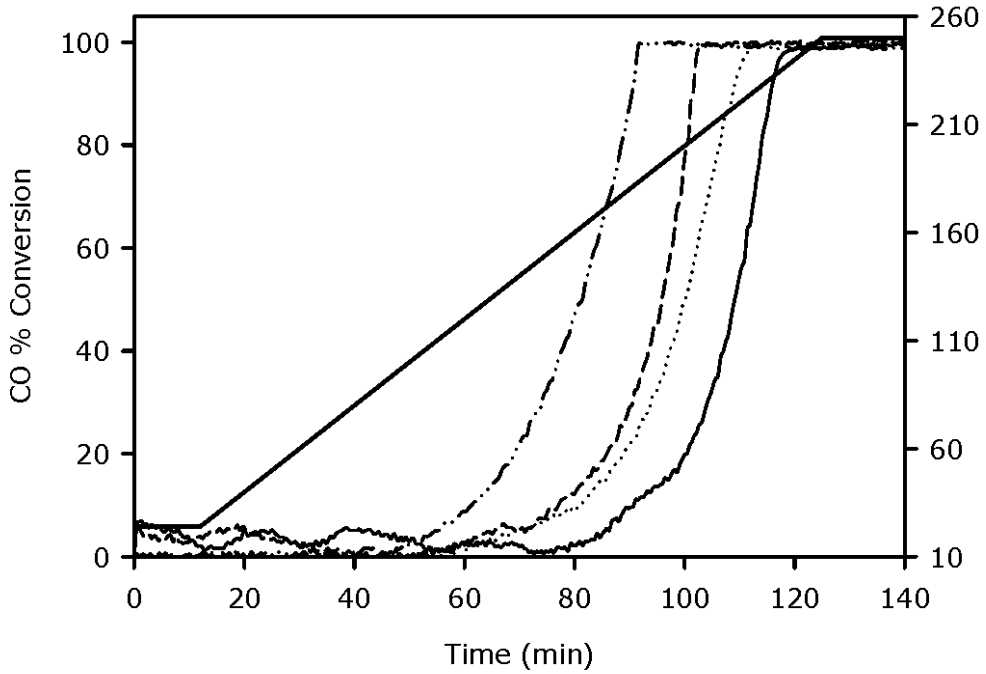

Figure 4.30 Rates of CO conversion over oxidized Li-PdO/SnO_2 (———), reduced Li-PdO/SnO_2 (·····), oxidized K-PdO/SnO_2 (------) and reduced K-PdO/SnO_2 (—··—··)

(*Reaction Conditions:* P = 1 atm; [CO]/[O] = 0.5; GHSV = 12 800 hr^{-1}; [CO] = 2400 ppm; catalyst weight = 100 mg, heating rate = 2°C/min)

4.2.4 Temperature Programmed Reduction (TPR) Studies with CO

The oxide (Reaction 4.1) and hydroxide (Reaction 4.2) reaction mechanisms have been observed to be responsible for CO oxidation$_2$-based catalysts thus, the reactivity and surface abundance of oxide and hydroxy species are the key factors that alter the activity of these catalysts towards CO oxidation. The previously discussed results on CO oxidation with PdO/SnO_2 and Na-PdO/SnO_2 catalysts also evidenced the important role played by the hydroxy reaction mechanism in the CO activity.

To investigate the modes of interaction of reducible surface species with PdO/SnO_2 and the influence of alkali-metal modifiers on the reduction characteristics of PdO/SnO_2-based catalysts CO-TPR technique was adopted. During the CO-TPR studies evolution of water vapor (m/z=18) from the surfaces was also monitored along with the evolution of CO_2 (m/z=44) to provide further insights to the role of hydroxy groups in CO oxidation. Control experiments were performed on the bare support to test the contribution of the support and the interaction of the noble metal and the alkaline modifiers with the support.

As it is observed form the CO_2 and H_2O traces, SnO_2 samples subjected to oxidation and reduction pretreatment exhibited similar reduction behavior suggesting that reduction pretreatment did not alter the abundance and reactivity of reducible species (Figures 4.31a and 4.31b). No evolution of CO_2 and H_2O was observed below 200°C and two broad CO_2 evolution bands corresponding to 200°C-375°C region (with temperature at peak maximum (T_{max}) corresponding to 315°C) and 380°C-480°C (T_{max} = 438°C) were resolved above 200°C. These two bands were accompanied by water evolution at the same temperature ranges (Figures 4.32a and 4.32b). These water evolutions bonds may be associated with condensation of hydroxy species. On tin dioxide surfaces, condensation of rooted hydroxy groups have been reported to give rise to water evolution around 130°C whereas, water evolution due to reactions involving isolated hydroxy groups was observed above 400°C [127]. Therefore, these high temperature evolution bands may be attributed to the condensation of isolated hydroxyl groups. However, the coincidence of the temperatures at which the CO_2 and H_2O evolution bands were observed and the correlation of the intensities of these bands may also suggest the involvement of hydroxy groups in CO oxidation reaction (Reaction 4.2) and consequent formation of water through Reaction 4.3. Therefore, the species leading to the CO_2 evolutions bands could be oxide and/or hydroxide species however, regardless of their nature two types reduction sites have been identified over bare SnO_2 in 20°C-500°C temperature range.

The reduction behavior of reduced PdO/SnO_2 was similar to bare support, where two CO_2 evolution bands corresponding to 200°C-342°C (T_{max} = 320°C) and 342°C-470°C (T_{max} = 390°C) and which are accompanied by water evolution in the same temperature range, were observed (Figures 4.31c and 4.32c). A comparison of the CO_2 trace of reduced PdO/SnO_2 with the CO_2 traces of oxidized and reduced support suggest a shift in the high temperature band towards lower temperatures while, the low temperature band remained intact. The promotion of the reduction of the support in the presence of palladium has been documented in literature and has been attributed to the spillover of activated CO species from noble metal centers, which have a high affinity for CO adsorption, to tin dioxide surface [106]. The current CO-TPR results provide further support for these observations but also, they suggest that palladium additions facilitates the reduction of only one type of reducible specie. A similar interaction between Pd and Sn above 300°C was also observed in the CO_2 trace of oxidized PdO/SnO_2 sample (Figure 4.31d). In addition to the abovementioned

CO_2 bands, another CO_2 evolution band, which is resolved as a doublet and corresponded to 50°C-315°C region (T_{max} = 276°C), was resolved. Its disappearance in CO_2 traces of SnO_2 samples and reduced PdO/SnO_2 implies that this band is associated with the reduction of palladium oxide (PdO_X) species. This CO_2 band was observed to be accompanied with an increase in the water evolution in the same temperature range (Figure 4.32d). Although it is possible that condensation of hydroxy groups to vacate sites for CO adsorption/oxidation may be responsible for the correlation between CO_2 and H_2O evolution bands, it is also plausible that palladium addition resulted in the incorporation of another active site which would promote either the formation of hydroxy species or their reduction through interaction with chemisorbed CO. Regarding the nature of the palladium species resulting in the promotion of the reduction of the support at high temperatures, the presence of metallic palladium might be expected to lead to the observed effect as reduction of palladium oxide would take place at much lower temperatures.

The elaboration of the CO-TPR data for PdO/SnO_2 suggest that the influence of palladium addition on the reduction behavior of tin oxide is (i) incorporation of another active site to the structure, for which the reduction took place at much lower temperatures than bare tin oxide and, (ii) promotion of the reduction of oxide species of SnO_2 at lower temperatures, possibly through an interaction between palladium and one of the two types of oxide species over SnO_2 surface. These results are in good agreement with our previous report, where we have reported an additional CO adsorption/oxidation site over PdO/SnO_2 through temperature-programmed adsorption/desorption experiments and have ascribed this low temperature site to the presence of palladium atoms.

Unlike the noble metal, the effect of alkali-metal addition on the reduction behavior of PdO/SnO_2 was not observed as the incorporation of other reactive sites but rather, as the promotion or retardation of the reduction the oxide species present over the surface. The effect of sodium and potassium on the low temperature reduction sites that have been incorporated into the structure by the addition of palladium was observed as the promotion of the reduction of these sites, which is manifested by a shift in the CO_2 evolution band to lower temperatures (Figures 4.31f and 4.31h). The CO_2 band corresponded to 50°C-315°C (T_{max} = 276°C) region in the CO_2 trace of oxidized PdO/SnO_2 was observed in 80°C-296°C region (T_{max} = 256°C) over K-PdO/SnO_2. Detailed investigation of the structure of this band suggests the presence of a weakly

resolved shoulder corresponding to the same temperature as the low temperature component of the CO_2 doublet resolved in the CO_2 trace of oxidized PdO/SnO_2 and this suggest that potassium addition modified the reduction characteristic of PdO/SnO_2 by interacting with a specific type of palladium oxide species. Further promotion of the reduction of these sites was evidenced by the CO_2 trace of oxidized Na-PdO/SnO_2 (Figure 4.31h). The CO_2 evolution band under consideration was resolved in 140°C-276°C region (T_{max} = 218°C) region and corresponded to lower temperatures than its counterparts resolved over PdO/SnO_2 and K-PdO/SnO_2. This observation further evidences the promotion of the reduction of PdO_X sites by alkali-metal addition.

The H_2O traces of oxidized Na-PdO/SnO_2 and K-PdO/SnO_2 exhibit a well-resolved H_2O desorption band in 170°C-280°C region and a slight shift in the peak maxima was observed in the alkali metal promoted samples such that $T_{max}(PdO/SnO_2) > T_{max}(K\text{-}PdO/SnO_2) > T_{max}(Na\text{-}PdO/SnO_2)$ (Figures 4.32f and 4.32h). As the shift in the H_2O band is correlated with the shift in the high temperature component of the CO_2 doublet, it is most meaningful to appoint the species giving rise to the high temperature component to the species that have been postulated to promote the formation/reduction of hydroxy species giving rise to the H_2O evolution band.

Regarding the effect of lithium on the reduction characteristics of PdO/SnO_2; the CO_2 band ascribed to the reduction of palladium related sites was resolved in 100°C-340°C region (T_{max} = 290°C) which suggested a lithium induced suppression of the reduction of these sites (Figure 4.31j). Similar observations on the effect of lithium addition was reported by Luo et *al.* [193] and have been attributed to the modification of the binding state of CO through the alteration of the dispersion of the noble metal in lithium modified Rh/SiO_2.

It is interesting to note the significant decrease in the intensity of well-resolved water bands of Na-PdO/SnO_2 and K-PdO/SnO_2 over Li-PdO/SnO_2 which provides further importance of hydroxy groups in the low temperature CO_2 evolution (Figure 4.32j). In this respect, the high reduction temperatures observed in the TPR profile of Li-PdO/SnO_2 show that lithium promotion either hinders the formation of these hydroxy species on the surface by blocking the sites for water dissociation. In fact, through IR studies on Li promoted Ni/SiO_2, Pereira et *al.* [133] have reported a decrease in the concentration of OH groups when the catalyst was promoted with Li. Yet, lithium may promote the interaction of hydroxy species with the surface such that these species can only be reduced at

elevated temperatures. It is also plausible that interaction of lithium with hydroxy species retarded the reduction of these species. Furthermore, the XRD data evidenced the formation of another phase when lithium was introduced in the catalysts and the suppression of the reduction of the oxide species of lithium promoted PdO/SnO_2 may also be associated with the formation of this phase. This phase has been postulated to form through the interaction of lithium with the proton of the surface hydroxy species and such an interaction would retard the reduction of such species.

At higher temperatures than the reduction palladium oxide samples subjected to reducing pretreatment and their counterparts subjected to oxidizing pretreatment exhibit similar bands in the CO_2 profiles (Figure 4.31). CO_2 traces of K-PdO/SnO_2 and Li-PdO/SnO_2 were observed to exhibit a well resolved CO_2 evolution band that corresponded to 380°C-490°C (T_{max} = 436°C) and this band shifted to 356°C-480°C region (T_{max} = 382°C) over Na-PdO/SnO_2. These bands correspond to the temperature region where the reduction of SnO_2 was observed to take place and palladium addition has been postulated to promote the reduction of the species that give rise to CO_2 evolution at this temperature. The shift in these bands with alkali-metal modification suggests an influence of the alkali-metals on the interaction of palladium with the support.

In attempts to identify the influence that the alkali-metals might have on the reduction behavior of tin dioxide rather than on palladium and on the interaction of palladium with tin, control CO-TPR experiments have been performed with oxidized and reduced palladium-free Li/SnO_2, Na/SnO_2, and K/SnO_2 samples. These catalysts have been synthesized by the abovementioned sol-gel route with the addition of the same amount of alkali-metals as alkali-metal promoted PdO/SnO_2 catalysts.The CO_2 evolution profiles of all alkali-metal promoted SnO_2 samples provided further evidence that, the CO_2 evolution band observed in 100°C – 350°C region over alkali-metal promoted and unpromoted PdO/SnO_2 arise from the contribution of palladium to the structure (Figure 4.33). CO_2 evolution traces of oxidized and reduced Na/SnO_2 resembled those of oxidized and reduced SnO_2 suggesting that the reduction of two different species took place in the temperature range studied (Figures 4.33c and 4.33d). The two bands corresponding to the reduction of these species were resolved at 170°C – 375°C (T_{max}=315°C) and 375°C – 460°C (T_{max}= 430°C) regions. All of these bands matched the bands observed in the CO_2 evolution trace of oxidized and reduced SnO_2. Unlike sodium, the CO_2 evolution traces of oxidized and reduced

lithium and potassium promoted SnO_2 were slightly differed from that of bare SnO_2, suggesting that these alkali-metals interacted with tin dioxide to a greater extent than sodium.

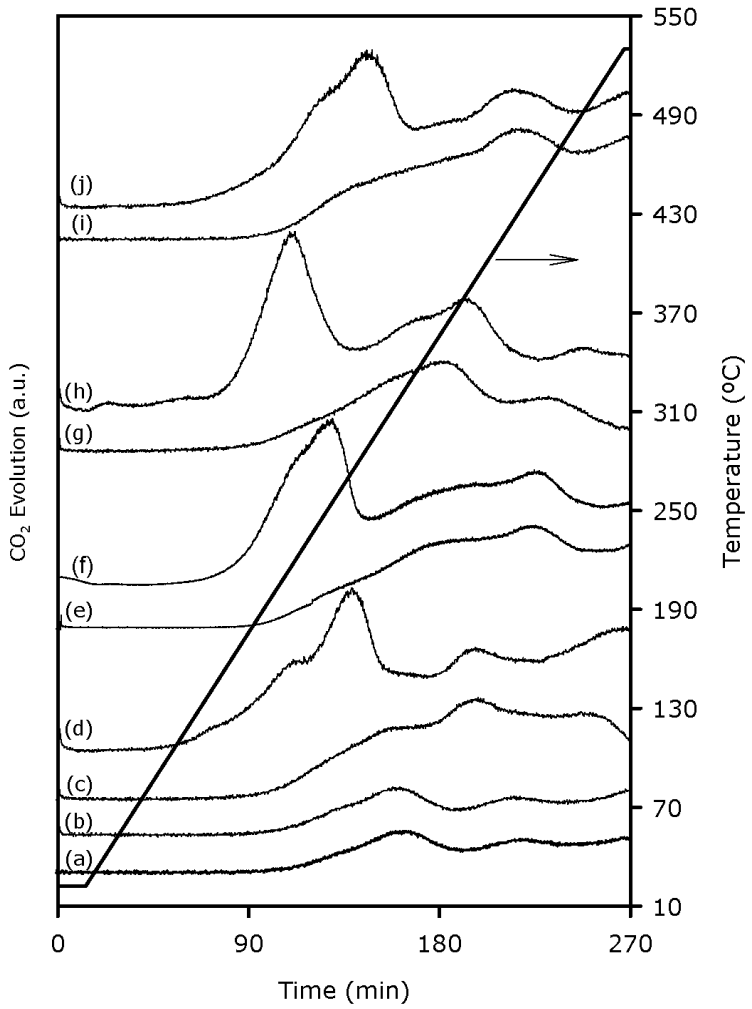

Figure 4.31 Temperature-programmed reduction CO_2 traces of (a) reduced SnO_2, (b) oxidized SnO_2, (c) reduced PdO/SnO_2, (d) oxidized PdO/SnO_2, (e) reduced K-PdO/SnO_2, (f) oxidized K-PdO/SnO_2, (g) reduced Na-PdO/SnO_2, (h) oxidized Na-PdO/SnO_2 (i) reduced Li-PdO/SnO_2 and (j) oxidized Li-PdO/SnO_2

(*Conditions:* P = 1 atm; GHSV = 12 800 hr^{-1}; [CO] = 2000 ppm; catalyst weight = 100 mg, heating rate = 2°C/min)

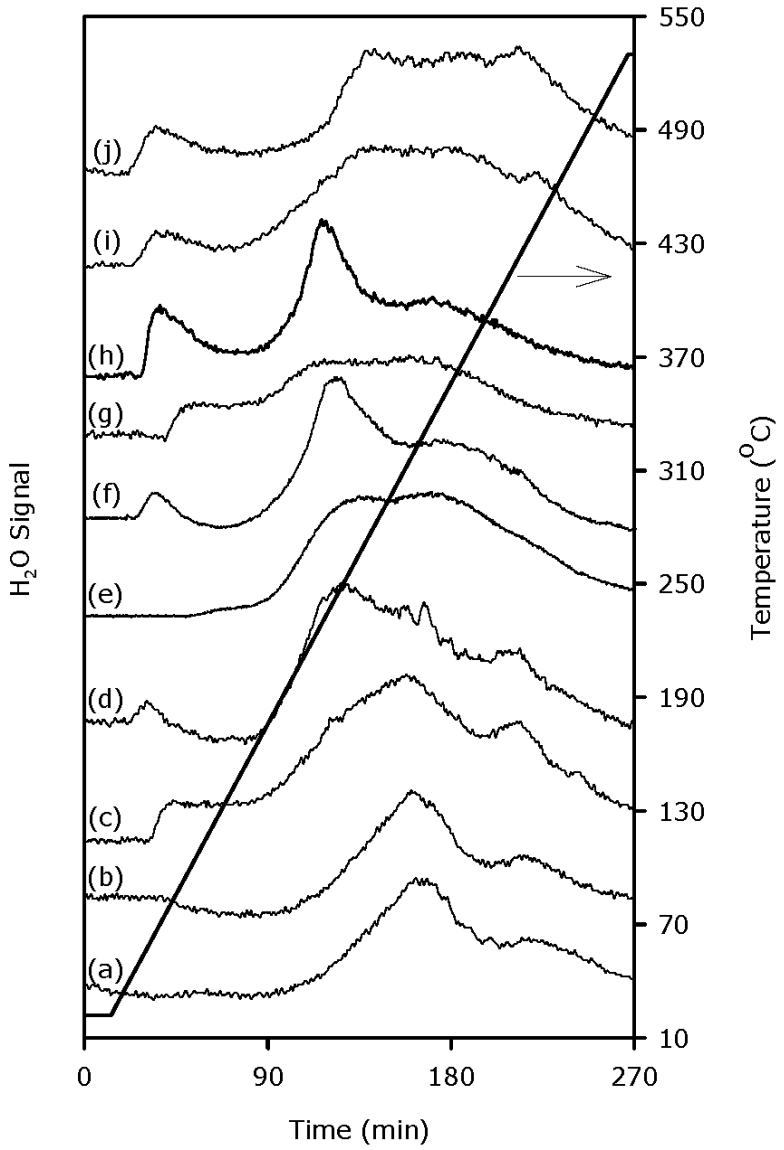

Figure 4.32 Temperature-programmed reduction H_2O traces of (a) reduced SnO_2, (b) oxidized SnO_2, (c) reduced PdO/SnO_2, (d) oxidized PdO/SnO_2, (e) reduced K-PdO/SnO_2, (f) oxidized K-PdO/SnO_2, (g) reduced Na-PdO/SnO_2, (h) oxidized Na-PdO/SnO_2 (i) reduced Li-PdO/SnO_2 and (j) oxidized Li-PdO/SnO_2

(*Conditions:* P = 1 atm; GHSV = 12 800 hr^{-1}; [CO] = 2000 ppm; catalyst weight = 100 mg, heating rate = 2°C/min)

In the experiments conducted with PdO/SnO_2-based samples, palladium was observed to interact with some oxide species of the support altering their reducibility and alkali-metals added to the catalysts acted either to promote or to offset this effect of palladium. As a result, the CO_2 evolution band observed at 436°C over SnO_2 has shifted to 400°C over PdO/SnO_2 and further down to 390°C over Na-PdO/SnO_2 and lithium promotion of PdO/SnO_2 delayed the reduction of these species till 436°C whereas, potassium delayed till 446°C. Such effects were not observed over alkali-metal promoted SnO_2, showing that the changes in the reduction behavior of SnO_2 in the corresponding to this temperature range need be associated with the ternary interaction of Sn-Pd and the alkali-metal added.

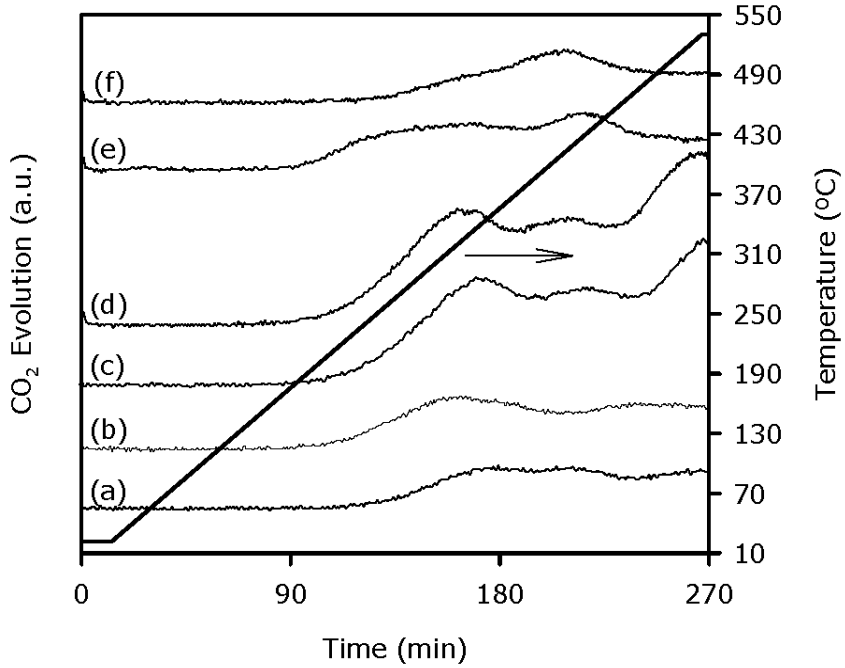

Figure 4.33 Temperature-programmed reduction CO_2 traces of (a) reduced K/SnO_2, (b) oxidized K/SnO_2, (c) reduced Na/SnO_2, (d) oxidized Na/SnO_2, (e) reduced Li/SnO_2 and (f) oxidized Li/SnO_2

(*Conditions:* P = 1 atm; GHSV = 12 800 hr^{-1}; [CO] = 2000 ppm; catalyst weight = 100 mg, heating rate = 2°C/min)

4.3 Competitive Oxidation of CO and H_2 over Alkali-metal Modified PdO/SnO_2

The influence of the presence of other reducing agents is particularly important for catalyzed low temperature oxidation of CO due to its relevance in selective oxidation of CO in hydrogen-rich streams for fuel cell applications and in elimination of carbon monoxide from automobile exhaust gases. Alkali metal modified PdO/SnO_2 catalysts, with their demonstrated low temperature CO oxidation activity, are potential candidates for CO oxidation catalysts in the presence of other reducing agents and the effect of the presence of hydrogen on the interaction of CO with alkali metal modified PdO/SnO_2 surfaces and competitive oxidation of CO and hydrogen with these catalysts were investigated for providing additional inputs to the investigation of the role and mechanism of alkali metal promotion and assessing the applicability of these catalysts in CO elimination in H_2 containing streams.

4.3.1 Temperature Programmed Reduction with CO-H_2 Mixtures

TPR technique utilizing a single or binary reducing agents was used in the investigation of the influence of carbon monoxide and hydrogen on the interaction of each other with PdO/SnO_2 based catalysts. CO/H_2-TPR experiments were carried out under CO lean conditions and the results of these experiments were elaborated with reference to the results of previously discussed CO-TPR experiments and control H_2-TPR experiments.

The CO_2 evolution traces of the catalysts are presented in Figure 4.34. A well resolved CO_2 band was observed in the CO_2 traces of all of samples in 90°C-230°C region with the maxima corresponding to 130°C over PdO/SnO_2, Na-PdO/SnO_2 and K-PdO/SnO_2 and to slightly higher temperatures over Li-PdO/SnO_2. This CO_2 band appeared to be more intense and had a well resolved shoulder in 175°C-275°C region in the case of K-PdO/SnO_2 (Figure 4.34a). Contrarily, the amount of CO_2 evolution from lithium modified sample appeared to be much lower than its counterparts (Figure 4.34c).

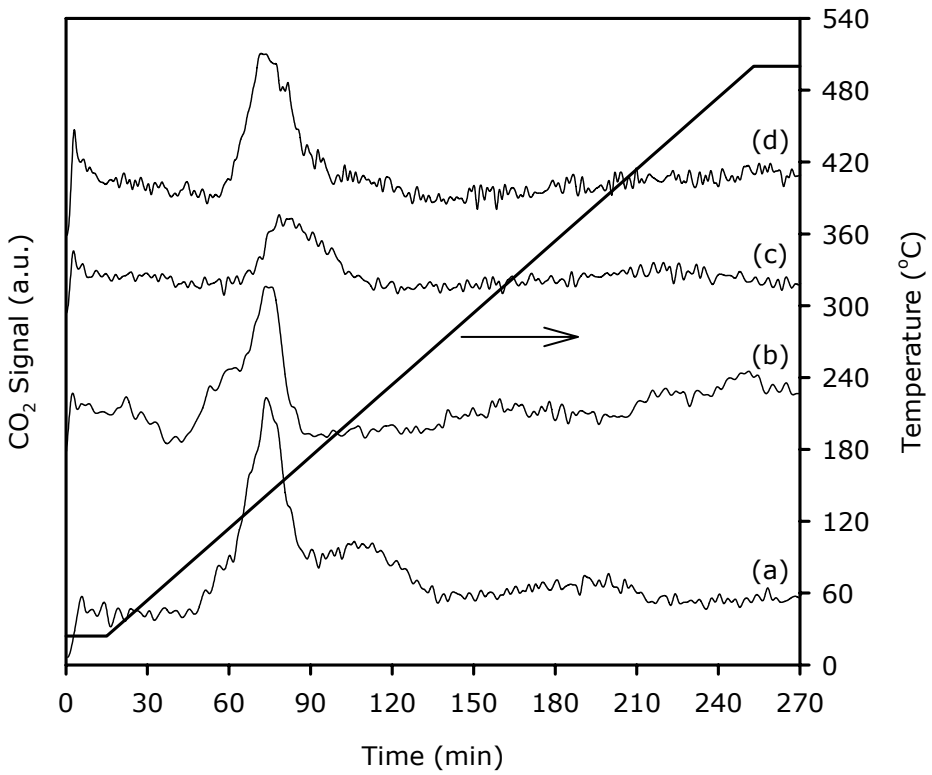

Figure 4.34 CO_2 evolution profiles during CO/H_2-TPR (a) K-PdO/SnO_2, (b) Na-PdO/SnO_2, (c) Li-PdO/SnO_2 and (d) PdO/SnO_2

(*Conditions:* P = 1 atm; GHSV = 6 400 hr^{-1}; [CO] = 2000 ppm and $[H_2]$ = 9000 ppm; catalyst weight = 100 mg, heating rate = 2°C/min)

Temperature programmed reduction of PdO/SnO_2-based catalysts with CO as the reducing agent yielded a CO_2 evolution band corresponding to 100°C-310°C with maxima corresponding to 275°C and a comparison of the position of the CO_2 bands resolved in CO/H_2-TPR traces of the catalysts with the results of CO-TPR experiments shows a shift in the CO_2 evolution bands towards lower temperatures implying the promotion of the activity CO adsorption/oxidation sites in the presence of hydrogen.

The water evolution traces collected during the CO/H_2-TPR experiments are presented in Figure 4.35. All of the water evolution profiles presented in Figure 4.35 exhibit a water evolution band right after the admittance of the reagents to the reactor, suggesting that the reduction of the catalysts with hydrogen can take place to a certain extent even at room temperature and an increase in the amount of water evolution from the surface was observed at the onset of the temperature program.

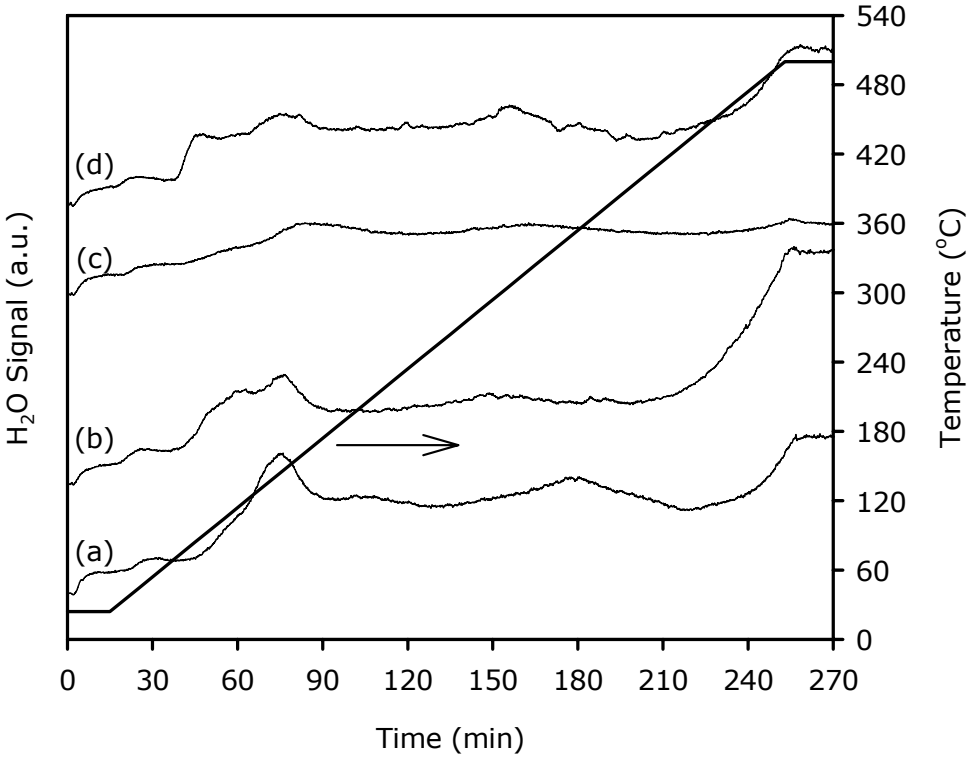

Figure 4.35 H_2O evolution profiles during CO/H_2-TPR (a) K-PdO/SnO_2, (b) Na-PdO/SnO_2, (c) Li-PdO/SnO_2 and (d) PdO/SnO_2

(*Conditions:* P = 1 atm; GHSV = 6 400 hr^{-1}; [CO] = 2000 ppm and [H_2] = 9000 ppm; catalyst weight = 100 mg, heating rate = 2°C/min)

Apart from the abovementioned H_2O bands, the water evolution profile of Li-PdO/SnO_2 was observed to be fundamentally different from its counterparts, exhibiting no well-resolved H_2O evolution bands in the temperature region studied (Figure 4.35c). Similarly, the CO oxidation activity under these reaction conditions was inferior to those of the other catalysts (Figure 4.34c), indicating that lithium promotion suppressed the reduction of the oxide species of the catalyst. Similar observations on the adverse effect of lithium on the reduction behavior of PdO/SnO_2 have already been reported through previous CO-TPR studies and the effect has been attributed to the formation of an anomalous phase, which has been observed through XRD analysis of Li-PdO/SnO_2 samples.

In addition to the water evolution bands observed during the isothermal reduction stage and at the onset of temperature program, a sharp increase in the level of H_2O evolution from PdO/SnO_2 was observed at 70°C and water evolution continued at a certain level throughout the temperature range studied

(Figure 4.35d). Such a water evolution profile implies that the reduction of the surfaces with hydrogen takes place at a certain rate which is probably limited to hydrogen adsorption because of the blanketing effect CO. In addition to this feature, another weak desorption band was also resolved in 120°C-180°C (Tmax=145°C) range. Both of these bands were also resolved over sodium and potassium modified catalysts (Figures 4.35a and 4.35b). The onset of the former band was observed to shift towards higher temperatures with alkali addition and the latter band was observed at the same temperature range in the H_2O traces of Na-PdO/SnO_2 and K-PdO/SnO_2 with an increase in its intensity. Both of these effects were more pronounced in the case of K-PdO/SnO_2. The shift in the onset of the first band towards higher temperatures supports the assumption that the rate of reduction of the surfaces is limited to hydrogen adsorption. Alkali metal mediated suppression of the adsorption the electropositive adsorbate may account for the mechanism leading to the suppression of hydrogen chemisorption. The electropositive character of the alkali-metals increase from top to bottom in the periodic table thus, the observed increase in the poisoning effect from sodium to potassium provides futher support for the proposed electrochemical mechanism. The second band that was resolved in 120°C-180°C region might be attributed to decomposition some surface complex that retains hydrogen on the surface at low temperatures. The interaction of hydrogen with alkali metal modified palladium is subject to formation of alkali-metal hydrides [148,158] as well as palladium hydride [80]. Furthermore, in the presence of CO, adsorbed CO and hydrogen may form H-CO complexes [68,80,198,199]. Each of these species may cause retention of hydrogen on the surface and result in the latter H_2O evolution band upon decomposition. It is interesting to note that this water evolution band was accompanied by CO_2 evolution from the surface thus, it would be more meaningful to associate this band with the decomposition of H-CO type surface complexes. The formation of H-CO complexes is further supported by H_2-TPR experiments discussed below as, no distinct water evolution bands that could be associated with decomposition of abovementioned hydride species were observed in the H_2-TPR profiles of the catalysts in the absence of CO.

Control H_2-TPR experiments were carried out to investigate the interaction of hydrogen with alkali modified PdO/SnO_2 surfaces and the influence of CO on this interaction. The water evolution profiles of unpromoted and alkali-metal promoted PdO/SnO_2 collected during H_2-TPR experiments are presented in Figure 4.36. For all of the catalysts the onset of a well resolved water evolution band

was observed just after the admittance of H_2 to the reactor. This low temperature water evolution band appeared in the temperature range 24-80°C and was observed as a weakly resolved doublet over all of the catalysts. The water evolution profiles clearly demonstrate that, regardless of the promoter, the PdO/SnO_2 surfaces can be reduced with hydrogen even at room temperature. At such a low temperature the reduction of bare SnO_2 support cannot be expected thus, it is most meaningful to associate this evolution band with the reduction of PdO_X species and reduction of the support sites by spillover of activated species from the noble metal centers. For the alkali-metal free sample the maxima of the water evolution band corresponded to lower temperatures when compared to the alkali promoted samples, where the maxima was observed around 50°C. The shift in the maxima towards higher temperatures in the case of alkali-metal promoted samples indicates that in the absence of alkali-metal promotion the PdO_X species of PdO/SnO_2 are more labile and thus, they can be reduced at slightly lower temperatures. Another important observation of the H_2-TPR studies is that, higher amount of water evolves from the potassium modified catalyst when compared to its counterparts. The higher amount of water evolution from the K-PdO/SnO_2 surface can be attributed to the facilitation of the reduction of the support through a potassium-assisted spillover mechanism. Apart from the low temperature evolution, no distinct water evolution bands were clearly resolved over any of the catalysts till 430°C, where the onset of another water evolution band was present. Water evolution at such high temperatures need be associated with the reduction of the oxide species of the support.

A comparison of the water evolution profiles collected during H_2-TPR experiments with the ones collected during CO/H_2-TPR experiments suggest an increase in the water evolution bands in the presence of CO in the reactor feed. When CO and H_2 coexist in the reactor feed; hydrogen consumption, thus water evolution form the surfaces, take place at around 100°C which corresponds to temperatures approximately 70°C higher relative to the absence of CO in the reactor feed, implying that reduction of the surface by hydrogen is suppressed in the presence of CO. These results are in agreement with previous studies on the competitive oxidation of CO and H_2 over noble metal catalysts [62, 66-69] where the promoting effect of hydrogen have been attributed to the formation of H-CO surface complexes. The interaction of H and CO to form formyl-like complexes have been postulated to lead to desorption of CO at lower temperatures eliminating the site blocking effect arising from the strong interaction of CO with noble metals.

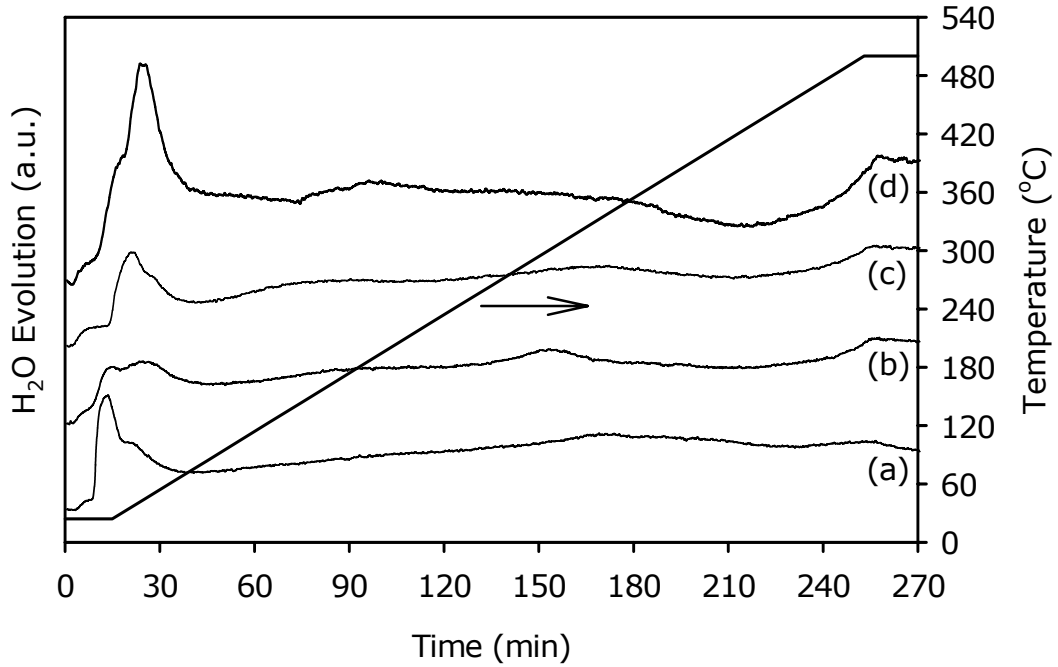

Figure 4.36 H_2O Evolution profiles during H_2-TPR (a) PdO/SnO_2, b) Li-PdO/SnO_2, (c) Na-PdO/SnO_2 and (d) K-PdO/SnO_2

(*Conditions:* P = 1 atm; GHSV = 6 400 hr^{-1}; $[H_2]$ = 9000 ppm; catalyst weight = 100 mg, heating rate = 2°C/min)

In addition to the shift in the water evolution bands to higher temperatures, the coexistence of CO with H_2 in the reactor feed during TPR experiments resulted in a decrease in the amount of H_2 consumption of the catalysts, which was manifested by a decrease in the intensity of the water evolution bands relative to the H_2-TPR experiments (Figures 4.36 and 4.35). Given that the oxygen content of the catalysts are limited, this evidences that CO and H_2 interact over the surface and some of the oxide species over the surface preferentially oxidize CO even in the presence of excess amount of H_2 in the gas phase.

As the catalysts were observed to exhibit selectivity towards CO oxidation under these reaction conditions the sustainability of this selective oxidation activity and the ability to replenish the CO active surface sites were investigated through temperature programmed reaction spectroscopy experiments and by time-on-stream activity tests with different oxygen concentrations at the gas phase. The results of these experiments will be presented in the next section.

4.3.2 Temperature-Programmed Reaction Spectroscopy (TPRS) Studies

In addition to the interaction of CO and H_2 on PdO/SnO_2-based surfaces and their influence on the adsorption/desorption dynamics of each other, the effect of hydrogen on CO oxidation with these catalysts was investigated from a mechanistic point of view. The CO and H_2 activity and, CO selectivity of unmodified and alkaline modified PdO/SnO_2 were studied with temperature-programmed reaction spectroscopy experiments by considering the gas phase concentration of the oxidizing component as a parameter. For this purpose, the gas phase concentration of oxygen was changed to yield CO-to-O ratios of 1, 0.5, 0.25 and 0.17 while, the concentration of the reducing components were kept constant. The presented conversion versus temperature curves and, the reported light-off temperature and CO selectivity values are obtained from the CO, H_2 and O_2 traces collected during TPRS experiments. Moreover, the CO oxidation steady-state activity and selectivity of alkali metal modified catalysts were studied under conditions resembling upstream fuel processing system in the H_2 fuel cell. The reactor feed for these experiments constituted 70% H_2, 2000 ppm CO with [CO]/[O]=0.5. For these experiments, the reported conversion and selectivity values represent the activity of the catalysts after 20 minutes on stream.

When the gas phase concentration of CO and O_2 are adjusted to correspond to a CO-to-O ratio of 1, all of the catalysts except for K-PdO/SnO_2 were observed to exhibit an insignificant CO oxidation activity although a considerable portion of hydrogen was consumed (Figure 4.37). In the 25°C-175°C region, a maximum hydrogen conversion of approximately 20% was observed over all of the catalysts. In the same temperature range, the maximum CO conversion achieved over PdO/SnO_2, Li-PdO/SnO_2 and Na-PdO/SnO_2 was in the order of 10% while this value was tripled in the case of K-PdO/SnO_2. It is worthwhile to note that, the previously mentioned TPRS experiments with CO-O_2 mixtures have evidenced the suppression CO oxidation activity of PdO/SnO_2 by the addition of potassium. However, CO-H_2-O_2 TPRS experiments showed that, under reducing conditions, K-PdO/SnO_2 exhibits significantly higher CO oxidation activity than both PdO/SnO_2 and its alkaline modified counterparts.

The H_2O traces of the catalysts in 20°C-230°C region is presented in Figure 4.38. Two water evolution bands, corresponding to the admittance of the reagents to the reactor and the onset of the temperature program were resolved in the H_2O

traces before the onset of significant water evolution from the surfaces due to hydrogen oxidation. The weakly resolved bands might be associated with the reduction of the catalysts at low temperatures which take place at a limited extent. The band resolved in 120°C-150°C region has previously observed during CO/H_2-TPR studies and has been associated with the decomposition of a CO-H complex as the band was accompanied by CO_2 evolution. No other water evolution bands that could evidence the formation and decomposition of palladium hydride or alkali-metal hydride species was resolved in the H_2O traces.

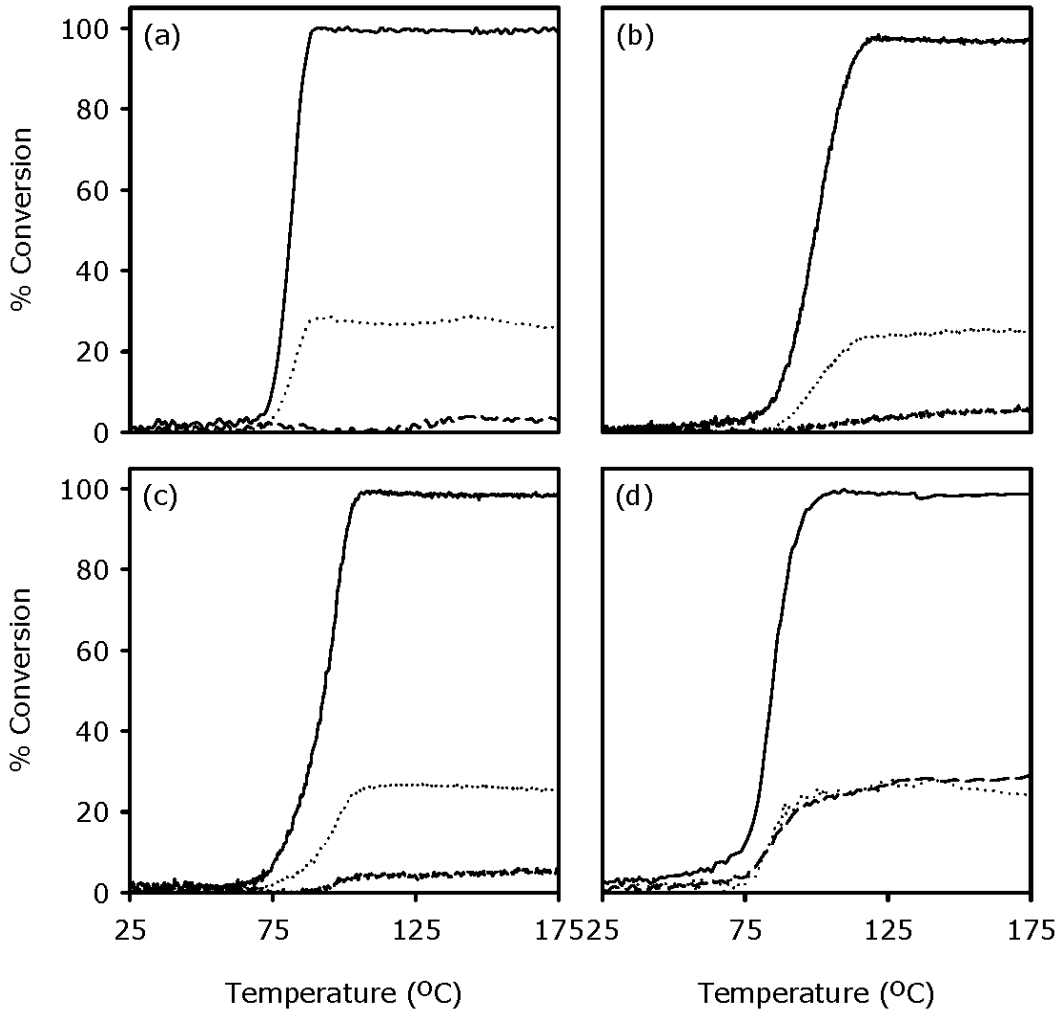

Figure 4.37 CO (------), O_2 (———) and H_2 (.....) conversion over oxidized (a) PdO/SnO_2, (b) Li-PdO/SnO_2, (c) Na-PdO/SnO_2 and (d) K-PdO/SnO_2

(*Reaction Conditions:* P = 1 atm; GHSV = 6 400 hr^{-1}; [CO]/[O] = 1; [CO] = 2000 ppm and $[H_2]$ = 9000 ppm; catalyst weight = 100 mg, heating rate = 2°C/min)

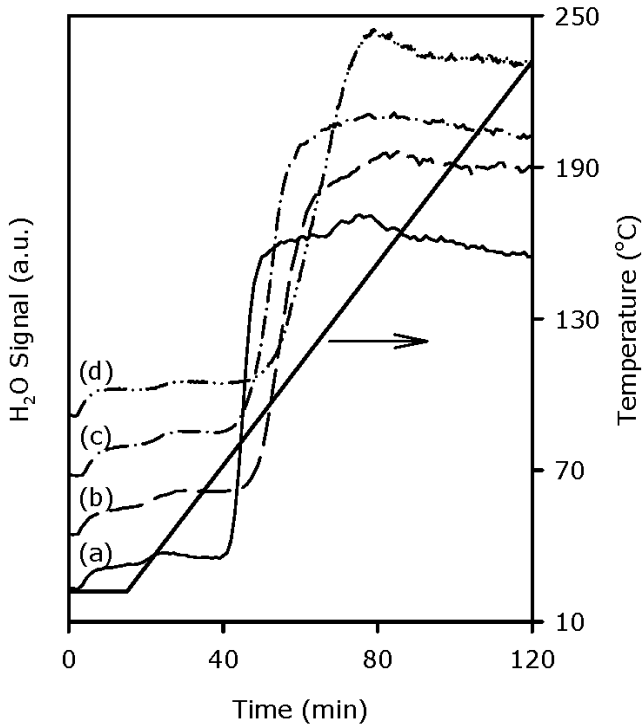

Figure 4.38 Water evolution profiles of (a) PdO/SnO_2, (b) Li-PdO/SnO_2, (c) Na-PdO/SnO_2 and (d) K-PdO/SnO_2

(*Reaction Conditions:* P = 1 atm; GHSV = 6 400 hr^{-1}; [CO]/[O] = 1; [CO] = 2000 ppm and $[H_2]$ = 9000 ppm; catalyst weight = 100 mg, heating rate = 2°C/min)

Doubling the oxygen concentration in the feed, i.e. [CO]/[O] = 0.5, resulted in approximately two-fold increase in the H_2 conversion rates (Figures 4.39). An insignificant increase in maximum CO conversion in 25°C-175°C region over oxidized PdO/SnO_2 was present whereas, the rates of CO conversion were doubled over Li-PdO/SnO_2 and Na-PdO/SnO_2 under this feed condition (Figures 4.39a to 4.39c). The highest CO oxidation activity was observed over K-PdO/SnO_2 where, CO conversions in the order of 40-45% are achieved (Figure 4.39d). When the light-off temperatures for O_2 are compared, the lowest light-off temperature (73°C) was observed over PdO/SnO_2 the corresponding values for Li-PdO/SnO_2 and Na-PdO/SnO_2 were 78°C and 76°C, respectively. A higher light-off temperature (88°C) was observed in the case of K-PdO/SnO_2. The variation of light-off temperatures may be correlated with H_2 oxidation activity of the catalysts in the presence of CO as, no significant CO oxidation activity was observed around 70-80°C over any of the catalysts.

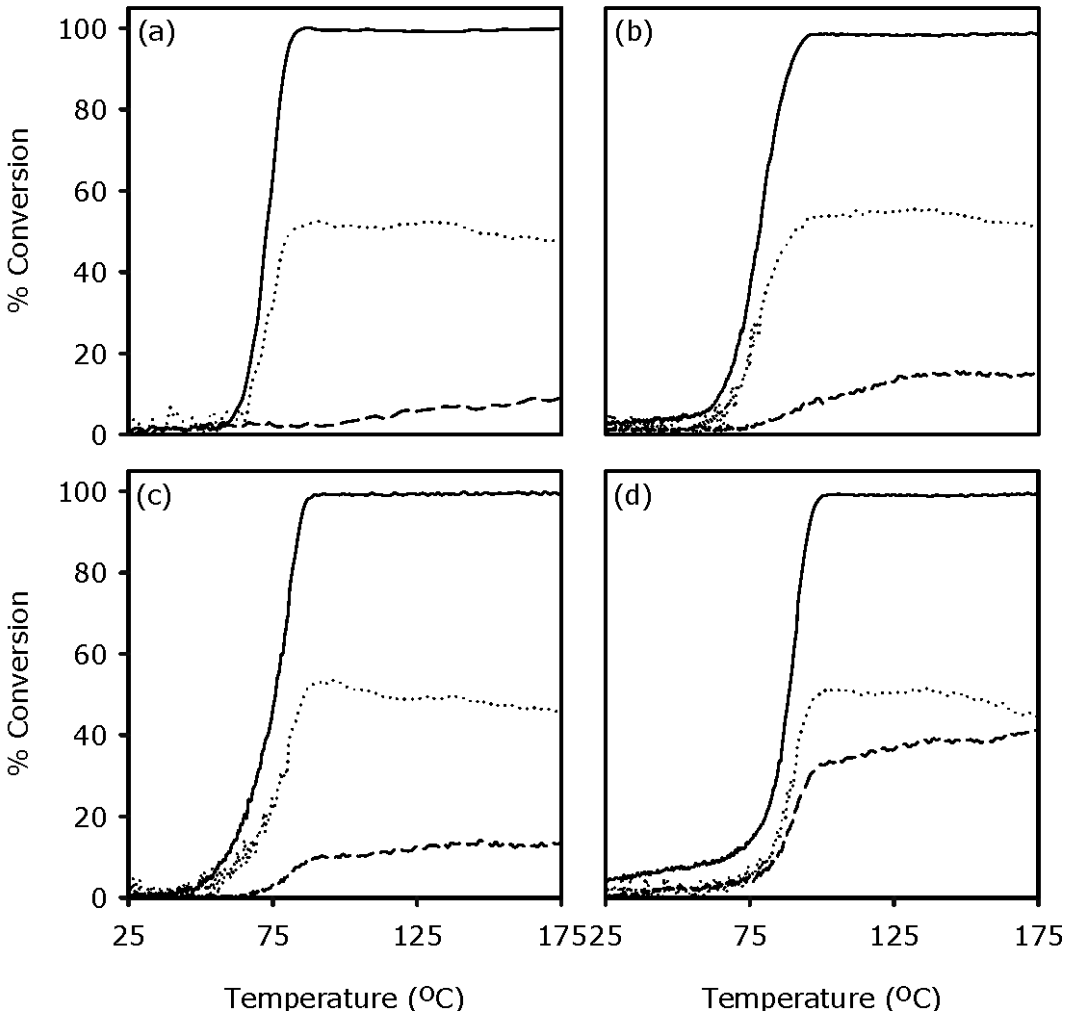

Figure 4.39 CO (------), O_2 (———) and H_2 (.....) conversion over oxidized (a) PdO/SnO_2, (b) Li-PdO/SnO_2, (c) Na-PdO/SnO_2 and (d) K-PdO/SnO_2

(*Reaction Conditions:* P = 1 atm; GHSV = 6 400 hr^{-1}; [CO]/[O] = 0.5; [CO] = 2000 ppm and [H_2] = 9000 ppm; catalyst weight = 100 mg, heating rate = 2°C/min)

The oxygen concentration in the reactor feed was further doubled to correspond to a CO-to-O ratio of 0.25. Under this reactor feed condition, maximum CO conversions observed over PdO/SnO_2, Li-PdO/SnO_2 and Na-PdO/SnO_2 were in the order of 35-40% while, approximately 60% of CO in the reactor feed was oxidized over K-PdO/SnO_2 (Figure 4.40). When the light-off temperatures for H_2 are considered the highest light-off temperature corresponded to the potassium modified sample with 94°C and the lowest to PdO/SnO_2 with 70°C. The H_2 light-off temperatures corresponding to Li-PdO/SnO_2 and Na-PdO/SnO_2 were 89°C and 82°C, respectively.

The effect of interference of hydrogen on the CO oxidation activity of alkaline modified PdO/SnO_2 catalysts was also tested under oxidizing conditions where, CO-to-O_2 ratio corresponded to 0.17. Under this feed condition, reduced catalyst samples were also studied with regard to their CO oxidation activity for observing the effect of initial oxygen coverage on the activity. For oxidized PdO/SnO_2, the light-off temperatures for CO and H_2 were 136°C and 65°C, respectively (Figure 4.41a). Reduction pretreatment resulted in a decrease in the CO oxidation activity and the light-off temperatures of CO and H_2 were observed as 150°C and 100°C, which are 25°C and 35°C higher than the respective the light-off values observed over the oxidized counterpart (Figure 4.41b). In contrast to the current TPRS data with CO-H_2-O_2 mixtures, previous temperature-programmed characterization data presented in Section 4.1.3 for the CO oxidation activity of PdO/SnO_2-based catalysts in CO-O_2 mixtures have shown that reduction pretreatment had a promoting effect on the CO oxidation activity of PdO/SnO_2 catalysts. The lower reaction rates observed over oxidized samples have been associated with the competition between CO and O_2 for the same adsorption sites. As oxidation pretreatment would saturate the surfaces with oxygen ad-species, the adsorption of CO over oxygen precovered surfaces would be hindered, resulting in lower rates of CO oxidation. Reduction pretreatment would result in significant decrease in the abundance of oxygen ad-species and during the course of the CO-O_2 TPRS experiments, when oxygen is supplied to the reactor, oxygen species would be replenished by adsorption from the gas phase and the effective oxidation of the catalyst surface coupled with CO adsorption vacancies created during reduction pretreatment would lead to enhancement of the rates over prereduced samples. However, incorporation of hydrogen to the reactor feed significantly alters the picture for unmodified PdO/SnO_2 and leads to lower rates of both CO and H_2 oxidation over reduced samples.

Palladium is a well-known Mars-van-Krevelen catalyst and the oxidation of species chemisorbed on Pd proceeds through the involvement of lattice oxygen species which are then replenished by adsorption from the gas phase. The involvement of lattice oxygen species in CO oxidation over PdO/SnO_2-based catalysts has been reported through CO-impulse studies over these catalysts (see Section 4.1.6). The replenishment of these sites with oxygen from the gas phase is a critical step in palladium catalyzed oxidation reactions and the abovementioned decrease in the reaction rates of both H_2 and CO need be

associated with surface oxygen content related limitations. Although the reactor feed was oxygen rich in terms of oxidation of both CO and H_2, it is probable that this gas phase composition is not reflected in the relative surface coverage of oxidizing and reducing components at low temperatures. As CO-O_2 TPRS experiments have shown the enhancement of CO oxidation rates with reduction pretreatment, adsorbed hydrogen and/or CO-H complexes may be considered as the potential candidates that could interfere with oxygen adsorption. The competitive oxidation of CO and H_2 over palladium and platinum surfaces has been observed to result in a new adsorption state for both of these molecules [197-199]. In the TPD spectra of CO and H_2, this new adsorption state was observed as the appearance of another desorption band and the band was associated with the formation –COH complexes [198,199] whose presence was reported through DRIFTS studies on supported palladium catalysts [80]. Further support for the formation of –COH complexes have been provided by CO/H_2-TPR experiments discussed in Section 4.3.1 where, bands of simultaneous CO_2 and H_2O desorption were resolved in 120°C-180°C region and has been attributed to the decomposition of such surface complexes.

The TPRS data for the lithium modified sample suggested a simultaneous shift in the H_2 and CO conversion curves towards higher temperatures relative to the unpromoted sample and the light-off temperatures for CO and H_2 were recorded as 160°C and 82°C, respectively (Figure 4.41c). Reduction pretreatment of Li-PdO/SnO_2 had opposite effects on the CO and H_2 oxidation behavior of this catalyst such that, the H_2 conversion versus temperature curve shifted to higher temperatures when compared to oxidized Li-PdO/SnO_2 whereas, CO conversion versus temperature curve shifted to lower temperatures (Figure 4.41d). The light-off temperature for CO was 140°C which accounts to a 20°C decrease relative to the light-off temperature observed over the oxidized counterpart. For H_2, the light-off temperature increased by 24°C to 106°C. These observations imply that reduction pretreatment of Li-PdO/SnO_2 resulted in the promotion of CO oxidation over the catalyst surface whereas; it suppressed H_2 oxidation over this catalyst.

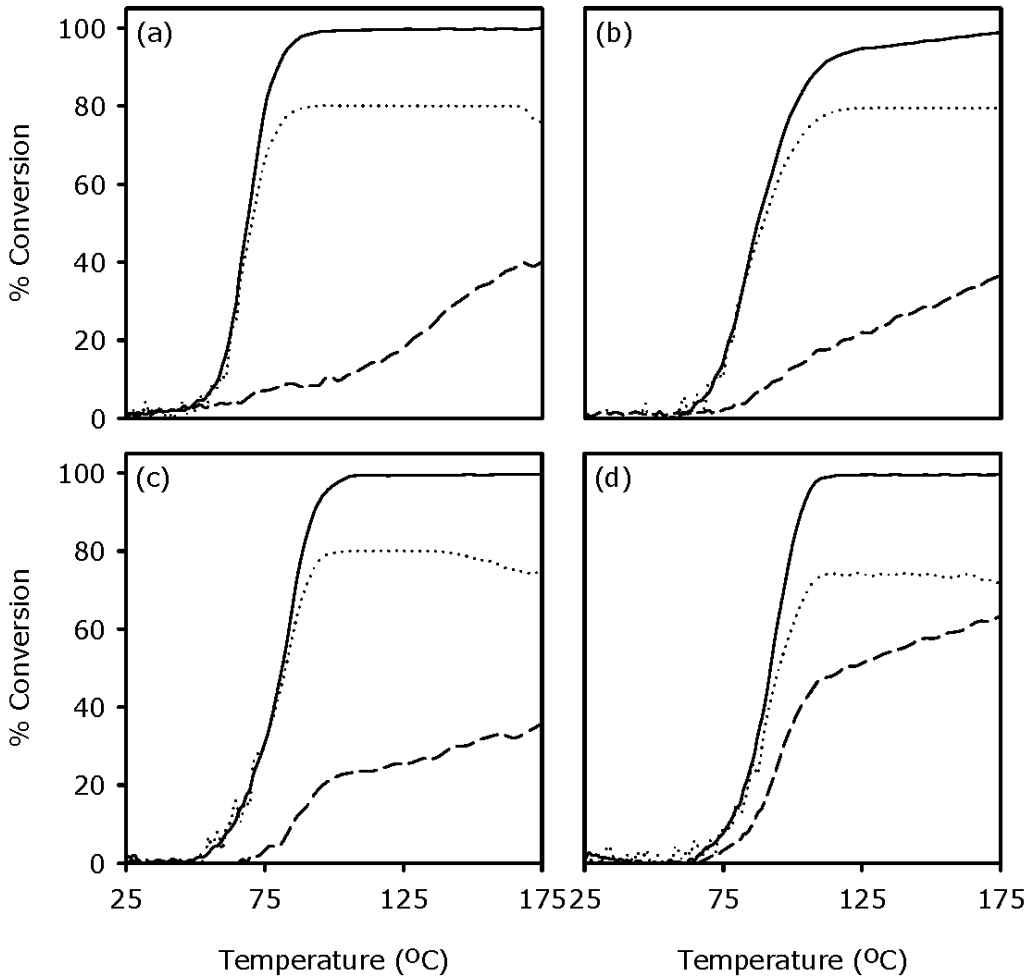

Figure 4.40 CO (------), O_2 (———) and H_2 (.....) conversions over oxidized (a) PdO/SnO_2, (b) Li-PdO/SnO_2, (c) Na-PdO/SnO_2 and (d) K-PdO/SnO_2

(*Reaction Conditions:* P = 1 atm; GHSV = 6 400 hr^{-1}; [CO]/[O] = 0.25; [CO] = 2000 ppm and $[H_2]$ = 9000 ppm; catalyst weight = 100 mg, heating rate = 2°C/min)

In the case of oxidized Na-PdO/SnO_2, retardation of H_2 oxidation to result in a 15°C increase in the light-off temperature relative to PdO/SnO_2 was observed (Figure 4.41e). However, this fact is not reflected in the CO conversion rates and the light-off temperature for CO was recorded as 137°C indicating that sodium modification has no effect on the CO activity. Subjecting this catalyst to reduction pretreatment had no significant effect on the H_2 oxidation activity of Na-PdO/SnO_2 while, it shifted the CO conversion curve to lower temperatures with respect to the oxidized sample (Figure 4.41f). The light-off temperatures for CO and H_2 were 116°C and 80°C, respectively.

Among the alkali-metal modifiers, potassium had the most striking effect on the H_2 and CO oxidation activity. A shift in H_2 conversion curve towards higher temperatures with respect to PdO/SnO_2 was coupled with a shift in the CO conversion curve towards lower temperatures (Figure 4.41g). The light-off temperature for H_2 was recorded as 92°C as opposed to 108°C for the light-off temperature of CO. Upon reduction pretreatment the light-off temperature for H_2 increased by 4°C with respect to the oxidized counterpart while; the light-off temperature of CO decreased by 8°C (Figure 4.41h). For prereduced K-PdO/SnO_2, CO conversion was slightly higher than the H_2 conversion at temperatures below 95°C where, the conversion curves for CO and H_2 intersect and 100°C represents the light-off temperature of both of the species.

The CO-H_2-O_2 TPRS results suggest that alkali-metal promotion may serve as an alternative for promoting the CO oxidation activity of PdO/SnO_2 catalysts in the presence of hydrogen. The shift of hydrogen conversion versus temperature curves of the alkali-metal modified samples towards higher temperatures relative to unmodified PdO/SnO_2 imply the suppression of hydrogen adsorption/oxidation by the presence of alkali-metals. The suppression of hydrogen adsorption in the presence of alkali-metals have previously been reported by several authors [145-147,157] and an interpretation of the results have been provided by Vayenas et *al.* [129]. As it has been stated before, alkali-metals tend to enhance the chemisorption of electron acceptor adsorbates and suppress the adsorption of electron donor adsorbates thus, the lower rate of H_2 conversion over the alkaline modified sample may arise from alkali-mediated decrease in the relative surface coverage of hydrogen while, the adsorption of O_2 and CO, which are electron acceptor adsorbates, is promoted. However, as it is apparent from the CO and H_2 oxidation behavior of Li-PdO/SnO_2 suppression of H_2 adsorption/oxidation is not sufficient for obtaining high CO oxidation rates.

Though alkali-metals tend to suppress the adsorption of hydrogen they simultaneously promote the interaction of oxygen and carbon monoxide with the surface. Promotion of the adsorption of the former would result in poor CO oxidation activity due to the increased stability of these species on the surface. Alternatively, the promotion of the adsorption of the latter would suppress the CO oxidation activity by retaining CO on the surface or leading to the dissociation of the molecule. As they lead to the weakening of C-O bond of chemisorbed CO which might result in the cleavage of the bond alkali-metals are frequently applied in CO hydrogenation catalysis [130-132]. It is obvious that the cleavage of the C-O bond needs to be avoided for selective oxidation of CO in the presence of H_2. Therefore, the aim in promoting the CO activity by alkali-metals should be to promote the adsorption of CO without leading to the dissociation of the molecule.

The suppression of the CO oxidation activity of PdO/SnO_2 by introduction of lithium to the structure may arise from either one of these factors. In fact, this light-off behavior of CO over Li-PdO/SnO_2 is in line with previous *in-situ* dynamic characterization results where, lithium modification was observed to suppress the CO oxidation activity of PdO/SnO_2. Through CO-TPR experiments lithium addition has been shown to suppress the reduction of oxide and hydroxide species possibly through an interaction between these species and lithium and, the inferior activity of lithium modified catalysts have been attributed to this observation. In addition to the stabilization of oxide species in the presence of lithium, CO dissociation may also act to suppress CO oxidation over Li-PdO/SnO_2 and such a mechanism would also account for the suppression of H_2 adsorption on a surface covered with C and O from CO.

Another important point that needs to be mentioned is a high CO oxidation rate region observed in 80°C-110°C region over alkali-metal promoted catalysts (Figure 4.41). This unusual temperature dependence of the rate of CO conversion is much well resolved over potassium modified sample that its counterparts and is not resolved in the case of the unpromoted sample. At the onset of this band an increase in the CO conversion rate was observed where CO conversion curve closely follows H_2 conversion curve and the inflection of the CO conversion profile occurs at around 100°C over oxidized Li-PdO/SnO_2 and Na-PdO/SnO_2 and at 125°C over oxidized K-PdO/SnO_2, where CO conversion significantly diverges from that of H_2. In the case of the samples subjected to reduction pretreatment, the inflection point has shifted to higher temperatures

and was less clearly resolved than the oxidized samples. The initial increase in the CO oxidation rate might be attributed to the reduction of palladium oxide species to metallic palladium, which are more active in CO oxidation than palladium oxide. The disappearance of the onset of this high rate region with reduction pretreatment supports this view as, reduction of a considerable amount of palladium oxide species has already been completed during the preceding reduction stage. As the reaction mixture was oxidizing in nature, the oxidation of these palladium sites is to be expected with increasing temperature and the transition between high rate region to low rate region observed in the vicinity of 110°C might be associated with the oxidation of palladium to result in the low CO oxidation rate regime due to the low activity of PdO in CO oxidation. Over samples subjected to reduction pretreatment, the initial concentration of Pd^0 would be higher and oxidation of these sites would be suppressed because of the enhanced rates of CO and H_2 conversion over these samples therefore, the transition from the high rate regime to the low rate regime was less clearly resolved over the samples subjected to reduction pretreatment. A similar temperature dependence of the CO conversion profile in the presence of H_2 was also observed by Oh and Sinkevitch [65] over Pd/Al_2O_3 and has been attributed to the oxidation of highly active Pd centers to PdO, which are less active than Pd in CO oxidation.

It is also plausible that hydrogen oxidation might lead to localized temperature increase in the vicinity of the metal centers and this localized increase may give rise to enhanced CO oxidation rates that are observed as the high rate regions in the CO versus temperature profiles. Although this possibility should not be ruled out, the disappearance of the hig rate regime in the CO conversion profile of PdO/SnO_2 where highest hydrogen oxidation rate was present suggests that another mechanism rather than localized temperature rise should be effective.

The rates of CO and H_2 oxidation and CO selectivity were calculated at 50% conversion of O_2 in the reactor feed (Table 4.4). The reaction rate data also evidence the high CO activity and selectivity exhibited by K-PdO/SnO_2 under all of the conditions studied. Although an increase in the rates of both of the reactions over all of the catalysts was observed by increasing oxygen concentration, the ratio of the rates of CO oxidation to H_2 oxidation increase by alkali-metal addition, especially under oxidizing conditions suggesting that alkali-metals act to favor CO oxidation reaction, the effect being more readily observed in the case of potassium.

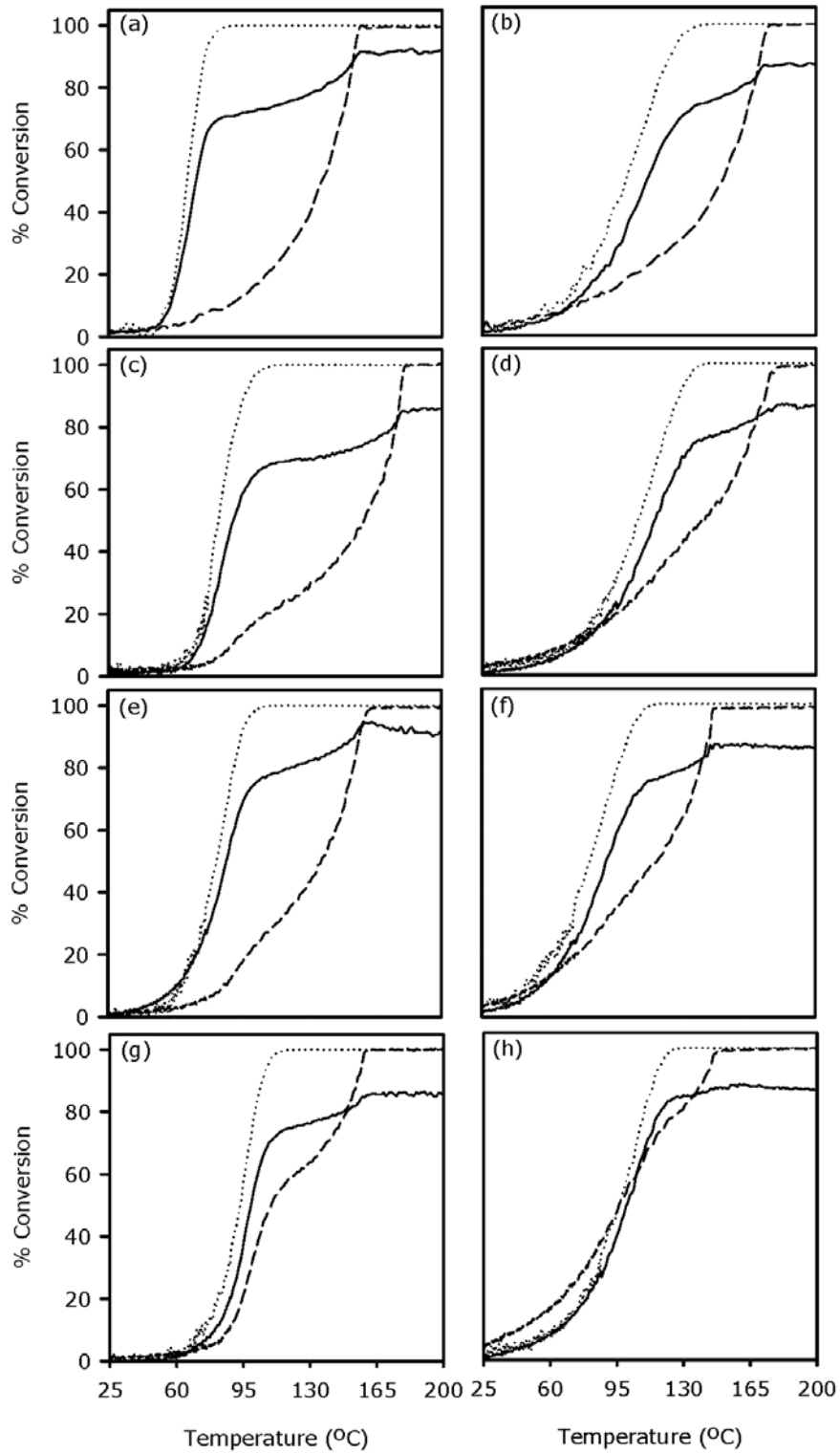

Figure 4.41 CO (------), O_2 (———) and H_2 (.....) conversion over (a) oxidized PdO/SnO_2, (b) reduced PdO/SnO_2, (c) oxidized Li-PdO/SnO_2, (d) reduced Li-PdO/SnO_2, (e) oxidized Na-PdO/SnO_2 (f) reduced Na-PdO/SnO_2, (g) oxidized K-PdO/SnO_2 and (h) reduced K-PdO/SnO_2

(*Reaction Conditions:* P = 1 atm; GHSV = 6 400 hr^{-1}; [CO]/[O] = 0.17; [CO] = 2000 ppm and $[H_2]$ = 9000 ppm; catalyst weight = 100 mg, heating rate = 2°C/min)

Table 4.4 Rates of CO and H_2 oxidation (μmol/m^2.min) and CO Selectivity at $X_{O_2} = 0.5$ *

		PdO/SnO_2	Li-PdO/SnO_2	Na-PdO/SnO_2	K-PdO/SnO_2
[CO]/[O_2] = 2	R_{H_2}	0.408	0.351	0.351	0.450
	R_{CO}	0.010	0.010	0.009	0.085
	S_{CO}	2.8	3.2	2.8	24.0
	R_{CO}/R_{H_2}	0.023	0.029	0.026	0.189
[CO]/[O_2] = 1	R_{H_2}	0.782	0.734	0.682	0.813
	R_{CO}	0.019	0.017	0.019	0.118
	S_{CO}	2.8	2.6	2.9	16.6
	R_{CO}/R_{H_2}	0.024	0.023	0.028	0.144
[CO]/[O_2] = 0.5	R_{H_2}	1.426	1.308	1.433	1.327
	R_{CO}	0.037	0.043	0.045	0.134
	S_{CO}	5.5	6.7	6.8	9.5
	R_{CO}/R_{H_2}	0.026	0.033	0.031	0.101
[CO]/[O_2] = 0.17	R_{H_2}	2.212	2.253	2.011	0.600
	R_{CO}	0.037	0.068	0.068	0.235
	S_{CO}	1.80	3.50	3.43	11.07
	R_{CO}/R_{H_2}	0.017	0.030	0.034	0.392

**Reaction Conditions:* P = 1 atm; GHSV = 6 400 hr^{-1}; [CO] = 2000 ppm and [H_2] = 9000 ppm; catalyst weight = 100 mg

4.3.3 Time-on-stream Activity – Under Fuel-Cell Conditions

Under conditions that resemble the fuel-cell upstream fuel processing conditions, the steady-state CO oxidation activity and selectivity of oxidized PdO/SnO_2, Na-PdO/SnO_2 and K-PdO/SnO_2 were tested to investigate the applicability of these catalysts as selective CO oxidation catalysts in H_2 fuel cells. The reactor feed for these steady-state activity measurements constituted 2000 ppm CO, 2000 ppm O_2 and 70% H_2 and, the CO conversion and selectivity are reported at 50°C-140°C region, which is the relevant range of operation for a selective CO oxidation catalyst under fuel cell operating conditions. The time-on-stream CO and O_2 conversions and CO selectivities are presented in Figure 4.42 and these values are representative of the activity of the catalysts after 20 minutes on stream.

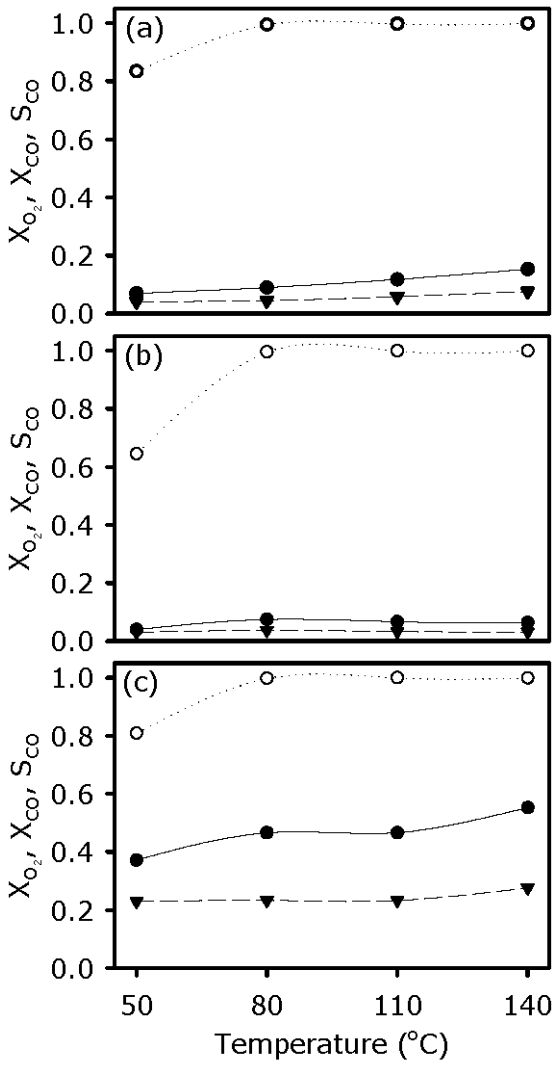

Figure 4.42 Steady-state CO (●) and O_2 (○) conversions and CO selectivity (▼) (a) PdO/SnO_2, (b) Na-PdO/SnO_2 and (c) K-PdO/SnO_2

(*Reaction Conditions:* P = 1 atm; GHSV = 6 400 hr^{-1}; [CO]/[O] = 0.5; [CO] = 2000 ppm and $[H_2]$ = 9000 ppm; catalyst weight = 100 mg)

It is evident from Figure 4.42 that, under fuel cell operating conditions PdO/SnO_2 and Na-PdO/SnO_2 exhibit insignificant CO oxidation activity and thus, selectivity towards CO oxidation and, nearly all of the oxygen present in the reactor feedstream was consumed by the side reaction to oxidize hydrogen. In line with the previous TPRS experiments with CO-H_2-O_2 mixtures, potassium modified PdO/SnO_2 was observed to be more active and selective than PdO/SnO_2 and Na-PdO/SnO_2 towards CO oxidation under steady-state conditions. In the case of the potassium promoted sample CO conversions around 50% were attained in 50°C-140°C region and the selectivity of this catalyst as calculated to be in the order of 20% indicating that this catalyst has the potential for being applied in CO elimination from H_2 containing gases.

4.4 Effect of Alkali-Metal Concentration on Properties of PdO/SnO_2-Based Catalysts

Alkaline modifiers are known to alter the relative surface coverage of electron donor and electron acceptor adsorbates and two factors have direct influence on the promotion of oxidation reactions by alkali-metal modifiers:

1. The relative molar ratios of oxidizing and reducing species in the gas phase which, would impose surface concentration and coverage limitations on the surface. The gas phase composition has been observed to have significant influence on the promoting action of sodium in CO-O_2 TPRS experiments discussed above. Moreover, the results of the TPRS experiments with CO-H_2-O_2 gas mixtures have also evidenced the influence of relative molar ratios of oxidizing and reducing species on the modification of catalytic properties by alkali metals.

2. The amount of modifier loading is the other factor that has been reported to have significant influence on the promotion of oxidation reactions by alkali metals [194-196]. In general, the promotion of supported noble metal catalysts exhibit a volcano type behavior as a function of alkali metal content of the catalyst, which goes through a maximum at the alkali metal loading and decreases by the inhibition of the rates beyond the optimum alkali metal loading. Therefore, optimization of the alkali metal content is of great importance for designing catalyst formulations for high activity and selectivity.

The former tool for the control of relative surface coverages of oxidizing and reducing species has been utilized in the preceding sections and in this section the effect of the latter on CO oxidation with alkaline modified PdO/SnO_2 catalysts is discussed. For this purpose, PdO/SnO_2 catalysts with different sodium and potassium contents were tested with CO-TPR, $CO-O_2$ and $CO-H_2-O_2$ TPRS experiments. All the alkali metal modified catalysts tested characterized and dynamically tested so far have alkali metal (A)-to-palladium atomic ratio of 0.53, which corresponds to 0.1 wt. percentage sodium loading in the case of Na-PdO/SnO_2. Na-PdO/SnO_2 and K-PdO/SnO_2 catalysts with A-to-Pd ratios of 0.32, which corresponds to 0.1 wt. percentage potassium loading in the case of K-PdO/SnO_2, and 1.50 were synthesized and characterized and, the results are discussed together with previous results to elucidate the influence of alkali metal content on catalytic properties of PdO/SnO_2-based catalysts.

Lithium modified catalysts were not subject to these tests as lithium modification has been observed to lead to formation of an anomalous crystallographic phase (see Figure 4.26), which has been tested at various lithium loadings and, this phase has been postulated to result in the poor catalytic activity of Li-PdO/SnO_2.

The BET surface areas of Na/0.32 and Na/1.50 are 48 m^2/g and 52 m^2/g, respectively and similarly, the active surface areas of K/0.32 and K/1.50 are 58 m^2/g and 53 m^2/g, respectively.

4.4.1 Effect of Modifier Concentration on the Crystal Structure

Na-PdO/SnO_2 (Na/0.32 and Na/1.50) and K-PdO/SnO_2 (K/0.32 and K/1.50) catalysts with different alkali-metal modifier contents were characterized with XRD to investigate the influence of the alkali-metal content on the crystal structure. Regardless of the type of the alkali metal and content, the major crystallographic phase present in the samples was cassiterite (mineral tin dioxide), which has anatase structure (Figure 4.43). As a consequence of the difficulties mentioned earlier, the identification of palladium oxide phase that co-exists with tin dioxide is a formidable task especially when the palladium oxide content is very low and, only weakly resolved reflections that could be assigned to palladium oxide phase exist in the diffraction patterns. First of these bands that could be associated with reflection from (103) plane of palladium oxide was resolved at 60.1° and was observed in the XRD pattern of Na/0.32 (Figure 4.43a). Two other weakly resolved peaks were observed at 29.2° and 70.4° in the pattern of Na/1.50. These bands may be associated with reflections from

(100) and (004) of palladium oxide, respectively Figure 4.43b). One of these bands was also resolved in the XRD pattern of K/0.32 (Figure 4.43c).

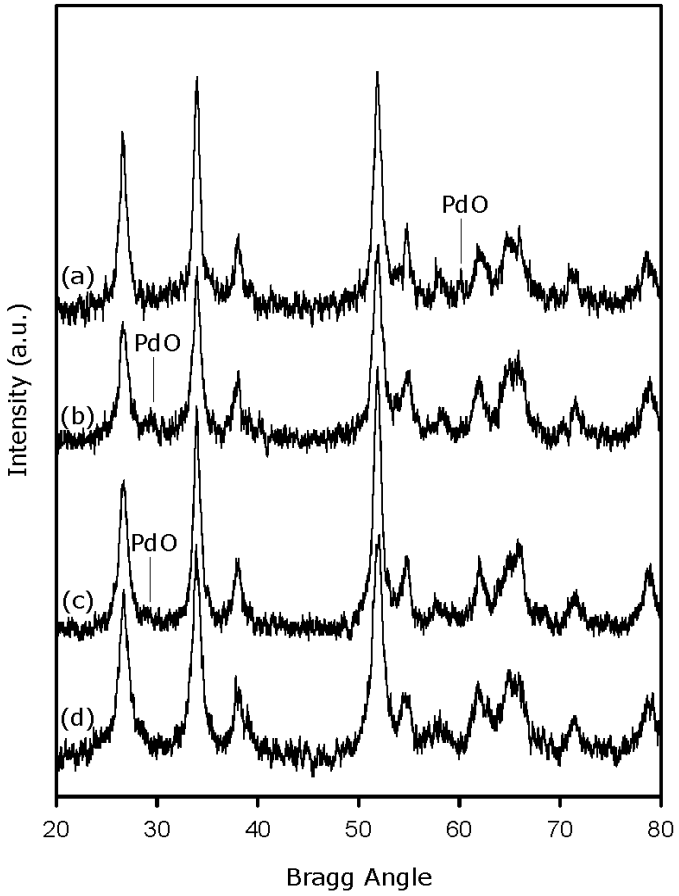

Figure 4.43 XRD patterns of (a) Na/0.32, (b) Na/1.50, (c) K/0.32 and (d) K/1.50

The broadening of the XRD peaks with increasing alkali-metal content was another artifact observed from the XRD patterns (Figure 4.44). The broadening of the XRD peaks suggest a decrease in the crystallite size and the XRD data was utilized to investigate the effect of alkali-metal concentration on the crystallite size by using Scherrer's method. The calculations were performed on the reflection from (211) plane of cassiterite. In line with the peak broadening evident in Figure 4.44 a decrease in the crystallite size from 14.8 nm to 11.2 nm was observed for both of the families of catalysts upon increasing the alkali-to-palladium ratio from 0.32 to 1.50. The decrease in the crystallite size with increasing alkali-metal content evidences the development of less ordered crystals in the presence of the alkali-metals.

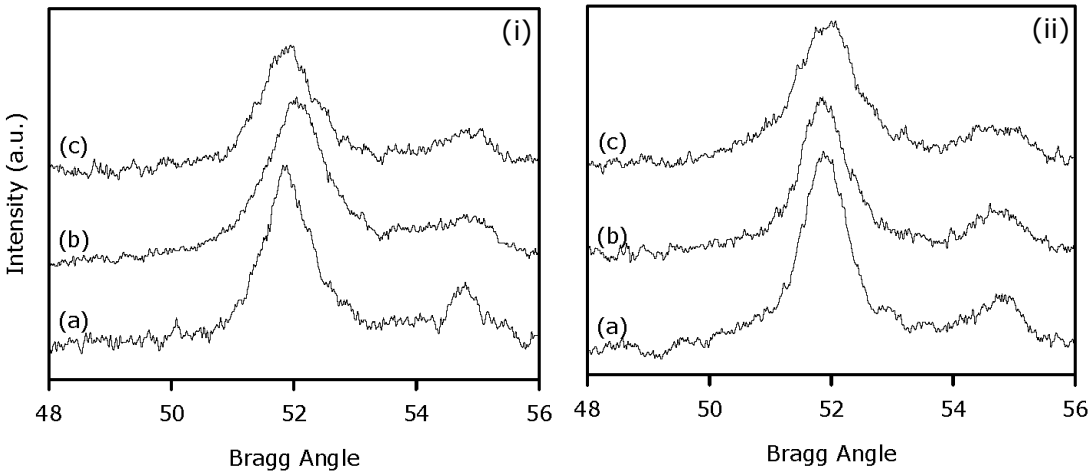

Figure 4.44 Broadening of (211) reflection from cassiterite with sodium (i) and potassium (ii) content: (a) A:Pd = /1.50, (b) A:Pd = 0.53 and (c) A:Pd = 0.32

4.4.2 Effect of Modifier Concentration on the CO Oxidation Activity

The CO oxidation activity of oxidized and reduced samples of Na-PdO/SnO_2 and K-PdO/SnO_2 catalysts with different alkali-metal contents was investigated with temperature programmed reaction spectroscopy (TPRS) under oxygen-rich conditions. For the comparability of the results with TPRS data presented above, the CO concentration of the gas phase was kept at 2400 ppm and the [CO]/[O] was adjusted to 0.91.

Through similar TPRS experiments it has been shown that, enhancements in the CO oxidation activity of PdO/SnO_2 catalysts, which are already known as effective catalysts for low temperature CO oxidation, can be achieved by sodium promotion of this catalyst and complete conversion of CO around 160°C was observed over Na-PdO/SnO_2. The CO conversion versus temperature curves of Na-PdO/SnO_2 catalysts with different sodium contents show that the CO activity and sodium content are correlated and further enhancements in the reported CO oxidation activity of Na-PdO/SnO_2 (Na/0.53) can be achieved by increasing the sodium content (Figure 4.45).

The rates of CO versus temperature curves for Na-PdO/SnO_2-based catalysts namely, Na/0.32 and Na/1.50 are presented in Figure 4.45. The CO conversion curve for oxidized and reduced Na/0.53 obtained under the same experimental conditions has already been presented above in Figure 4.6. The CO conversion versus temperature curves suggest an increase in the CO oxidation activity with increasing sodium content. The light-off temperature of CO over oxidized

Na/0.32 was higher than that of oxidized Na/0.53 and was recorded as 186°C as opposed to 174°C recorded over Na/0.53. Contrarily, by increasing the sodium content (Na/1.50) a 30°C decrease in the light-off temperature relative to oxidized Na/0.53 was achieved. Therefore, the activities of oxidized Na-PdO/SnO_2 catalysts decrease in the order Na1.50 > Na/0.53 > Na/0.32.

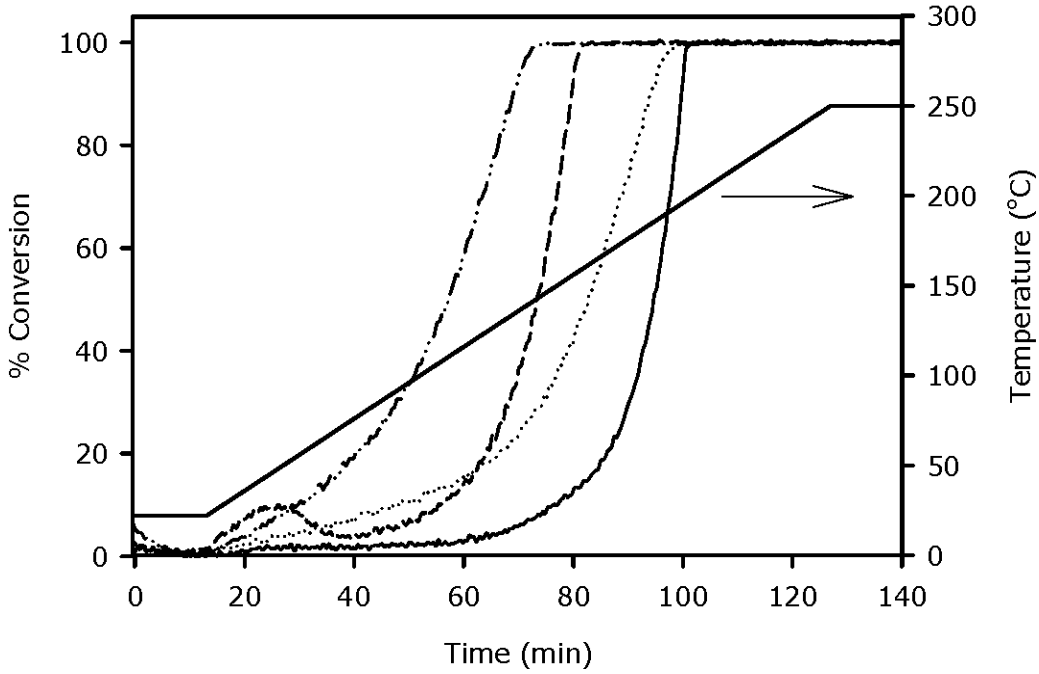

Figure 4.45 CO conversion rates over oxidized Na-PdO/SnO_2 (Na/0.32) (———), reduced Na-PdO/SnO_2(Na/0.32) (·····) , oxidized Na-PdO/SnO_2 (Na/1.50) (-----), reduced Na-PdO/SnO_2(Na/1.50) (–··–·)

(*Reaction Conditions:* P = 1 atm; GHSV = 12 800 hr^{-1}; [CO] = 2400 ppm; [CO]/[O] = 0.91, catalyst weight = 100 mg; heating rate = 2°C/min)

Reduction pretreatment has been observed to increase the CO oxidation activity of PdO/SnO_2 based catalysts. In the case of the Na-PdO/SnO_2 catalysts, the promoting effect of reduction pretreatment on the CO oxidation increased with increasing sodium content such that reduction pretreatment reduced the light-off temperature by 24°C over Na/0.32 while this decrease accounted to 30°C over Na/0.53 and to 35°C over Na/1.50. The positive correlation between the CO oxidation activity and the alkali content of the catalysts observed in the case of oxidized catalysts was also valid in the case of samples subjected to reduction pretreatment and thus, the CO oxidation activity of reduced Na-PdO/SnO_2-based catalysts decreased in the order Na1.50 > Na/0.53 > Na/0.32.

The CO conversion versus temperature curves for oxidized and reduced K-PdO/SnO_2-based catalysts are presented in Figures 4.46 and 4.47. The light-off temperatures for oxidized K/0.32, K/0.53 and K/1.50 were 202°C, 176°C and 156°C, respectively. Reduction pretreatment promoted the activity of all of the potassium modified samples with the effect reduction pretreatment increasing by increasing alkali content of the catalyst. Reduction pretreatment decreased the light-off temperature of K/0.32 by 14°C to 188°C while the light-off temperatures of K/0.53 and K/1.50 were decreased by 38°C and 40°C to 138°C and 116°C, respectively.

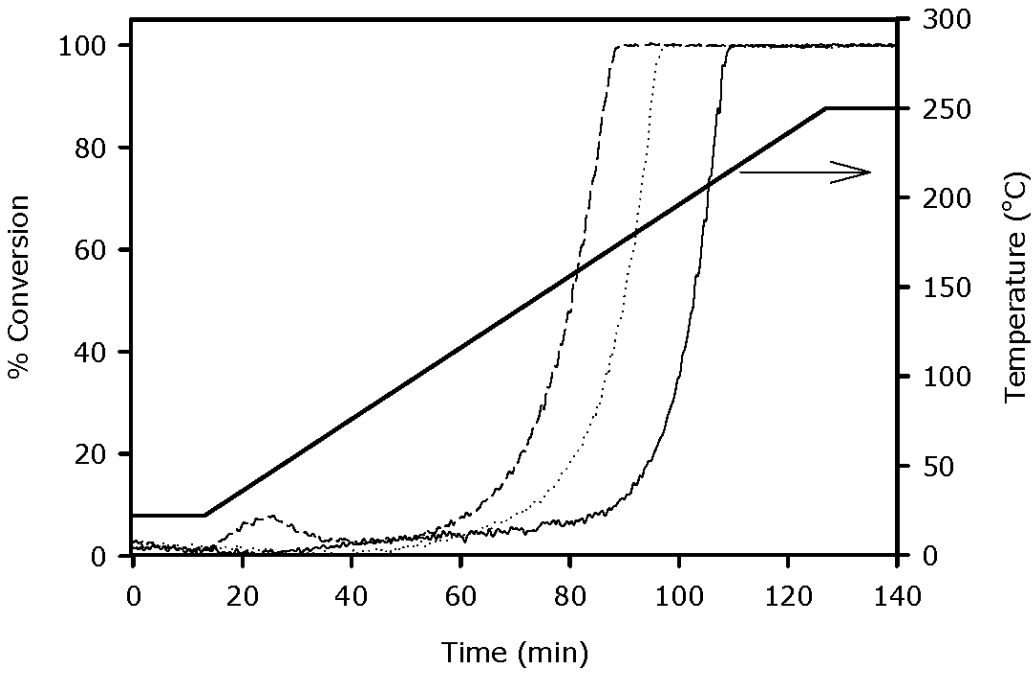

Figure 4.46 CO conversion rates over oxidized K-PdO/SnO_2(K/1.5) (------), oxidized K-PdO/SnO_2(K/0.53) (.....), oxidized K-PdO/SnO_2(K/0.32) (———)

(*Reaction Conditions:* P = 1 atm; GHSV = 12 800 hr^{-1}; [CO] = 2400 ppm; [CO]/[O] = 0.91, catalyst weight = 100 mg; heating rate = 2°C/min)

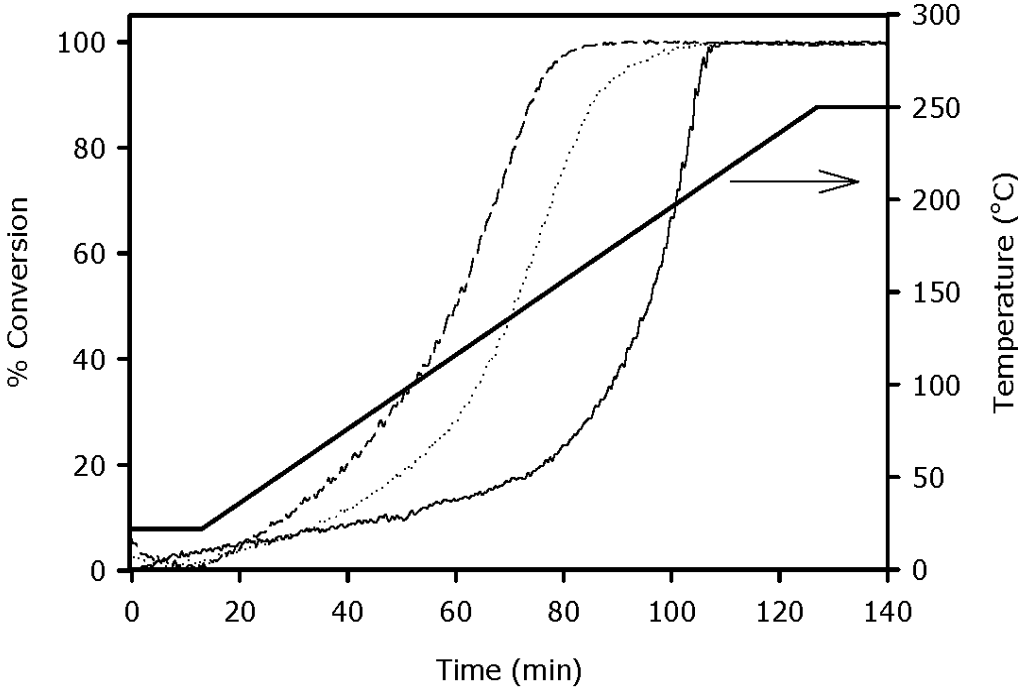

Figure 4.47 CO conversion rates over reduced K-PdO/SnO_2(K/1.5) (------), reduced K-PdO/SnO_2(K/0.53) (.....), reduced K-PdO/SnO_2(K/0.32) (———)

(*Reaction Conditions:* P = 1 atm; GHSV = 12 800 hr^{-1}; [CO] = 2400 ppm; [CO]/[O] = 0.91, catalyst weight = 100 mg; heating rate = 2°C/min)

The rates of CO oxidation were calculated at 150°C and the variation of rates of CO oxidation with alkali metal content and pretreatment conditions have been plotted in Figure 4.48. In line with the foregoing discussion, regardless of the type of the modifier, the rates of reaction increases with alkali-metal content and subjecting the catalysts to reduction pretreatment also promotes the reaction. The increase in the CO oxidation activity of the samples subjected to reduction pretreatment with alkali content is understandable in terms of the promotion of the oxygen affinity of the catalysts by the alkali metals. As it as been discussed earlier, the interaction of CO with noble metal surfaces is much stronger than the interaction of O_2 and the kinetics of CO-O_2 reaction over noble metal-based surfaces is governed by CO desorption from the surface that would create vacant sites for oxygen chemisorption. Alkali-metals can be expected to counteract this effect by promoting oxygen chemisorption so that oxygen can compete with CO for active sites.

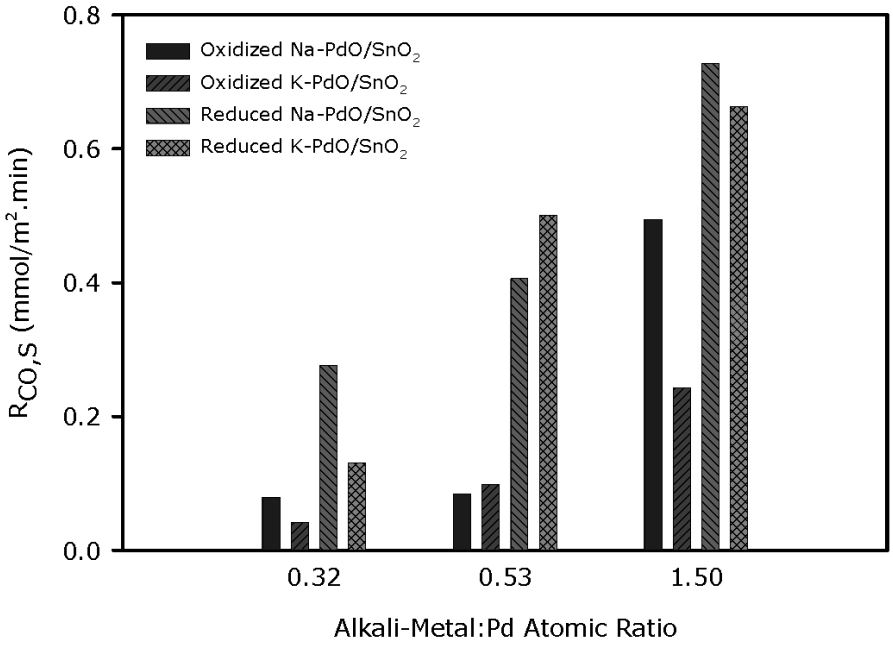

Figure 4.48 Variation of CO oxidation rate with alkali-metal content

(*Reaction Conditions:* P = 1 atm; GHSV = 12 800 hr^{-1}; [CO] = 2400 ppm; [CO]/[O] = 0.91, catalyst weight = 100 mg; heating rate = 2°C/min)

4.4.3 Effect of Modifier Concentration on the Reduction Characteristics

Alkali-metal modified PdO/SnO_2 catalysts with different modifier contents were investigated by CO-TPR to systematically investigate the observed alkali-induced changes in the reduction characteristics of PdO/SnO_2 catalysts. The same experimental procedure as the previously discussed CO-TPR experiments was adopted for the comparability of the TPR-spectra.

For the investigation of the influence of alkali metal modifiers on the interaction of oxide and hydroxide species, the reduction behavior of unmodified and alkali metal modified (A:Pd = 0.53) PdO/SnO_2 catalysts were tested with CO-TPR technique. The results of these CO-TPR experiments have been discussed in detail above and the major findings were the incorporation of other reducible sites to tin dioxide with palladium addition and the promotion or retardation of the reduction of these palladium related sites by the introduction of alkali metals. The reduction of palladium related sites were observed as a doublet in the 50°C-315°C region and surface hydroxy groups were postulated to be involved in the reaction mechanism leading to the evolution of CO_2 in this temperature range (Figure 4.31d). Sodium and potassium addition was observed to cause a shift in the high temperature component of the doublet to lower temperatures (Figures

4.31f and 4.31h). The effect was more pronounced over oxidized Na-PdO/SnO_2 and the shift in this band was correlated with shifts in the H_2O evolution bands in the same temperature region (Figures 4.32f and 4.32h). Thus, it was postulated that sodium and potassium interacted with one of the reducible species introduced in to the structure by palladium.

The CO_2 and H_2O traces of oxidized and reduced Na-PdO/SnO_2 samples with different sodium content (Na/0.32 and Na/1.50) are presented in Figures 4.49 and 4.50 together with the CO_2 and H_2O profiles of oxidized and reduced Na/0.53 discussed in Section 4.2.4 and reproduced here for better visualization. In line with previously discussed CO-TPR results on PdO/SnO_2 and alkaline modified PdO/SnO_2 (Li/0.53, Na/0.53 and K/0.53), two CO_2 bands were resolved in the CO_2 traces of oxidized samples and these bands were accompanied by water evolution bands in the H_2O profiles. Over oxidized Na/0.32, the first of these bands corresponded to 120°C-300°C and was observed as a doublet with peak maxima appearing at 224°C and 262°C (Figure 4.49b). The doublet structure of this band closely resembles the CO_2 bands observed in the same temperature range over oxidized PdO/SnO_2 (Figure 4.31d). In fact, the maxima of the low temperature components appear at the same temperature in the CO_2 traces of PdO/SnO_2 and Na/0.32 while, the high temperature component appears to be shifted to lower temperatures, 262°C as opposed to 276°C over PdO/SnO_2, in the case of Na/0.32. As it has been discussed earlier, over oxidized Na/0.53, this band was resolved in 140°C-275°C region with peak maximum corresponding to 218°C (Figure 4.49d) and further increase in the sodium content further shifted this band to lower temperatures such that the CO_2 band was resolved in 120°C-260°C with T_{max} = 212°C (Figure 4.49f). It is interesting to note that, the shift in the position of this band with alkali content of the catalysts was accompanied by water evolution bands which exhibit parallel behavior in terms of temperature. Over Na/0.32, a water evolution band was resolved in 155°C-316°C range (T_{max} = 248°C) which shifted to 218°C over Na/0.53 and to 212°C over Na/1.50 (Figures 4.50b, 4.50d and 4.50f). The CO_2 evolution band resolved in the same temperature range over oxidized PdO/SnO_2 was also accompanied by water evolution and the TPR results show that the H_2O band resolved over the sodium promoted samples exhibit a shift relative to their counterpart resolved over PdO/SnO_2.

Through previous TPR studies, sodium and potassium have been postulated to promote the reduction of one of the two palladium related species, whose activity was correlated with evolution water. The CO-TPR experiments with catalysts that have different sodium content provide further evidence for the promotion of the reduction these palladium related sites. Furthermore, the increase in the intensity of water bands with increasing alkali content and increasing CO_2 evolution also suggest that alkali addition promotes either the formation of hydroxy species or their availability to participate in CO oxidation reaction.

Regardless of the sodium content, reduction pretreatment was observed to lead to the elimination of the CO_2 band in the 120°C-300°C region (Figures 4.49a, 4.49c and 4.49e) and simultaneously resulted in significant decrease in water evolution in the same temperature range (Figures 4.50a, 4.50c and 4.50e). Over reduced Na/0.32, a broad band in 162°C-490°C region was resolved and the maximum of this band shifted to 362°Cand 330°C with increasing sodium content. In the case of the oxidized counterparts of these reduced samples, these high temperature bands appear at slightly higher temperatures. Previously, reduction of SnO_2 was observed in this temperature range however, the reduction behavior was unaffected by the pretreatment procedure. The changes in the CO_2 evolution profile in this temperature range suggest that sodium either had a direct influence on the reduction behavior of SnO_2 or affected the interaction of Pd and Sn to result in the observed effects. The effect of sodium on the reduction behavior of SnO_2 has already been investigated and the CO_2 and H_2O profiles of oxidize and reduced Na/SnO_2 samples have been observed to resemble those of bare SnO_2 thus, an influence of sodium on the interaction of Pd and Sn resulting in the alteration of the reduction behavior of the reduction behavior of the sodium modified samples in 300°C-500°C region might be considered as a more plausible explanation.

The CO_2 and H_2O evolution profiles of oxidized and reduced K-PdO/SnO_2 samples (K/0.32 and K/1.50) are presented in Figures 4.51 and 4.52. The CO_2 and H_2O traces of oxidized and reduced K-PdO/SnO_2 (K/0.53) have also been reproduced for providing better visualization of the results. Like Na-PdO/SnO_2, the CO_2 profile of oxidized K-PdO/SnO_2 (K/0.32) closely resembles the CO_2 trace of oxidized PdO/SnO_2, with a doublet observed in the 140°C-290°C (Figure 4.51b). The high temperature component of the doublet was resolved at lower temperatures than its counterpart observed over oxidized PdO/SnO_2 while, the

low temperature component corresponded to the same temperature. Likewise the other palladium containing catalysts investigated with CO-TPR, reduction pretreatment of K/0.32 led to the disappearance of this CO_2 band (Figure 4.51a). When the H_2O profiles of oxidized and reduced samples were compared, a weakly resolved H_2O evolution band that diminished with reduction pretreatment was observed in the H_2O profile of oxidized K/0.32 (Figures 4.52a and 4.52b). As it has been discussed earlier, an increase in the potassium content resulted in a shift in the high temperature component of the doublet toward lower temperatures and this shift was also coupled with a shift in the H_2O band so that, the maximum of the CO_2 band was observed at 256°C with a 10°C decrease relative to K/0.32 and the maximum of the H_2O was observed at 258°C.

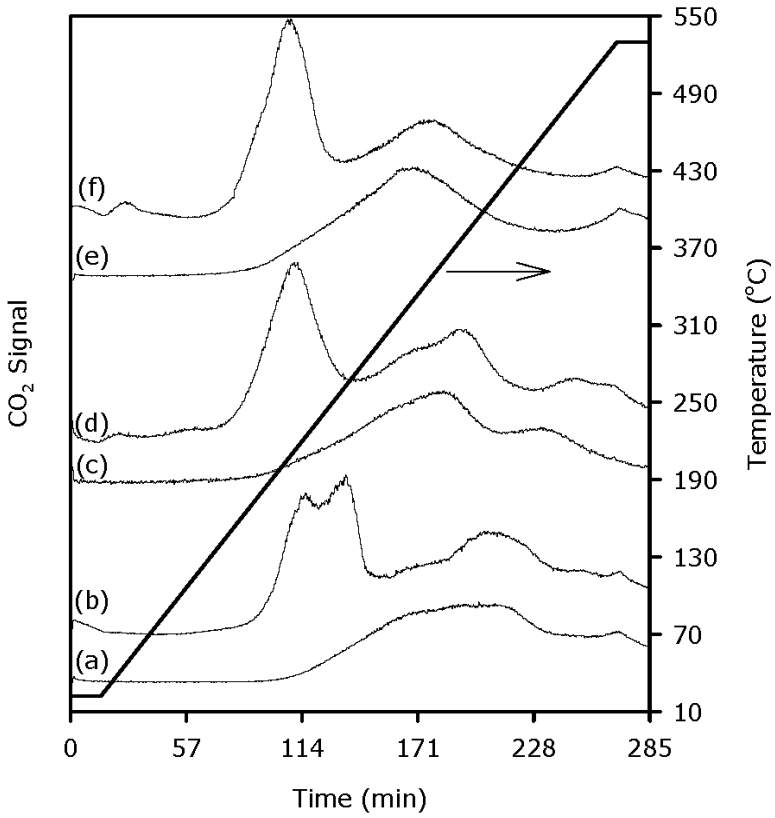

Figure 4.49 CO_2 evolution profiles (a) reduced Na-PdO/SnO_2 (Na/0.32), (b) oxidized Na-PdO/SnO_2 (Na/0.32), (c) reduced Na-PdO/SnO_2 (Na/0.53), (d) oxidized Na-PdO/SnO_2 (Na/0.53), (e) reduced Na-PdO/SnO_2 (Na/1.50) and (f) oxidized Na-PdO/SnO_2 (Na/1.50)

(*Conditions:* P = 1 atm; GHSV = 12 800 hr^{-1}; [CO] = 2000 ppm; catalyst weight = 100 mg, heating rate = 2°C/min)

Unlike sodium, further increase in the potassium content of PdO/SnO_2 resulted in significant changes in both CO_2 trace (Figures 4.51f). In the CO_2 trace, two bands that correspond to 140°C-300°C (T_{max} = 254°C) and 300°C-460°C (T_{max} = 354°C) were resolved and, the first of these bands was coupled with H_2O evolution in 140°C-320°C (T_{max} = 252°C) region (Figure 4.52f). In line with previous discussion on the reduction behaviour of the catalysts its meaningful to associate the low temperature band with reduction of palladium oxide species and the high temperature band with the reduction of the support. However, the broadening and increase in the intensity of both of the bands suggest more effective reduction of the catalyst in the presence of higher amount of potassium which could arise from potassium induced distortions in the sturucture.

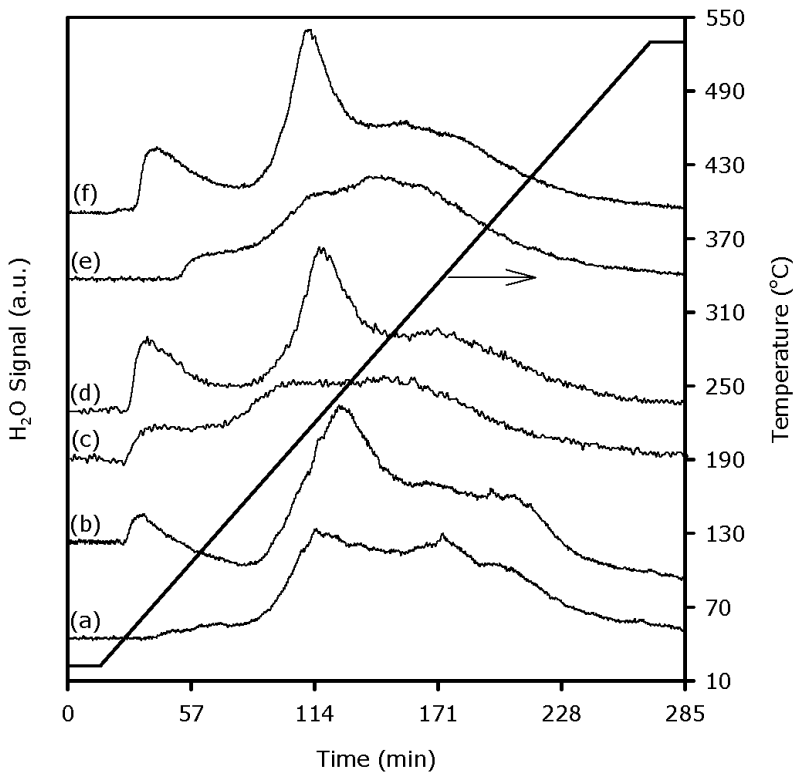

Figure 4.50 H_2O evolution profiles (a) reduced Na-PdO/SnO_2 (Na/0.32), (b) oxidized Na-PdO/SnO_2 (Na/0.32), (c) reduced Na-PdO/SnO_2 (Na/0.53), (d) oxidized Na-PdO/SnO_2 (Na/0.53), (e) reduced Na-PdO/SnO_2 (Na/1.50) and (f) oxidized Na-PdO/SnO_2 (Na/1.50)

(*Conditions:* P = 1 atm; GHSV = 12 800 hr^{-1}; [CO] = 2000 ppm; catalyst weight = 100 mg, heating rate = 2°C/min)

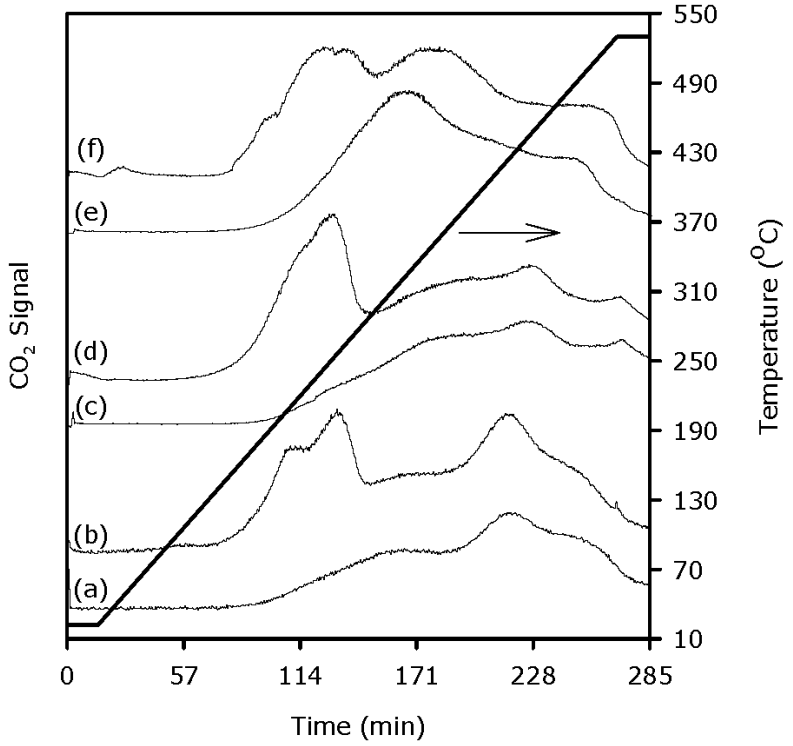

Figure 4.51 CO_2 evolution profiles (a) reduced K-PdO/SnO_2 (K/0.32), (b) oxidized K-PdO/SnO_2 (K/0.32), (c) reduced K-PdO/SnO_2 (K/0.53), (d) oxidized K-PdO/SnO_2 (K/0.53), (e) reduced K-PdO/SnO_2 (K/1.50) and (f) oxidized K/PdO/SnO_2 (K/1.50)

(*Conditions:* P = 1 atm; GHSV = 12 800 hr^{-1}; [CO] = 2000 ppm; catalyst weight = 100 mg, heating rate = 2°C/min)

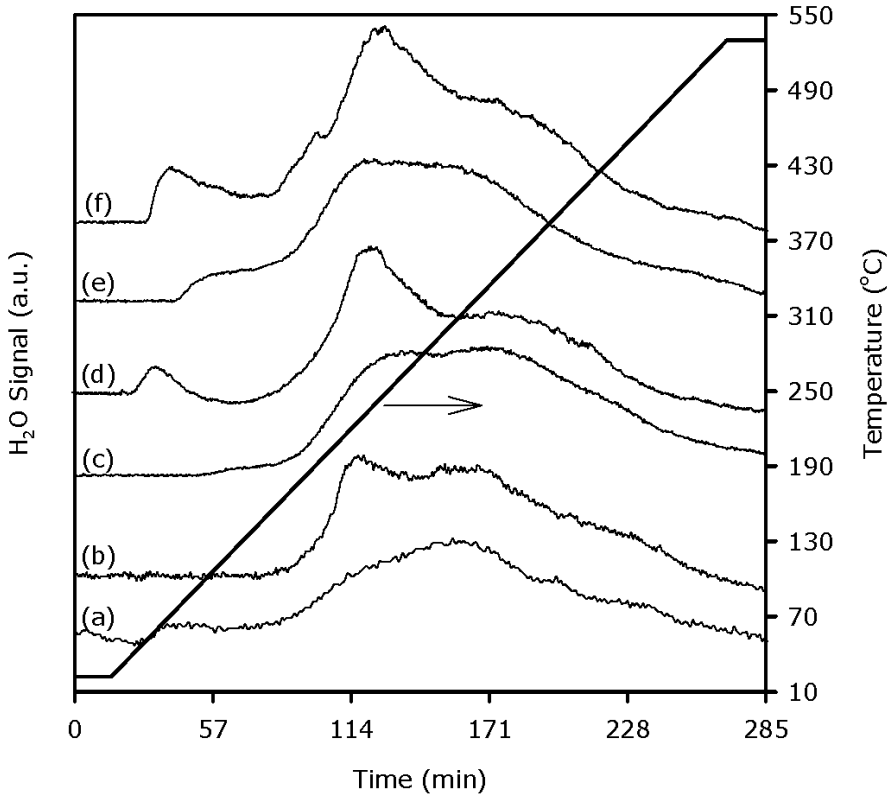

Figure 4.52 H_2O evolution profiles (a) reduced K-PdO/SnO_2 (K/0.32), (b) oxidized K-PdO/SnO_2 (K/0.32), (c) reduced K-PdO/SnO_2 (K/0.53), (d) oxidized K-PdO/SnO_2 (K/0.53), (e) reduced K-PdO/SnO_2 (K/1.50) and (f) oxidized K/PdO/SnO_2 (K/1.50)

(*Conditions:* P = 1 atm; GHSV = 12 800 hr^{-1}; [CO] = 2000 ppm; catalyst weight = 100 mg, heating rate = 2°C/min)

CHAPTER 5

CONCLUSION

The basic motive of this research was to investigate CO oxidation over tin dioxide based catalysts to develop an understanding of the reactive sites, metal-support and adsorbate-surface interactions and, reaction mechanisms of low temperature CO oxidation with PdO/SnO_2 which, exhibits strong-metal-support-interaction (SMSI) behavior to result in the synergistic effects reported for this catalyst. Furthermore, alkali-metal modifiers were introduced to this system to promote the catalytic properties and the influence of the alkali-metal additives on the structure and reduction/oxidation behavior of PdO/SnO_2 was investigated at the molecular scale.

Although no clear-cut boundaries exist, the conducted research work can be divided in to four consecutive phases. In the first phase, the CO activity and active sites of sol-gel derived PdO/SnO_2 were investigated and alkali-metal promotion was applied by selecting sodium as the representative alkali-metal. During this phase, PdO/SnO_2 and Na-PdO/SnO_2 were characterized by XPS, SEM and *in-situ* dynamic techniques, namely, temperature programmed reaction, temperature programmed desorption and impulse experiments. The following observations have been made:

- SEM and EDX analysis of sol-gel derived PdO/SnO_2 and Na-PdO/SnO_2 nanopowders showed that the average particle size was 80nm and palladium was uniformly dispersed over SnO_2. Sodium addition was not observed to alter the particle morphology.

- PdO/SnO_2 and Na-PdO/SnO_2 were investigated by XPS to elucidate the influence of the modifier on the chemical state of palladium and tin atoms. In the case of sodium modified sample great amount of palladium was observed to exist in higher oxidation states and also, the XPS data evidenced an alkali-mediated increase in the oxygen storage capacity of PdO/SnO_2 by the formation of super-oxide species and by the presence of

greater amount of palladium in higher oxidation states. The quantification of the XPS data suggested the segregation of palladium atoms at the surface of the sodium modified catalyst. The formation of sodium oxopalladate species with the formula $Na_xPd_3O_4$ to promote oxygen storage and to stabilize Pd species at the surface was postulated. Quantification of the XPS data further suggested an increase in the surface palladium content with reduction pretreatment. The palladium enrichment of the surface layers during reduction pretreatment was attributed to the diffusion of palladium ions from the subsurface layers to the surface where, they are reduced and stabilized due to the increase in the ionic radius with reduction.

- Through TPRS experiments carried out at a number of different reactor feed conditions, it has been demonstrated that improvements in the CO oxidation activity of PdO/SnO_2, which is known as an active low temperature CO oxidation catalyst, can be achieved by sodium addition. Na-PdO/SnO_2 was demonstrated to be an active low-temperature CO oxidation catalyst especially under oxygen-lean conditions and under oxygen-rich conditions, sodium promotion was observed to have adverse effect on the activity of PdO/SnO_2 due to the oxygen blockage of the active sites for CO adsorption. The oxidation activity of PdO/SnO_2 and Na-PdO/SnO_2 was promoted by activation in reducing atmosphere and the effect of reduction pretreatment was observed to be more pronounced in the alkali-metal-promoted catalyst. The effect has been attributed to the elimination of the inhibition effect of oxygen species. In addition to the oxidation of chemisorbed CO with oxygen ad-species another reaction pathway involving hydroxy species was postulated and the hydroxy reaction mechanism was postulated to play a key role in low-temperature CO oxidation with PdO/SnO_2-based catalysts under oxygen-lean conditions. Evidences for significant contribution of hydroxy mechanism to the overall activity of the catalysts are obtained through TPRS experiments. The role of sodium in promoting the CO oxidation activity was associated with the surface segregation of palladium atoms, increasing the reactive sites for CO oxidation and as well, to the presence of super-oxide species was observed over Na-PdO/SnO_2.

- The steady-state activity tests of unmodified and sodium modified PdO/SnO_2 catalysts carried out under oxygen-rich and oxygen-lean reactor feed conditions also demonstrated the promoting effect of sodium on CO oxidation with PdO/SnO_2 catalysts. Although unmodified and sodium-modified catalysts exhibited similar activity under oxygen-rich conditions, the rates of CO oxidation reaction over Na-PdO/SnO_2 was observed to be higher than PdO/SnO_2 under oxygen lean conditions. The enhanced rates of CO oxidation have been attributed to the alkali-promotion of the oxidation of the catalyst by oxygen adsorption from the gas phase.

- The reactivity of surface oxygen and the extent of the incorporation of the bulk oxygen in the observed CO oxidation activity of the catalysts were investigated by impulse technique to further elucidate the mechanism of alkali-metal promotion in PdO/SnO_2 catalysts. When no oxygen was supplied to the reactor, oxidation of chemisorbed CO was observed to proceed through the incorporation of surface and lattice oxygen species. Diffusion of oxygen from the subsurface layers has been observed to effectively promote oxidized and reduced Na-PdO/SnO_2 at 150°C and 20°C, whereas it was sufficient to a limited extent to promote oxidized and reduced PdO/SnO_2 at 150°C and had no effect at 20°C.

- O_2-TPD studies following the adsorption of CO and co-adsorption of CO and O_2 were carried out to investigate the active sites for CO oxidation. Through these experiments, tin dioxide was observed to exhibit a high temperature CO oxidation activity, which corresponded to temperatures above 250°C. Addition of the alkali and noble metal had a positive effect on the high-temperature activity of tin dioxide, indicating the influence of these metals on tin dioxide catalytic behavior. This influence was attributed to the spillover of activated species from the metal centers to tin dioxide surface, which does not readily adsorb reducing species. The CO_2 trace of PdO/SnO_2 exhibited a low-temperature CO_2 desorption band in addition to the high-temperature band that has been ascribed to the activity of SnO_2. This low-temperature activity has been ascribed to the activity of PdO_X centers, and subjecting the catalyst to reduction pretreatment deactivated these centers. Sodium addition promoted the activity of PdO/SnO_2, especially in the reduced state. A shift of the CO_2 desorption band towards lower temperatures was observed when

PdO/SnO_2 catalyst was promoted with sodium and this has been attributed to a decrease in the activation energy of CO to CO_2 conversion. Furthermore, sodium addition was observed to promote the interaction of oxygen with the surface which facilitated the replenishment of oxide species consumed during CO oxidation and reduction pretreatment.

During the second phase, lithium an potassium were introduced to PdO/SnO in attempts to further promote the CO oxidation activity of PdO/SnO_2 and gain further insights to the mechanism of alkali-metal promotion of CO oxidation activity of PdO/SnO_2-based catalysts. Li-PdO/SnO_2 and K-PdO/SnO_2 were characterized with XRD and XPS and, tested dynamically with temperature programmed techniques.

- XRD analysis of Li-PdO/SnO_2 and K-PdO/SnO_2 confirmed the presence of tin dioxide as the major phase. The identification of palladium containing phase has not been possible because of the low level of palladium loading and the overlap of major reflection peaks with those of tin dioxide. Unlike K-PdO/SnO_2, the powder diffraction pattern of Li-PdO/SnO_2 exhibited reflections that could not be associated with palladium oxide or tin oxide phases. This phase was associated with $LiSnO_X$ type oxides that could form through lithium intercalation to tin dioxide which has anatase structure.

- Lithium and potassium modified PdO/SnO_2 catalysts were characterized with TPRS with regard to their CO oxidation activity under oxygen-rich conditions in 20 – 250°C range. The initial oxygen content of the surfaces was considered as a parameter and catalysts subjected to oxidation and reduction pretreatment were studied. Regardless of the pretreatment procedure, lithium and potassium were observed to act as catalyst poisons and suppress the activity. Furthermore, the interaction between lithium and hydroxy species, which suppresses the activity of these species, was postulated to result in the poor CO oxidation activity of Li-PdO/SnO_2.

- The modes of interaction of surface oxide/hydroxy species and their activity in CO oxidation were investigated by CO-TPR experiments. The CO-TPR data evidenced the presence of two types of reactive oxide species in 20°C-500°C region over bare SnO_2. Palladium addition to tin

dioxide was observed to influence the reduction behavior of this material in two different ways: (i) incorporation of another active site that is reduced at much lower temperatures than the oxide species of the support, (ii) promotion of the reduction of the support. The TPR traces also provided further support for the incorporation of hydroxy species in CO oxidation. Sodium and potassium addition were observed to promote the hydroxy reaction mechanism and CO oxidation tookplace at relatively lower temperatures. On the other hand, lithium suppressed the reduction of the oxide/hydroxide species. The poisoning effect of lithium postulated to arise either from the promotion of the interaction of chemisorbed CO with the surface to result in cleavage of C-O bond or from lithium-mediated stabilization of surface hydroxy species to suppress their reduction.

The third phase comprises the investigation of the competitive oxidation of CO and H_2 with PdO/SnO_2 surfaces and the influence of H_2 on the CO oxidation activity of PdO/SnO_2-based catalysts with temperature programmed techniques.

- Temperature programmed reduction of the catalysts with CO, H_2 and $CO+H_2$ mixture showed that hydrogen acted as a promoter of CO oxidation over PdO/SnO_2-based catalysts. The interaction of chemisorbed H and CO to form formyl-like surface complexes was postulated to lead to desorption of CO at lower temperatures and eliminate the self-inhibitory effect of CO. H_2-TPR and CO/H_2-TPR studies suggested that the catalysts might be reduced with hydrogen even at room temperature and CO acted as a poison for the oxidation of chemisorbed hydrogen. Introduction of sodium and potassium further retarded the oxidation of hydrogen, the effect being more pronounced over K-PdO/SnO_2. The effect of alkali-metals was understandable in terms of alkali-mediated changes in the relative surface coverage of CO and H_2, where alkali-metals act to suppress H_2 adsorption due to its electropositive nature.

- Simultaneous oxidation of H_2 and CO over alkali-metal modified PdO/SnO_2 catalysts was studied with TPRS under oxygen-lean and oxygen rich conditions. Furthermore, the selective CO oxidation activity at steady-state was tested under conditions resembling upstream fuel processing conditions for the H_2 fuel cell. Under all of the conditions, potassium modified sample was observed to exhibit significant CO oxidation activity

and the results suggest that K-PdO/SnO_2 catalysts deserve more attention for elucidating their potential for application in fuel cell applications. The CO oxidation activity and selectivity of potassium modified catalysts need be investigated in the presence of significant amounts of CO_2 and water vapor, in addition to H_2, CO and O_2.

The final phase comprised the investigation of the effect of alkali-metal content on the catalytic behavior of PdO/SnO_2 catalysts. Na-PdO/SnO_2 and K-PdO/SnO_2 samples with different alkali-metal contents were prepared, characterized and tested dynamically with temperature programmed techniques.

- The XRD peaks of the samples exhibited broadening with increasing alkali content suggesting either the formation of smaller crystallites and/or less ordered more defective structures. The crystallite size was calculated using Scherrer's method and was found to decrease with increasing alkali content.

- The CO conversion versus temperature curves obtained by TPRS showed that CO oxidation activity and alkali-metal content of the catalysts were correlated and improvement of the CO oxidation activity of the alkaline modified catalysts can be achieved by increasing the alkali-metal content. The pretreatment conditions altering the initial oxygen coverage of the surfaces was observed to have significant effect on the catalytic properties. Reduction pretreatment acted to promote the CO oxidation activity and the effect of reduction pretreatment in promoting the CO activity was observed to increase with increasing alkali-metal content. The effect was postulated to arise from the promotion of the oxygen chemisorption to compete with CO adsorption which normally interferes with the O_2 adsorption mechanism by blocking the active sites.

- The investigation of the reduction behavior of sodium and potassium modified catalysts with CO-TPR provided support for the postulated hydroxy mechanism for CO oxidation. Sodium and potassium have been postulated to promote the reduction of one of the palladium related sites whose activity was correlated with hydroxy species. The TPR data further suggested that alkali addition promoted either the formation or the availability of surface hydroxy species resulting in an increase in the extent of hydroxy mechanism.

The presented spectroscopic and dynamic characterization data has shown that promoting PdO/SnO_2 with alkaline metals such as Li, Na and K, alters the chemical properties of the catalyst as well as the catalyst morphology and offers a range of catalysts which exhibit different reduction behaviors and reactivity towards oxidation reactions and; present promising outcomes for various applications.

REFERENCES

[1] D.S. Stark, M.R. Harris, "Catalysed recombination of CO and O_2 in sealed $CO_{2\ TEA}$ laser gases at temperatures down to -27°C", Journal of Physics: Scientific Instruments, 16, 1983, pp. 492-496.

[2] D.S. Stark, M.R. Harris, "Platinum-catalysed recombination of CO and O_2 in sealed $CO_{2\ TEA}$ laser gases", Journal of Physics E: Scientific Instruments, 11, 1978, pp. 316-319.

[3] D.S. Stark, A. Crocker, G.J. Steward, "A sealed 100-Hz $CO_{2\ TEA}$ laser using CO_2 concentrations and ambient-temperature catalysts", Journal of Physics E: Scientific Instruments, 16, 1983, pp. 158-161.

[4] D.S. Stark, A. Crocker, N.A. Lowde, "A semiconductor-preionized sealed TEA laser operating at high CO_2 concentrations and repetition rates up to 100 Hz", Journal of Physics E: Scientific Instruments, 16, 1983, pp. 1069-1071.

[5] S.D. Gardner, G.B. Hoflund, D.R. Schryer, J. Schryer, B.T. Upchurch, E.J. Kielin, "Catalytic behavior of noble metal/reducible oxide materials for low-temperature carbon monoxide oxidation. 1. Comparison of catalyst performance", Langmuir, 7, 1991, pp. 2135-2139.

[6] S.D. Gardner, G.R. Hoflund, B.T. Upchurch, D.R. Schryer, E.J. Kielin, J. Schryer, "Comparison of the performance characteristics of Pt/SnO_X and Au/MnO_X catalysts for low-temperature CO oxidation", Journal of Catalysis, 129, 1991, pp. 114-120.

[7] R.M. Heck, R.J. Farrauto, "Automobile exhaust catalysis", Applied Catalysis A: General, 221, 2001, pp. 443-457.

[8] P.A.J. Bagot, "Fundamental surface science studies of automobile exhaust catalysis", Materials Science and Technology, 20, 2004, pp. 679-694.

[9] M. Skoglundh, E. Fridell, "Strategies for enhancing low-temperature activity", Topics in Catalysis, 28, 2004, pp. 79-87.

[10] J.R. Gonzalez-Velasco, J.A. Botas, R. Ferret, MP. Gonzalez-Markos, J.L. Marc, M.A. Guiterrez-Ortiz, "Thermal aging of Pt/Pd/Rh automotive catalysts under a cycled oxidizing-reducing environment", Catalysis Today, 59, 2000, pp. 395-402.

[11] R.J. Farrauto, R.M. Heck, "Catalytic converters: state of the art and perspectives", Catalysis Today, 51, 1999, pp. 351-360.

[12] H. Gandhi, G. Graham, R. McCabe, "Automotive exhaust catalysis", Journal of Catalysis, 216, 2003, pp. 433-442.

[13] H. Gandhi, W. Williamson, E. Logothetis, J. Tabock, C. Peters, M. Hurley, M. Shelef, Surface and Interface Analysis, 6, 1984, pp. 149-

[14] J. Kummer, "Catalysts for automobile emission control", Progress in Energy and Combustion Science, 6, 1980, pp. 177-199.

[15] Y. Yao, "Oxidation of alkanes over noble metal catalysts", Industrial and Engineering Product Research and Development, 19, 1980, pp. 293-298.

[16] J. Summers, B. Williamson, "Palladium-only catalysts for closed loop control", Environmental Catalysis, 552, 1993, pp. 94-113.

[17] A. Boudghene Stambouli, E. Traversa, "Fuel cells, an alternative to standard sources of energy", Renewable and Sustainable Energy Reviews, 6, 2002, pp. 297-306.

[18] D.L. Trimm, "Minimisation of carbon monoxide in a hydrogen stream for fuel cell application", Applied Catalysis A: General, 296, 2005, pp. 1-11.

[19] A.F. Ghenciu, "Review of fuel processing catalysts for hydrogen production in PEM fuel cell systems", Current Opinion in Solid State and Materials Science, 6, 2002, pp. 389-399.

[20] F. de Brujin, "The current status of fuel cell technology for mobile and stationary applications", Green Chemistry, 7, 2005, pp. 132-150.

[21] M.A.J. Cropper, S. Geiger, D.M. Jollie, "Fuel cells: a survey of current developments", Journal of Power Sources, 131, 2004, pp. 57-61.

[22] P.G. Gray, M.I. Petch, "Advances with HotSpot™ fuel processing", Platinum Metals Review, 44(3), 2000, pp. 108-111.

[23] A. T-Raissi, D.L. Block, "Hydrogen: automotive fuel of the future", IEEE Power and Energy Magazine, 2(6), 2004, pp. 40-45.

[24] W. Ruettinger, O. Illinich, R.J. Farrauto, "A new generation of water gas shift catalysts for fuel cell applications", Journal of Power Sources, 118, 2003, pp. 61-65.

[25] F.A. de Brujin, D.C. Papageorgepoulos, E.F. Sitters G.J.M. Janssen, "The influence of carbon dioxide on PEM fuel cell anodes" Journal of Power Sources, 110, 2002, pp. 117-124.

[26] D.L. Trimm, Z.I. Onsan, "Onboard fuel conversion for hydrogen-fuel-cell-driven vehicles", Catalysis Reviews, 43(1&2), 2001, pp. 31-84.

[27] R.W. McCabe, P.J. Mitchell, "Exhaust-catalyst development for methanol-fueled vehicles: 2. Synergism between palladium and silver in methanol and carbon monoxide oxidation over an alumina-supported palladium-silver catalyst", Journal of Catalysis, 103, 1987, pp. 419-425.

[28] S. Takenaka, T. Shimizu, K. Otsuka, "Complete removal of carbon monoxide in hydrogen-rich gas stream through methanation over supported metal catalysts", International Journal of Hydrogen Energy, 29, 2004, pp. 1065.

[29] R. Farrauto, S. Hwang, L. Shore, W. Ruettinger, J. Lampert, T. Giroux, Y. Liu, O. Illinich, "New material needs for hydrocarbon fuel processing: generating hydrogen for the PEM fuel cell", Annual Review of Materials Research, 33, 2003, pp. 1-27.

[30] R.J. Farrauto, R. M. Heck, "Environmental catalysis into the 21st century", Catalysis Today, 55, 2000, pp. 179-187.

[31] A. Törncrona, M. Skoglundh, P. Thormählen, E. Fridell and E. Jobson, "Low temperature catalytic activity of cobalt oxide and ceria promoted Pt and Pd: -influence of pretreatment and gas composition", Applied Catalysis B: Environmental, 14, 1997, pp. 131-145.

[32] F. Duprat, H.R. Moreno, "Oxidation of carbon monoxide with air on supported palladium catalysts: effect of mass transfer limitation on the kinetics", Journal of Chemical Engineering of Japan, 33 (3), 2000, pp. 400-406.

[33] A.V. Kalinkin, V.I. Savchenko, A.V. Pashis, "Mechanism of low-temperature CO oxidation on a model Pd/Fe_2O_3 catalyst", Catalysis Letters, 59, 1999, pp. 115-119.

[34] T. Maillet, C. Solleau, J. Barbier Jr., D. Duprez, "Oxidation of carbon monoxide, propene, propane and methane over a Pd/Al_2O_3 catalyst. Effect of the chemical state of Pd", Applied Catalysis B: Environmental, 14, 1997, pp. 85-95.

[35] L.S. Sun, S.Y. Li, B.L. Li, "Kinetics of low temperature CO oxidation over Pt/SnO_2 catalyst", Reaction Kinetics and Catalysis Letters, 62(1), 1997, pp. 151-156.

[36] S.K. Kulshrestha, M.M. Gadgil, "Physico-chemical characteristics and CO oxidation over $Pd/(Mn_2O_3+SnO_2)$ catalyst", Applied Catalysis B: Environmental, 11, 1997, pp. 291-305.

[37] A. Martinez-Arias, A.B. Hungria, M. Fernandez-Garcia, A. Iglesias-Juez, J.A. Anderson, J.C. Conesa, "Light-off behavior of $PdO/\gamma\text{-}Al_2O_3$ catalysts for stoichiometric $CO\text{-}O_2$ and $CO\text{-}O_2\text{-}NO$ reactions: a combined catalytic activity-in situ DRIFTS study", Journal of Catalysis, 221, 2004, pp. 85-92.

[38] T.J. Huang, T.C. Yu, S.H. Chang, "Effect of calcination atmosphere on $CuO/\gamma\text{-}Al_2O_3$ catalyst for carbon monoxide oxidation", Applied Catalysis, 52, 1989, pp. 157-163.

[39] W. Lin, M. Fyltzani-Stephanopoulos, "Total Oxidation of Carbon Monoxide and Methane over Transition Metal Fluorite Oxide Composite Catalysts : I. Catalyst Composition and Activity", Journal of Catalysis, 153, 1995, pp. 304-316.

[40] M.F. Luo, Y.J. Zhong, X.X. Yuan, X.M. Zheng, "TPR and TPD studies of CuO/CeO_2 catalysts for low temperature CO oxidation", Applied Catalysis A: General, 162, 1997, pp. 121-131.

[41] L. Simonot, F. Garin, G. Maire, A comparative study of $LaCoO_3$, Co_3O_4 and $LaCoO_3\text{-}Co_3O_4$ I. Preparation, characterisation and catalytic properties for the oxidation of CO", Applied Catalysis B: Environmental, 11, 1997, pp. 167-179.

[42] H. Falcon, M.J. Martinez-Lope, J.A. Alonso, J.L.G. Fierro, "Defect $LaCuO_{3-\delta}$ (δ=0.05−0.45) perovskites: Bulk and surface structures and their relevance in CO oxidation", Applied Catalysis B: Environmental, 26, 2000, pp. 131-142.

[43] T. Engel, G. Ertl, "A molecular beam investigation of the catalytic oxidation of CO on Pd(111)", Journal of Chemical Physics, 69(3), 1978, pp. 1267-1281.

[44] K. Kimura, Y. Ohno, T. Matsushima, "Translational energy change of desorbing product in steady-state carbon monoxide oxidation on palladium (110)", Surface Science Letters, 429, 1999, pp. L455-L461.

[45] S. Fuchs, T. Hahn, H.G. Lintz, "The oxidation of carbon monoxide by oxygen over platinum, palladium and rhodium catalysts form 10-10 to 1 bar", Chemical Engineering and Processing, 33, 1994, pp. 363-369.

[46] B.L.M. Hendriksen, S.C. Bobaru, J.W.M. Frenken, "Looking at heterogeneous catalysis at atmospheric pressure using tunnel vision", Topics in Catalysis, 36, 2005, pp. 43-53

[47] A.K. Santra, D.W. Goodman, "Catalytic oxidation of CO by platinum group metals: from ultrahigh vacuum to elevated pressures", Electrochimica Acta, 47, 2002, pp. 3595-3609.

[48] G. Vaporciyan, A. Annapragada, E. Gulari, "Rate enhancements and quasi-periodic dynamics during forced concentration cycling of CO and O_2 over supported Pt-SnO_2", Chemical Engineering Science, 43(11), 1988, pp. 2957-2966.

[49] O. Yepez, B.R. Scharifker, "Oxidation of CO on hydrogen-bonded palladium", Journal of Applied Electrochemistry, 29, 1999, pp. 1185-1190.

[50] P.J. Berlowitz, C.H.F. Peden, D.W. Goodman, "Kinetics of CO oxidation on single-crystal Pd, Pt and Ir", Journal of Physical Chemistry, 92, 1988, pp. 5213-5221.

[51] A.K. Tripathi, N.M. Gupta, "Pretreatment effect on the catalyst activity and on the enthalpy changes during exposure of Pd/SnO_2 and Pd metal to CO, O_2 and CO+O_2", Journal of Catalysis, 153, 1995, pp. 208-217.

[52] J. Goschnick, M. Grunze, J. Loboda-Cackovic, J.H. Block, "Sticking probability of CO on an oxygen covered Pd(110) surface under reaction conditions", Surface Science, 189, 1987, pp. 137-146.

[53] L. Piccolo, C. Becker, C.R. Henry, "Reaction between CO and pre-adsorbed oxygen layer on supported palladium clusters", Applied Surface Science, 164, 2000, pp. 156-162.

[54] R.M. Ziff, E. Gulari, Y. Barshad, "Kinetic phase transitions in an irreversible surface-reaction model", Physical Review Letters, 56, 1986, pp. 2553-2556.

[55] V.M. Belousov, M.A. Vasylev, L.V. Lyashenko, N.Y. Vilkova, B.E. Nieuwenhuys, "The low-temperature reduction of Pd-doped transition metal oxide surfaces with hydrogen", Chemical Engineering Journal, 91, 2003, pp. 143-150.

[56] M.M. Wolf, H. Zhu, W.H. Green, G.S. Jackson, "Kinetic model for polycrystalline Pd/PdOX in oxidation reduction cycles", Applied Catalysis A: General, 244, 2003, pp. 323-340.

[57] D. Ciuparu, L. Pfefferle, "Contributions of lattice oxygen to the overall oxygen balance during methane combustion over PdO-based catalysts", Catalysis Today, 77, 2002, pp. 167-179.

[58] J.A. Yeung, A.T. Bell, E. Iglesia, "The dynamics of oxygen exchange with zirconia-supported PdO", Journal of Catalysis, 185, 1999, pp. 213-218.

[59] C.A. Müller, M. Maciejewski, R.A. Koeppel, A. Baiker, "Combustion of methane over palladium/zirconia derived form a glassy Pd-Zr alloy: Effect of Pd particle size on catalytic behavior", Journal of Catalysis, 166, 1997, pp. 36-43.

[60] R. Burch, F.J. Urbano, "Investigation of the active state of supported palladium catalysts in the combustion of ethane", Applied Catalysis A: General, 124, 1995, pp. 121-138.

[61] S.H. Oh, G.B. Fisher, J.E. Carpenter, D.W. Goodman, "Comparative kinetic studies of CO-O_2 and CO-NO reactions over single crystal and supported rhodium catalysts", Journal of Catalysis, 100, 1986, pp. 360-376.

[62] J.R. Stetter, K.F. Blurton, "Catalytic oxidation of CO and H_2 mixtures in air", Industrial and Engineering Chemistry Product Research and Development, 19, 1980, pp. 214-215.

[63] A. Czerwinski, S. Zamponi, R. Marassi, "The influence of carbon monoxide on hydrogen absorption by thin films of palladium", Journal of Electroanalytical Chemistry, 304, 1991, pp. 233-239.

[64] M. Lischka, C. Mosch, A. Groß, "CO and hydrogen adsorption on Pd(210)", Surface Science, 570, 2004, pp. 227-236.

[65] S.H. Oh, R.M. Sinkevitch, "Carbon monoxide removal from hydrogen-rich fuel cell feedstreams by selective catalytic oxidation", Journal of Catalysis, 142, 1993, pp. 254-262.

[66] R.L. Goldsmith, M. Modell, R.F. Baddour, "Hydrogen promotion of the palladium-catalyzed carbon monoxide oxidation", Journal of Physical Chemistry, 75(13), 1971, pp. 2065-2066.

[67] J.R. Stetter, K.F. Blurton, "Selective oxidation of hydrogen in carbon monoxide/air streams. Application to environmental monitoring", Industrial and Engineering Chemistry Product Research and Development, 16(1), 1977, pp. 22-25.

[68] D.W. Dabill, S.J. Gentry, H.B. Holland, A.J. Jones, "The oxidation of hydrogen and carbon monoxide mixtures over platinum", Journal of Catalysis, 53, 1978, pp. 164-167.

[69] H. Muraki, S. Matunaga, H. Shinjoh, M.S. Wainwright, D.L. Trimm, "The effect of steam and hydrogen in promoting the oxidation of carbon monoxide over a platinum on alumina catalyst", Journal of Chemical Technology and Biotechnology, 52, 1991, pp. 415-424.

[70] M.J. Kahlich, H.A. Gasteiger, R.J. Behm, "Kinetics of the selective CO oxidation in H_2-rich gas on Pt/Al_2O_3", Journal of Catalysis, 171, 1997, pp. 93-105.

[71] S. Golunski, "HotSpot™ fuel processor. Advancing the case for fuel cell powered cars", Platinum Metals Review, 42 (1), 1998, pp. 2-7.

[72] O. Korotkikh, R. Farrauto, "Selective catalytic oxidation of CO in H_2: fuel cell applications", Catalysis Today, 62, 2000, pp. 249-254.

[73] A. Manasilp, E. Gulari, "Selective CO oxidation over Pt/alumina catalysts for fuel cell applications", Applied Catalysis B: Environmental, 37, 2002, pp. 17-25.

[74] G.K. Berthke, H.H. Kung, "Selective CO oxidation in a hydrogen-rich stream over $Au/\gamma\text{-}Al_2O_3$ catalysts", Applied Catalysis A: General, 194-195, 2000, pp. 43-53.

[75] M.J. Kahlich, H.A. Gasteiger, R.J. Behm, "Kinetics of the Selective Low-Temperature Oxidation of CO in H_2-Rich Gas over $Au/\alpha\text{-}Fe_2O_3$", Journal of Catalysis, 182, 1999, pp. 430-440.

[76] C. He, H.R. Kunz, J.M. Fenton, "Selective oxidation of CO in hydrogen under fuel cell operating conditions", Journal of the Electrochemical Society, 148(10), 2001, pp. A1116-A1124.

[77] J.G.E. Cohn, "Process for selectively removing carbon monoxide from hydrogen-containing gases", US Patent, 3 216 783, Nov. 9, 1965.

[78] P.V. Snytkov, V.A. Sobyanin, V.D. Belyaev, P.G. Tsyrulnikov, N.B. Shitova, D.A. Shlyapin, "Selective oxidation of carbon monoxide in excess hydrogen over Pt-, Ru- and Pd-supported catalysts", Applied Catalysis A: General, 239, 2003, pp. 149-156.

[79] F. Marino, C. Descorme, D. Duprez, "Noble metal catalysts for the preferential oxidation of carbon monoxide in the presence of hydrogen (PROX)", Applied Catalysis B: Environmental, 54, 2004, pp. 59-66.

[80] O. Pozdnyakova, D. Teschner, A. Wootsch, J. Krohnert, B. Steinhauer, H. Sauer, L. Toth, F.C. Jentoft, A. Knop-Gericke, Z. Pall, R. Schogl, "Preferential CO oxidation in hydrogen (PROX) on ceria-supported catalysts, part II: oxidation states and surface species on Pd/CeO_2 under reaction conditions, suggested reaction mechanism", Journal of Catalysis, 237, 2006, pp. 17-28.

[81] M. Batzill, U. Diebold, "Surface and Materials Science of Tin Dioxide", Progress in Surface Science, 79, 2005, pp. 47-154.

[82] D. Kohl, "Surface Processes in the detection of reducing gases with SnO_2-based devices", Sensors and Actuators, 18, 1989, pp. 71-113.

[83] P.T. Moseley, "Solid state gas sensors", Measurement Science and Technology, 8, 1997, pp. 223-237.

[84] W. Gopel, K. D. Schierbaum, "SnO_2 sensors: Current status and future prospects", Sensors and Actuators B: Chemical, 26, 1995, pp. 1-12.

[85] N. Bârsan, U. Weimar, "Understanding the fundamental principles of metal oxide based gas sensors; the example of CO sensing with SnO_2 sensors in the presence of humidity", Journal of Physics: Condensed Matter, 15, 2003, pp. R813-R839.

[86] N. Yamazoe, "New approaches for improving semiconductor gas sensors", Sensors and Actuators B: Chemical, 5, 1991, pp. 7-19.

[87] P. Siciliano, "Preparation, characterization and applications of thin films for gas sensors prepared by cheap chemical method", Sensors and Actuators B: Chemical, 70, 2000, pp. 153-164.

[88] A. Chiorino, G. Ghiotti, M.C. Carotta, G. Martinelli, "Electrical and spectroscopic characterization of SnO_2 and Pd/SnO_2 thick films studied as

CO gas sensors", Sensors and Actuators B: Chemical, 47, 1998, pp. 205-212.

[89] G. Kiss, V.K Josepovits, K. Kovács, B. Ostrick, M. Fleischer, H. Meixner, F. Réti, "CO sensitivity of the PtO/SnO_2 and PdO/SnO_2 layer structures: Kelvin probe and XPS analysis", Thin Solid Films 436, 2003, pp. 115-118.

[90] A. Cabot, A. Vila, J.R. Morante, "Analysis of the catalytic activity and electrical characteristics of different modified SnO_2 layers for gas analysis", Sensors and Actuators B: Chemical, 84, 2002, pp. 12-20.

[91] B. Gautheron, M. Labeau, G. Delabouglise, U. Schmatz, "Undoped and Pd-doped SnO_2 thin films for gas sensors", Sensors and Actuators B: Chemical, 15-16, 1993, pp. 357-362.

[92] M.I. Ivanovskaya, P.A. Bogdanov, D.R. Orlik, A. Ch. Gurlo, V.V. Romanovskaya, "Structure and properties of sol-gel obtained SnO_2 and SnO_2-Pd films", Thin Solid Films, 296, 1997, pp. 41-43.

[93] L. Delabie, M. Honoré, S. Lenaerts, G. Huyberechts, J .Roggen, G. Maes, "The effect of sintering and Pd-doping on the conversion CO to CO_2 on SnO_2 gas sensor materials", Sensors and Actuators B: Chemical, 44, 1997, pp. 446-451.

[94] G. Korotcenkov, V. Brinzari, Y. Boris, M. Ivanov, J. Schvank, J. Morante, "Influence of surface Pd doping on gas sensing characteristics of SnO_2 thin films deposited by spray pyrolysis", Thin Solid Films 436, 2003, pp. 119-126.

[95] R. Rella, A. Serra, P. Siciliano, L. Vasanelli, G. De, A. Licciulli, A. Quirini, "Tin oxide-based gas sensors prepared by the sol-gel process", Sensors and Actuators B: Chemical, 44, 1997, pp. 462-467.

[96] J. Kappler, N. Bársan, U. Weimar, A. Dièguez, J.L. Alay, A. Romano-Rodriguez, J.R. Morante, W. Göpel, "Correlation between XPS, Raman and TEM measurements and the gas sensitivity of Pt and Pd doped SnO_2 based gas sensors", Fresenius Journal of Analytical Chemistry, 361, 1998, pp. 110-114.

[97] S. Emiroglu, N. Bârsan, U. Weimar, V. Hoffmann, "In situ diffuse reflectance infrared spectroscopy study of CO adsorption on SnO_2", Thin Solid Films 391, 2001, pp. 176-185.

[98] H.J. Michel, H. Leiste, K.D. Schierbaum, J. Halbritter, "Adsorbates and their effects on gas sensing properties of sputtered SnO_2 films", Applied Surface Science, 126, 1998, pp. 57-64.

[99] N. Sergent, P.Gélin, L. Périer-Camby, H. Praliaud, G. Tomas, "Preparation and characterization of high surface area stannic oxides: structural, textural and semiconducting properties", Sensors and Actuators B: Chemical, 84, 2002, pp. 176-188.

[100] S.H. Hahn, N. Bârsan, U. Weimar, S.G. Ejakov, J.H. Visser, R.E. Soltis, "CO sensing with SnO_2 thick film sensors: role of oxygen and water vapour", Thin Solid Films 436, 2003, pp. 17-24.

[101] M.I. Baraton, L. Merhari, H. Ferkel, J.F. Castagnet, "Comparison of the gas sensing properties of tin, indium and tungsten oxides nanopowders: carbon monoxide and oxygen detection", Materials Science and Engineering C, 19, 2002, pp. 315-321.

[102] M.J. Fuller, M.E. Warwick, "The catalytic oxidation of carbon monoxide on tin(IV) oxide", Journal of Catalysis, 29, 1973, pp. 441-450.

[103] M.M. Gadgil, R. Sasikala, S.K. Kulshreshtha, "CO oxidation over Pd/SnO_2 catalyst", Journal of Molecular Catalysis, 87, 1994, pp. 297-310.

[104] J.E. Drawdy, G.B. Hoflund, S.D. Gardner, E. Yngvadottir, D.R. Schryer, "Effect of pretreatment on a platinized tin oxide catalyst for low-temperature CO oxidation", Surface and Interface Analysis, 16, 1990, pp. 369-374.

[105] N.D. Gangal, N.M. Gupta, R.M. Iyer, "Microcalorimetric study of the interaction of CO, O_2 and $CO+O_2$ with Pt/SnO_2 and SnO_2 catalysts", Journal of Catalysis, 126, 1990, pp. 13-25.

[106] M. Sheintuch, J. Schmidt, Y. Lecthman, G. Yahav, "Modeling catalyst-support interactions in carbon monoxide oxidation catalysed by Pd/SnO_2", Applied Catalysis, 49, 1989, pp. 55-65.

[107] S.K. Kulshreshtha, R. Sasikala, "Pd/SnO_2 and Pt/SnO_2 catalysts: spill over effects", Indian Journal of Chemistry, 33A, 1994, pp. 115-119.

[108] D. Amalric-Popescu, F. Bozon-Verduraz, "SnO_2-supported palladium catalysts: activity in $deNO_X$ at low temperature", Catalysis Letters, 64, 2000, pp. 125-128.

[109] A. Boulahouache, G. Kons, H. G. Lintz, "Oxidation of carbon monoxide on platinum-tin dioxide catalysts at low temperatures", Applied Catalysis A: General, 91, 1992, pp. 115-123.

[110] K. Grass, H.G. Lintz, "The kinetics of carbon monoxide oxidation on tin(IV) oxide supported platinum catalysts", Journal of Catalysis, 172, 1997, pp. 446-452.

[111] D.R. Schryer, B.T. Upchurch, J.D. van Norman, K.G. Brown, J. Schryer, "Effects of pretreatment conditions on a Pt/SnO_2 catalyst for the oxidation of CO in CO_2 lasers", Journal of Catalysis, 122, 1990, pp. 193-197.

[112] D.R. Schryer, B.Y. Upchurch, B.D. Sidney, K.G. Brown, G.B. Hoflund, R.K. Herz, "A proposed mechanism for Pt/SnO_X-catalyzed CO oxidation", Journal of Catalysis, 130, 1991, pp. 314-317.

[113] T. Takeguchi, O. Takeoh, S. Aoyama, J. Ueda, R. Kikuchi, K. Eguchi, "Strong chemical interaction between PdO and SnO_2 and the influence on catalytic combustion of methane", Applied Catalysis A: General, 252, 2003, pp. 205-214.

[114] N. Tsud, V. Johanek, I. Stara, K. Veltruska, V. Matolin, "XPS,ISS and TPD study of Pd-Sn interactions on Pd-SnO_X systems", Thin Solid Films 391, 2001, pp. 204-208.

[115] P.A. Sermon, V.A. Self, E.P.S. Barrett, "Analysis of Pt/SnOx during catalysis of CO oxidation", Journal of Molecular Chemistry, 65, 1991, pp. 377-384.

[116] J. Araña, P. Ramirez de la Piscina, J. Llorca, J. Sales, N. Homs, J. L. G. Fierro, "Bimetallic silica-supported catalysts based on Ni-Sn, Pd-Sn and Pt-Sn as materials in the CO oxidation reaction", Chemistry of Materials, 10, 1998, pp. 1333-1342.

[117] A. Hammoudeh, S. Mahmoud, "Selective hydrogenation of cinnamaldehyde over Pd/SiO_2 catalysts: selectivity promotion by alloyed Sn", Journal of Molecular Catalysis A: Chemical, 203, 2003, pp. 231-239.

[118] S. Verdier, B. Didillon, S. Morin, D. Uzio, "Pd-Sn/Al_2O_3 catalysts from colloidal oxide synthesis, II. Surface characterization and catalytic properties for buta-1,3-diene selective hydrogenation", Journal of Catalysis, 218, 2003, pp. 288-295.

[119] D. Koziej, N. Barsan, U. Weimar, J. Szuber, K. Shimanoe, N. Yamazoe, "Water-oxygen interplay on tin dioxide surface: implication on gas sensing", Chemical Physics Letters, 410, 2005, pp.321-323.

[120] M. Caldararu, D. Sprinceana, V.T. Popa, N.I. Ionescu, "Surface dynamics in tin dioxide-containing catalysts, II. Competition between water and oxygen adsorption on polycrystalline tin dioxide", Sensors and Actuators B: Chemical, 30, 1996, pp. 35-41.

[121] R. Burch, F.J. Urbano, P.K. Loader, "Methane combustion over palladium catalysts: the effect of carbon dioxide and water on activity", Applied Catalysis A: General, 123, 1995, pp. 173-184.

[122] D. Ciuparu, N. Katsikis, L. Pfefferle, "Temperature and time dependence of water inhibition effect on supported palladium catalyst for methane combustion", Applied Catalysis A: General, 216, 2001, pp. 209-215.

[123] R. Kikuchi, S. Maeda, K. Sasaki, S. Wennerström, K. Eguchi, "Low-temperature methane oxidation over oxide-supported Pd catalysts: inhibitory effect of water vapor", Applied Catalysis A: General, 232, 2002, pp. 23-28.

[124] J.C. van Giezen, F.R. van den Berg, J.L. Kleinen, A.J. van Dillen, J.W. Geus, "The effect of water on the activity of supported palladium catalysts in the catalytic combustion of methane", Catalysis Today, 47, 1999, pp. 287-293.

[125] G. Croft, M.J. Fuller, "Water-promoted oxidation of carbon monoxide over tin(IV) oxide-supported palladium", Nature 269, 1977, pp. 585-586.

[126] W. Schmid, N. Barsan, U. Weimar, "Sensing of hydrocarbons and CO in low oxygen conditions with tin dioxide sensors: possible conversion paths", Sensors and Actuators B: Chemical, 103, 2004, pp. 362-368.

[127] E.W. Thornton, P.G. Harrison, "Tin oxide surfaces", Journal of Chemical Society Faraday Transactions, 71, 1975, pp. 461-472.

[128] W. Thoren, D. Kohl, G. Heiland, "Kinetic studies on the decomposition of CH_3COOH and CH_3COOD on SnO_2 single crystals", Surface Science, 162, 1985, pp. 402-410.

[129] C.G. Vayenas, S. Bebelis, C. Pliangos, S. Brosda, D. Tsiplakides, Electrochemical Activation of Catalysis, Kluver Academic/Plenum, New York, 2001.

[130] A.E. Gusovius, R. Prins, "Alloy formation in Li-promoted Pd/SiO_2 catalysts for the synthesis of methanol", Journal of Catalysis, 211, 2002, pp. 273-277.

[131] A. Gotti, R. Prins, "Basic metal oxides as Co-catalysts in the conversion of synthesis gas to methanol on supported palladium catalysts", Journal of Catalysis, 175, 1998, pp. 302-311.

[132] C. Diagne, H. Idriss, J.P. Hindermann, A. Kiennemann, "Promoting effects of lithium on Pd/CeO_2 catalysts in carbon monoxide-hydrogen reactions", Applied Catalysis, 51, 1989, pp.165-180.

[133] E.B. Pereira, G.A. Martin, "Alcohol synthesis from syngas over nickel catalysts: effect of copper and lithium addition", Applied Catalysis A: General, 103, 1993, pp. 291-309.

[134] H.Y. Luo, P.Z. Lin, S.B. Xie, H.W. Zhou, C.H. Xu, S.Y. Hung, L.W. Lin, D.B. Liang, P.L. Yin, Q. Xin, "The role of Mn and Li promoters in supported rhodium catalysts in the formation of acetic acid and acetaldehyde", Journal of Molecular Catalysis A: Chemical, 122, 1997, 115-123.

[135] V.R. Choudhary, S.D. Sansare, A.M. Rajput, D.B. Akolekar, "Oxidative conversion of methane to C_2 hydrocarbons over Li, Mn, Cd and Zn promoted MgO catalysts", Applied Catalysis, 69, 1991, pp. 187-200.

[136] I.V. Yentekakis, R.M. Lambert, M. Konsolakis, V. Kiousis, "The effect of sodium on the Pd-catalyzed reduction of NO by methane", Applied Catalysis B: Environmental, 18, 1998, pp. 293-305.

[137] N. Macleod, J. Isaac, R.M. Lambert, "Sodium promotion of $Pd/\gamma\text{-}Al_2O_3$ catalysts operated under simulated "three-way" conditions", Journal of Catalysis, 198, 2001, 128-135.

[138] P. Vernoux, A.-Y. Leinekugel-Le-Cocq, F. Gaillard, "Effect of the addition of Na to Pt/Al_2O_3 catalysts for the reduction of NO by C_3H_8 and C_3H_6 under lean-burn conditions", Journal of Catalysis, 219, 2003, pp. 247-257.

[139] H. Wu, L. Liu, S. Yang, "Effects of additives on supported noble metal catalysts for oxidation of hydrocarbons and carbon monoxide", Applied Catalysis A: General, 211, 2001, pp. 159-165.

[140] T. Seiki, A. Nakato, S. Nishiyama, S. Tsuruya, "Effect and role of alkali metals added to cobalt ion-exchanged X and Y zeolite catalysts in the gas-phase catalytic oxidation of benzyl alcohol", Physical Chemistry Chemical Physics, 5, 2003, pp. 3818-3826.

[141] A.J. Urquhart, F.J. Williams, R.M. Lambert, "Electrochemical promotion by potassium of Rh-catalysed Fischer-Tropsch synthesis at high pressure", Catalysis Letters, 103(1-2), 2005, pp. 137-141.

[142] V. Pitchon, M. Guenin, H. Praliaud, "X-ray photoelectron spectroscopic study of the electronic state of palladium in alkali metal doped Pd/SiO_2 solids", Applied Catalysis, 63, 1990, pp. 333-343.

[143] A.M. Venezia, D. Duca, M.A. Floriano, G. Deganello, A. Rossi, "Chemical effect on the XPS spectra of the valence band and on O KLL and Pd MNN Auger-spectra in pumice-supported catalysts", Surface and Interface Analysis, 18, 1992, pp. 619-622.

[144] G.A. Somorjai, "The catalytic hydrogenation of carbon monoxide. The formation of C_1 hydrocarbons", Catalysis Reviews Science and Engineering, 23, 1981, pp. 189-202.

[145] H. Shi, G.K. Jacobi, "Hydrogen chemisorption on cesium-predosed Ru(001) surfaces", Surfce Science, 315, 1994, pp. 1-8.

[146] C. Resch, V. Zhukov, A. Lugstein, H.F. Berger, A. Winkler, K.D. Rendulic, "Dynamics of hydrogen adsorption on promoter-and inhibitor-modified nickel surfaces", Chemical Physics, 177, 1993, pp. 421-431.

[147] F. Solymosi, I. Kovacs, "Adsorption of hydrogen and deuterium on potassium-promoted Pd(100) surfaces", Surface Science, 260, 1992, pp. 139-150.

[148] J. Paul, F.M. Hoffmann, "Hydrogen adsorption on alkali modified aluminum", Surface Science, 194, 1988, pp. 419-437.

[149] L. Surnev, G. Rangelov, M. Kiskinova, "Interaction of oxygen with alkali modified Ru(001) surface", Surface Science, 179, 1987, pp. 283-296.

[150] M. Kiskinova, G. Rangelov, L. Surnev, "Coadsorption of oxygen ans cesium on Ru(001)", Surface Science, 172, 1986, pp. 57-70.

[151] M. Kiskinova, G. Rangelov, L. Surnev, "Coadsorption of oxygen and sodium on Ru(001)", Surface Science, 150, 1985, pp. 339-350.

[152] M. Gravelle-Rumeau-Maillot, V. Pitchon, G.A. Martin, H. Praliaud, "Complementary study by calorimetry and infrared spectroscopy of alkali metal doped Pd/SiO_2 solids: adsorption of hydrogen and carbon monoxide", Applied Catalysis A: General, 98, 1993, pp. 45-59.

[153] J. Paul, F.M. Hoffmann, "Alkali promoted CO bond weakening on aluminum: a comparison with transition metal surfaces", Journal of Chemical Physics, 86, 1987, pp. 5188-5195.

[154] S.J. Pratt, D.A. King, "Coverage dependent promoter action: K coadsorption and reactions with CO and CO_2 on Pd{100}", Surface Science, 540, 2003, pp. 185-206.

[155] L.F. Liotta, G.A. Martin, G. Deganello, "The influence of alkali metal ions in the chemisorption of CO and CO_2 on supported palladium catalysts: a Fourier transform infrared spectroscopic study", Journal of Catalysis, 164, 1996, pp. 322-333.

[156] G. Sijta, C.R. Henry, "Infrared study of CO adsorption on Pd particles supported on NaCl(100)", Surface Science, 517, 2002, pp. 155-122.

[157] A.M.Lanzillotto, M.J. Dresser, M.D. Alvey, J.T. Yates, Jr., "Alkali sensitization of H^+ electron stimulated desorption from H adsorbed on Ni(111)", Journal of Chemical Physics, 89, 1988, pp. 570-576.

[158] M. Rogozia, H. Niehus, A. Böttcher, "Formation of Cs-H surface compounds", Surface Science, 519, 2002, pp. 101-114.

[159] J.J. Scheer, A.E. van Arkel, R.D. Heyding, "Oxide complexes formed in the systems platinum metals: alkali carbonates : oxygen", Canadian Journal of Chemistry, 33, 1955, pp. 683-686.

[160] B.L. Dubey, J.A. Gard, F.P. Glasser, A.R. West, "Synthesis, structure and stability of phases in the system Li_2O-Pd-O_2", Journal of Solid State Chemistry, 6, 1973, pp. 329-334.

[161] H. Müller-Buschbaum, "Zur kristallchemie der oxopalladate", Zeitschrift fur Anorganische und Allgemeine Chemie, 631, 2005, pp. 239-259.

[162] B. Mitra, X. Gao, I.E. Wachs, A.M. Hirt, G. Deo, "Characterization of supported rhenium oxide catalysts: effect of loading, support and additives", Physical Chemistry Chemical Physics, 3, 2001, pp. 1144-1152.

[163] H. Tanaka, S. Ito, S. Kameoka, K. Tomishige, K. Kunimori, "Promoting effect of potassium in selective oxidation of CO in hydrogen-rich stream on Rh catalysts", Catalysis Communications, 4, 2003, pp. 1-4.

[164] C. Pedrero, T. Waku, E. Iglesia, "Oxidation of CO in H_2-CO mixtures catalyzed by platinum: alkali effects on rates and selectivity", Journal of Catalysis, 233, 2005, pp. 242-255.

[165] C. Kwak, T.J. Park, D.J. Suh, "Effects of sodium addition on the performance of PtCo/Al_2O_3 catalysts for preferential oxidation of carbon monoxide from hydrogen-rich fuels", Applied Catalysis A: General, 278, 2005, pp. 181-186.

[166] B. Mirkelamoglu, "Investigation of Carbon Monoxide Oxidation Over Tin Dioxide Based Catalysts by Dynamic Methods", M.Sc. Thesis, 2002, Ankara.

[167] X. Cao, L. Cao, W. Yao, X. Ye, "Structural characterization of Pd-doped SnO_2 thin films using XPS", Surface and Interface Analysis, 24, 1996, pp. 662-666.

[168] M. Hara, K. Asami, K. Hashimoto, T. Masumoto, "An X-ray photoelectron study of electrocatalytic activity of platinum group metals for chlorine evolution", Electrochimica Acta 28, 1983, pp. 1073-1081.

[169] K. Otto, L.P. Haack, J.E. deVries, "Identification of two types of oxidized palladium on γ-alumina by X-ray photoelectron spectroscopy", Applied Catalysis B: Environmental, 1, 1992, pp. 1-12.

[170] M. Moroseac, T. Skala, K. Veltruska, V. Matolin, I. Matolinova, "XPS and SSIMS studies of Pd/SnO_x system: reduction and oxidation in hydrogen containing air", Surface Science, 566-568, 2004, pp. 1118-1123.

[171] K.S. Kim, A.F. Gossmann, N. Winograd, "X-ray photoelectron spectroscopic studies of palladium oxides and palladium-oxygen electrode", Analytical Chemistry, 46, 1974, pp. 197-200.

[172] J.G. McCarty, "Kinetics of PdO combustion catalysis", Catalysis Today, 26, 1995, pp. 283-293.

[173] V. Chausse, P. Regull, L. Victori, "Formation of a higher palladium oxide in the oxygen evolution potential range", Journal of Electroanalytical Chemistry, 238, 1987, pp. 115-128.

[174] J.M. Tura, P. Regull, L. Victori, M.D. de Castellar, "XPS and IR (ATR) analysis of Pd oxide films obtained by electrochemical methods", Surface and Interface Analysis, 11, 1988, pp. 447-449.

[175] J. F. Geiger, K.D. Schierbaum, W. Gopel, "Surface spectroscopic studies on Pd-doped SnO_2", Vacuum, 41, 1990, 1629-1632.

[176] V.M. Jimenez, J. P. Espinos, A.R. Gonzalez-Elipe, "Effect of texture and annealing treatments in SnO_2 and Pd/SnO_2 gas sensors", Sensors and Actuators B: Chemical, 61, 1999, 23-32.

[177] I.N. Yakovkin, V.I. Chernyi, A.G. Naumovetz, "Oxidation of CO on Li-precovered Pt", Surface Science, 442, 1999, pp. 81-89.

[178] N. Yamazoe, J. Fuchigami, M. Kishikawa, T. Seiyama, "Interactions of tin oxide surface with O_2, H_2O and H_2", Surface Science, 86, 1979, pp. 335-344.

[179] M. Konsolakis, N. Macleod, J. Isaac, I.V. Yentekakis, R.M. Lambert, "Strong promotion by Na of Pt/γ-Al2O3 catalysts operated under simulated exhaust conditions", 193, 2000, pp. 330-337.

[180] P.G. Harrison, B. Maunders, "Tin oxide surfaces", Journal of Chemical Society Faraday Transactions I, 81, 1985, pp. 1345-1355.

[181] N. Pavlenko, P.P. Kostrobij, Y. Suchorski, R. Imbihl, "Alkali metal effect on catalytic CO oxidation on a transition metal surface: a lattice-gas model", Surface Science, 489, 2001, pp. 29-36.

[182] O. Wurzinger, G. Reinhardt, "CO-sensing properties of doped SnO_2 sensors in H_2-rich gases", Sensors and Actuators B: Environmental 103, 2004, pp. 104-110.

[183] R.A. Huggins, "Lithium alloy negative electrodes formed from convertible oxides", Solid State Ionics, 113-115, 1998, 57-67.

[184] I. A. Courtney, R.A. Dunlap, J.R. Dahn, "In-situ ^{119}Sn Mössbauer effect studies on the reaction of lithium with SnO and SnO:0.25 B_2O_3:0.25 P_2O_5 glass", Electrochimica Acta, 45, 1999, 51-58.

[185] K. Furuya, K. Ogawa, Y. Mineo, A. Matsufuji, J. Okuda, T. Erata, "Solid ^{7}Li-NMR and in situ XRD studies of the insertion reaction of lithium with tin oxide and tin-based amorphous composite oxide", Journal Physics: Condensed Matter, 13, 2001, 3519-3532.

[186] P. Sreeraj, R.D. Hoffmann, Z. Wu, R. Pöttgen, "Structure and bonding of $Li_{1.42(5)}Pd_2Sn_{5.58(5)}$: a lithium intercalated palladium stannide", Chemistry of Materials, 17, 2005, 911-915.

[187] R.V. Krol, A. Gossens, J. Schoonman, "Spatial extent of lithium intercalation in anatase TiO_2", Journal of Physical Chemistry B, 103, 1999, pp. 7151-7159.

[188] L. Kavan, M Gratzel, S.E. Gilbet, C. Klemenz, H.J. Scheel, "Electrochemical and photoelectrochemical investigation of single-crystal anatase", Journal of American Chemical Society, 118, 1996, pp. 6716-6723.

[189] R.J. Cava,D.W. Murphy, S. Zahurak, A. Santoro, R.S. Roth, "The crystal structures of the lithium-inserted metal oxides $Li_{0.5}TiO_2$ anatase, $LiTi_2O_4$ spinel, and $Li_2Ti_2O_4$" Journal of Solid State Chemistry, 53, 1984, pp. 64-75.

[190] J. Kim, P. Fulmer, A. Manthiram, "Sythesis of $LiCoO_2$ cathodes by an oxidation reaction in solution and their electrochemical properties", Materials Research Bulletin, 34, 1999, pp. 571-579.

[191] A. Fritsch, P. Legare, "Metal vapor deposition on carbon: an XPS study of Pd and Au cluster growth", Surface Science, 162, 1985, 742-746.

[192] G. Zhuang, Y. Chen, P.N. Ross, "The reaction of lithium with carbon dioxide studied by photoelectron spectroscopy", Surface Science, 418, 1998, pp. 139-149.

[193] H.Y. Luo, P.Z. Lin, S.B. Xie, H.W. Zhou, C.H. Xu, S.Y. Hung, L.W. Lin, D.B. Liang, P.L. Yin, Q. Xin, "The role of Mn and Li promoters in supported rhodium catalysts in the formation of acetic acid and acetaldehyde", Journal of Molecular Catalysis A: Chemical, 122, 1997, 115-123.

[194] I.V. Yentekakis, M. Konsolakis, R.M. Lambert, N. Macleod, L. Nalbantian, "Extraordinarily effective promotion by sodium in emission control catalysis: NO reduction by propene over Na-promoted Pt/γ-Al_2O_3", Applied Catalysis B: Environmental, 22, 1999, pp. 123-133

[195] M. Konsolakis, I.V. Yentekakis, "Strong promotional effects of Li, K, Rb and Cs on the Pt-catalysed reduction of NO by propene", Applied Catalysis B: Environmental, 29, 2001, pp. 103-113.

[196] I.V. Yentekakis, V. Tellou, G. Botzolaki, I.A. Rapakousios, "A comparative study of the C_3H_6+NO+O_2, C_3H_6+O_2 and NO+O_2 reactions in excess oxygen over Na-modified Pt/γ-Al_2O_3 catalysts", Applied Catalysis B: Environmental, 56, 2004, pp. 215-225.

[197] V. H. Baldwin, Jr., J.B. Hudson, "Coadsorption of hydrogen and carbon monoxide on (111) platinum", The Journal of Vacuum Science and Technology, 8(1), 1971, pp. 49-52.

[198] J.H. Craig, Jr., "Adsorption of hydrogen and carbon monoxide on platinum", Surface Science, 111, 1981, pp. L695-L700.

[199] N.V. Hieu, J.H. Craig, "Effect of CO on hydrogen adsorption on palladium", Surface Science, 160,1985, pp. L483-L487.

APPENDIX A

MASS SPECTROMETRY

A.1 Basic Principles

Mass spectrometry is an analytical technique that is used for determining the composition of a sample, which can be solid, liquid or gas, by separating the gas phase ions according to the their mass-to-charge (m/z) ratios. The mass spectrometer operates on the basic physics principle that the mass of an electrically charged particle may be determined by deflecting the particle in electric or magnetic field. For the mass spectrometric analysis of a gaseous sample, the sample needs to be ionized first. Each constituent in the gaseous sample has a specific mass and an identifiable charge carried by its ion. The ions formed in the ionization source of the mass spectrometer are sorted in the mass analyzer according to their m/z ratios and then, they are collected by a detector, where the ion flux is converted to proportional electrical current. These electrical signals are collected as a function of m/z ratio and the mass spectra are obtained.

A.2 Quantitative Analysis of Mass Spectra

During charging, some molecules may remain intact during charging and these ions are called the molecular ions or the parent ions. However, the cleavage of some of the bonds of some of the molecules take place, which results in the appearance of a fraction of ions at lower m/z values than the m/z value that corresponds to the molecular mass of the traced specie. Such ions are called fragments and the m/z values of the fragments of a parent ion may correspond to those of other molecular ions or fragments in multicomponent mixtures. Such an incidence would result in attenuated signals for some species for which overlap occurs and thus, the evaluation of the mass spectra would lead to misinterpretations.

To avoid the misinterpretation of the collected mass spectra, the spectra need be corrected for the elimination of the contribution from the fragment ions and for the quantitative analysis of the data. In addition to the corrections in the mass spectra due to the fragmentation of the molecular species, the collected mass spectra need also be corrected for the relative ionization gauge sensitivities, which is an indication of the capability of the instrument in ionizing the specific specie. Thus, relative ionization gauge sensitivity represents the sensitivity of the instrument for changes in the concentration of the specific specie in the analyte. The relative ionization gauge sensitivities of the traced molecular and atomic species and their cracking patterns which presents the mass-to-charge ratios of the parent ions and the two most intense fragments are presented in Table A.1.

Table A.1. Cracking patterns of traced species

Substance	Formula	Relative Ionization Gauge Sensitivity (RS)	Fragments (mass number/percent of major peak)		
			1	2	3
Argon	Ar	1.2	40/100	20/10	
Carbon Dioxide	CO_2	1.4	44/100	28/11	16/9
Carbon Monoxide	CO	1.05	28/100	16/10	12/5
Formic Acid	HCOOH	1.0	29/100	46/61	45/47
Hydrogen	H_2	0.44	2/100	1/5	
Methane	CH_4	1.6	16/100	15/85	14/16
Methanol	CH_3OH	1.8	31/100	32/66	29/64
Oxygen	O_2	0.86	32/100	16/11	
Water	H_2O	0.9	18/100	17/25	1/6

For the collection of the time-resolved mass spectra of the abovementioned species the ions listed in Table A.2 were traced during the in-situ characterization experiments. Table A.2 also shows the molecular ions and fragments of molecular species that have contributions to the traced ions. Carbon (m/z=12) was traced for monitoring the carbon balance within the system. Argon (m/z=40) signal was traced for monitoring possible air leak incidences. Although argon is a trace component of air, identification of air leaks

trough nitrogen (m/z=28) and oxygen (m/z=32) is not possible as m/z ratio of nitrogen corresponds to that of carbon monoxide and oxygen is supplied to the system.

The molecular ion of CO and the fragment of CO_2, where the cleavage of one of the C-O bonds of the molecule has occurred during ionization have the same m/z ratio thus, the contribution of CO_2 to the m/z=28 need be taken into account to arrive at the CO component of m/z=28 signal. For this purpose, the m/z=28 contribution, which accounts to 11% of the intensity of the CO_2 molecular ion (Table A.1) need be subtracted from the raw m/z=28 signal and the remaining is the contribution of CO (Equation A.1).

$$\left(I_{corrected}\right)_{m/z=28} = \left[\left(I_{raw}\right)_{m/z=28} - \left(I_{raw}\right)_{m/z=44} * \frac{11}{100} * \frac{1}{RS_{CO_2}}\right] * \frac{1}{RS_{CO}} \tag{A.1}$$

Similarly, m/z=32 and m/z=29 signals- which were traced to identify oxygen and formic acid species, respectively, have contributions from fragments of other molecular species that need be subtracted from the traced signals for arriving at the contributions of these molecular species. Both, m/z=29 and m/z=32 signals have contributions from methanol, which accounts for 66% and 64% of the intensity of the molecular ion of methanol, respectively, and the contributions of formic acid and oxygen to these signals can be calculated through Equations A.2 and A.3.

$$\left(I_{corrected}\right)_{m/z=29} = \left[\left(I_{raw}\right)_{m/z=29} - \left(I_{raw}\right)_{m/z=31} * \frac{65}{100} * \frac{1}{RS_{CH_4}}\right] \tag{A.2}$$

$$\left(I_{corrected}\right)_{m/z=32} = \left[\left(I_{raw}\right)_{m/z=32} - \left(I_{raw}\right)_{m/z=31} * \frac{67}{100} * \frac{1}{RS_{CH_4}}\right] * \frac{1}{RS_{O_2}} \tag{A.3}$$

The molecular ion of methane has a m/z ratio of 16, which would have contributions from carbon monoxide, carbon dioxide and oxygen. For the better assessment of methane content of the feed stream, CH_3^+ (m/z=15) species, which is the most abundant fragment of methane accounting to 85% of the peak for molecular methane ion, was traced. The methane signal (m/z=16) may be calculated through the m/z=15 component of methane with the help of Equation A.4.

$$\left(I_{corrected}\right)_{m/z=16} = \left(I_{raw}\right)_{m/z=15} * \frac{100}{85} * \frac{1}{RS_{CH_4}} \tag{A.4}$$

Table A.2 Traced ions and species contributing to traced ions

Traced Ion (m/z)	**Contributing Species**
2	Hydrogen, water
12	Carbon monoxide, carbon dioxide
15	Methane
16	Methane, oxygen
18	Water
28	Carbon monoxide, carbon dioxide
29	Formic acid, methanol
31	Methanol
32	Oxygen, methanol
40	Argon
44	Carbon dioxide

The collected mass spectra were corrected to account for relative ionization gauge sensitivity (RS) only, whenever no contributions to the collected signal for the molecular ion of a specie exist form the fragments of other species. Therefore, the collected mass spectra were corrected by the RS for hydrogen (Equation A.5), water (Equation A.6), methanol (Equation A.7) and argon (Equation A.8).

$$\left(I_{corrected}\right)_{m/z=2} = \left(I_{raw}\right)_{m/z=2} * \frac{1}{RS_{H_2}} \tag{A.5}$$

$$\left(I_{corrected}\right)_{m/z=18} = \left(I_{raw}\right)_{m/z=18} * \frac{1}{RS_{H_2O}} \tag{A.6}$$

$$\left(I_{corrected}\right)_{m/z=31} = \left(I_{raw}\right)_{m/z=31} * \frac{1}{RS_{CH_3OH}} \tag{A.7}$$

$$\left(I_{corrected}\right)_{m/z=40} = \left(I_{raw}\right)_{m/z=40} * \frac{1}{RS_{Ar}} \tag{A.8}$$

APPENDIX B

FORTRAN 90 CODE FOR AREA UNDER THE CURVE CALCULATIONS FOR IMPULSE EXPERIMENTS

The following F90 code that computes the area under a curve by numerical integration using 2nd order Lagrange polynomial on non-uniform grid was utilized for the calculation of areas under mass signal traces of CO and CO_2.

```
!##################################################
      program area_under_the_curve
      implicit none
!##################################################
      integer, parameter :: prec  = 8
      integer :: i,j,k,n
      integer :: jstart,jend, npeak, ispc
      integer :: inp1, inp2, out, status, nvar, ndim, stat
      character(len=20) :: inputfile1, inputfile2, outputfile
      real (kind=prec)  :: tstr, tend, avg1, avg2, slope, tendi, tinterval
      real (kind=prec)  :: area, area_extracted, area_residual
      real (kind=prec), allocatable, dimension(:,:) :: variables
      integer, allocatable, dimension(:)            :: ipeak
      real (kind=prec), allocatable, dimension(:)   :: tstart,ttend
      real (kind=prec), allocatable, dimension(:)   :: f,x
!##################################################
      ispc       = 3          ! 2=CO2, 3=CO
      tinterval  = 110.0d0    ! seconds
      slope      = 3.0d0      ! ratio of avg2/avg1 (slope)
      inputfile1 = 'data.inp' ! name of the input file
      inputfile2 = 'time.inp' ! name of the input file containing peaks loc.s
      outputfile = 'data.out' ! name of the output file
      inp1       = 11
          inp2       = 12
      out        = 13
      nvar       =  3
      open(unit=inp1, file=inputfile1, iostat=status)
      open(unit=inp2, file=inputfile2, iostat=status)
      open(unit=out, file=outputfile, iostat=status)
      read(inp1,*,iostat=status)
      ndim = 0
      do
        read(inp1,*,iostat=status)
        if(status /= 0) exit
        ndim = ndim + 1
      enddo
!      write(*,*) ndim,status
```

```
      rewind(unit=inp1)
      allocate (variables(nvar,ndim), stat=stat)

      read(inp1,*,iostat=status)
      do j=1,ndim
      read(inp1,*,iostat=status) (variables(i,j), i=1,nvar)
      enddo
!...
!...  read the number of peaks
      read(inp2,*,iostat=status)
      read(inp2,*,iostat=status) n
      read(inp2,*,iostat=status)
!...
!...  allocate the arrays for peak starting locations
      npeak = n
      write(*,*) 'number of peaks = ',npeak
      allocate ( ipeak(n), stat=stat)
      allocate (tstart(n), stat=stat)
      allocate ( ttend(n), stat=stat)
!...
!...  read the starting and ending of peaks
      do i=1,npeak
      read(inp2,*,iostat=status) jstart,jend
      do j=1,ndim
            if(j == jstart) then
        tstart(i) = variables(1,j)
      endif
            if(j == jend) then
        ttend(i) = variables(1,j)
        write (*,1000) i,jstart,jend,tstart(i),ttend(i)
      exit
      endif
      enddo
      enddo
!...
!...  perform area calcuations
      do i=1,npeak
      tstr  = tstart(i)
      tend  = ttend(i)

      n = 0
      do j=1,ndim
      if(variables(1,j) >= tstr .and. variables(1,j) <= tend) then
      n = n + 1
      endif
      if(variables(1,j) == tstr ) jstart = j
      if(variables(1,j) == tend ) jend   = j
      enddo
      if(mod(n,2) == 0) jend = jend + 1
      if(mod(n,2) == 0) n    = n    + 1

      allocate (f(n), stat=stat)
      allocate (x(n), stat=stat)

      k = 0
      do j=jstart,jend
```

```
      k = j-jstart+1
      f(k) = variables(ispc,j)
      x(k) = variables(1,j)
      enddo
      area_extracted = (f(n)+f(1))/2.0d0*(x(n)-x(1))
      call intlg2(f,x,n,area)
           area_residual  = area - area_extracted
      write(out,1002) i,tstr,tend,n,area,area_extracted,area_residual,f(n),f(1)
      deallocate(f)
      deallocate(x)

!      pause
      enddo
!...  formats
1000  format(3i8,2f12.6)
1001  format(1i,1f12.6,2e16.6,1e16.6)
1002  format(i8,2f16.6,i8,5e16.6)
!##################################################
       end program
!##################################################
!
!
!##################################################
      subroutine intlg2(f,x,n,area)
      implicit none
!##################################################
!...
!...  this subroutine computes the integral by using 2nd order
!...  lagrange polynomial on non-uniform grid for numerical integration
      integer :: i, n
      real (kind=8) :: f(n),x(n)
      real (kind=8) :: sum, area
!...
      sum = 0.0d0
      do i=1,n-1,2
      sum =   sum                                          &
           +(x(i+2)-x(i))                                  &
           *(                                        &
             f(i)*(x(i+1)-x(i+2))*(2.0d0*x(i)-3.0d0*x(i+1)+x(i+2))  &
           +  f(i+1)*(x(i)-x(i+2))**2.0d0                        &
           -  f(i+2)*(x(i)-3.0d0*x(i+1)+2.0d0*x(i+2))*(x(i)-x(i+1))  &
            )                                        &
           /(       6.0d0*(x(i)-x(i+1))*(x(i+1)-x(i+2))       )
      enddo
!...
      area = sum
!...
!##################################################
      return
      end subroutine intlg2
    !##################################################
```

APPENDIX C

FORTRAN 90 CODE FOR AREA UNDER THE CURVE CALCULATIONS FOR O_2-TPD EXPERIMENTS

The following F90 code that computes the area under a curve by numerical integration using 2nd order Lagrange polynomial on non-uniform grid was utilized for the calculation of areas under mass signal traces of CO_2 and H_2O.

```
!##############################################
      program area_under_the_curve
      implicit none
!##############################################
      integer, parameter :: prec  = 8
      integer :: i,j,k,n
      integer :: jstart,jend, npeak, ispc, itime
      integer :: inp, out, status, nvar, ndim, stat
      character(len=20) :: inputfile, outputfile
      real (kind=prec)  :: area, tstr, tend, tend2,triangle !, avg1, avg2, slope,
tendi, tinterval
      real (kind=prec), allocatable, dimension(:,:) :: variables
!      integer, allocatable, dimension(:)           :: ipeak
!      real (kind=prec), allocatable, dimension(:)   :: tstart
      real (kind=prec), allocatable, dimension(:)   :: f,x
!##############################################
      tstr       =  7.0000583333d+01
      tend       =  130.00691666d+01
      tend2      =  140.00441666d+01
      itime      =  1
      ispc       =  2         !
      inputfile  = 'data.inp' ! name of the input file
      outputfile = 'data.out' ! name of the output file
      inp        = 11
      out        =  6 !12
      nvar       = 14
      open(unit=inp, file=inputfile, iostat=status)
!      open(unit=out, file=outputfile, iostat=status)
!      read(inp,*,iostat=status)
      ndim = 0
      do
        read(inp,*,iostat=status)
        if(status /= 0) exit
        ndim = ndim + 1
      enddo
      write(*,*) ndim,status
      rewind(unit=inp)
```

```
      allocate (variables(nvar,ndim), stat=stat)
!
!      read(inp,*,iostat=status)
      do j=1,ndim
      read(inp,1003,iostat=status) (variables(i,j), i=1,nvar)
!      write(*,1003) (variables(i,j), i=1,nvar)
      enddo

      n = 0
      do j=1,ndim
      if(variables(itime,j) >= tstr .and. variables(itime,j) <= tend) then
      n = n + 1
!      write(*,*) j,n
      endif
      if(variables(itime,j) == tstr ) jstart = j
      if(variables(itime,j) == tend ) jend   = j
      enddo
      if(mod(n,2) == 0) jend = jend + 1
      if(mod(n,2) == 0) n    = n    + 1

      allocate (f(n), stat=stat)
      allocate (x(n), stat=stat)

      k = 0
      do j=jstart,jend
      k = j-jstart+1
      f(k) = variables(ispc,j) !-variables(ispc,1)
      x(k) = variables(itime,j)
      enddo

!      write(*,*) jstart,jend,jend-jstart,n,k
!
      call intlg2(f,x,n,area)

      triangle = (tend2-tend)*(variables(ispc,k)-variables(ispc,1))/2.0d0
      area     = area-variables(ispc,1)*(tend-tstr)
!
!      deallocate(f)
!      deallocate(x)
!
      write(out,1002) tstr,tend,n,area,triangle
!!      pause
!      enddo
!!...  formats
!1001  format(1i,1f12.6,2e16.6,1e16.6)
1002  format(2f16.6,i8,2e16.6)
1003  format(2x,18(f16.10,2x))
!##################################################
    end program
!##################################################
!
!
!
!##################################################
      subroutine intlg2(f,x,n,area)
      implicit none
```

```
!##################################################
!...
!...  this subroutine computes the integral by using 2nd order
!...  lagrange polynomial on non-uniform grid for numerical integration
     integer :: i, n
     real (kind=8) :: f(n),x(n)
     real (kind=8) :: sum, area
!...
     sum = 0.0d0
     do i=1,n-1,2
     sum =   sum                                          &
          +(x(i+2)-x(i))                                  &
          *(                                          &
            f(i)*(x(i+1)-x(i+2))*(2.0d0*x(i)-3.0d0*x(i+1)+x(i+2))  &
          +  f(i+1)*(x(i)-x(i+2))**2.0d0                        &
          -  f(i+2)*(x(i)-3.0d0*x(i+1)+2.0d0*x(i+2))*(x(i)-x(i+1))  &
           )                                          &
          /(      6.0d0*(x(i)-x(i+1))*(x(i+1)-x(i+2))      )
     enddo
!...
     area = sum
!...
!##################################################
     return
     end subroutine intlg2
!##################################################
```

APPENDIX D

SAMPLE CALCULATIONS

D.1 Calculation of Crystallite Size

The crystallite size was calculated by using the method developed by Scherrer. The crystallite size for a specific peak or a reflection can be calculated by using Scherrer Equation:

$$t = \frac{K\lambda}{B\cos\theta_B}$$

where, K is Scherrer constant, λ is the wavelength of radiation ($\lambda_{Cu,K\alpha}$ = 0.154nm), and B is the integral breadth of peak (in radians 2θ) located at angle θ_B. The crystallite size of palladium and alkali metal incorporated cassiterite was calculated from the (211) plane.

For K-PdO/SnO_2 (K/1.50),

$$B=1.1^{\circ} = 1.1^{\circ} * 2 * \frac{\pi}{360^{\circ}} = 0.0192 \text{ rad}$$

$2\theta = 52°$

$$t = \frac{0.9 * 0.154}{0.0192 * \cos\left(52/2\right)} = 11.2nm$$

D.2 Calculation of Rates of CO Oxidation Reaction

System: Reactor

Assumptions: Differential reactor operating at steady-state

$$\begin{Bmatrix}\text{Rate of CO in}\\ \text{to the system}\end{Bmatrix} - \begin{Bmatrix}\text{Rate of CO out}\\ \text{of the system}\end{Bmatrix} - \begin{Bmatrix}\text{Rate of CO}\\ \text{consumption}\\ \text{within the system}\end{Bmatrix} = \begin{Bmatrix}\text{Rate of CO}\\ \text{accumulation}\\ \text{within the system}\end{Bmatrix}$$

$$F_{CO,in} - F_{CO,out} + R_{CO,s} m_{cat} S_{cat} = 0$$

$$R_{CO,s} = \frac{F_{CO,in} - F_{CO,out}}{m_{cat}S_{cat}} = \frac{F_{CO,in} - F_{CO,in}\left(1 - X_{CO,out}\right)}{m_{cat}S_{cat}} = \frac{F_{CO,in}X_{CO,out}}{m_{cat}S_{cat}}$$

Calculation of Molar Flow Rate of Carbon Monoxide at the Inlet ($F_{CO_{in}}$)*:*

Total volumetric flow rate: $\upsilon = 40\ \mathrm{ml}/\mathrm{min}$

Inlet carbon monoxide concentration: $C_{CO_{in}} = 2400$ ppm

$$F_{CO_{in}} = \frac{P\upsilon}{\Re T} = \frac{97.272\ \mathrm{kPa} \times 40\,\frac{\mathrm{ml}}{\mathrm{min}} \times \frac{0.24}{100} \times \frac{1\mathrm{m}^3}{10^6\mathrm{ml}}}{8.314 \times 10^{-3}\,\frac{\mathrm{kPa}\cdot\mathrm{m}^3}{\mathrm{mol}\cdot\mathrm{K}} \times 297\mathrm{K}}$$

$$F_{CO_{in}} = 3.78 \times 10^{-6}\ \mathrm{mol}/\mathrm{min} = 3.78\ \mu\mathrm{mol}/\mathrm{min}$$

Calculation of Carbon Monoxide Conversion: The CO $\left(m/z = 28\right)$ signals corresponding to 100% and 0% conversion of carbon monoxide are obtained from $\left(m/z = 28\right)$ traces collected while pure carrier gas and the analysis gas are flowing through the by-pass line.

$\left(m/z = 28\right)$ *signal corresponding to 100% conversion :* $\left(m/z = 28\right)_{100\%}$

$\left(m/z = 28\right)$ *signal corresponding to 0% conversion :* $\left(m/z = 28\right)_{0\%}$

$\left(m/z = 28\right)$ *signal corresponding to* X_{CO}*% conversion :* $\left(m/z = 28\right)_{X_{CO}}$

$$X_{CO}(\%) = \frac{100}{\left(m/z = 28\right)_{100\%} - \left(m/z = 28\right)_{0\%}}\left(\left(m/z = 28\right)_{X_{CO}} - \left(m/z = 28\right)_{0\%}\right)$$

For reduced Na-PdO/SnO_2 and S = 0.91,

$\left(m/z = 28\right)_{100\%} = 9 \times 10^{-10}$ *Torr*

$\left(m/z = 28\right)_{0\%} = 6.50 \times 10^{-9}$ *Torr*

@ t=93min, $\left(m/z = 28\right)_{X_{CO}} = 3.25 \times 10^{-9}$ *Torr*

$$X_{CO}(\%) = \frac{100}{9\times10^{-10} - 6.5\times10^{-9}}\left(3.25\times10^{-9} - 6.5\times10^{-9}\right) = 57.9\%$$

Table D.1 Rates of CO conversion (%) at 150°C under different reactor feed conditions

	Oxidized PdO/SnO_2	Reduced PdO/SnO_2	Oxidized Na-PdO/SnO_2	Reduced Na-PdO/SnO_2
S= 1.25	6.5	22	10	59
S = 0.91	19	45	12	58
S = 0.50	20	54	14	71

For oxidized PdO/SnO_2,

Weight of catalyst: m_{cat} = 0.1 g

Surface area of catalyst: S_{cat}=52 m^2/gr

CO conversion: $X_{CO} = 0.065$

$$R_{CO,s} = \frac{F_{CO,in}X_{CO,out}}{m_{cat}S_{cat}} = \frac{3.78\ \frac{\mu\text{mol}}{\text{min}}\times0.065}{0.1\ \text{g}\times52\ \frac{\text{m}^2}{\text{g}}} = 0.047\ \mu\text{mol}/\text{m}^2\cdot\text{min}$$

Table D.2 Rates of CO reaction (μmol/m^2.min) at 150°C under different reactor feed conditions

	Oxidized PdO/SnO_2	Reduced PdO/SnO_2	Oxidized Na-PdO/SnO_2	Reduced Na-PdO/SnO_2
S= 1.25	0.047	0.160	0.070	0.413
S = 0.91	0.138	0.327	0.084	0.406
S = 0.50	0.145	0.389	0.096	0.501

D.3 Calculation of CO Selectivity in the Presence of H_2

$$S_{CO} = \frac{\text{moles of oxygen consumed for the desired reaction}}{\text{total moles of oxygen consumed}}$$

$$S_{CO} = \frac{= 0.5F_{CO_2,\,out}}{F_{O_{2,in}} - F_{O_{2,out}}} = \frac{0.5X_{CO}F_{CO_{in}}}{F_{O_{2,in}} - F_{O_{2,in}}\left(1 - X_{O_2}\right)} = \frac{0.5X_{CO}F_{CO_{in}}}{X_{O_2}F_{O_{2,in}}}$$

For reduced K-PdO/SnO_2 (K/0.53) and [CO]/[O]=0.17,

CO conversion when 50% O_2 conversion is achieved: $X_{CO} = 0.557$

$$S_{CO} = \frac{0.5X_{CO}F_{CO_{in}}}{X_{O_2}F_{O_{2,in}}} \times 100 = 0.5\frac{F_{CO_{in}}}{F_{O_2,in}}\frac{X_{CO}}{X_{O_2}} \times 100 = 0.5 \times 0.33 \times \frac{0.557}{0.500} \times 100 = 22.58$$

APPENDIX E

N_2 ADSORPTION ISOTHERMS FOR BET AND PSD ANALYSIS

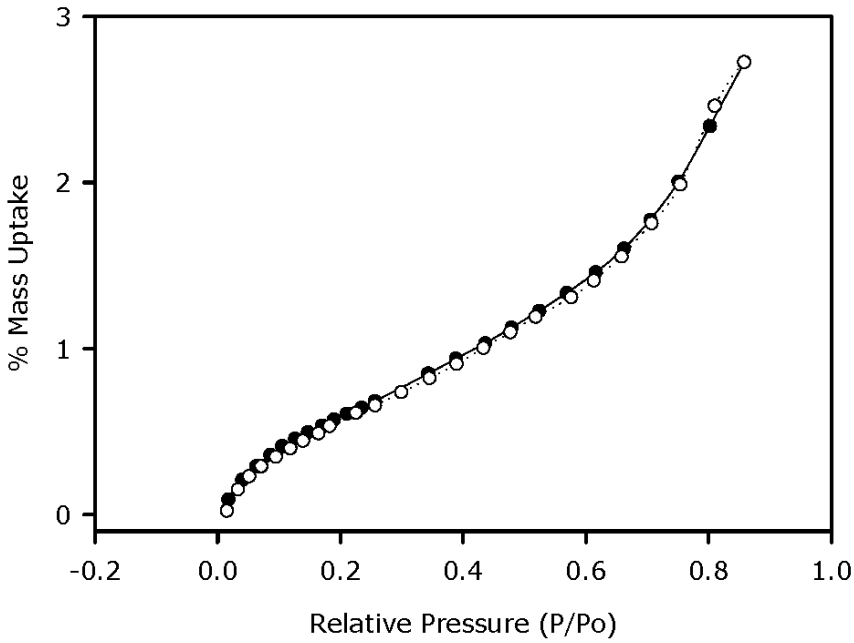

Figure E.1 N_2 adsorption (•) and desorption (o) isotherm for SnO_2

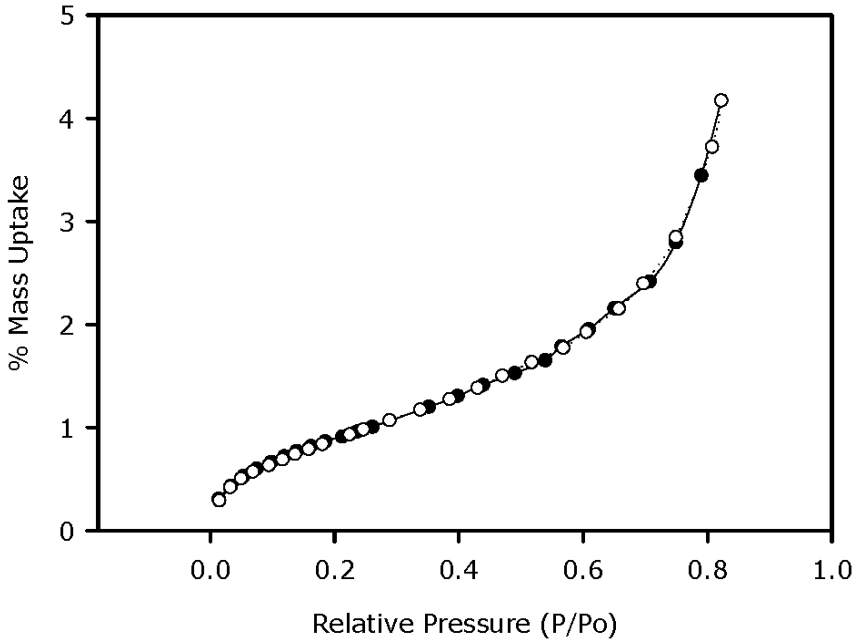

Figure E.2 N_2 adsorption (•) and desorption (o) isotherm for PdO/SnO_2

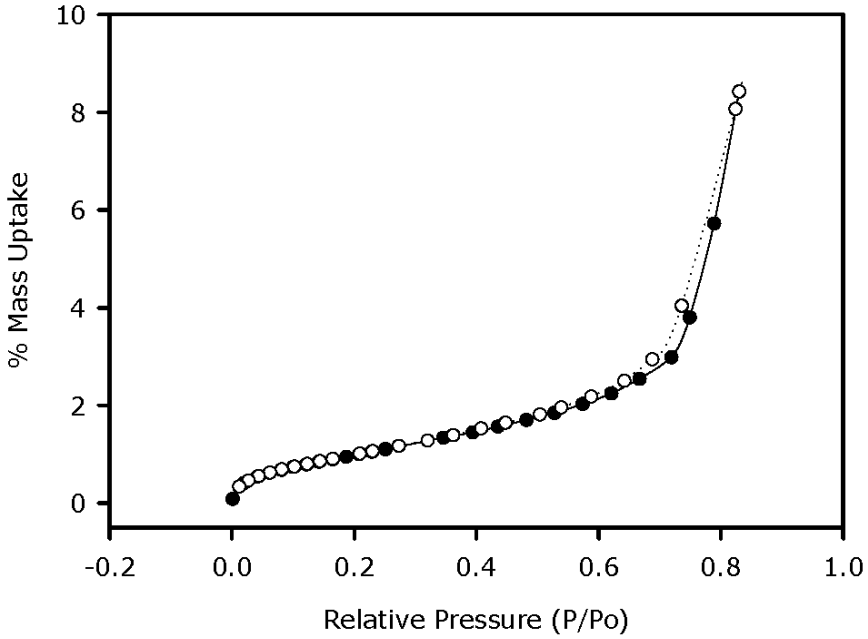

Figure E.3 N_2 adsorption (•) and desorption (o) isotherm for Na-PdO/SnO_2

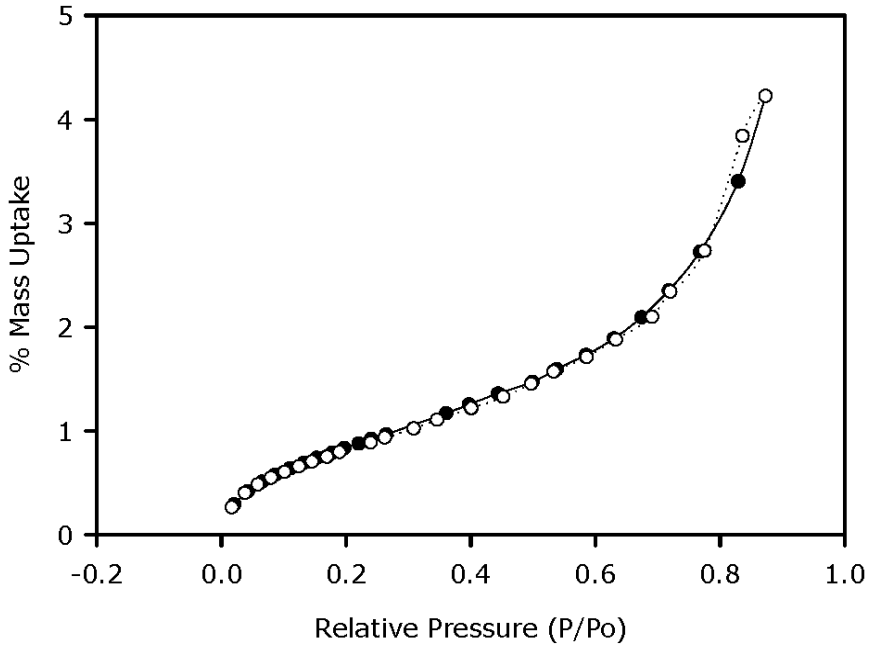

Figure E.4 N_2 adsorption (●) and desorption (o) isotherm for K-PdO/SnO_2

CURRICULUM VITAE

BURCU MİRKELAMOĞLU

SEPTEMBER 2006

PERSONAL INFORMATION

Nationality: Turkish (TC)
Date and Place of Birth: 7 May 1977, Ankara
Marital Status: Single
Phone: +90 312 210 43 90
Fax: +90 312 210 12 64
email: bmirkelamoglu@gmail.com

EDUCATION

Degree	Institution	Year of Graduation
MS	METU Chemical Engineering	2002
MS	METU Business Administration	2000
BS	METU Chemical Engineering	1998
High School	TED Ankara College, Ankara	1994

WORK EXPERIENCE

Year	Place	Enrollment
2001 – present	METU Department of Chemical Engineering	Teaching Assistant
2000 – 2001	METU Computer Center	Financial and Administrative Assistant
1996 July	Ankara Cement Factory	Intern Engineering Student

FOREIGN LANGUAGES

English; full-fluency

HONORS AND AWARDS

- 2006, Awarded by Middle East Technical University, Department of Chemical Engineering with Hasan Orbey Award in Graduate Studies
- 2005, Awarded by the Graduate School of Natural and Applied Sciences of Middle East Technical University for outstanding CGPA among Ph.D. students of Department of Chemical Engineering
- 1998, Ranked 1st among senior Chemical Engineering students
- 1996, Ranked 3rd among sophomore Chemical Engineering students

PUBLICATIONS

1. Research Articles

[1] B. Mirkelamoglu, G. Karakas, *"Characterization of Li, Na and K doped PdO/SnO_2 catalysts for low-temperature CO oxidation"*, to be published.

[2] B. Mirkelamoglu, G. Karakas, "The role of alkali-metal promotion on CO oxidation over PdO/SnO_2 catalysts", Applied Catalysis A: General, 299, 2006, p. 84-94.

[3] B. Mirkelamoglu, G. Karakas, *"CO oxidation over palladium- and sodium-promoted tin dioxide: catalyst characterization and temperature-programmed studies"*, Applied Catalysis A: General, 281, 2005, p. 275-284.

2. Book Chapters

[1] B. Mirkelamoglu, G. Karakas, *"Low temperature oxidation of carbon monoxide over alkali-metal promoted palladium-tin oxide catalysts"*, Eds. J.P. Blitz and V. Gun'ko, Pure and Applied Surface Chemistry and Nanomaterials for Human Life and Environmental Protection, Springer, in print.

3. International Conference Publications

[1] B. Mirkelamoglu, G. Karakas, *"Characterization and Temperature-Programmed Studies on CO Oxidation Activity of Alkaline Promoted PdO/SnO_2"* International Workshop on Nanostructured Materials – Nanomat2006, Antalya, Turkey (2006).

[2] B. Mirkelamoglu, G. Karakas, *"Effect of Na- addition on the low-temperature oxidation of CO over SnO_2-based catalysts"*, 2nd International Congress on Operando Spectroscopy – Operando-II, Spain (2006).

[3] G. Karakas, B. Mirkelamoglu, *"The enhanced CO oxidation over alkaline doped Pd/SnO_2 catalysts"*, NATO-ARW Meeting on Pure and Applied Surface Chemistry and Nanomaterials for Human Life and Environmental Protection, Ukraine (2005).

[4] B. Mirkelamoglu, B. Kurbanoglu, G. Karakas, *"Carbon monoxide oxidation and sensing behavior of noble metal and alkali metal promoted tin dioxide"*, 7th International Conference on Nanostructured Materials – Nano2004, Germany (2004).

[5] B. Mirkelamoglu, G. Karakas, *"Adsorption properties of emission gases over noble metal and alkali metal promoted stannic oxide"*, 3rd Chemical Engineering Conference for Collaborative Research in Eastern Mediterranean – EMCC3, Greece (2003).

4. National Conference Publications

[1] B. Mirkelamoğlu, G. Karakaş, *"Na-Pd/SnO_2 katalizörü ile düşük sıcaklıkta karbon monoksit oksidasyonu"*, XVIII. Ulusal Kimya Kongresi (2004).

[2] B. Kurbanoğlu, B. Mirkelamoğlu, G. Karakaş, *"Pd/SnO_2 ince tabaka filmlerin gaz algılayıcısı olarak uygulanabilirliklerinin incelenmesi"*, XVIII. Ulusal Kimya Kongresi (2004).

[3] B. Mirkelamoğlu, G. Karakas, *"%1 Pd/SnO_2 ince tabaka gaz algılayıcılarında CO ve CH_4 adsorpsiyonunun incelenmesi"*, V. Ulusal Kimya Mühendisliği Kongresi (2002).